AIIM
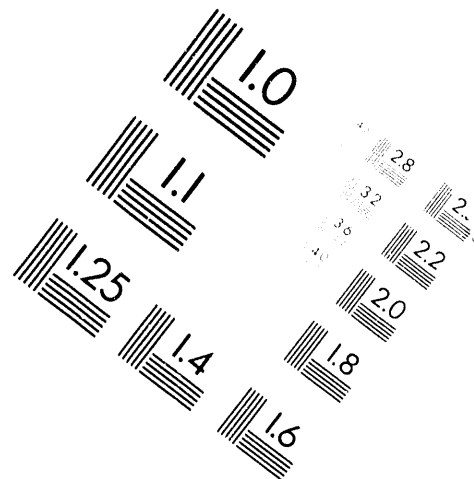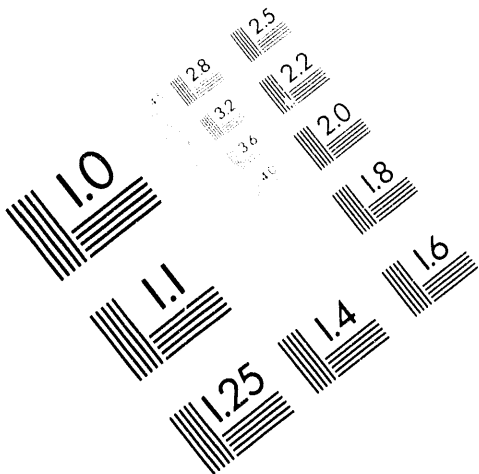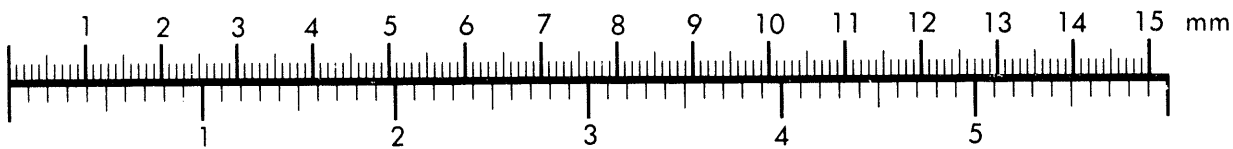
Association for Information and Image Management

1100 Wayne Avenue, Suite 1100
Silver Spring, Maryland 20910

301/587-8202

Centimeter
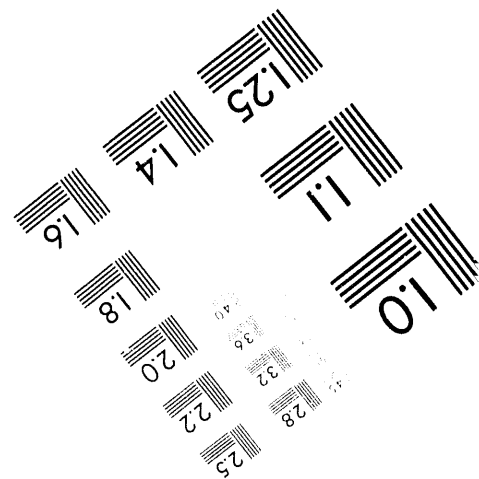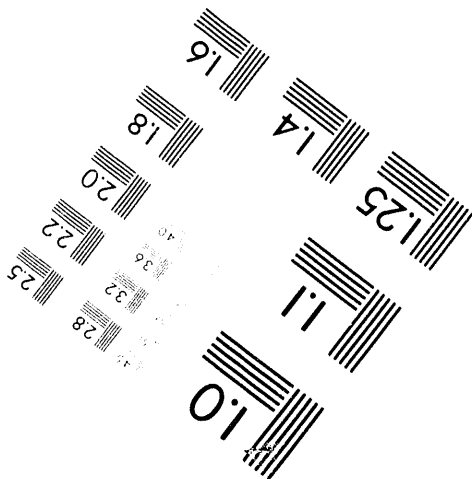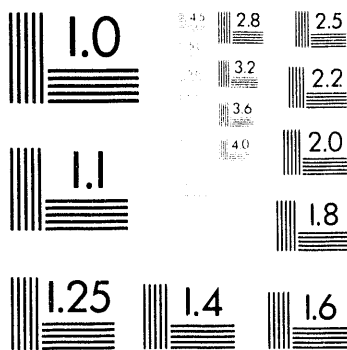
1   2   3   4   5   6   7   8   9   10   11   12   13   14   15 mm

1   2   3   4   5

Inches

1.0   2.8   2.5
       3.2   2.2
       3.6
       4.0   2.0
              1.8

1.1

1.25   1.4   1.6

Dynamic Characterization and

Damage Detection in the

I-40 Bridge Over the Rio Grande
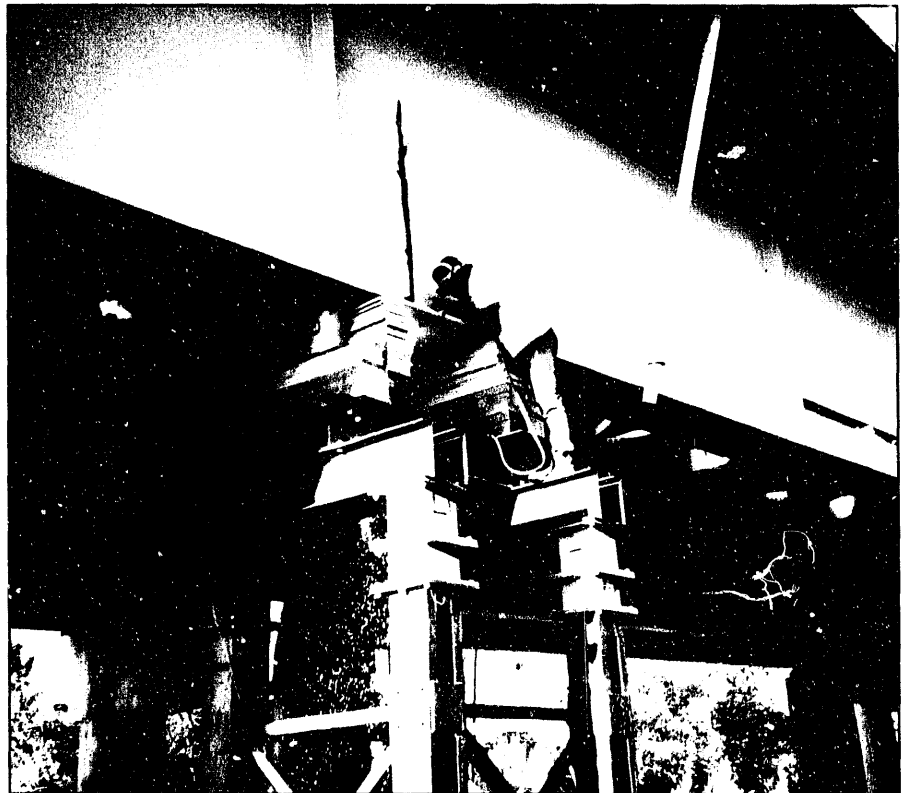
Los Alamos
NATIONAL LABORATORY

Cover photo: *A New Mexico State University technician introduces damage into the I-40 Bridge over the Rio Grande in Albuquerque, New Mexico. Using an acetylene torch, he has made a 6-ft-long cut (the line above and to the left of his head) in the web of the steel plate girder and is now cutting across the 21-in. flange. Vibration tests were performed after each cut to assess changes in structural properties resulting from the damage.*

Dynamic Characterization and Damage Detection in the I-40 Bridge Over the Rio Grande

C. R. Farrar
W. E. Baker
T. M. Bell
K. M. Cone
T. W. Darling
T. A. Duffey
A. Eklund
A. Migliori

CONTENTS

FIGURES

TABLES

DYNAMIC CHARACTERIZATION AND DAMAGE DETECTION IN THE I-40 BRIDGE OVER THE RIO GRANDE

by

C. R. Farrar, W. E. Baker, T. M. Bell, K. M. Cone,
T. W. Darling, T. A. Duffey, A. Eklund, and A. Migliori

ABSTRACT

In the 1960's and 1970's over 2500 bridges were built in the U.S. with a design similar to those on Interstate 40 over the Rio Grande in Albuquerque, New Mexico. These bridges were built without structural redundancy and typically have only two plate girders carrying the entire dead and live loads. Failure of either girder is assumed to produce catastrophic failure of the bridge, hence these bridges are referred to as fracture-critical bridges. The Federal Highway Administration (FHWA) and the National Science Foundation (NSF) have provided funds to New Mexico State University (NMSU) through the New Mexico State Highway and Transportation Department (NMSH&TD) and The Alliance For Transportation Research (ATR) for evaluation and testing of the existing fracture critical bridges over the Rio Grande.

Because the I-40 bridges over the Rio Grande were to be razed during the summer of 1993, the investigators were able to introduce simulated fatigue cracks, similar to those observed in the field, into the structure in order to test various damage identification methods and to observe the changes in load paths through the structure caused by the cracking. To support this research effort, NMSU contracted Los Alamos National Laboratory (LANL) to perform experimental modal analyses, and to develop experimentally verified numerical models of the bridge. Scientists from the LANL's Condensed Matter and Thermal Physics Group (P-10) applied state-of-the-art sensors and data acquisition software to the modal tests. Engineers from the LANL's Advanced Engineering Technology Group (MEE-13) conducted ambient and forced vibration tests to verify detailed and simplified finite element models of the bridge. Forced vibration testing was done in conjunction with engineers from Sandia National Laboratory (SNL) who provided and operated a hydraulic shaker. SNL also provided consultation on the use of the their NExT method, a state-of-the-art method for system identification from ambient vibration data. This report summarizes the experimental procedures and results obtained by P-10 and MEE-13 personnel. A subsequent report will summarize the numerical models of the bridge and compare results obtained with these models to the measured dynamic response of the bridge.

Consistent results for identified dynamic properties of the bridge were obtained from the ambient vibration data analyzed using the NExT method, swept sine tests using non-contact microwave interferometer absolute displacement sensors, and conventional random forced vibration experimental modal analyses. After various stages of damage the dynamic tests were

repeated, but changes in modal properties were only observed after considerable damage had been introduced . Significant contributions of this work include (1) the demonstration of the NExT method for identification of bridge dynamic properties from ambient response to traffic excitation and the benchmarking of this procedure against conventional forced vibration test results; (2) the demonstration of the microwave interferometer non-contact absolute displacement dynamic measurement system and the benchmarking of results obtained from it with a conventional modal analysis data acquisition system; and (3) a quantification of the amount of damage that must be present before conventional modal analysis methods identify a change in the structure's global dynamic properties.

I. INTRODUCTION

In the 1960's and 1970's over 2500 bridges were built in the U.S. with a design similar to those on Interstate 40 over the Rio Grande in Albuquerque, New Mexico, Fig. 1. These bridges were built without structural redundancy and typically have only two plate girders carrying the entire dead and live loads. Failure of either girder is assumed to produce catastrophic failure of the bridge. For this reason the bridges, which have been found to exhibit fatigue cracking from out of plane bending, are referred to as fracture-critical bridges. The Federal Highway Administration (FHWA) and the National Science Foundation (NSF) have provided funds to New Mexico State University (NMSU) through the New Mexico State Highway and Transportation Department (NMSH&TD) and The Alliance For Transportation Research (ATR) for evaluation and testing of the existing fracture critical bridges over the Rio Grande. The project is intended to develop and field test new nondestructive testing technology and to create a detailed bridge management data base for this class of bridges. NSF is providing funds to investigate the seismic capacity of bridges such as these that were built prior to the adoption of modern seismic design standards.

Because the bridges over the Rio Grande were to be razed during the summer of 1993, the investigators were able to introduce simulated fatigue cracks, similar to those observed in the field, into the structure in order to test various damage identification methods and to observe the changes in load paths through the structure caused by the cracking. To support this research effort, NMSU contracted Los Alamos National Laboratory (LANL) to perform experimental modal analyses, and to develop experimentally verified numerical models of the bridge. Scientists from the LANL's Condensed Matter and Thermal Physics Group (P-10) applied state-of-the-art sensors and data acquisition software for the modal tests. Engineers from the LANL's Advanced Engineering Technology Group (MEE-13) conducted ambient and forced vibration tests to verify detailed and simplified finite element models of the bridge. Forced vibration testing was done in conjunction with engineers from Sandia National Laboratory (SNL) who provided and operated a hydraulic shaker. SNL also provided consultation on the use of the their NExT method, a state-of-the-art method for system identification from ambient vibration data. This report summarizes the experimental procedures and results obtained by P-10 and MEE-13 personnel. A subsequent report will summarize the numerical models of the bridge and compare results obtained with these models to the measured dynamic response of the bridge.

2

Fig. 1. I-40 bridges over the Rio Grande in Albuquerque, New Mexico.

II. LITERATURE REVIEW

Before a contract between NMSU and LANL was put in place, LANL allocated internal research and development funds to perform a literature search of topics related to highway bridge testing and damage detection. Such a literature search allowed engineers and scientists at LANL to become familiar with the current "state-of-the-art" in these fields and helped in the planning of the experimental portion of this program. This search also highlighted areas where LANL could extend the state-of-the-art both in experimental measurements and in numerical modeling of highway bridges.

There have been a large number of studies related to static and dynamic testing of bridges reported in the open literature, and, hence, the initial phase of this effort was to conduct an extensive review of this body of literature. Also reviewed were literature pertaining to testing of large civil engineering structures, in general, because test methods and data analysis procedures used for any large structure, say a nuclear reactor building, may also be applicable to bridges. The survey is concluded by reviewing the much more limited body of literature pertaining to damage detection in civil engineering structures, particularly bridges.

Before the literature review is presented several terms related to spectral analysis are defined along with synonyms for these terms that are often found in the technical literature. These terms are used extensively in the literature review as well as the rest of this report.

For a continuous time series, x(t), defined on the interval from 0 to T, the Fourier Spectrum (Fourier Transform), X(f), is defined as

$$X(f) = \int_0^T x(t)e^{-i2\pi ft}dt,$$ (1)

where $i = \sqrt{-1}$, and
   f = cyclic frequency (Hz).

This function is complex and the magnitude is typically plotted in engineering units (EU), such as m/s^2 or g's, versus frequency.

The power spectrum is defined as

$$|X(f)|^2 = X(f)X^*(f),$$ (2)

where * denotes complex conjugate. The power spectrum is a real-valued frequency domain function and has the units of $(EU)^2$.

The power spectral density (autospectral density), $G_{xx}(f)$ is defined as

$$G_{xx}(f) = \frac{2}{T} E\left[|X(f)|^2\right],$$ (3)

where $E[\ ]$ indicates an ensemble average for a specific f over n samples of $X(f)$. This function will often be referred to by the abbreviation **PSD**. Again, this is a real-valued frequency domain function and has the units of EU^2/Hz.

The cross-power spectrum (cross-spectral density), $G_{xy}(f)$, relating two time histories, $x(t)$ and $y(t)$, is defined as

$$G_{xy}(f) = \frac{2}{T} E\left[X^*(f)Y(f)\right].$$ (4)

The abbreviation **CPS** will be used to denote cross-power spectrum.

For a linear system the frequency response function (transfer function), $H(f)$, which relates an input, $X(f)$, to a response, $Y(f)$, is defined as

$$H(f) = \frac{Y(f)}{X(f)} = \frac{G_{xy}(f)}{G_{xx}(f)}.$$ (5)

This function is abbreviated as **FRF** throughout this report.

In actual dynamic testing discrete time series are measured. The reader is referred to Bendat and Piersol (1980) for the discrete representations of the functions listed in Eqs. 1-5.

A. Testing of Large Civil Engineering Structures in General

Hudson (1970,1977) presented two extensive reviews on the dynamic testing of full-scale structures covering 160 references. Free and forced vibration tests as well as shake table tests were surveyed. One feature noted by Hudson (1977) was the lack of structural tests taken to the point of complete destruction. Structures discussed in detail ranged from a steel-fran.e building to a radio telescope, with limited treatment of dynamic bridge testing. A comparison of mode shapes obtained from ambient tests with those of forced-vibration tests was presented. Various types of ambient and forced loading on structures were discussed.

More recently, Srinivasan, et al. (1981) reviewed a large number of dynamic tests performed on as-built nuclear power plant buildings. The types of structures tested varied widely, ranging from box-like concrete-wall/steel-roof reactor buildings to a spherical steel containment shell. Loading on the various nuclear power plant structures also varied widely: ambient loading; steady-state forced vibrations; impulsive loading with rockets; impulse/seismic simulation with buried explosives; and free vibrations resulting from step-relaxation tests (a large static force is applied and

suddenly released). The authors suggested that dynamic low-level testing is useful for verifying analytical models. For this class of structures, proof testing at design-level excitation is considered impractical. The authors further stated that high-level excitation response is best predicted by a combined program of low-level testing and analytical modeling.

Several years later, Srinivasan, et al. (1984) extended the review to dynamic testing of other (i.e., non-nuclear) as-built civil engineering structures. A wide variety of different types of structures - subjected to dynamic testing - were discussed, including buildings, dams, bridges, towers, tall chimneys and off-shore structures. Loading included both ambient and forced steady-state testing. The authors concluded that dynamic testing at low levels of excitation is of limited value for predicting response to strong excitation because of the nonlinear nature of the dynamic behavior at higher amplitudes. Further, they cited the need for more systematic testing of as-built structures at various excitation levels. A discussion was also presented on ambient versus forced-vibration testing.

Finally, a review of a large number of dynamic tests, primarily on concrete and steel structures, has just appeared (Hashimoto, et al., 1993). The review was directed toward establishing appropriate structural damping levels at different values of excitation and for different types of construction. The work was based on an extensive literature survey of over 1,000 references.

A number of other papers on testing of large civil engineering structures which have relevance to the present work are as follows:

Chen (1977) performed forced vibration tests on a full-scale four-story reinforced concrete test structure to investigate dynamic response before, after and during the time it underwent structural damage. Based on results from the nondestructive and post-destructive tests, it was found that the damaged structure had a longer period, higher damping, and some mode shape "discontinuity". The paper is an example of early work on the influence of damage on the vibration characteristics of a structure.

Other fundamental, early forced vibration tests on large building structures were reported by Hudson, et al. (1964) for a 150 ft. high concrete intake tower and a nine-story steel frame building. Natural period and damping of several of the tower modes were obtained. Jennings, et al. (1972) tested a twenty-two story steel frame structure, and obtained frequencies, mode shapes, and damping values for the first 18 modes of the structure. Ellis and Jeary (1979) presented a comparison of forced and ambient vibration results for the first three modes of a tower. For the ambient (wind) tests, the amplitudes of motion were smaller than corresponding forced vibration tests with corresponding higher frequencies.

In the proceedings of a workshop on earthquake resistance of highway bridges conducted by the Applied Technology Council (1979), Hall and Newmark have suggested ranges of damping values that bridges can be expected to exhibit during seismic excitation based on the type of construction and stress level. The lower values are considered to be a "nearly lower bound" and the upper level is considered "average or slightly above average." These values were not developed from an

experimental program for bridges, but rather they represent slight modifications to damping values that had previously been suggested for nuclear power plant structures.

Galambos and Mayes (1979) performed a series of dynamic tests on an eleven story building, initially using small amplitude testing sufficient to result in major damage. Changes in modal response as a result of damage are discussed in detail.

Weaver (1980) presents a summary of test methods and parameter identification computer programs to be applied in the dynamic testing of nuclear power plant structures. He discusses many practical aspects of dynamic testing of large civil engineering structures such a safety considerations, budgeting and scheduling, and extrapolation of results to higher levels of excitation. Agbabian (1980) summarizes methods of conducting steady-state and transient forced vibration tests for verification of nuclear power plant dynamic properties. This paper discusses a new method of generating simulated seismic inputs using a series of impulsive loads. A recent review of the development in methods of dynamic testing of prototype civil engineering structures (forced and ambient methods) was presented by Severn, et al. (1988), along with the application of these methods to prototype structural testing of dams and bridges. Both forced and ambient testing methodologies were developed in detail.

Gersch and Martinelli (1979) reviewed time series methods for the estimation of structural system parameters from random vibration data. They estimated resonant frequency and damping parameters of a building subjected to ambient wind excitation. A methodology was introduced for the treatment of non-stationary time series ambient vibrations. (Long duration vibration records needed for ambient vibration studies may be non-stationary). Gersch and Brotherton (1982) later developed an improved locally stationary model for the estimation of stationary structural system parameters from non-stationary random vibration data.

Methods of data reduction for determining modal characteristics (resonant frequencies, mode shapes, and damping) of structures for ambient vibrations were described in detail by Benuska, et al. (1981) in a study of a tall chimney undergoing ambient wind vibrations. Carne, et al. (1988) recently used a similar PSD/CPS method to determine modal frequencies and mode shapes of a wind-excited, vertical axis turbine. Briefly, modal parameters are extracted from FRFs calculated as the ratio of the CPS between two measured responses to the power spectrum of a designated reference response signal. Forced testing of the wind turbine using step relaxation was also performed. Luz and Wallaschek (1992) developed a method for estimating the resonant frequency and mode shapes of a structure from ambient vibration measurements when the input is assumed to be a stationary random process and applied the technique to a 12-story office building.

As can be seen from the above reviews and papers, a wealth of testing has been performed on a wide variety of civil engineering structures, such as buildings, dams, bridges, towers, chimneys, and off-shore structures. Testing generally falls into either the ambient- or forced-vibration categories, with several authors comparing results using both ambient and forced excitation techniques on the same structure. Further, a wide variety of different ambient and forced excitation methods have been used.

One unresolved issue appears to be the utility of low-level testing. For large civil engineering structures, design-level excitation often is impractical, and low-level testing is a necessary consequence. Also, there are few test programs in which large structures are reported to have been taken to failure.

B. Bridge Testing in General

Static and dynamic testing of bridges has been performed for many years for a variety of different purposes. Early deflection and vibration measurements performed on fifteen bridges loaded by a constant load truck were summarized by Oehler (1957). These tests were intended to identify the resonant frequencies of the bridge, measure their amplitude of vibration, and determine the susceptibility of these bridges to vibration. The types of bridges tested include simple-span, continuous-span, and cantilever-type construction from either steel or reinforced concrete. Many practical observations regarding vibration response were presented. Further, an early summary of dynamic testing of highway bridges in the U.S. (simple, continuous and cantilever spans) performed between 1948 and 1965 was presented by Varney (1966). The tabulation (without conclusions) was restricted to dynamic vehicular loading. Measured quantities were typically deflections and strains although a limited number of acceleration measurements were made.

Iwasaki, et al. (1972) summarized tests performed in Japan to determine the dynamic properties of bridge structures. Excitation methods included eccentric mass shakers and, in one case, a rocket engine. Resonant frequencies and damping ratios determined for individual piers and for the complete structures were summarized. Based on the results of 26 highway bridge tests performed between 1958 and 1969, an empirical relationship was established between the damping exhibited by the horizontal modes and the modal frequencies. Instrumentation of bridges for the purpose of measuring seismic response was reported along with a comparison of the response measured on one bridge during a forced vibration test and a subsequent seismic event.

A more recent summary of field and laboratory tests on bridge systems was presented by Ganga Rao (1977). The work summarized several static test programs on short span bridges that utilized various types of construction. Finally, Cantieni (1984) summarized dynamic load testing of 226 beam and slab-type highway bridges conducted in Switzerland between 1958 and 1981. This paper discussed the evolution of dynamic testing in Switzerland from the use of test vehicles and data digitized by hand to servohydraulic actuators and impact testing using modern data acquisition systems. Cantieni pointed out that dynamic testing of highway bridges was required in Switzerland between 1892 and 1913. Practical, general information, such as fundamental frequency as a function of maximum span, was presented along with information regarding damping.

Considerable recent work has been reported on the evaluation of dynamic amplification factor (also known as impact factor or impact fraction), an important parameter in the design of highway bridges. This parameter accounts for the increase in stress or deflection caused by the dynamic nature of traffic loads. O'Connor (1985) reported experimental studies on a short span steel and concrete highway bridge. Bakht and Pinjarkar (1989) presented a review of literature dealing with bridge

dynamics in general and dynamic testing of highway bridges in particular, giving special attention to impact factors, their various definitions, and factors that influence these parameters. Paultre, et al. (1992) presented an extensive recent review of dynamic amplification factor for highway bridges. Finally, a detailed analysis of the dynamic behavior of multi-girder bridges caused by vehicles moving across rough bridge decks was presented by Wang, et al. (1992), along with a favorable comparison to experimental data reported earlier. They found that road surface roughness greatly influences impact factor for bridges.

Static testing of highway bridges to failure has been reported in a few cases. Burdette and Goodpasture (1972) tested four highway bridges to failure and compared the results to analytical models and American Association of State Highway Organizations (AASHO) specifications. These specifications were found to give an adequate lower bound for the measured ultimate load capacity of the bridges. Jorgenson and Larson (1972) reported on the test of a reinforced concrete highway bridge statically loaded by hydraulic rams to collapse. Deflections and strains were measured and good comparison with design calculations was found at the load causing first permanent set and at the collapse load. More recently, McClure and West (1984) reported on the static testing of a prestressed concrete segmental bridge, incrementally loaded to failure. Results to failure were found to compare reasonably well with a finite element analysis. Finally, Scanlon and Mikhailovsky (1987) presented results on the static loading to failure on a three-span continuous reinforced concrete highway bridge. Failure loading was accomplished by a combination of weight applied at the center of the span and jacking.

Scale model testing of bridges offers obvious advantages. Green and Strevel (1977) performed a small scale model study of simple span girders (open and closed section), with particular attention placed on torsional loading. It was found that for the open simple span girder tested, the response can be predicted with available theories of mixed torsion. However, the "quasi" closed girder tested was found to have only 40% of the theoretical torsion stiffness value. Scordelis, et al. (1982) presented analytical and experimental results for a large scale skew reinforced concrete box girder bridge. The bridge was statically tested before and after the overload stress levels were induced. Breen, et al. (1987) performed static loading tests on both 1/2 scale and full size prototypes of a composite bridge design. The scale model was taken to destruction. Grace and Kennedy (1988) performed experiments on a 1/4 scale continuous composite bridge excited by a hydraulic actuator and compared results to orthotropic plate theory. For a relatively wide rectangular bridge, the torsional flexural mode of vibration was found to be important. The paper emphasized the importance of determining resonant frequencies of a bridge beyond its lowest frequency. Finally, Kennedy and Grace (1990) investigated the dynamic and fatigue response of continuous composite bridges, particularly the influence of prestressing.

The extensive use of testing in the evaluation of bridges has resulted in the American Society of Civil Engineers' (ASCE) Committee on Bridge Safety publishing a guide for field testing of bridges in 1980. This guide includes an extensive reference list of papers summarizing previous bridge tests. Also discussed are static and dynamic load application methods, instrumentation, data acquisition, and methods for measuring *in situ* material characteristics.

Other recent bridge testing includes the following:

Thoman, et al. (1984) presented an experimental analytical comparison of the static response (to vertical loading) of a prestressed concrete segmental box girder bridge. The vertical load was applied by pulling against concrete blocks on the ground below using threaded tension rods. Deflections and strains were measured. Results were compared to design analytical models. Further, Saiidi and Douglas (1984) looked at the effects of design seismic loads on a five-span reinforced concrete highway bridge. Lateral loads were applied statically using hydraulic jacks.

Lee, et al. (1987) performed static and dynamic tests on a three-span reinforced concrete bridge and compared static results with a structural analysis. The study demonstrates the importance of making appropriate assumptions regarding the boundary conditions in a bridge analysis. Further, they found that within the design load range, the moment of inertia of a reinforced concrete bridge deck can be taken as that of a plain cross section, as the effects of steel reinforcement and concrete cracking tend to compensate each other.

Finally, an assessment of existing bridge condition by static and dynamic tests and comparison with static and dynamic analytical models was presented by Kohoutek (1993). Comparisons of frequencies and mode shapes for the five-span bridge were found to be good.

Clearly, there have been a vast number of static and dynamic tests performed on a variety of different types of highway bridges covering many years, including considerable work on the evaluation of dynamic amplification factor (impact-factor). As with testing of other large civil engineering structures (see subsection A), most tests are performed at nondestructive loading levels, although a few tests on bridges have been taken to failure. Not surprisingly, scale modeling has also found extensive application for the experimental investigation of bridge structures.

C. Ambient Vibration Testing of Bridges

Ambient vibrations in bridges may be caused by traffic, wind, water waves, seismic ground motions or other environmental factors. These vibrations can be characterized in terms of the resonant frequencies, mode shapes, and damping of the lower modes of the structure.

One difficulty with determining the dynamic parameters of a structure undergoing ambient vibrations is that the forcing function is not precisely characterized, ruling out conventional FRF spectral analysis techniques, which require the measurement of the forcing function.

The first attempt at fully characterizing the dynamic parameters of a bridge undergoing ambient vibrations appears to be due to McLamore, et al. (1971), using an extension of a spectral technique developed by Crawford and Ward (1964). In this work, the recorded motion of the bridge was measured with a series of seismometers. The PSD of each recorded motion provided estimates of resonant frequencies and modal damping. Then a CPS between a reference record and the other records provided estimates of modal shapes. McLamore, et al., applied the technique to

10

obtain resonant frequencies, mode shapes, and modal damping for a number of modes determined from data measured on two suspension bridges. Modal damping was estimated by the half-power bandwidth method (HPBW) applied to resonant peaks in the PSDs. Difficulties with applying the HPBW method to ambient vibration measurements were discussed by Abdel-Gaffar and Housner (1978). In an experimental program on vehicular traffic induced vibrations of a suspension bridge, these investigators found that satisfactory estimation of damping values was not possible because of closely spaced spectral peaks and spectral overlap that resulted in widening of the peaks.

Buckland, et al. (1979) investigated both ambient and forced vibrations of an existing suspension bridge. Using accelerometers, time histories were obtained, transformed into Fourier spectra and CPS, and then analyzed to determine damping, resonant frequencies, and mode shapes. Ambient vibrations were induced by traffic and wind loading. Structural damping was measured in two ways: (1) by applying the HPBW method to the Fourier spectrum; and (2) from the decay rate for any particular frequency using forced-vibration excitation (vehicle impact caused by a truck being driven off a timber). Response of the bridge was also calculated. It was found that for vertical bridge motion, calculated and measured resonant frequencies were in reasonably good agreement. However, for torsional motion, measured values were inconsistent (either higher or lower) with those calculated. For this suspension bridge, it was found that strong coupling exists between torsion and horizontal motions. Further, the effective center of rotation can vary greatly from one vibration mode to another.

Shepherd, Brown and Wood (1979) report ambient (wind) and forced vibration testing of a three span steel truss bridge. Damping exhibited by the bridge, determined by decay in displacement measurements after excitation terminated, was low (less than 1%) and the authors attribute the perceived "liveliness" of the bridge to this low damping.

Douglas, et al. (1981) reported determining mode shapes, resonant frequencies, and modal damping for a reinforced concrete bridge and a composite girder bridge. While the primary loading is forced (in both horizontal and vertical directions - see the following subsection), ambient vibrations caused by vehicular traffic were also investigated. Mode shapes and resonant frequencies were determined from the Fourier Spectra. Damping was estimated from decay in spectral peaks determined from a moving spectral window.

Pardoen, et al. (1981) summarized an ambient vibration test on a steel truss bridge in New Zealand. Power spectra were used to identify resonant frequencies and modal amplitudes while FRFs were used to determine modal phasing information. These authors reported difficulties with ambient vibration testing. Power spectra plots showed shifts in resonant frequencies on the order of one to two times the frequency resolution of the spectra. The shifts were attributed to the discrete nature of these functions.

Gates and Smith (1982) summarized the ambient testing procedures applied to 57 highway bridges in California. Resonant frequencies and mode shapes were identified from modified FRF measurements. These authors presented detailed discussions of problems associated with ambient vibration testing. Problems that were identified included: (1) Peaks in the Fourier spectra that result from non-stationary inputs can be interpreted as resonant responses of the structure, and (2) Structural properties can change when acquiring long time windows of data.

Van Nunen and Persoon (1982), as a part of a larger study on the vibration of a cable-stayed bridge under wind loads, determined the modal characteristics of the bridge by driving a truck back and forth across its deck. Road surface irregularities were accentuated by placing wooden beams on the deck. These irregularities resulted in a random excitation of the bridge. The method used to determine the modal characteristics was, in principle, similar to those discussed above: For the excitation, which was assumed to be a stochastic random process, the (unknown) input spectrum was considered to have a constant amplitude with frequency. Therefore, the output spectrum (measured with accelerometers) was assumed to be linearly related to the input spectrum through the FRF, which contains both resonant frequency and damping information of the vibrating system. Resonant frequencies can be determined from peaks in the output spectrum and damping values can be determined by the half-power bandwidth (HPBW) method. The CPS plot between the signals from two accelerometers can then be used to determine vibration mode shape information based on the relative phase of the two signals (one signal is termed the reference signal, and the process is repeated at various stations on the bridge to map out the mode shapes).

Tanaka and Davenport (1983) investigated previously obtained accelerometer data from wind-induced response of the Golden Gate Bridge by spectral analysis . Coupling of vertical and torsion motions, and the role of wind speed on the modes which are amplified are discussed in particular. A subsequent investigation of the same bridge (new data) has been reported in a two-part paper by Abdel-Ghaffar and Scanlan (1985). They determined damping, three-dimensional mode shapes, and associated frequencies of bridge vibration induced by a combination of ambient wind, wave and traffic excitation. The methods of data reduction (14 accelerometers were used) were similar to those discussed above, that is, use of a reference station measurement to generate mode shapes and determination of damping values by the HPBW method of the Fourier spectrum peaks. Finally, White and Pardoen (1987) used ambient vibration data reported earlier to perform a modal analysis of one of the towers of the Golden Gate Bridge. The authors chose to interpret the longitudinal acceleration of the reference channel as an "excitation", so that a FRF corresponding to each accelerometer location on the structure could be calculated. Then, a least-squares curve-fitting algorithm was used to express the FRFs in rational polynomial form. Next, the least squares rational polynomials were expanded in partial fraction form. The modal parameters of frequency, damping, and mode shapes were then obtained from the poles and residues of the partial fraction expressions.

Ward (1984), with a goal of determining the physical condition of bridges with minirum inconvenience to the road user, obtained ambient vibration measurements from normal traffic passage on 18 bridges. He demonstrated that it is possible to

determine resonant frequencies and damping from traffic-generated vibrations of bridges based on a number of simple procedures. Because resonant frequencies are a direct measure of the bridges stiffness, he suggested that such determinations might form a basis for evaluating structural integrity.

Wilson (1986) reported on the response of a highway bridge to an actual strong motion earthquake, comparing results with finite element analysis. This ambient vibration problem differed from previously cited examples, as the input to the structure was rather well defined ground motion. A similar study on the response of a previously instrumented, two-span concrete bridge subjected to a strong motion earthquake was reported by Werner, et al. (1987). Despite the intense levels of shaking that were involved, classical linear models of modal response provided an excellent fit to the measured motions of the bridge. Related studies using the same two-span bridge data were subsequently reported by Levine and Scott (1989) and by Wilson and Tan (1990). Finally, ambient vibration testing of a suspension bridge anchorage subjected to both seismic motions and microtremors was presented by Higashihara, et al. (1987). These authors bring out one major difficulty with applying ambient vibration measurements: confounding of data by extraneous input sources.

A comparison of ambient and forced vibration testing methods was presented by Taskov (1988), who expanded upon the difficulties mentioned by Higashihara, et al. (1987) above regarding the effect of external sources of much higher intensity than the random noise input. He also applied the ambient vibration method to a six-span bridge.

Other recent ambient vibration studies on existing bridges are as follows:

Brownjohn, et al. (1987), Brownjohn, et al. (1989), and Kumarasena, et al. (1989) utilized traffic and wind excitations to obtain the dynamic modal characteristics of suspension bridges. Wilson and Liu (1991) also utilized wind and traffic excitations to obtain the dynamic modal characteristics of a cable-stayed bridge. Modal frequencies were identified by the locations in peaks in the power spectra and CPS (using the reference location approach described earlier). As before, mode shapes were identified using the ratios of Fourier spectral peaks at the measurement and reference locations. CPS phases were used to determine directions of relative motion. Difficulty was had in determining damping ratios, because the small-valued damping ratios were very sensitive to the non-stationary nature of the ambient vibrations and other parameters.

Muria-Vila. et al. (1991) experimentally determined frequencies and mode shapes for a 3-span cable-stayed bridge based on traffic and wind induced excitations. Forced "step-relaxation" tests were also performed. Resulting frequency values were in good agreement with those from ambient excitation.

Kussmaul, et al. (1992) applied the ambient vibration testing methods developed by Luz and Wallaschek (see previous discussion in II. A.) to a 9 span prestressed concrete bridge. Analytical results compared well with those measured during the ambient vibration tests.

Finally, Brownjohn, et al. (1992) reported on an ambient vibration (wind and traffic excitation) study of a suspension bridge, providing resonant frequencies, mode shapes, and damping ratios. Data processing techniques were similar to those reported above. Frequencies and damping ratios were determined by fitting the best curve (in the least squares sense) representing the response of a single degree of freedom oscillator to the power spectra from individual acceleration measurements in the region of a resonance. The authors again pointed out errors implicit in the random vibration method: the assumption of a random input with a flat power spectrum.

Summarizing, it is seen that ambient vibrations in bridges can be induced by a wide variety of different environmental factors, such as traffic, wind, water waves, and seismic ground motions. With the possible exception of strong earthquake ground motions, the forcing function is not precisely characterized, ruling out conventional FRF analysis techniques for determining resonant frequencies, mode shapes and damping of the structure. However, spectral techniques have been developed, as summarized by Bendat and Piersol (1980), for system identification based only upon response measurements. The methods require assumptions regarding the spectral content of the unknown input signal (a random process, which traffic excitation on bridges may approximate). Such ambient vibration methods have been used for characterization of the modal properties of a number of highway bridges since the 1970's. Table I summarizes the ambient vibration tests that have been reviewed including the type of excitation and analysis methods employed to extract the structures' dynamic properties from the measured response.

Table I					
Summary of Ambient Vibration Testing on Highway Bridges					
			Parameter I.D. Method		
Investigator/location/ structure	Year	Excitation	Frequency	Mode Shapes	Damping
Mclamore, Hart, Stubbs Newport Bridge, RI 3 Span Suspension William Preston Lane Memorial Bridge, MD 3 Span Suspension	1971	traffic	PSD	CPS	HPBW-PSD
Abdel-Gaffar, Housner Vincent-Thomas Bridge, CA 3 Span Suspension	1978	traffic	FS	FS	HPBW-FS

Table I *continued*

Buckland, et al. Lions' Gate Bridge, Vancouver, BC 3 Span Suspension	1979	traffic wind	FS	CPS	HPBW-FS
Shepherd, et al. Mohaka River Bridge, New Zealand 3 Span steel truss	1979	wind	Method not described	Method not described	Method not described
Pardoen, et al. Toe Toe Stream Bridge, New Zealand Single span steel truss	1981	method not described	PS	PS	N/A
Douglas, Brown, Gordon Deeth Railroad Overpass, NV 3 Span skewed composite girder bridge	1981	traffic	FS	FS	Decay of moving FS amplitudes
Gates and Smith 57 Highway Bridges, CA	1982	traffic	FS	FRF	N/A
Van Nunen, Persoon Wall River Bridge, Netherlands Cable stayed steel box girder	1982	traffic	PSD	CPS	HPBW-FS
Tanaka, Davenport Golden Gate, CA 3 Span suspension	1983	wind	PS	N/A	HPBW
Ward Numerous highway bridges mostly 1-4 spans	1984	traffic	PSD	N/A	Auto- correlation function Analysis (decay rate)

Table I *continued*

Abdel-Gaffar, Scanlan Golden Gate Bridge, CA 3 Span suspension	1985	traffic, wind, and wave	FS	FS	HPBW-FS
Wilson San Juan Bautista Separation Bridge, CA 6 Span steel girder composite	1986	seismic, 0.12 PGA	Time Domain Least Squares Curve Fitting	N/A	Time Domain Least Squares Curve Fitting
Brownjohn, Dumanoglu, Severn, Taylor Humber Bridge 3 Span suspension	1987	wind and traffic	Least squares CF to PS	Amplitude from PS peaks, Phase from FRF	Least squares CF to PS
Higashihara, Moriya, Tajima South Bisen-Seto Bridge Japan 3 Span suspension	1987	seismic	PSD	N/A	N/A
Werner, Beck, Levine Meloland Road Overpass, CA 2 Span concrete box girder bridge	1987	seismic	Time Domain Least Squares Curve Fitting	N/A	Time Domain Least Squares Curve Fitting
White, Pardoen Golden Gate Bridge, CA 3 Span suspension	1987	traffic, wind, and wave simult.	FRF curve fitting	FRF curve fitting	FRF curve fitting
Taskov Spiljie Lake, Yugoslavia, 6 Span steel girder	1988	wind	FS	FS	N/A

16

Table 1 *continued*

Levine, Scott Meloland Road Overpass, CA 2 Span concrete box girder bridge	1989	seismic	Time Domain Least Squares Curve Fitting	N/A	Time Domain Least Squares Curve Fitting
Brownjohn, Dumanoglu, Severn, Blakeborough Bogazici Bridge, Turkey, 3 span suspension	1989	wind, and traffic	PS CF	FRF	PS, CF
Kumarasena, Scanlan, Morris Dear Isle Bridge, ME 3 Span suspension	1989	wind	PSD	Amplitude from area under PSD Peak, Phase from CPS	N/A
Wilson, Tan Meloland Road Overpass, CA 2 Span concrete box girder bridge	1990	seismic	Time Domain Least Squares Curve Fitting	N/A	Time Domain Least Squares Curve Fitting
Wilson, Liu Quincy Bayview Bridge, IL 2 Span cable stayed	1991	wind, and traffic	PS	Amplitude from FS, Phase from CPS	HPBW
Muria-Vila, Gomez, King Tampico Bridge, Mexico 5 Span cable stayed	1991	wind, and traffic	PS	PS	N/A
Brownjohn, Dumanoglu, and Severn Fatih Sultan Mehmet Bridge, Turkey 3 Span suspension	1992	wind, and traffic	PS CF	FRF	PS CF

Table I *continued*

Kussmaul, et al. Kocher Bridge, Germany 9 Span concrete box girder bridge	1992	method not described	PSD	PSD	N/A

CF - Curve Fit
CPS - Cross-power Spectrum
FS - Fourier Spectrum
HPBW - Half power Bandwidth
PS-Power Spectrum
PSD -Power Spectral Density

D. Forced Vibration Testing of Bridges

The determination of the modal characteristics (resonant frequencies, mode shapes, and modal damping ratios) of structures subjected to forced vibrations is well-established, e.g., Ewins (1985), particularly when the input forcing function is well-characterized. In the forced vibration testing of bridges, a wide variety of forcing techniques are used including variable frequency rotating dynamic shakers of various types, servo-hydraulic inertial actuators, step-relaxation, instrumented impact hammer, and controlled truck loading (this type of loading typically does not allow the input to be accurately measured).

Shepherd and Charleson (1971) determined resonant frequencies and damping for a multi-span continuous deck bridge at various stages of bridge construction using an eccentric mass shaker. Shepherd and Sidwell (1973) tested five concrete bridges by applying a steady state excitation and by driving a test vehicle over the bridge. Measured dynamic properties were compared to those determined analytically. The authors found that the analytical models accurately predicted the measured resonant frequencies of the bridges. Damping values associated with the horizontal mode were found to be significantly higher than those associated with the vertical modes. This increased damping was attributed to soil-structure interaction effects.

Kuribayashi and Iwasaki (1973) determined modal characteristics on 30 highway bridges when subjected to transverse harmonic excitation also using an eccentric mass shaker. Leonard (1974) described excitation techniques and instrumentation used in full scale highway bridge dynamic tests. He later demonstrated some of the techniques on eight composite, box girder bridges, obtaining resonant frequencies, mode shapes and, particularly, damping (Leonard and Eyre, 1975).

In one of the first investigations involving the transverse dynamic behavior of bridges, Douglas (1976) performed step-relaxation tests on a six-span continuous composite girder access ramp bridge. Resonant frequencies and mode shapes were determined from peaks in the Fourier spectrum. Modal damping values were calculated from the decay of spectral peaks from a moving Fourier spectrum. This method showed how the damping changes with the amplitude of response. Later,

Douglas and Reid (1982) reported on dynamic tests of a five-span reinforced concrete box girder bridge[1]. Transverse excitation was again accomplished using the step-relaxation method. Transverse mode shapes and resonant frequencies were obtained and used in conjunction with a system identification procedure introduced by the authors to obtain further information on the dynamic characteristics of the structure as well as the soil-structure interaction process.

Dorton, et al. (1979) reported dynamic tests using a test vehicle to generate the input. Information concerning the methods used to calculate the dynamic properties of the structure are not given.

Billing (1984) reported on testing of 27 bridges of various construction types (steel, timber and concrete) over a wide range in length. Accelerometer responses were used to determine the first few resonant frequencies, damping ratios, and mode shapes. Excitation was accomplished using special test vehicles driven in a closely controlled manner. The work was motivated by the need to verify dynamic load provisions for a highway bridge design code.

Radkowski, et al. (1984) performed a very similar study using test vehicles at various speeds to excite a plate girder bridge. Four vibration modes with damping ratios were determined: The first three (longitudinal flexural) modes compared well with an analytical beam model. However, no comparisons with the fourth mode (torsional) were presented.

Richardson and Douglas (1987) investigated the dynamic response of a reinforced concrete highway bridge vertically loaded by hydraulic jacks with quick-release mechanisms. The authors measured three translational and two rotational acceleration components and presented results in the form of a power spectral density "surface" which provides an overall view of the frequency response of the bridge deck. A second contribution of the paper was the development and illustration of a method for separating closely spaced modes in free vibration data.

Using harmonic forced vibration excitations, Crouse, et al. (1987) investigated the dynamic response of a single-span, prestressed concrete bridge (resonant frequencies, modal damping, and mode shapes). The forced excitation was in both transverse and longitudinal directions. Emphasis in the paper was on soil-structure interactions. Reasonable agreement with a three-dimensional finite element model of the bridge was obtained, with soil-structure interaction modeled using Winkler springs attached to the footings and abutment walls.

In an investigation very similar to the present I-40 Bridge investigation, Miller, et al. (1992) performed field tests on a three-span reinforced concrete slab bridge. The overall purpose of the work was to evaluate the strength deterioration of damaged bridges. Using an impact hammer, mode shapes were determined and compared with those from theoretical models to find damage to the shoulders of the bridge. It is notable that the damage was hidden by a layer of asphalt. This result is of concern

---

[1] Lateral behavior of bridges has direct application to earthquake loading. At least in the U.S., strong seismic loading was not recognized as a major threat to highway bridges until the 1971 San Fernando Earthquake in Southern California (Crouse, et al., 1987).

because the American Association of State Highway and Transportation Organizations (AASHTO) uses capacity reduction factors based largely on visual inspection. This paper represents an attempt to quantify the bridge deterioration process. Following nondestructive testing, the bridge was taken to failure, resulting in an unexpected failure mode, but providing information on bridge failure mechanisms.

Recently, Filiatrault, et al. (1993) have reported on modal testing and analysis of an earthquake damaged, cable-stayed bridge. Testing was performed using dynamic excitation provided by a heavy test truck which crossed the bridge at constant speed. Braking tests using the same truck were also performed to excite higher bridge modes. System identification was accomplished using the "reference station" approach discussed in the previous Ambient Vibration Subsection. Comparisons of resonant frequencies with a finite element numerical model using three-dimensional beam elements were good. The comparisons included two torsional modes. An equivalent section approach was used with the beam elements for axial and bending stiffness. Details on the treatment of torsional stiffness were not presented explicitly. Difficulties in obtaining estimates of damping from field vibration data were discussed.

Green and Cebon (1993) presented a modal testing program for a 4-span continuous bridge of prestressed concrete box girder construction. Testing was performed using an instrumented hammer. Dynamic parameters were estimated from curve fitting analytical expressions to the measured frequency response functions. Resonant frequencies, damping ratios and mode shapes were found to be in good agreement with predictions of a simple mathematical model of the bridge. Similar impact tests that have been reported include those done by Lee, et al. (1987), Raghavendrachar and Aktan (1992), and Kohoutek (1993).

Finally, Cantieni and Pietrzko (1993), reported the modal testing of a wooden footbridge using a randomly driven servo-hydraulic shaker. Measurement of response with accelerometers was performed at 77 points on the bridge in three directions. Modal parameters were estimated for this single input test using conventional time-domain curve-fitting methods that analyze an impulse response function.

In addition to the forced vibration studies listed above, a number of references discussed in the previous subsection on ambient vibration testing also contained forced vibration studies as well, with comparison of results (i.e., mode shapes, frequencies, and modal damping) obtained from forced and ambient vibration. In particular, Buckland, et al. (1979) used two types of forced excitations for suspension bridge excitation (weighted pendulum swinging with varying pendulum length; vehicle impact) in addition to traffic- and wind-excited ambient vibrations discussed earlier. Unfortunately, the authors did not present explicit detailed comparisons of results obtained from forced and from ambient vibration excitation.

Shepherd, Brown, and Wood (1979) used a counter-rotating-eccentric-mass shaker to investigate the dynamic response of the previously discussed Mohaka River Bridge. The shaker provided a 50 kN force at 3 Hz. However, the bridge was found to have modes below 3 Hz. Details of the methods to estimate modal parameters were not given.

In the previously cited study by Douglas, et al. (1981), two bridges were tested dynamically, one of which was subjected to a combination of forced and ambient loading (transverse forced dynamic excitations by step-relaxation; vertical ambient excitation by normal vehicular truck traffic). However, again no explicit comparisons of forced versus ambient vibration results were presented.

Taskov (1988), also previously cited in the ambient vibration subsection, determined the dynamic characteristics (resonant frequencies, mode shapes, and modal damping) in both the transverse and longitudinal directions for the forced harmonic excitations of an 8-span prestressed concrete bridge. Forced harmonic excitations over a frequency range were excited using two electromechanical vibration generators. While he reported that forced vibration testing is less prone to error, he made no direct comparisons with the ambient vibration results on another bridge cited earlier.

Finally, Muria-Vila, et al. (1991), also cited earlier, found frequencies obtained from step-relaxation tests of a cable-stayed bridge to be in good agreement with ambient (traffic and wind) tests.

Summarizing, it appears that a large number of forced vibration tests have been performed on various types of bridges to determine modal properties (resonant frequencies, mode shapes, and modal damping). Forcing methods include variable-frequency eccentric-mass shakers, step-relaxation tests, instrumented impact hammer, and controlled truck loading. In cases for which the input is not well-defined, techniques of signal analysis similar to those discussed in II. C., Ambient Vibration Testing of Bridges, are utilized. Comparisons of modal properties of the structure determined by both forced and ambient techniques appears somewhat lacking. The need for additional comparisons is apparent. Table II lists some of the characteristics of the forced vibration tests that have been reviewed.

Table II					
Summary of Forced Vibration Testing on Highway Bridges					
			Parameter I.D. Method		
Investigator/location/structure	Year	Excitation	Frequency	Mode Shapes	Damping
Oehler 15 Highway bridges, Michigan 1-5 Spans, Concrete or Steel	1957	Test Vehicle	Free vibration decay	N/A	N/A

Table II *continued*

Shepherd and Charleson Waiau River Bridge New Zealand 6 Spans, prestressed concrete girder	1971	rotating disc dynamic shaker, (swept sine)	Spectrum generated from swept sine test	N/A	HPBW
Kuribayashi, Iwasaki 30 highway bridges from 1958 - 1969 Japan	1973	transverse force from centrifugal type shaker (swept sine?)	Details not provided	Details not provided	Details not provided
Shepherd and Sidwell 5 Prestressed and reinforced concrete bridges, New Zealand	1973	rotating disc dynamic shaker, (swept sine)	Spectrum generated from swept sine test	N/A	HPBW
Leonard, Eyre 8 Steel box girder bridges, England 1-5 spans	1975	swept sine using inertial excitation system,	Spectrum from swept sine test	FRF	log decrement
Douglas 6 Span composite girder access ramp, NV	1976	step-relaxation using cable and tractor	FS	FS	decay in amplitudes from moving FS
Dorton, Holowka, King Conestogo River Bridge, Canada 3 Span composite girder bridge	1977	test vehicle	Details not provided	Details not provided	Details not provided
Shepherd, Brown, and Wood Mohaka River Bridge, New Zealand 3 Span steel truss	1979	rotating disc dynamic shaker, (swept sine)	Details not provided	Details not provided	Details not provided

Table II *continued*

Douglas, Reid Ross Creak Interchange, NV **5 Span reinforced** concrete box girder	1982	step-relaxation using cable and tractor	FS	FS	N/A
Cantieni 226 beam and slab concrete bridges in Switzerland	1958 - 1981	test vehicle, servo hydraulic actuator, impact with hammer	Free Vibration Decay, PSD	Details not provided	Log decrement
Billings 27 steel, timber, and concrete highway bridges, 1-5 spans, Canada	1984	test vehicle	PSD	Details not provided	Log decrement
Radkowski, Bakht, Billings Madawaska River Bridge Canada 3 Span plate girder	1984	test Vehicle	Details not provided	Details not provided	Details not provided
Richardson, Douglas Dominion Road Bridge New Zealand 10 span curved prestressed concrete box girder bridge	1987	step-relaxation using hydraulic jacks	PSD	FS	Details not provided
Crouse, Hushmand, Martin Horsethief Road Undercrossing, CA, 1 Span prestressed concrete box girder ,	1987	eccentric mass shaker	Sine sweep spectra data	Sine sweep spectra data	HPBW - Sine sweep spectra data

Table II *continued*

Lee, Ho, Chung Hong Kong 3 Span concrete girder	1987	impact hammer, test vehicle	Vibration decay	N/A	N/A
Taskov Spiljie Lake, Yugoslavia 6 Span steel girder	1988	harmonic excitation from electro-mechanical shaker	FS	Details not provided	Details not provided
Muria-Vila, Gomez, King Tampico Bridge, Mexico 5 Span cable stayed	1991	test vehicle, step-relaxation	PS	PS	N/A
Miller, Aktan, Shahrooz 3 Span reinforced concrete slab bridge	1992	impact with instrumented hammer	FRF curve fitting	FRF curve fitting	FRF curve fitting
Raghavendrachar, Aktan 3 Span reinforced concrete slab bridge	1992	impact with instrumented hammer	FRF curve fitting	FRF curve fitting	FRF curve fitting
Filiatrault, Felber Shipshaw Bridge, Canada 2 Span cable stayed, steel box girder	1993	test vehicle	FS	Amplitude from FS, Phase from CPS	N/A
Kohoutek Talbragar River Bridge Australia 5 Span truss and girder bridge	1993	Impact	FRF curve fitting	FRF curve fitting	FRF curve fitting

Table II *continued*

Green, Cebon Drift Road Bridge, England, 4 Span prestressed concrete box girder Lodden River, England 3 span Prestressed Concrete Girder Bridge	1993	impact with instrumented hammer	FRF circle curve fitting	FRF circle curve fitting	FRF circle curve fitting
Cantieni, Pietrzko Wimmis Pedestrian Bridge, Switzerland 3 Span wooden girder bridge	1993	random input from servo-hydraulic shaker	Least square complex exponential curve fitting	Least square complex exponential curve fitting	Least square complex exponential curve fitting
CPS - Cross-power Spectrum FS - Fourier Spectrum HPBW - Half power Bandwidth PS-Power Spectrum PSD -Power Spectral Density					

E. Damage Detection In Bridges

An extensive, recent survey of bridge failures in the United States since 1950 is presented by Shirole and Holt (1991). These authors point out that recent responses of engineers to bridge failures have been reactive. Bridge design modifications and inspection program changes are often made in response to catastrophic failures. The collapse of the Tacoma Narrows Bridge a half century ago is, of course, classic and has led to the inspection and modification of other suspension bridges. The widespread introduction of systematic bridge inspection programs was directly attributed by Shirole and Holt to the catastrophic bridge collapse at Point Pleasant, WV, in 1967[2]. As pointed out earlier in this literature survey, design modifications for seismic response of bridges have been made as a direct consequence of the 1971 San Fernando Earthquake (Gates, 1976)

At present, bridges are generally rated and monitored during biennial inspections, largely using visual inspection techniques. There is the possibility that damage could go undetected at inspection or that growth of cracks in load-carrying members to critical levels, for instance, could occur between inspection intervals (e.g. see Gorlov, 1984). Sudden damage leading to bridge collapse also occurs due to collision, as evidenced by the recent AMTRAK railroad bridge collapse in the Southeastern US in 1993 involving collision of the bridge by a barge. (According to

---

[2] Details of current bridge inspection techniques are given by White, et al. (1992).

statistics presented by Shirole and Holt, more than 13% of identified failures of US bridges since 1950 are attributed to collision).

Based on the above, a quantitative, possibly continuous, mechanism of bridge damage detection may be appropriate for certain types of bridges, i.e., those with non-redundant structural members. As well, use of an active damage detection system may be indicated in some cases; i.e., such a system could detect sudden significant damage to the bridge structure due to collision and trigger a system to close the bridge to traffic.

Damage or fault detection in structures by the use of experimental modal data is a subject which has received considerable recent attention in the literature. The basic idea is that modal parameters, notably frequencies, mode shapes, and modal damping, are a function of the physical properties of the structure (mass, damping, and stiffness). The modal parameters can be interpreted as solutions to the governing equations of motion of the structure, written in terms of the structure's physical properties. Therefore, changes in physical properties of the structure, such as its stiffness, will cause changes in the modal properties. The numerous modal methods for detecting damage or changes in a structure that have been developed primarily over the past 15 years differ only in the techniques used to detect and quantify changes in the modal response and the method for relating such changes to physical damage in the structure.

A detailed survey of the technical literature and interviews of selected experts to determine the state-of-the-art of the damage detection field (using such modal changes) as of 1979 was presented by Richardson (1980). The survey focused on structural integrity monitoring for nuclear power plants, large structures, rotating machinery and offshore platforms, with by far the largest amount of literature associated with rotating machinery. The author stated that while monitoring of overall vibration levels for rotating machinery had become commonplace, attempts at relating structural damage to measured modal changes was still in its primitive stages. While modal testing of suspension bridges is discussed, the work was for system identification (i.e., determination of mode shapes, modal damping and resonant frequencies) and not specifically directed at damage determination.

Since 1979, numerous studies involving the development and application of damage detection techniques have been reported for bridge structures. Salane, et al. (1981) use changes in dynamic properties of a 3-span highway bridge during a fatigue test as a possible means of detecting structural deterioration due to fatigue cracks in the bridge girders. The authors found that changes in bridge stiffness and vibration signatures (mechanical impedance plots) are indicators of structural deterioration caused by fatigue. Stiffness coefficients were calculated from experimentally determined mode shapes. Excitation was by electrohydraulic actuator.

Kato and Shimada (1986) performed vibration measurements on an existing prestressed concrete bridge during a test to failure. A reduction in natural frequencies could be detected as a statically applied load approached the ultimate load. Damping values were little affected, however. The ambient vibration method of system identification was used.

Turner and Pretlove (1988) performed a numerical analysis of the vibration response of a simple beam representation of a bridge subjected to random traffic loading. The authors suggested that measurement of the response of a bridge to traffic appeared to provide a method of determining resonant frequencies. These frequencies could then be monitored: a 5% change would indicate significant damage. The motivation of the work was to develop a structural condition monitoring system without a measured source of vibrations.

Sanders, et al. (1989), presented a method, also based on the measurement of modal parameters, to detect not only the extent, but the location of damage in structures as well. The work was based on the use of modal sensitivity equations and is applied to fiber-reinforced composite beams.

Biswas, et al. (1990) discussed the state of degradation of bridges in the U.S., emphasizing that the current, 24-month inspection interval for highway bridges has two major drawbacks: Bridge failure could occur between inspection intervals; and incipient failures may go unnoticed during inspection. They performed modal testing on a 2-span continuous composite bridge in undamaged and "damaged" condition. "Damage" consisted of a large fatigue crack simulated by unfastening a set of bolts at a steel girder splice connection. Changes in frequency response functions obtained by using a shaker were found to be detectable and quantifiable. Modal frequencies showed small but consistent drops due to the presence of the simulated crack.

In related work by the same authors (Samman, et al., 1991), a scale model of a typical highway bridge was used to investigate the change in FRF signals caused by the development of girder cracks. The authors used a procedure from the field of pattern recognition to accentuate the differences in the FRF's between cracked and uncracked bridges. The method also provided some crack location information.

Spyrakos, et al. (1990) performed an experimental program on test beams which were designed to respond in a dynamically similar fashion to actual bridges. Each beam was given different damage scenarios (type, location, degree), on which low-level free vibration tests were performed. The authors found a definite correlation between level of damage and dynamic characteristics of the structure. It was found that frequency change may be insufficient to be a useful indicator of structural safety (less than 5% change in frequency was associated with "critical" damage). However, the study suggests that the method may be applicable to more severely damaged structures, giving an indication of remaining serviceability.

Ismail, et al. (1990) investigated the effect of fatigue crack closure on the frequency changes of cracked cantilever beams. Based upon a combined experimental-numerical program, the authors conclude that the drop in resonant frequencies, especially for the higher modes, is an insufficient measure of crack severity when considered alone. The reliability of the vibration testing method for detecting the presence and nature of the crack was, however, demonstrated.

Mazurek and DeWolf (1990) again presented strong arguments for the need of a continuous automated vibration monitoring system for highway bridges, citing several unexpected collapses and near collapses of bridges (the collapse of one Rhode Island

bridge was prevented when a passerby observed severe cracking of a primary girder at mid span). In their experimental study of a bridge monitoring technique, the authors performed laboratory model tests on a 2-span aluminum plate-girder bridge, with vibrations induced by vehicular excitation. The authors found that major structural degradation can cause significant changes to both resonant frequencies and mode shapes. The greatest changes in mode shapes occur in the vicinity of the structural defect (e.g., crack). Therefore, once it is determined that a structural defect is present, mode shapes could be used for detection of the defect location.

Jain (1991), also using modal methods, investigated the performance characteristics of a continuously deteriorating railway bridge using as excitation a locomotive run at constant speed. Jain concluded that modal parameters, particularly frequencies and mode shapes, can furnish only general information on the damage state of the structure: deviation indicates that damage has occurred, but not its local extent or underlying cause.

Tang and Leu (1991) performed experiments on a defective prestressed concrete girder bridge. They found that mode shape changes may be a more effective indicator for damage detection in bridges than frequency shifts (for damage detection, they state a frequency shift on the order of 0.01 Hz must be detectable). Bridge excitation was accomplished by the step relaxation method.

Raghavendrachar and Aktan (1992) performed impact testing on a 3-span reinforced concrete bridge with a goal of detecting local or obscure damage, as opposed to severe, global damage. The authors concluded that modal parameters may not be reliable as damage indicators if only the first few modes are determined. For this type of damage, modal information for higher modes would be required.

Finally, an extensive survey and analysis of structural damage detection has just been completed by Kim and Stubbs (1993) as part of this overall bridge project. The authors assessed the relative impact of model uncertainty on the accuracy of nondestructive damage detection in structures. The authors applied their approach to a plate-girder bridge and a 3-dimensional truss-type bridge.

Summarizing, it appears that over the past fifteen years there has been repeated application of the use of modal properties of bridges to the fields of damage detection and structural monitoring, much of the work having been motivated by several catastrophic bridge failures. Earlier work utilized primarily modal frequency changes to detect damage, but others have lately shown that frequency changes are insufficient, and that changes in mode shapes are more sensitive indicators and might be useful for detection of the defect location as well. Damping changes have not been found useful for damage detection in bridges. Finally, other more sensitive methods of examining modal properties for damage are being developed (e.g., using pattern recognition to accentuate changes in FRFs measured on cracked and uncracked bridges).

III. EXPERIMENTS

A. Testing of the New Mexico State University Laboratory Bridge

Before tests were done on the I-40 Bridge, scientists from P-10 made preliminary measurements on a concrete bridge structure in a laboratory at NMSU. The purpose of the measurements was twofold, first it provided data on the resonant frequencies of the structure. This information was used to improve numerical models of the test structure being developed at NMSU. Second, these measurements provided a "test bed" for studying very low frequency transducers and data acquisition systems prior to actual testing of the I-40 Bridge.

The bridge is a 25 ft by 11 ft rectangular reinforced concrete slab, approximately 8" thick. The slab is supported by two prestressed concrete I-beams located under the long sides of the slab. Measurements on the concrete structure were made on March 30th and 31st, 1993. Further measurements were made on the surrounding steel structure on May 3rd, 1993.

The data acquisition equipment, diagrammed in Fig. 2, was set up in a low frequency homodyne detection mode. A dual programmable signal generator provided a sine wave source at a given frequency, ω, to a Crown, model PSR-2, 250W amplifier, which drove an electrodynamic shaker. This source is designated $A\sin(\omega t)$. The shaker (APS Dynamics Inc. model 120S, 75 lb. peak force) was placed at one corner of the slab (Fig. 3) and loaded with 70 lb. of steel weights. Vibrations were detected at other points on the slab by various accelerometers and a microwave interferometer, the output of which is amplified and fed into a mixer. For a linear system subjected to a harmonic excitation, the output will be at the same frequency as the input, but with different amplitude and phase. The output signal is designated $B\sin(\omega t+\phi)$. The same signal that was used to drive the shaker was also fed into the mixer along with a similar signal shifted 90 degrees in phase, which is designated $A\cos(\omega t)$. The homodyne mixer multiplies the output signal from the accelerometer by the two signals, $A\sin(\omega t)$ and $A\cos(\omega t)$, yielding (after some trigonometric manipulation)

$$0.5AB\cos(\phi)-0.5AB\cos(2\omega t+\phi), \text{ and} \tag{6}$$

$$0.5AB\sin(\phi)+0.5AB\sin(2\omega t+\phi), \text{ respectively.} \tag{7}$$

These signals are composed of a DC component represented by the first term in each equation, and an AC component that has a frequency of 2ω. Numerous time averages are taken causing the AC terms in Eqs. 6 and 7 to go to zero. The remaining DC components in Eqs. 6 and 7 are squared (to remove the phase angle dependence) and added yielding

$$0.25A^2B^2(\cos^2(\phi)+\sin^2(\phi))=0.25A^2B^2. \tag{8}$$

Because the amplitude of the source signal, A, is known, the amplitude of the response, B, can be extracted. The computer then steps to the next frequency, recording and plotting the response amplitude values as a function of the excitation (and response) frequency. The advantage of this method over conventional modal testing, which typically uses broad-band excitation from a shaker or impulse input, is

30
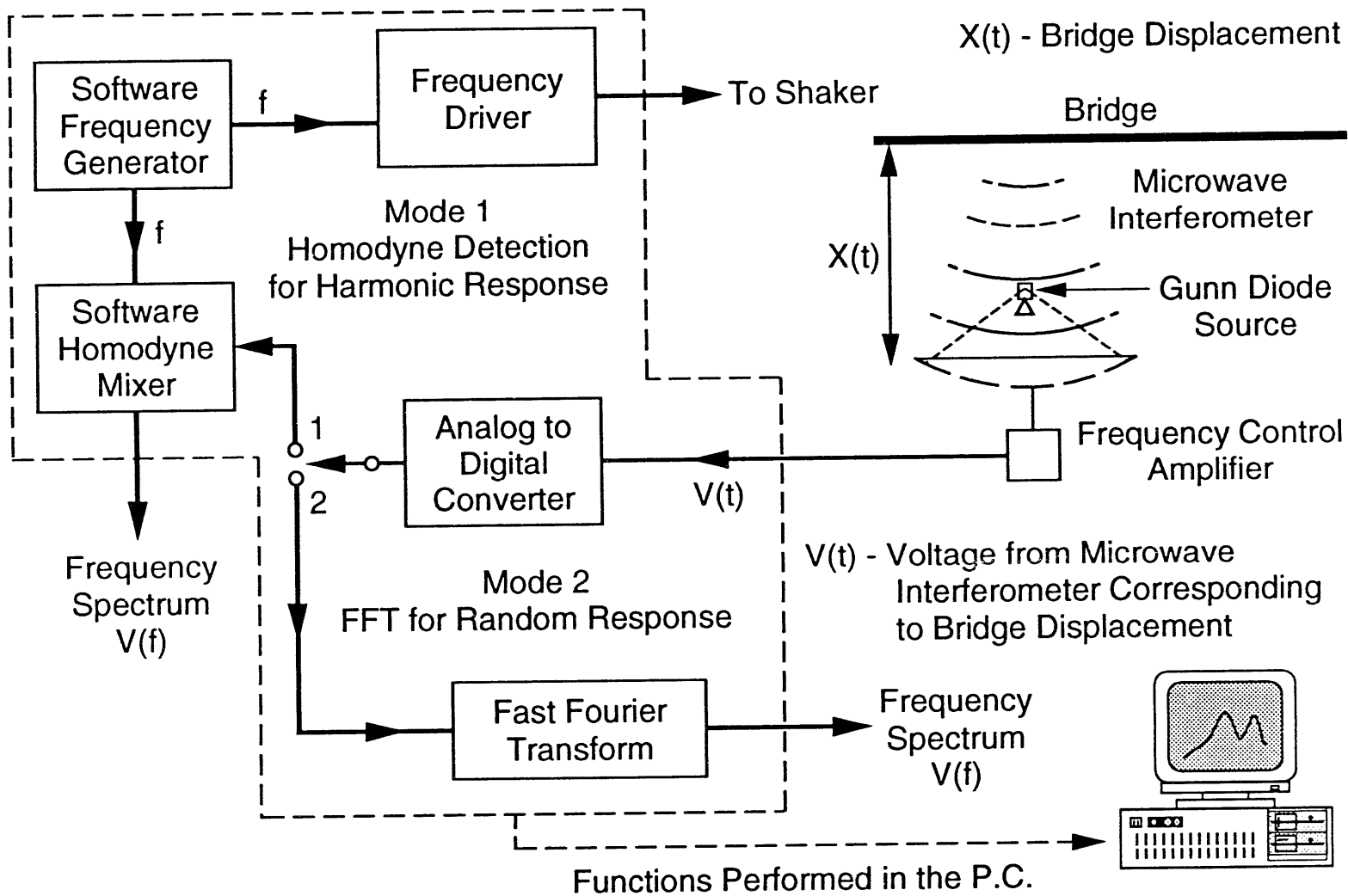
Fig. 2. Data acquisition system used on preliminary tests at NMSU.

NMSU Laboratory Bridge Deck
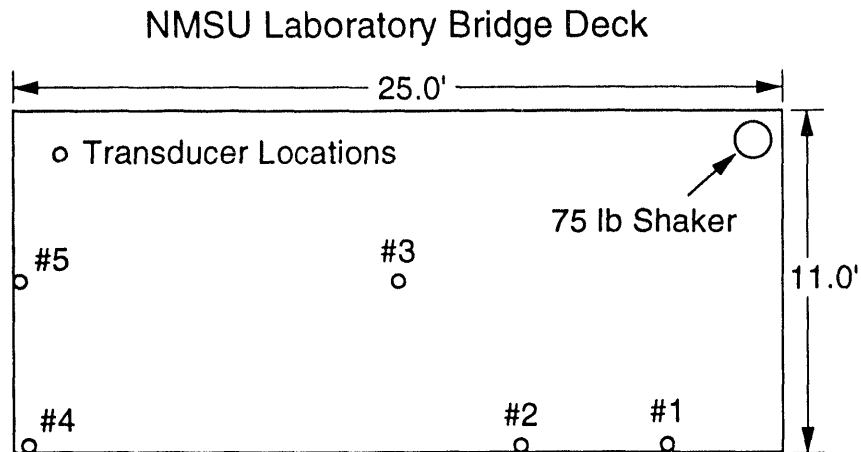
Fig. 3. Measurements and excitation locations for preliminary tests at NMSU.

that all the excitation energy is put in at a specified frequency thus identifying modes other than the predominant ones.

Five different transducers were tested including a magnetic borehole accelerometer, Model L-4 Seismometer from Mark Products, Inc., with a resonant frequency of 1 Hz. This is a large spring and mass sensor with a mass of nearly a kilogram. Also tested were an experimental cantilevered-arm bimorph piezoelectric accelerometer (a metallic conducting strip sandwiched between two thin layers of piezoelectric material), a small higher frequency piezoelectric transducer, and a 24.125 GHz Gunn diode microwave source, configured as an interferometer to detect absolute displacement. These transducers were tested at the points labeled 1-5 on Fig. 3. In all cases, the transducers were oriented such that they were primarily sensitive to vertical motion of the slab.

The vibrations of the slab were detected by all of the transducers. A spectrum from each of the transducers are plotted in Figs. 4 - 8. The lowest detected resonance was at 14 Hz and there were other resonances identified at 20, 25, 41, and 53 Hz (as well as others) which reproduced on nearly every scan. Most of the significant resonances were easily heard or felt. These identified frequencies can be used as parameters to verify the numerical models of the test structure being developed by NMSU. The microwave setup, which had a 26-in. (round trip) cavity with an aluminum plate at position 4 in Fig. 3, gave a flat response compared to the generally rising sensitivity of the piezoelectric sensors, indicating that this type of sensor would be most appropriate for the actual bridge tests.

B. Description of the I-40 Bridge

The existing I-40 bridge over the Rio Grande consists of twin spans (there are separate bridges for each traffic direction) made up of a concrete deck supported by two welded-steel plate girders and three steel stringers. Although plans for the bridge
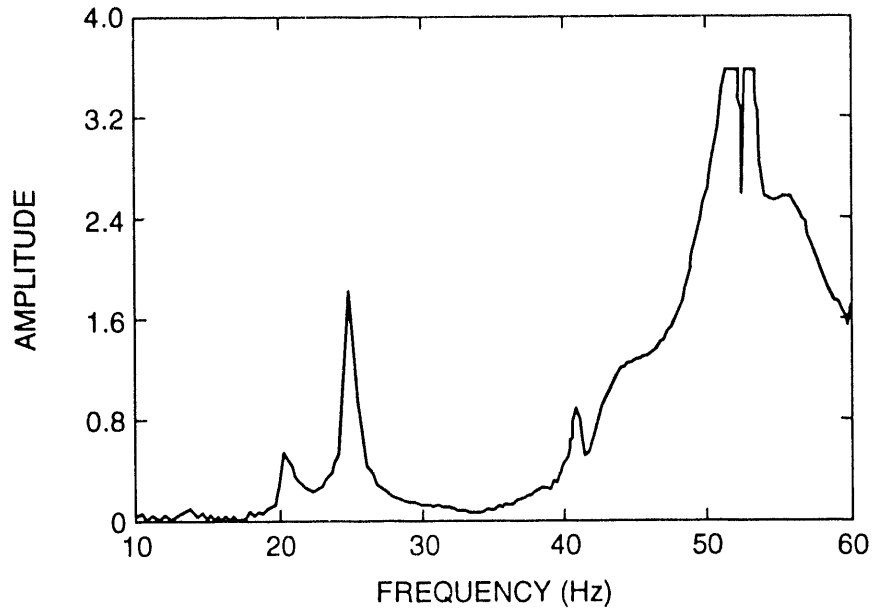
Fig. 4. Displacement spectrum measured on the NMSU laboratory bridge at location 5 using the large piezoelectric transducer
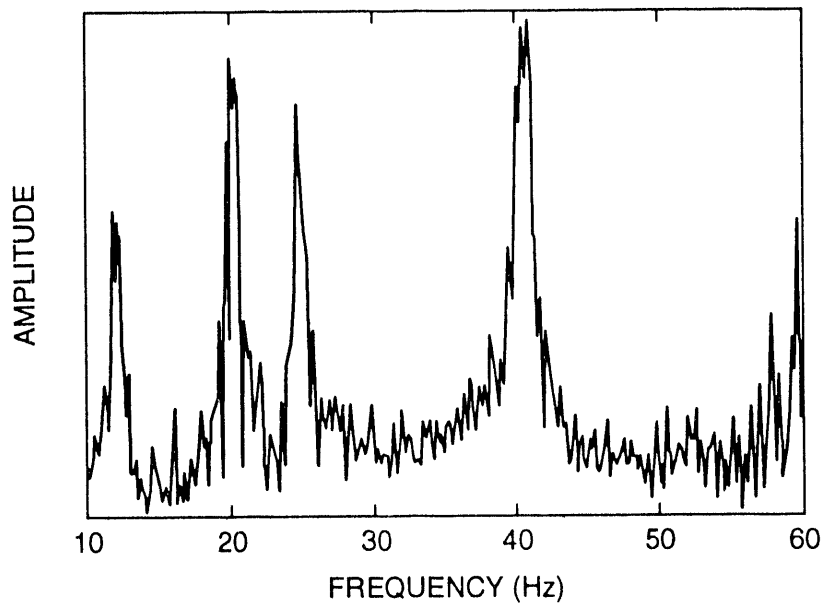
Fig. 5. Displacement spectrum measured on the NMSU laboratory bridge at location 3 using the spring-mass transducer.

32
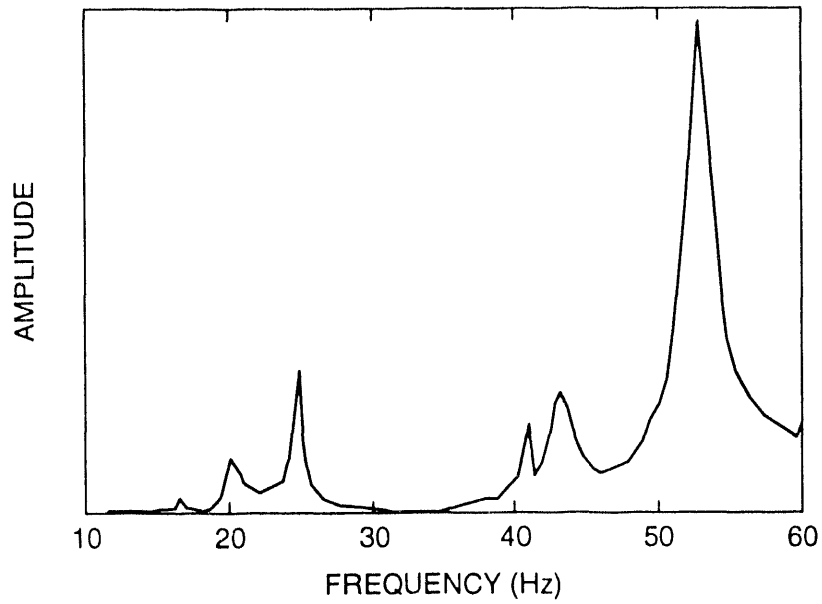
Fig. 6. Displacement spectrum measured on the NMSU laboratory bridge at location 4 using the piezoelectric cantilevered transducer.
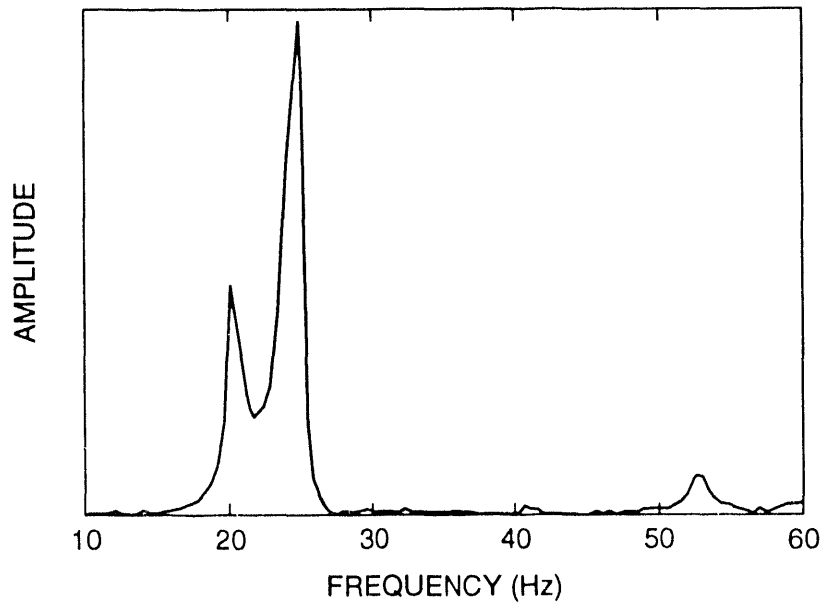
Fig. 7. Displacement spectrum measured on the NMSU laboratory bridge at location 4 using the small piezoelectric transducer.
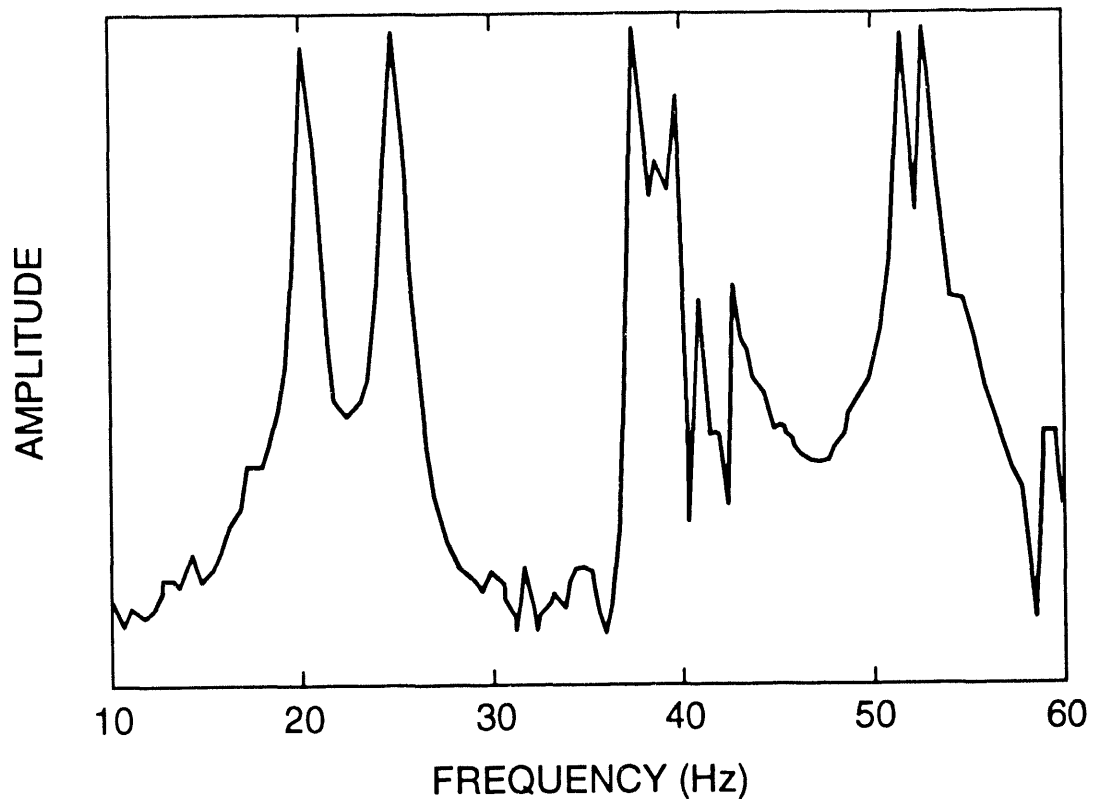
Fig. 8. Displacement spectrum measured on the NMSU laboratory bridge at location 4 using the microwave interferometer.

show studs welded to the flanges of the outer stringers, these studs would not be considered sufficient to produce composite action between the concrete deck and the steel beams. As can be seen in Fig. 9, the portions of the west end of the bridge that was being razed during the testing showed no studs on any of the stringers. Loads from the stringers are transferred to the plate girders by floor beams located at 20 ft intervals. Cross-bracing is provided between the floor beams. Figure 10 shows an elevation view of the portion of the bridge that was tested. The cross-section geometry of each bridge is shown in Fig. 11, and Fig. 12 shows the actual substructure of the bridge. It should be noted that the actual bridges have concrete crash barriers on either side of the concrete slab. These crash barriers were not shown in the original drawings for the bridge.

Each bridge is made up of three identical sections. Except for the common pier located at the end of each section, Fig. 13 , the sections are independent. A section has three spans; the end spans are of equal length, approximately 131 ft, and the center span is approximately 163 ft long. Five plate girders are connected with four bolted splices to form a continuous beam over the three spans. The portions of the

34
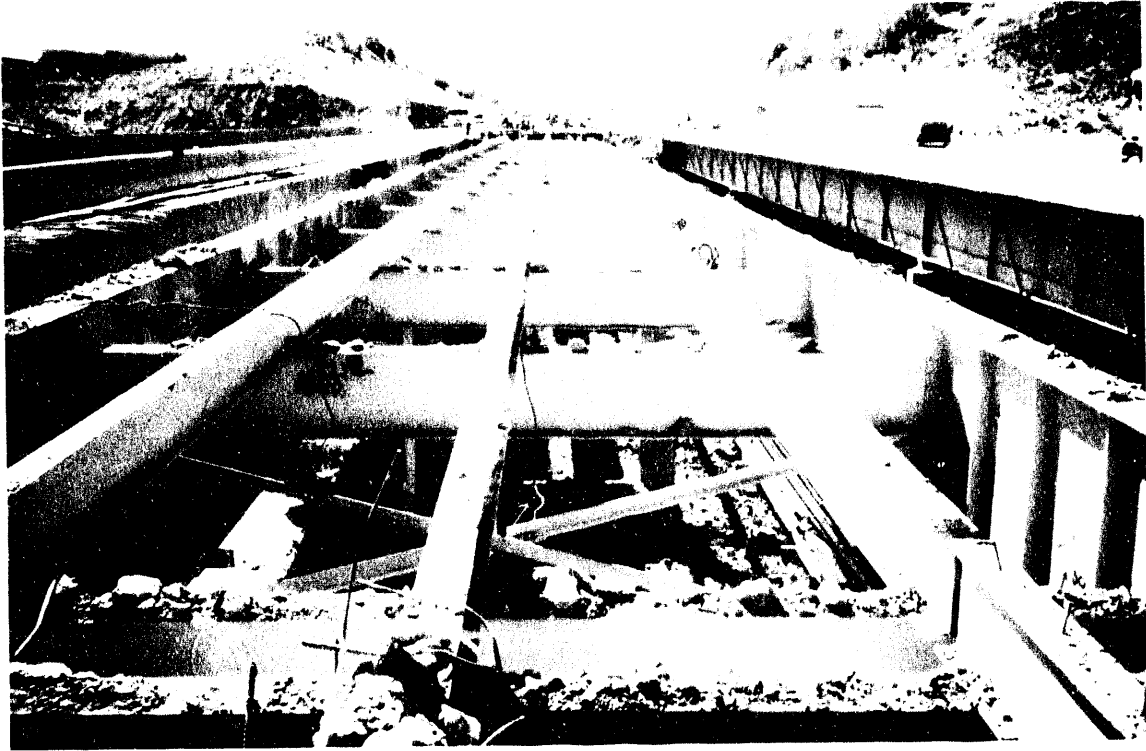
Fig. 9. Top flanges of stringers and plate girders after the concrete deck has been removed. Note the lack of shear studs on these flanges.
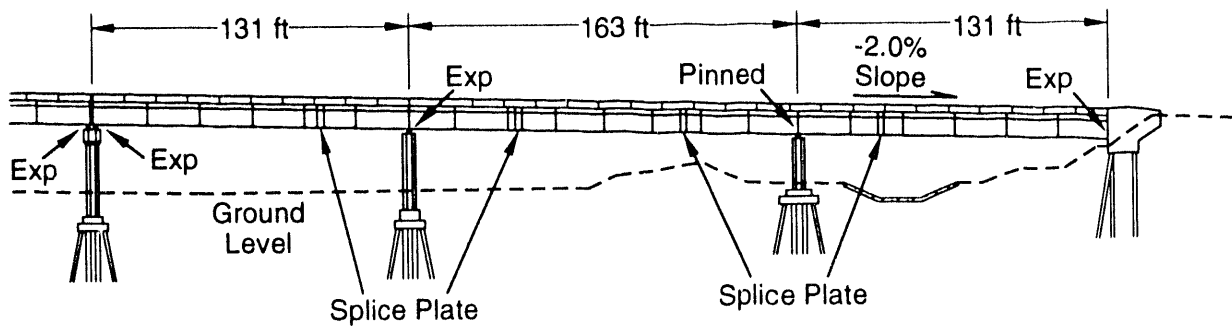
Fig. 10. Elevation view of the portion of the eastbound bridge that was tested.
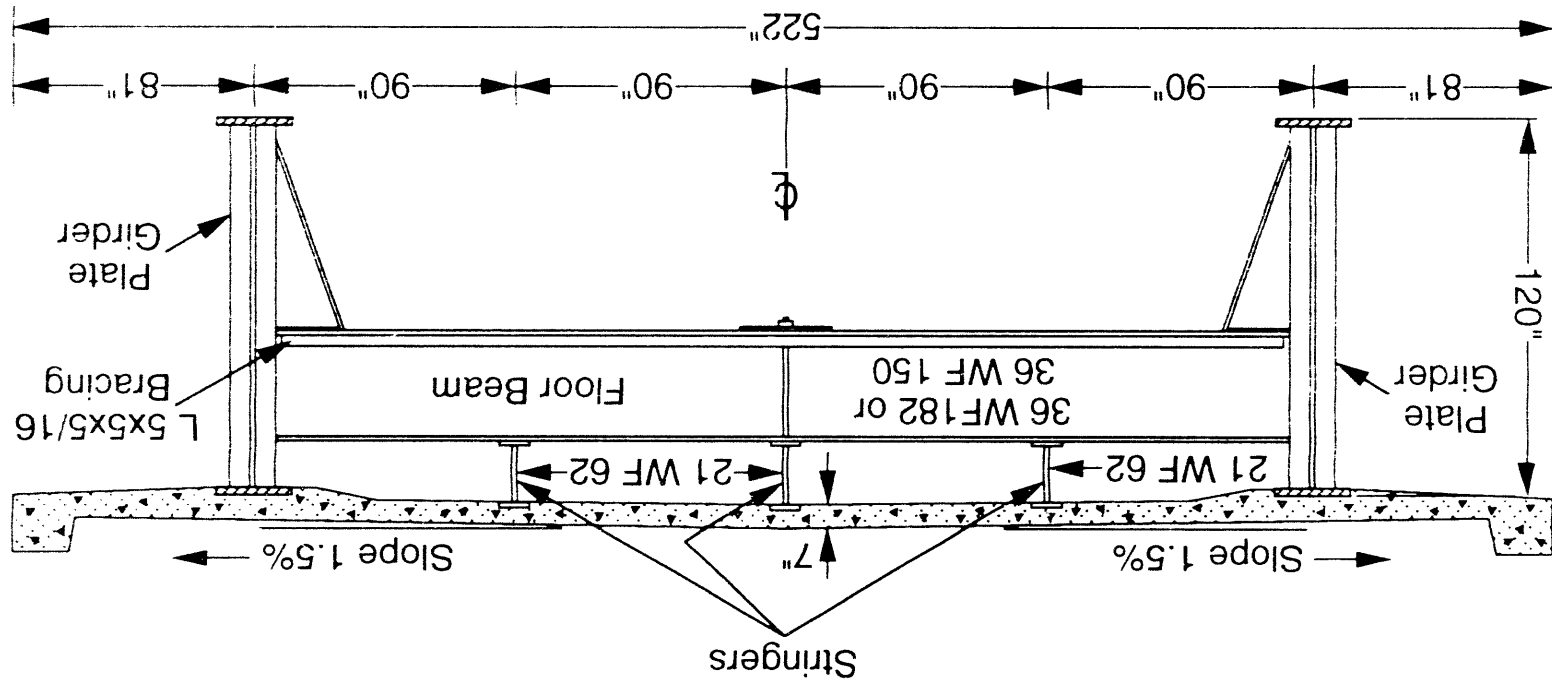
Fig. 11. Typical cross-section geometry of the bridge.

Fig. 12. Bridge substructure.
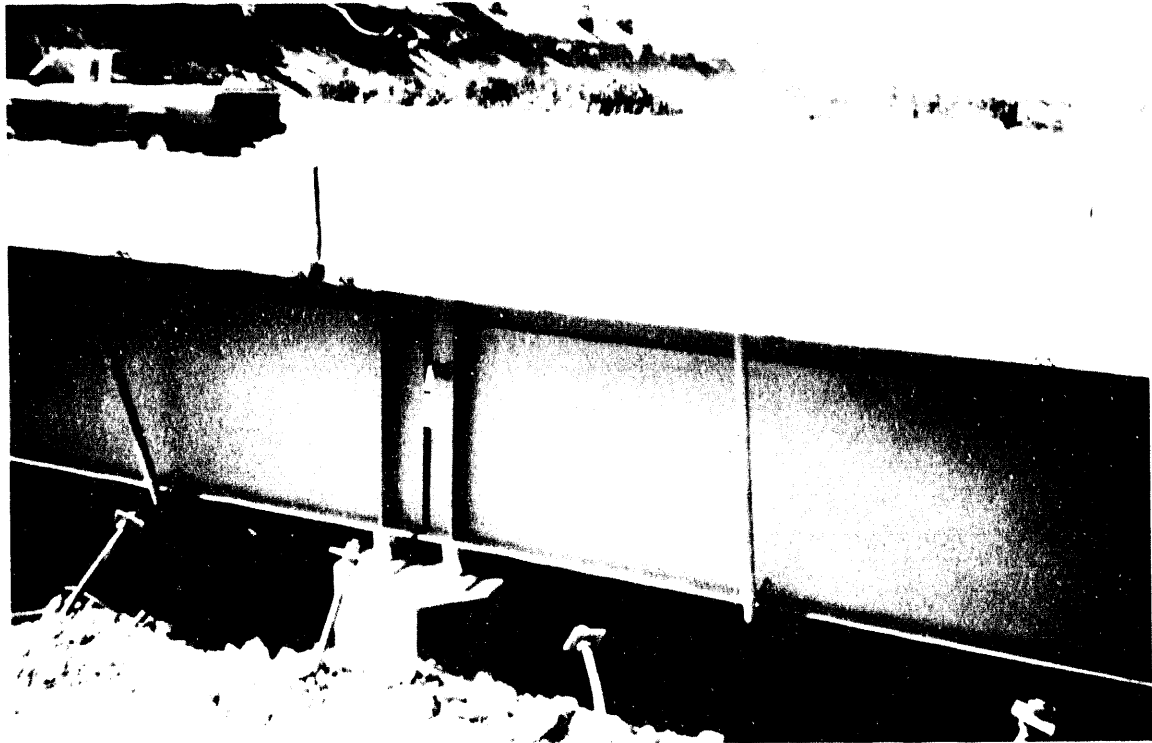
Fig. 13. Common pier shared by two independent plate girders.

plate girders over the piers have increased flange dimensions, compared with the midspan portions, to resist the higher bending stresses at these locations. Connections that allow for thermal expansion, Figs. 14 and 15, as well as connections that prevent longitudinal translation, Fig. 16 are located at the base of each plate girder, where the girder is supported by a concrete pier or abutment. These connections are labeled "exp" and "pinned" in Fig. 10.

All subsequent discussions of the bridge will refer to the bridge carrying east bound traffic, particularly the three eastern spans, which were the only ones tested.

C. Preliminary Vibration Measurements on the I-40 Bridge (MEE-13)

On March 30 and 31, 1993 preliminary vibration measurements were made on the I-40 bridge. These measurements were intended to give an indication of the required sensitivity and frequency range of the accelerometers that will be needed to perform a complete modal analysis of the bridge and to give initial estimates of the bridge's resonant frequencies. When these tests were performed, temperatures ranged from morning lows of 35 - 39 degrees F to afternoon highs of 57 - 58 degrees F. Although not measured, no significant wind was observed.
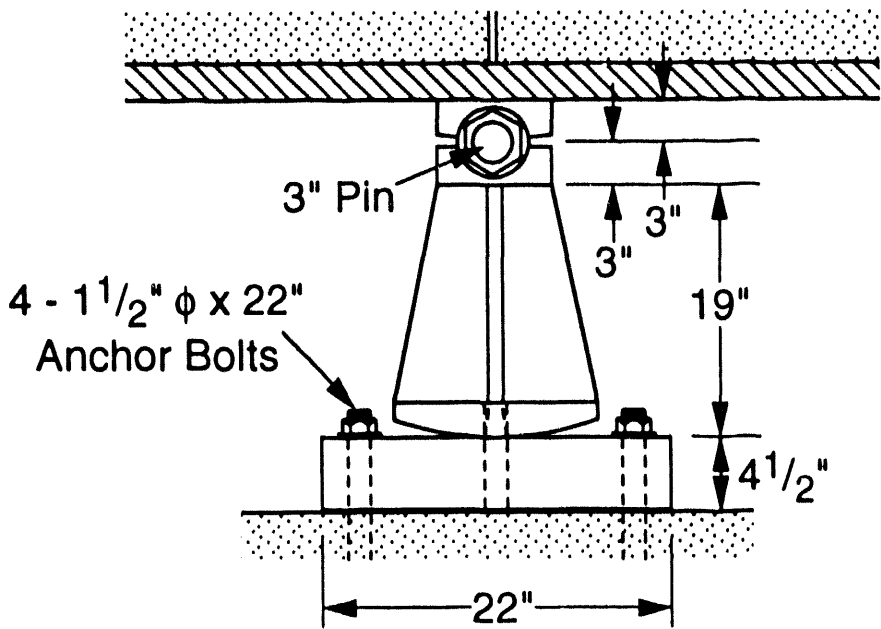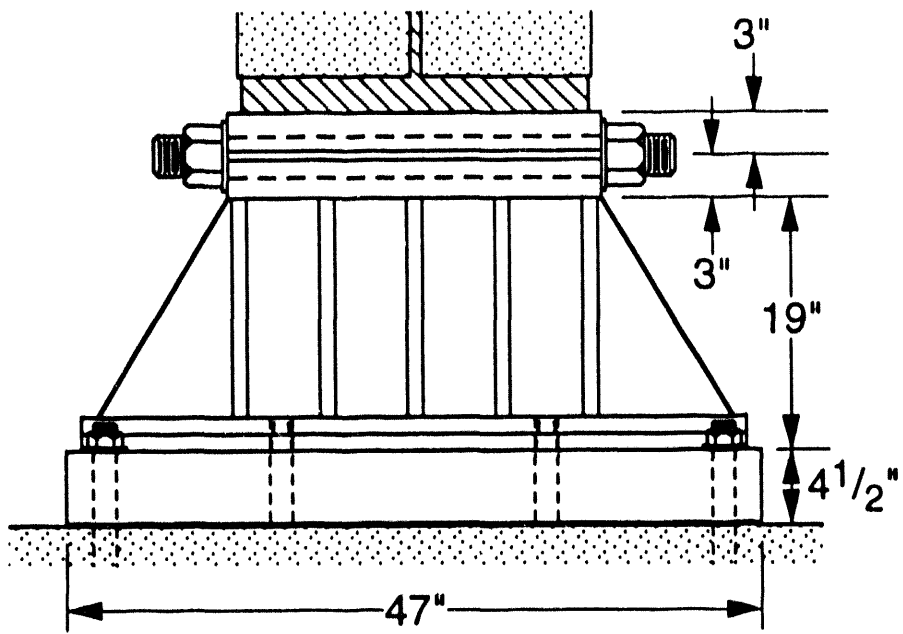
Fig. 14. Connection detail found at piers 1 and 4 that allows longitudinal displacement.
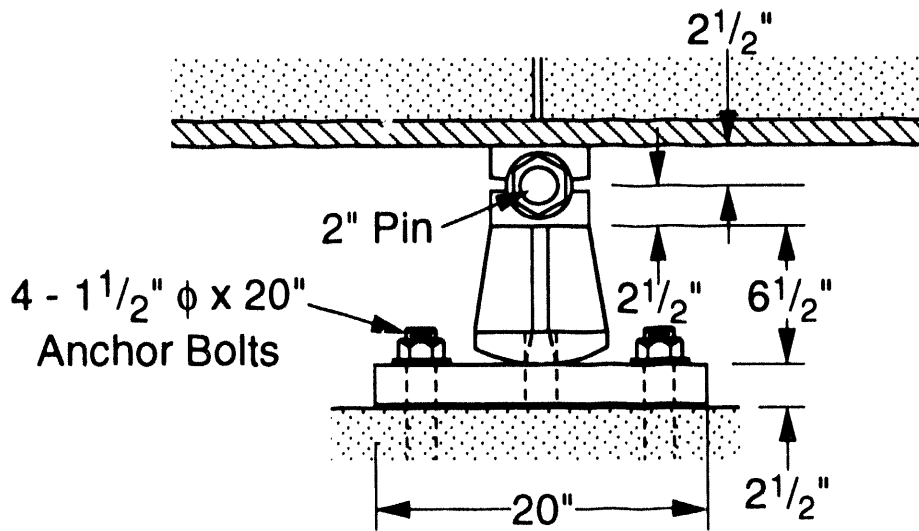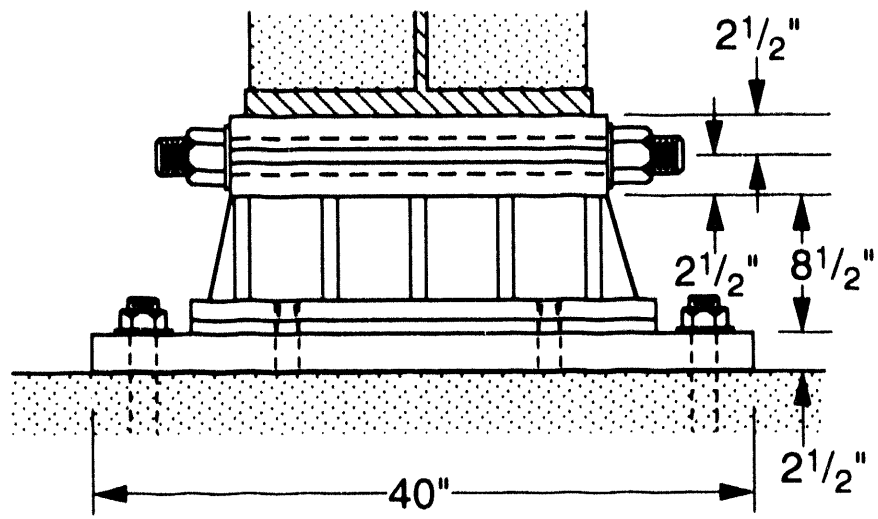
Fig 15. Connection detail found at pier 3 that allows longitudinal displacement.
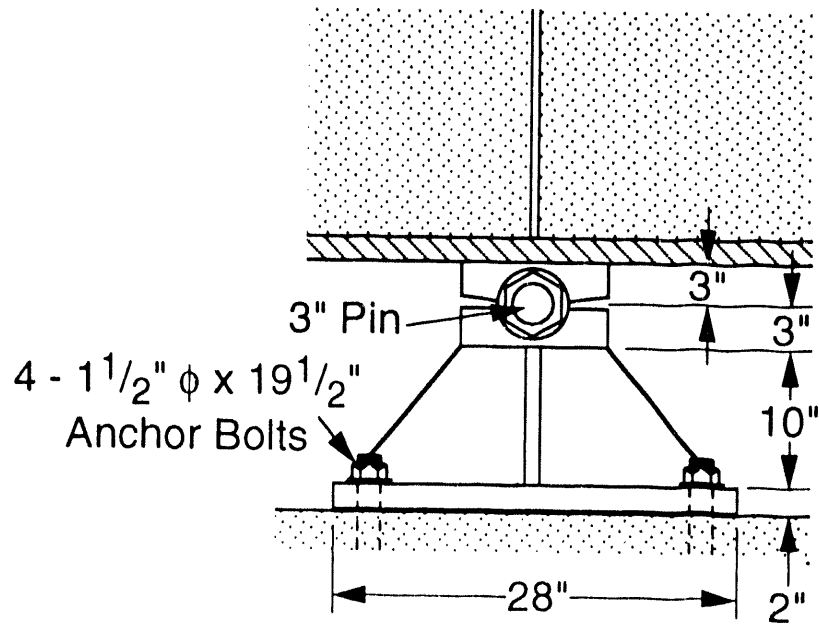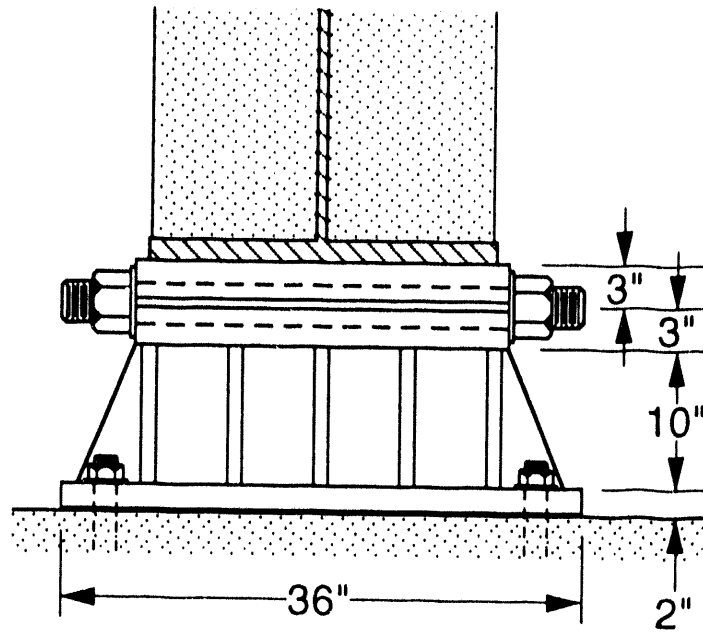
Fig. 16. Connection detail found at pier 2 that constrains longitudinal displacement.

1. Time domain data measurement and observed response. Vibration measurements were made on the middle and eastern spans of the eastern-most section of the eastbound bridge. Traffic, which had been funneled onto the two northern most lanes, provided an ambient vibration source for these measurements. No attempt was made to measure this input to the bridge. Acceleration response of the bridge was measured at the various locations shown in Figure 17. In most cases, an aluminum mounting block for the accelerometer was dental-cemented to the bottom, interior flange of the plate girders as shown in Fig. 18. For two locations the aluminum blocks were mounted adjacent to the plate girder web on the seats that support the floor beams (Pts. 2 and 3 in Fig. 17).

Two types of integral circuit piezoelectric accelerometers were used: PCB 302a's, with a nominal sensitivity of 10 mV/g and a specified minimum frequency (±5%) of 1 Hz, and PCB 393C's, with a nominal sensitivity of 1 V/g and a lower frequency bound of 0.01 Hz. These accelerometers were connected to the aluminum blocks with a single 10-32 stud. Power was supplied to the accelerometers by the HP 35665A two-channel spectrum analyzer.

Time domain analog data were acquired with the spectrum analyzer, and recorded in DOS format on floppy discs. The analyzer was mounted in a minivan and was powered by a portable 3 kW gasoline generator. Twelve and one-half foot lengths of low noise coaxial cables with 10-32 fittings were connected directly to the accelerometers. These cables were then connected to various lengths of RG-58 coaxial cable (75 ft for Pts. 1 and 4 in Fig. 17; 150 ft for Pts. 2 and 3; and 200 ft for Pts. 5, 6, and 7). The RG-58 coaxial cables were, in turn, connected to the analyzer.

Figure 19 shows two typical 64-s time histories recorded with the transducers mounted on the middle span of the south plate girder at the midpoint of this span (Pt. 1 in Fig. 17). These time histories were acquired simultaneously at nearly identical locations. The top plot corresponds to data obtained from a 302A accelerometer, and the bottom plot corresponds to data obtained with a 393C accelerometer. Note that the peaks highlighted with the cursor show an approximately 20% difference in amplitude between the two measurements. The abrupt changes in amplitude shown in these plots correspond to the large trucks passing over the bridge. Numerous time histories similar to those shown in Fig. 19, were acquired (0.08 g's was the largest amplitude response observed).

Figure 20 shows an additional set of 32-s time histories. The top plot corresponds to a measurement made at the pier supporting the east end of the midspan (Pt. 3 in Fig. 17), and the bottom plot corresponds, again, to a measurement made at Pt. 1 in Fig. 17. Both sets of data were acquired with 393C transducers. This measurement shows that although small, vertical accelerations within the resolution of this transducer are being measured at the pier.

2. Frequency domain data measurement and response. Power spectra were calculated from measurements made at various locations on the plate girders shown in Fig. 17. The power spectra show the frequencies at which the structure exhibits a strong response, indicative of its resonance frequencies. Sampling parameters were established that allowed frequency ranges of 6.25 Hz, 12 Hz, and 50 Hz to be

130'-2"

162'-9"

130'-2"

Note:
1 and 4 at midpoint
2 and 5 at quarter point
3 and 6 at piers
7 at midpoint

Drawing not to scale

East

East

43
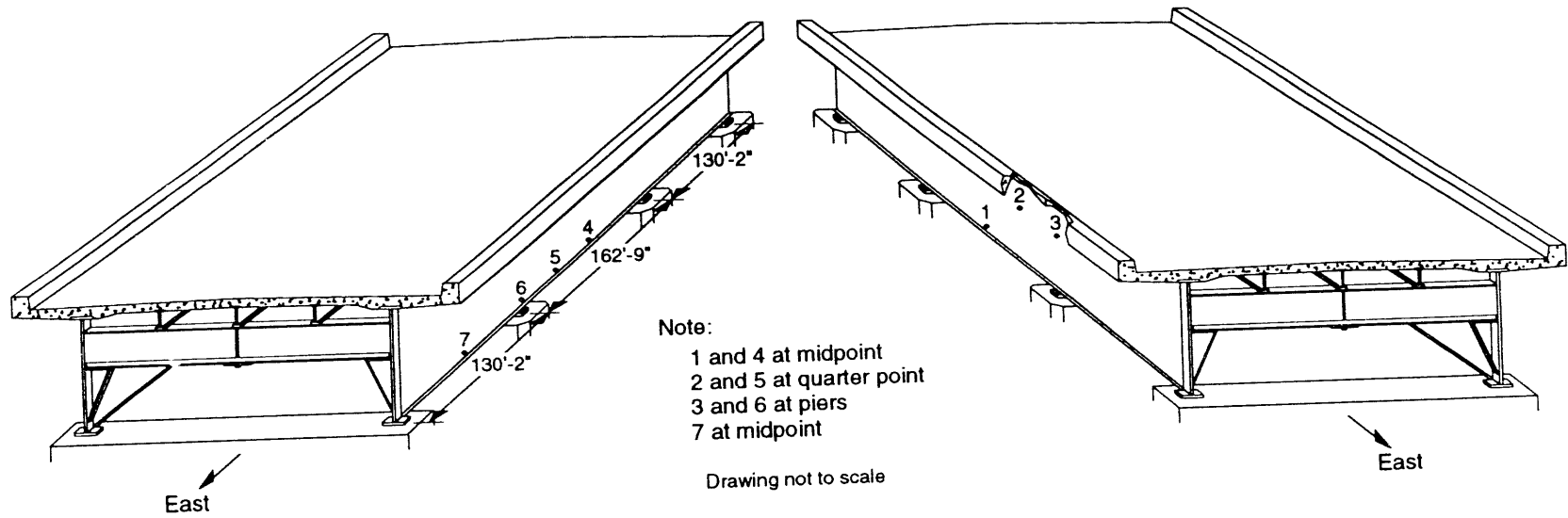
Fig. 17. Locations where preliminary vibration measurements were made.

Fig. 18. Typical accelerometer mounting scheme.
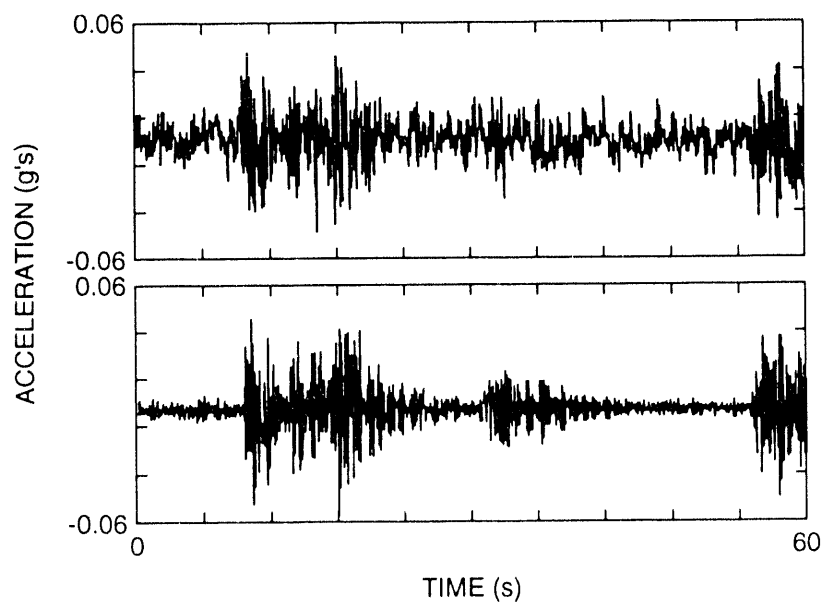
Fig. 19. Sixty-four second time histories measured at location 1 comparing the response of accelerometers with different sensitivity.

44
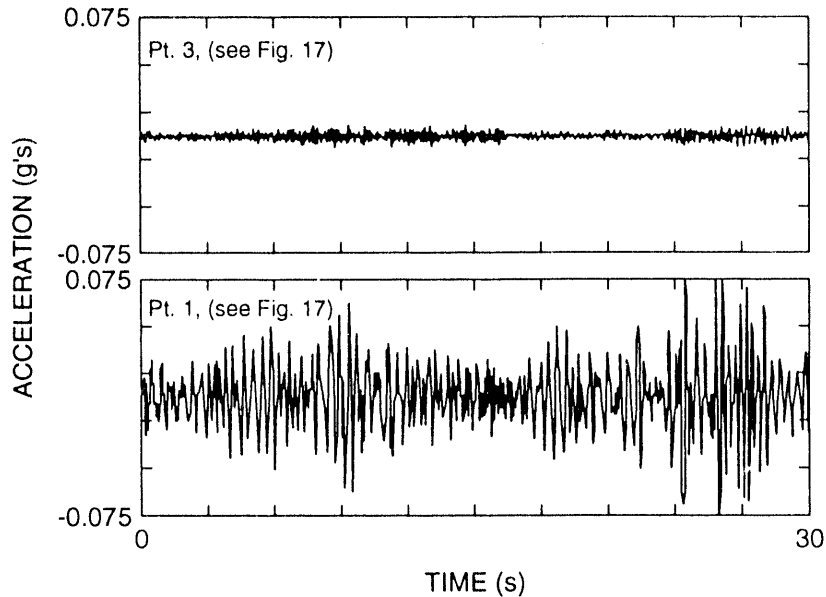
Fig. 20. Thirty-two second time histories comparing vertical accelerations measured on a pier (location 3) and on the plate girder (location 1).

displayed with 400 spectral lines. Estimates of the spectra were determined from 10 to 30 averages, with 20% overlap. The overlap allows for a more optimal use of the time samples because data that is eliminated in one sample (by the windowing function) will be used in the next sample if overlapping is permitted. Flattop or Hanning windows were used to minimize leakage. To eliminate problems associated with DC offsets, AC coupling of the input signals was specified. AC coupling applies a high-pass filter to the analog data, thus eliminating the DC component of the measured signal.

Because fairly low-frequency response (2-5 Hz) is of interest, there was some concern that the AC coupling would distort the data in this frequency range. The HP 35665A manual specifies that AC coupling attenuates the signal 3 dB at 1 Hz, with a 6 dB per octave roll off at frequencies below 1 Hz. The effect of AC coupling was measured by inputting a 1 Vrms, 0.08-Hz to 6.2-Hz swept sine signal into each data acquisition channel and plotting the RMS amplitude, as measured by the analyzer with the AC coupling. The results of this test are shown for both data channels in Fig. 21. These plots show that AC coupling provides a 3-dB signal reduction at approximately 0.5 Hz, and that virtually no attenuation occurs at frequencies of 2 Hz and above.

Figure 22 shows the effects of averaging and the repeatability of the spectra when ambient vibration data were collected over various time intervals at Pt. 1 in Fig 17. The top plot corresponds to a power spectrum estimated from 30 averages and the two plots below correspond to spectra obtained from 10 averages. These plots show that the frequency components of the primary bridge response are repeatable. However, the amplitudes of response vary almost 100%, and the effects of averaging on the amplitudes are masked by the variations in these results obtained at different times. The differences in amplitude are attributed to variations in the truck traffic during the different measurement windows.
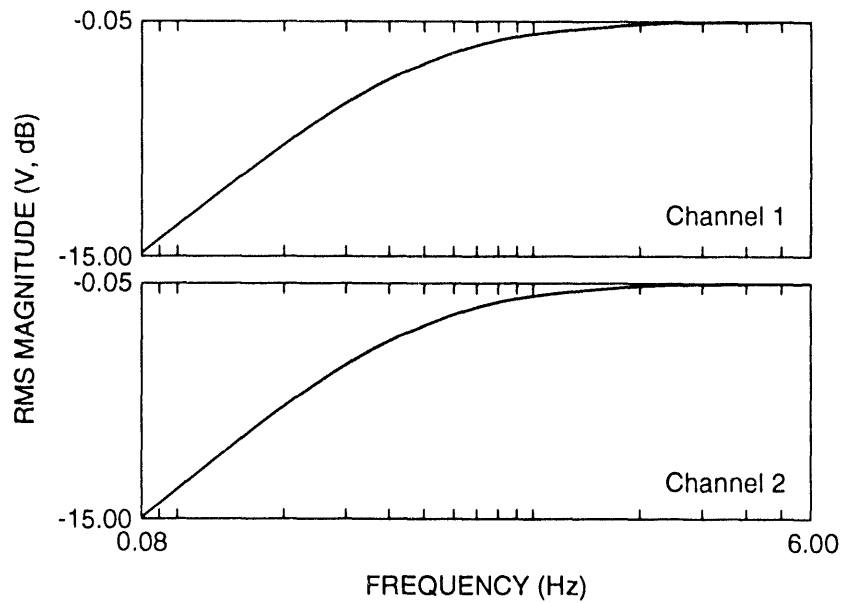
Fig. 21. Roll-off characteristics of the AC coupling filter in the HP-35665A Analyzer.
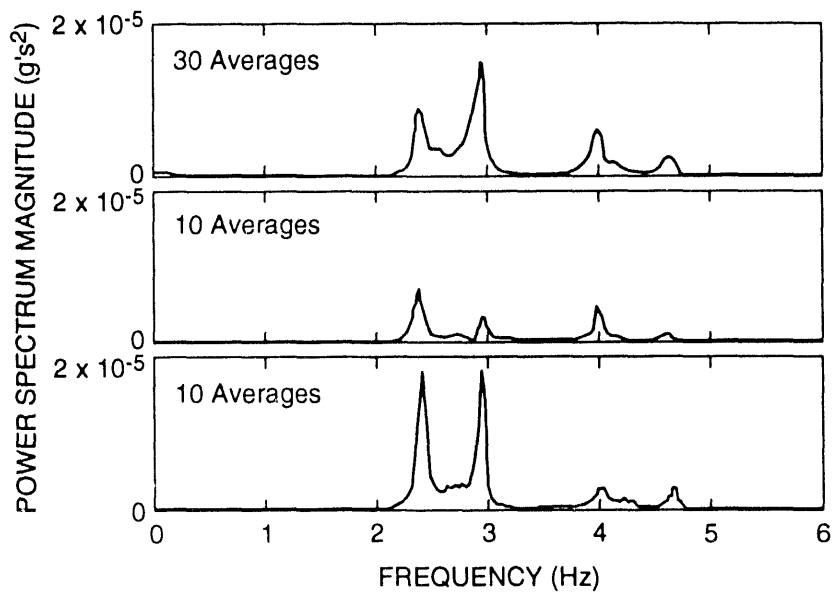
Fig. 22. The effects of averaging and taking measurements at different times on the power spectra measured at location 1.

3. Results of preliminary measurements.

The initial ambient vibration measurements made on the bridge showed that the lowest frequency mode of the structure occurs around 2.4 Hz. This resonant frequency is high enough that typical AC coupling filters should not interfere with the measurements. Commercially available accelerometers have the necessary sensitivity to measure the response caused by ambient traffic excitation. The spectra revealed several distinct resonances in the 0 - 6.25 Hz range which should allow mode shapes to be determined when more channels of data are available.

D. Preliminary Vibration Measurements on the I-40 Bridge (P-10)

On April 28th and May 13th several vibration measurements were made on the I-40 bridge by P-10 personnel. These measurements were used to test transducers, electronics, software and measurement techniques which were to be used by P-10 when damage was introduced into the bridge later during the year.

1. Experimental procedure and equipment.

Measurements were made on April 28th to compare the response of four different types of conventional accelerometers, and to compare data acquisition techniques. Three types of accelerometers, identical to the ones used during preliminary tests on the NMSU laboratory bridge were tested. The first was the magnetic borehole accelerometer, Model L-4 Seismometer from Mark Products, Inc. Also tested were two similar but smaller magnetic accelerometers, one attached for detecting horizontal motion and one for vertical motion. Finally, the experimental cantilevered-arm bimorph piezoelectric accelerometer was tested. All four sensors were clamped to the flange of the south I-beam of the westbound bridge, at a point similar to Pt. 1 shown in Fig. 17.

Cables ran from the accelerometers down to the receiver electronics and computer data acquisition system, which were battery powered. All couplings in the electronics were DC. Two modes of data acquisition were used with this setup, multiple channel time domain data acquisition, and frequency domain data acquisition using the homodyne detector, previously discussed in section III. A. Also, a Hewlett Packard Digital Spectrum Analyzer, model 3562A, was used for some measurements. Excitations for the vibration of the bridge was supplied by ambient traffic, most of which are attributed to impulses caused by heavy trucks as they came onto the bridge at speed.

The set of measurements taken on May 13th were made specifically to test the effectiveness of a microwave interferometer motion sensor. A 24 GHz Gunn diode oscillator unit with a detector diode in the cavity was placed near the focus of a 4' parabolic dish. The distance from the focus was adjusted until the image point was focused on the surface of interest. Microwaves reflected from this image are collected by the dish and refocused into the source cavity where they interfere with the original wave to change the amplitude measured by the detector diode. Any change in the distance from the source to the reflecting surface will produce a change in the output signal from the diode. The four previously used inertial accelerometers were once again set up on the bridge, at the same place as the April 28th measurements. The dish was placed on the ground and the spot focused on the bottom plate girder flange near the other sensors, and again, time domain measurements were made.

47

2. Results. The homodyne detection method requires the signal to be reasonably continuous, in order to have good noise performance. It was clear that the random and phase varying nature of the traffic-induced excitation made homodyne detection useless. This method will have advantages when harmonically driven shakers are used to excite the bridge modes, but it could not be tested under ambient vibration conditions. Therefore, all measurements were made in the time domain. The magnetic sensors performed very well, providing high signal levels and good frequency response. Figure 23 shows the Fourier spectrum calculated by the spectrum analyzer, using the signal from the small magnetic accelerometer oriented in the vertical direction. The resonant frequencies that can be identified from this signal correspond well with the results of preliminary measurements discussed in Section III C. Figures 24 through 26 show averaged power spectra for the three magnetic accelerometers. Again, the data are consistent with measurements made by MEE-13 . The data from the horizontal accelerometer suggests that the 3 Hz mode has a strong horizontal component. More detailed tests, discussed in Section III. E., subsequently showed this mode to be the first torsional mode which, in fact, does have a strong horizontal component of response. The piezoelectric bimorph sensor provided very small signals, mostly due to the effects of cable capacitance and no useful data was taken.

Figure 27 shows the simultaneously measured power spectra of signal from the microwave interferometer and the L-4 seismometer. The data from the microwave detector suggests that there is motion of the bridge at frequencies in the 0.3 - 0.5 Hz range. This is the only sensor that was able to measure response in this frequency region, since the inertial accelerometers move as a rigid body at frequencies below their lower cut-off frequency. The microwave interferometer measures the higher frequency signal accurately and it does not have the resonances that are associated with conventional accelerometers.

A variety of motion sensors were tested. Results of these tests showed that the microwave interferometer has many advantages over the low frequency conventional accelerometers. These advantages are flat response from DC upward, high signal level, and a non-contacting mounting scheme that requires no climbing on the bridge. Based on these results, the microwave interferometer was selected for use during the actual bridge testing to be performed later in the year.

E. Ambient Vibration Tests.

Following the preliminary measurements made in March, ambient (traffic) vibration tests were conducted in June 28 and 29, July 7 through 9, and August 31, 1993. These tests were intended to identify the structure's resonant frequencies, modal damping, and the corresponding modes shapes. Weather conditions were considerably different from those during the preliminary tests as temperatures would range from morning lows of 64 - 67 degrees F to afternoons highs ranging from 94 - 100 degrees F. The thermal expansion associated with these higher temperatures produced noticeable changes in the angles of the rocker bearings. It was also noted that the east end of the top flange on the south girder was in contact with the top of the concrete abutment. Although it is assumed that this contact was a result of thermal expansion, similar observations had not been made in March, hence, the state of this
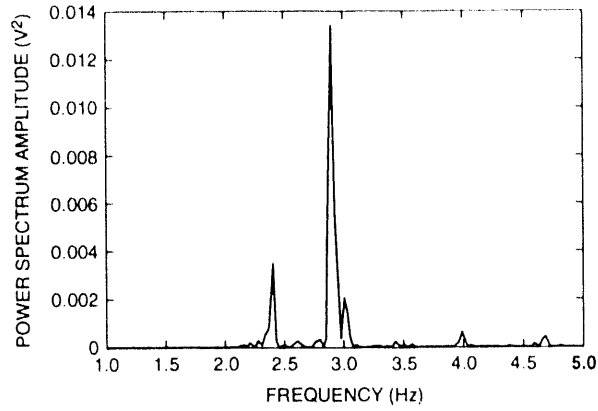
Fig. 23. Fourier spectrum obtained during P-10's preliminary measurements using a magnetic accelerometer oriented in the vertical direction.
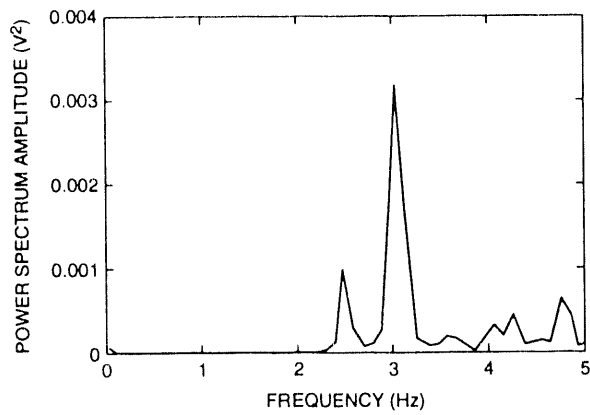
Fig. 24. Power spectrum from the L-4 Seismometer obtained during P-10's preliminary measurements.
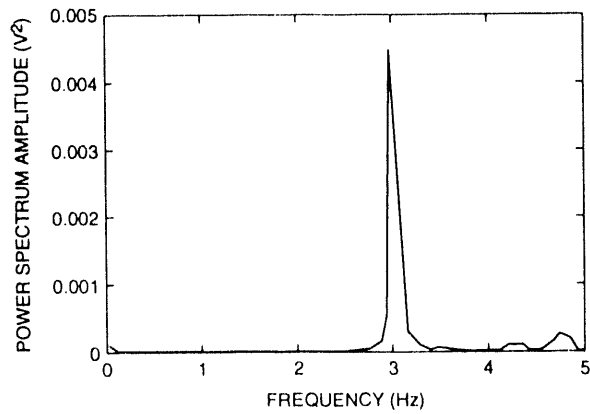
Fig. 25. Power spectrum from magnetic accelerometer oriented in the vertical direction obtained during P-10's preliminary measurements.

49
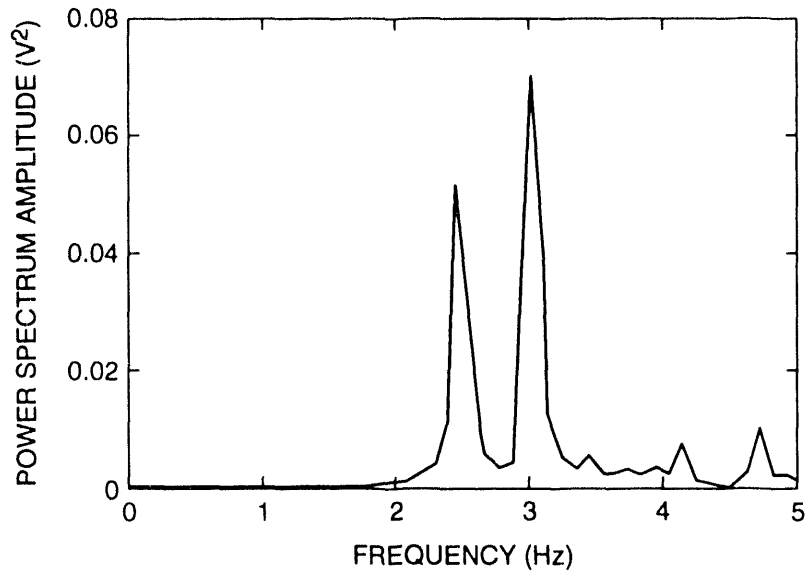
Fig. 26. Power spectrum from magnetic accelerometer oriented in the horizontal direction obtained during P-10's preliminary measurements.
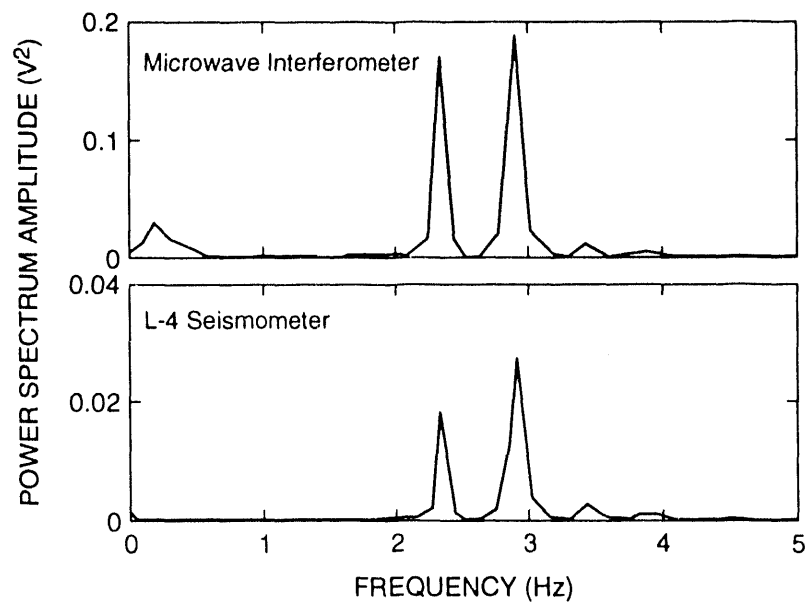
Fig. 27. A comparison of the power spectrum obtained from the microwave interferometer to the power spectrum obtained simultaneously with L-4 Seismometer during P-10's preliminary measurements.

boundary condition corresponding to cooler temperatures is unknown. Wind was very light during all ambient vibration tests and was not considered a significant input source.

As during the preliminary tests, traffic had been funneled onto the two northern lanes. Significantly different traffic flow could be observed at various times when data was being acquired. During morning and afternoon rush hours the traffic would slow down considerably thus producing lower level excitations in the bridge. At midday the trucks crossing the bridge at high speeds would cause high level excitations that would often over range some of the data acquisition channels. The ambient vibration test conducted on August 31 was done just prior to the forced vibration tests when all traffic had been removed from the eastbound bridge. For this test the ambient vibration source was provided by the traffic on the adjacent new eastbound bridge and the existing westbound bridge that was transmitted through the ground to the piers and abutment. During all ambient tests, no attempt was made to characterize the input to the bridge.

1. Experimental procedure and equipment. The data acquisition system used in the ambient vibration tests consisted of a Hewlett Packard 9000 Series 370 workstation with a 300 megabyte hard disk, 29 HP 35652A input modules that provide power to the accelerometers and perform analog to digital conversion of the accelerometer signals, an HP 35651A signal processing module that performs the needed fast Fourier transform calculations, and Vista, a commercial data acquisition/signal analysis software package from Hewlett Packard. The system is shown schematically in Fig. 28. A 3500 watt GENERAC Model R-3500 XL AC generator was used to power this system in the field.

PCB model no. 336C integrated circuit piezoelectric accelerometers were used for the ambient vibration measurements. These accelerometers had a nominal sensitivity of 1 V/g, a specified frequency range of 1 - 2000 Hz, and an amplitude range of ±4 g's. Twelve-inch-long 50-Ohm MicroDot cables were connected to the accelerometers. The Microdot cables were then connected to various lengths of two conductor PVC jacketed 20 gauge cable ranging from 70 ft to 291 ft that were, in turn, connected to the input modules. The cables were supported by the catwalks located along each plate girder, tied off, and dropped down to the van housing the input modules. The field configuration of this data acquisition system is shown in Fig. 29.

Before taking the data acquisition system into the field the entire system was tested in the laboratory by placing 26 accelerometers on an aluminum beam that had its first mode frequency in the range of 2 - 3 Hz. This test configuration is shown in Fig. 30. During these tests the system was powered by the generator to further simulate the actual field conditions. Tests were also conducted to examine the thermal drift properties of the accelerometers. The accelerometer was heated by two 250 watt bulbs located six inches away for 30 s, and then with just one bulb for 200 s while recording the background vibration signals. Results of these tests showed that the data acquisition system should perform well in the field as configured, and, if AC coupling is specified, thermal drift would not be a problem during the ambient vibration measurements.
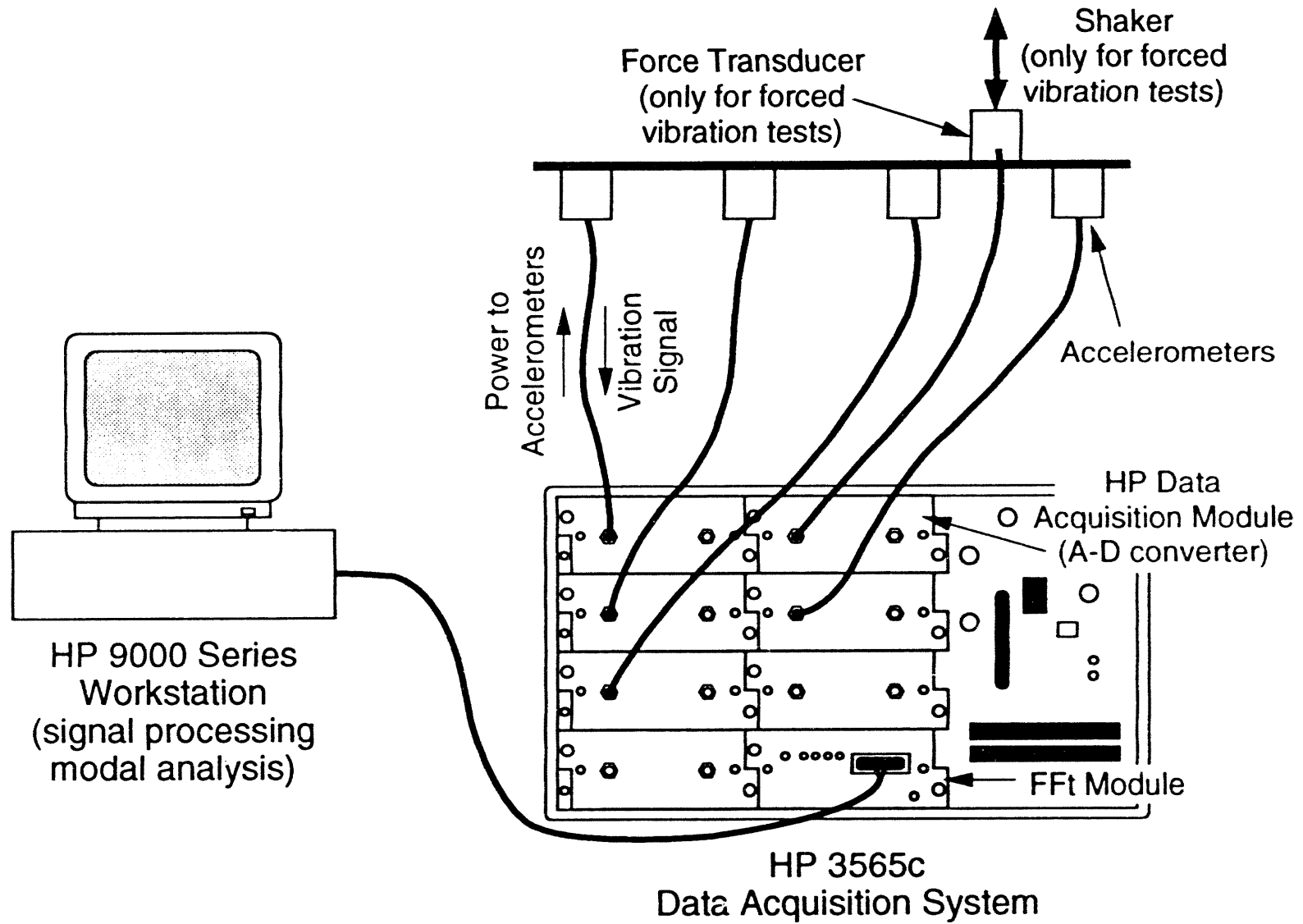
Fig. 28. Data acquisition system.
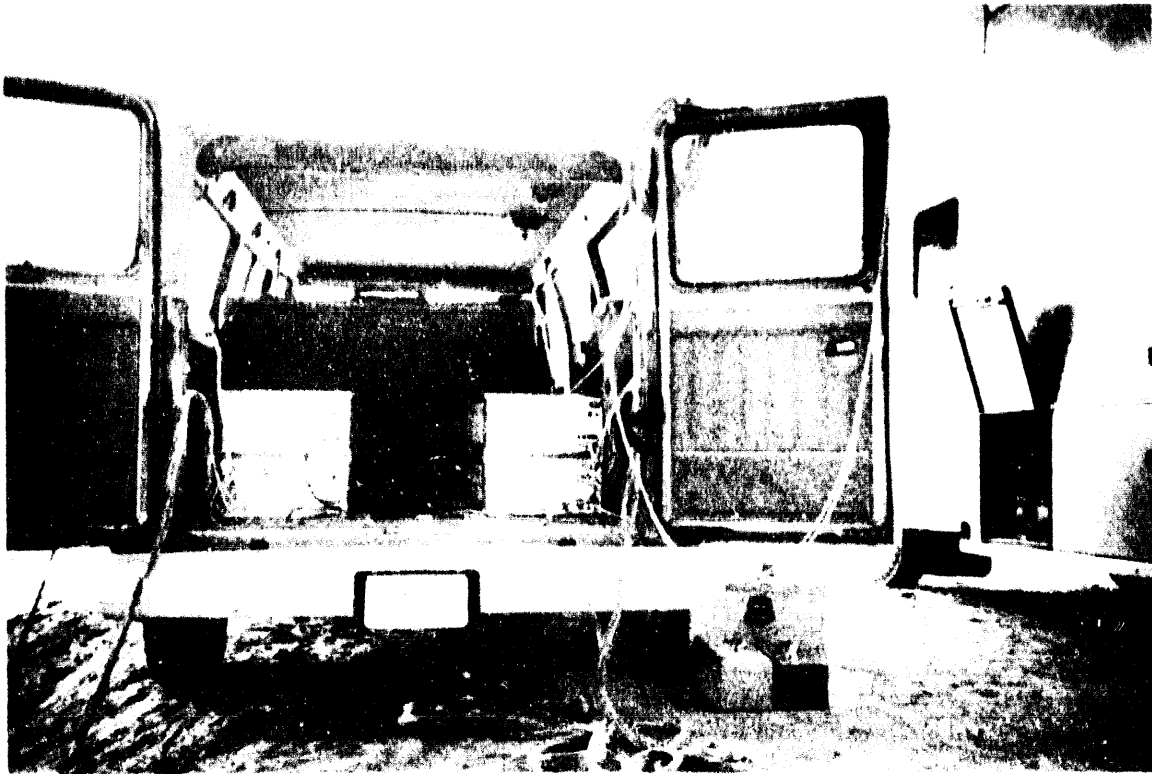
Fig. 29. Field setup of the data acquisition system.
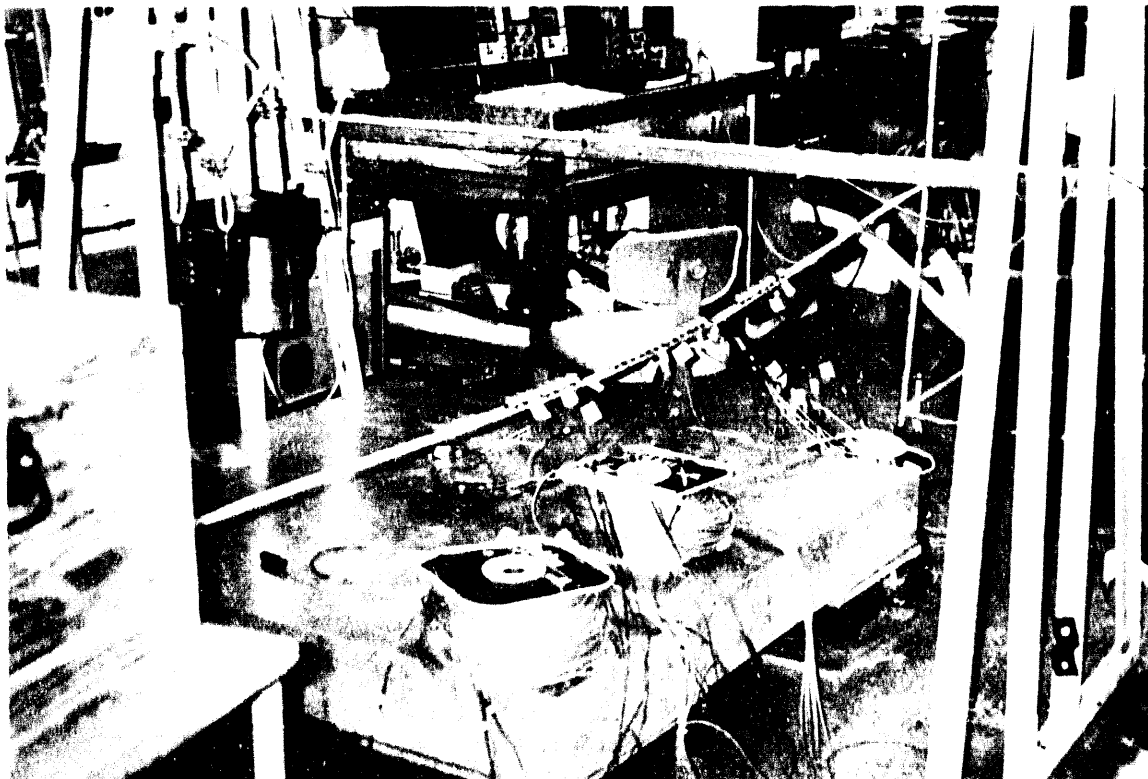
Fig. 30. Laboratory test of the data acquisition system.

Twenty-six one-inch square aluminum mounting blocks were dental cemented to the inside web of the plate girder at mid-height and at the axial locations shown in Fig. 31. Within a span the three blocks were equally spaced in the axial direction. Blocks at locations N-10 and S-10 were mounted directly to the splice plates on the girder. Finite element analysis shows that, when the dental cement is assumed to produce a fixed base condition, the blocks have a resonant frequency in excess of 20 kHz. Therefore, at the frequencies of interest in this study, the blocks are assumed to move as a rigid body with the structure. Accelerometers were mounted on the blocks with a 10-32 stud, either in the global X, Y, or Z direction as shown in Fig. 31. Note that on the south beam accelerometers were mounted in the negative X direction.
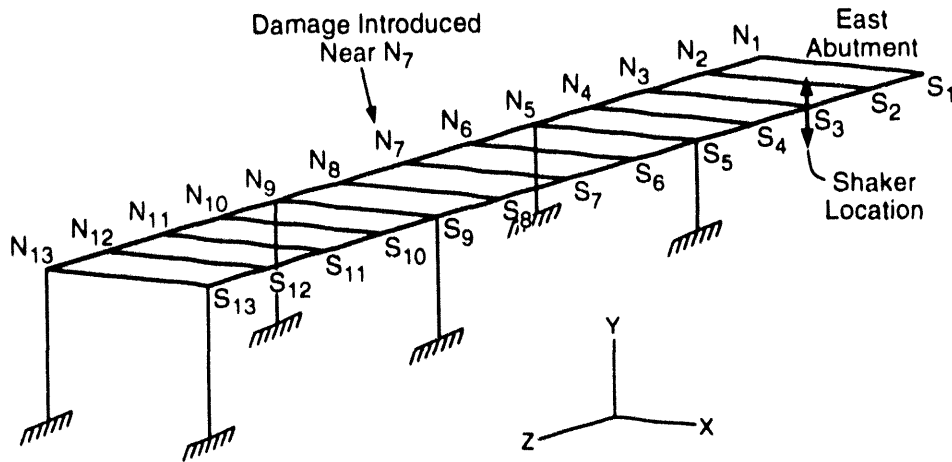
Fig. 31. Accelerometer locations.

Initially the dynamic range for data acquisition from the accelerometers was set at 0.25 g's, but after observing numerous overloads, this range was increased to 3.98 g's; close to the maximum level at which the accelerometers are rated. The overloads persisted implying that they were caused by inputs out of the frequency range being examined. Sampling parameters were adjusted so that frequencies up to 12.8 kHz could be resolved. When data were acquired with these sampling parameters it became evident that high frequency response was, in fact, causing the overloads. It was assumed that this high frequency response was caused by impacts from trucks on road surface irregularities and expansion joints.

The data acquisition system samples the analog signal from the accelerometer at 262 kHz (regardless of the frequency range being analyzed), passes the signal through an analog anti-aliassing filter, digitizes it, then passes the data through a digital anti-aliassing filter with the cutoff frequency based upon the Nyquist frequency for the specified sampling parameters. The signal is then decimates based on the particular sampling parameters. However the overload test is performed prior to the digital filtering and decimating process, hence, out of band inputs can cause overloads. The overloads have two adverse effects on the measured data. First, the

54

"clipped" signal is not representative of the actual signal and the abrupt changes in the clipped signal can show up as high frequency noise in the measured response. Second, the signal-to-noise ratio is reduced when a larger than necessary dynamic range has to be specified. To avoid these overloads and their associated problems, the accelerometers must be mechanically isolated from the high frequency inputs or the signal from the accelerometers must be passed through an analog filter before it is sent into the data acquisition system.

Analog filters were not available. Therefore a simple mechanical filter was devised that isolated the accelerometers from the high frequency inputs. The mechanical filter consisted of a piece of either Scotch "Heavy Duty Mounting Tape" or Manco "Wide Double-Sided Mounting Tape" placed between the accelerometer and the mounting block as shown in Fig. 32. Also shown in Fig. 32 is a test set-up used to measure the filtering characteristics of this isolation scheme. Figure 33 shows power spectra of the responses to 10 hammer impacts on the side of the aluminum block opposite the accelerometers. The top plot in Fig. 33 corresponds to isolated accelerometer and the bottom plot corresponds to the accelerometer mounted with a 10-32 stud. The attenuation of high frequency signals by the isolation system is evident in these plots. Comparisons of the amplitudes at the resonance of the accelerometers, approximately 7. 5 kHz, shows that the isolation system attenuates these high frequency components of the time signal by a factor of 11.86. Figure 34 shows that below 1 kHz the isolation system has no effect on the measured signal. Based on these results, each accelerometer was attached to its mounting block with the doubled sided-tape rather than the 10-32 stud.
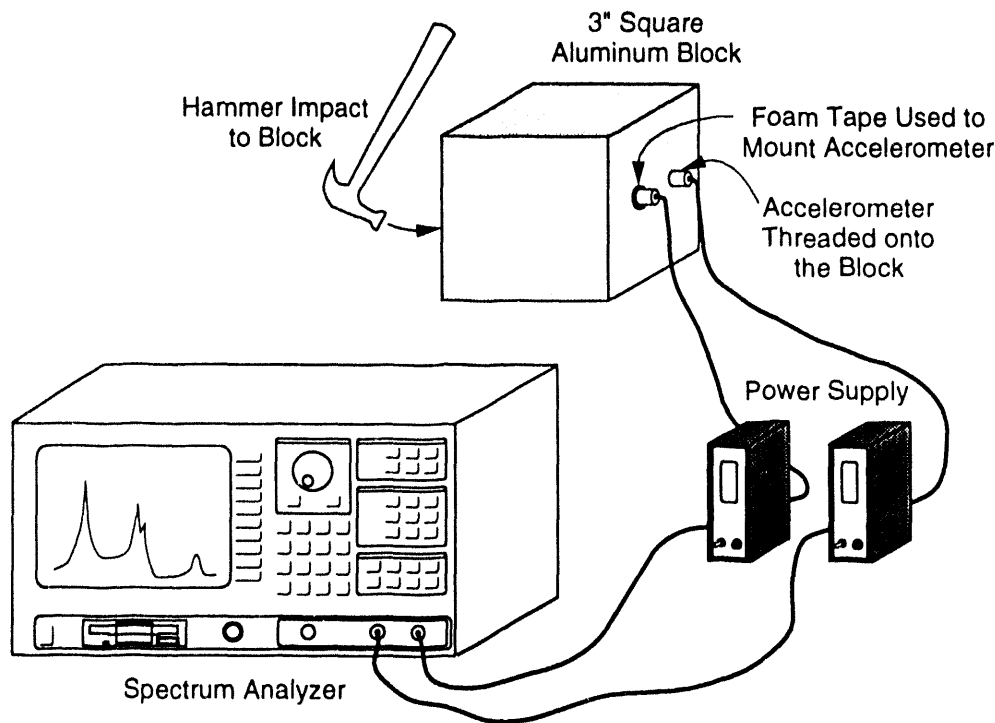
Fig. 32. Mechanical isolation scheme developed to filter high frequency inputs to the accelerometers and test set-up used to examine the filtering characteristics.

55
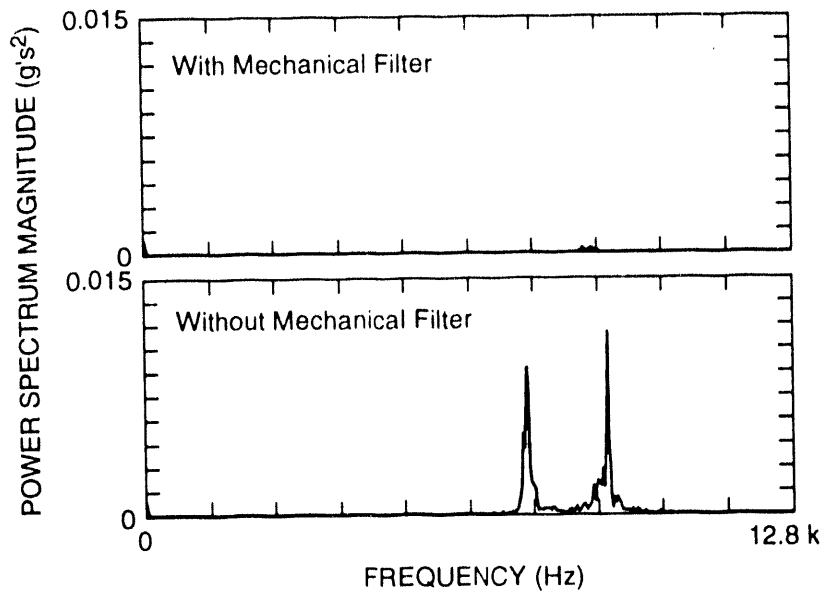
Fig. 33. Power spectra comparing the isolated and 10-32 stud mounted accelerometer response from 0 to 12.8 kHz.
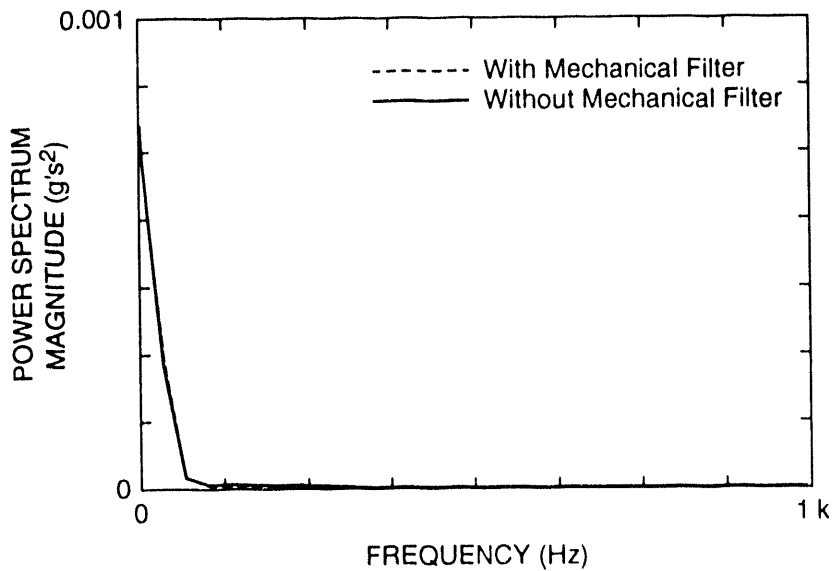
Fig. 34. Power spectra comparing the isolated and 10-32 stud mounted accelerometer response from 0 to 1 kHz.

The data acquisition system was set up to measure acceleration-time histories and calculate FRFs, CPS, and Power Spectra. The FRFs and CPS were calculated with either S-2 or S-6 in Fig. 31 specified as the reference channel. In both cases the reference accelerometers were oriented in the global Y direction. Sampling parameters were specified that calculated the FRFs from 64-s, 32-s, or 16-s time windows discretized with 1024 samples. Therefore, the FRFs were calculated for frequency ranges of 0 - 6.25 Hz, 0-12.5 Hz, and 0 - 25 Hz. Typically, 100 averages were used to calculate the 0 - 6.25 Hz FRFs, 30 averages were used to calculate the 0 - 12.5 Hz FRFs, and 75 averages were used to calculate the 0 - 25 Hz FRFs. Frequency resolutions of 0.015625 Hz, 0.03125 Hz, and 0.0625 Hz were obtained for the 0 - 6.25 Hz FRFs, the 0 -12.5 Hz FRFs, and the 0- 25 Hz FRFs, respectively. Hanning windows were applied to the time signals to minimize leakage and AC coupling was specified to minimize DC offsets.

A test of the AC coupling filter was performed similar to that done with the two channel analyzer discussed in Section III. C. 2. This test showed that the filter did not attenuate the signal at frequencies above 2 Hz, and it was concluded that the AC coupling filter would not adversely effect the data in the frequency ranges of interest. A dynamic range of 3.98 V was specified and time samples that overloaded this range were rejected. With these sampling parameters and the overload reject specified, data acquisition occurred over time periods ranging up to three hours. Table III summarizes the different ambient vibration tests that were conducted.

Table III					
Ambient Vibration Test Summary					
Test Designation[1]	Frequency Range (Hz)	No. of Averages	Reference Channel[1]	Date	Time
t1tr (y)	0 - 6.25	100	S-2 (y)	July 8	9:27 AM - 12:17 PM
t2tr (y)	0 - 25	75	S-2 (y)	July 8	12:24 - 1:01 PM
t3tr (y)	6.25 - 18.75	20	S-2 (y)	July 7	4:15 - 4:30 PM
t4tr (y)	0 - 6.25	5	S-2 (y)	July 7	4:54 - 5:02 PM
t5tr (y)	0 - 6.25	10	S-2 (y)	July 7	5:07 - 5:15 PM
t6tr (x)	0 - 6.25	100	S-2 (y)	July 8	2:25 - 4:35 PM
t7tr (x)	0 -25	75	S-2 (y)	July 8	4:43 - 5:30 PM
t8tr (z)	0 - 6.25	100	S-2 (y)	July 9	9:40 AM - 12:35 PM

Table III *continued*

t9tr (z)	0 - 25	75	S-2 (y)	July 9	12:36 - 1:16 PM
t10tr (y)	0 - 6.25	35	S-6 (y)	July 9	2:42 - 3:30 PM
t11tr (y)	0 - 25	35	S-6 (y)	July 9	3:31 - 3:45 PM
t15tr[2] (y)	0 - 12.5	15	S-2 (y)	August 31	4:45 - 5:00 PM

[1] Letters in parentheses refer to global orientation of the accelerometers.
[2] This test was performed immediately before forced vibration tests when traffic had been routed to new spans. Ambient excitation was caused by traffic on the adjacent spans.

2. Results. Figure 35 shows a typical time-history that was measured at location S-7 during the ambient vibration tests. Time histories such as these were subsequently transformed into the frequency domain so that estimates of the FRFs, CPS and power spectra could be obtained. These frequency domain functions were used to estimate the dynamic properties (resonant frequencies, mode shapes and modal damping values) of the structure.

Typically in vibration testing FRFs relating a measured input, usually force, to a measured response such as acceleration are used to estimate the dynamic properties of a structure. The use of measured input-measured response FRFs to identify a structure's dynamic properties is well documented in the technical literature (Ewins, 1989). However, when a bridge is subjected to traffic excitation, it is difficult, if not impossible, to measure the input to the structure. The extension of system identification methods to ambient vibration cases where an input can not be measured has received considerably less attention in the technical literature.

One alternative is to define an FRF based on a reference response measurement as was suggested by White and Pardoen (1987). From the definition of the CPS it is evident that two measured responses will be correlated only at the resonant frequencies of the structure. Therefore, the CPS will show peaks corresponding to the resonant frequencies. A typical CPS between channels N-7 and S-2 from test t11tr is shown in Fig. 36 and the power spectrum for S-2 is shown in Fig. 37. The corresponding FRF calculated with N-7 considered as the response and S-2 as the input is shown in Fig. 38. The FRF, which is formed from the quotient of the CPS and reference PSD, does not have well defined peaks corresponding to the resonant frequencies. Therefore identification of the structure's dynamic properties, particularly damping, from an FRF, where a response channel is considered the reference rather than a force input, is difficult.

A second alternative is to estimate the resonant frequencies from peaks in the response power spectra. Mode shapes are estimated from the relative magnitudes of these peaks (relative phase information must be obtained from either the CPS or FRF) and modal damping values can be obtained by applying the HPBW method to these
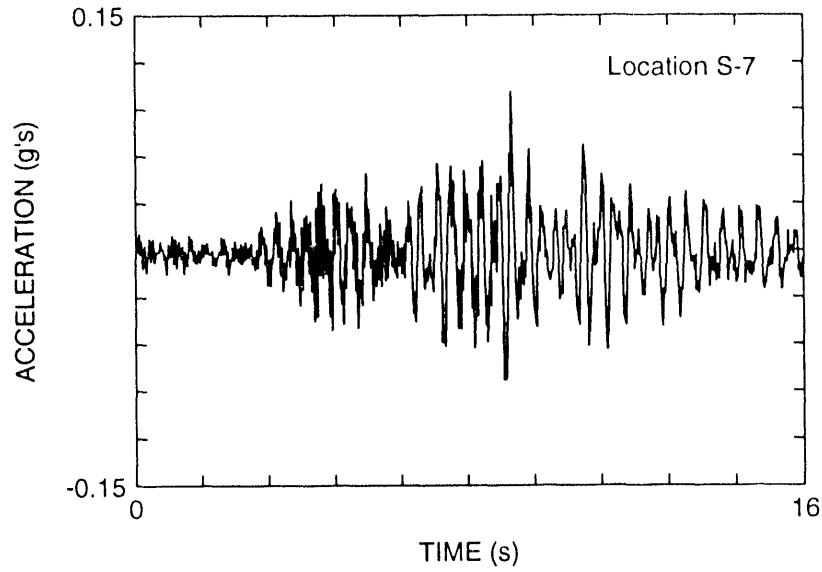
Fig. 35. Typical time-history measured at location S-7 during ambient vibration tests.
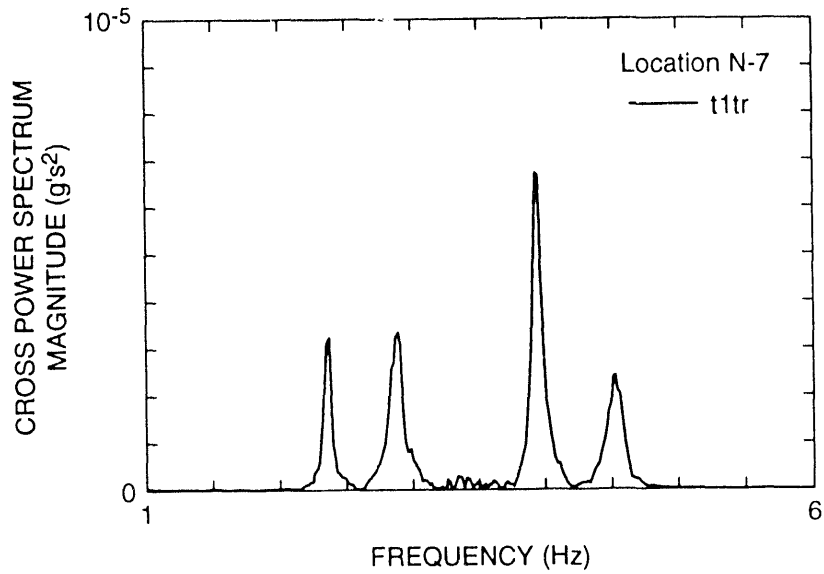
Fig. 36. The cross-power spectrum between channels N-7 and S-2 measured during test t1tr.
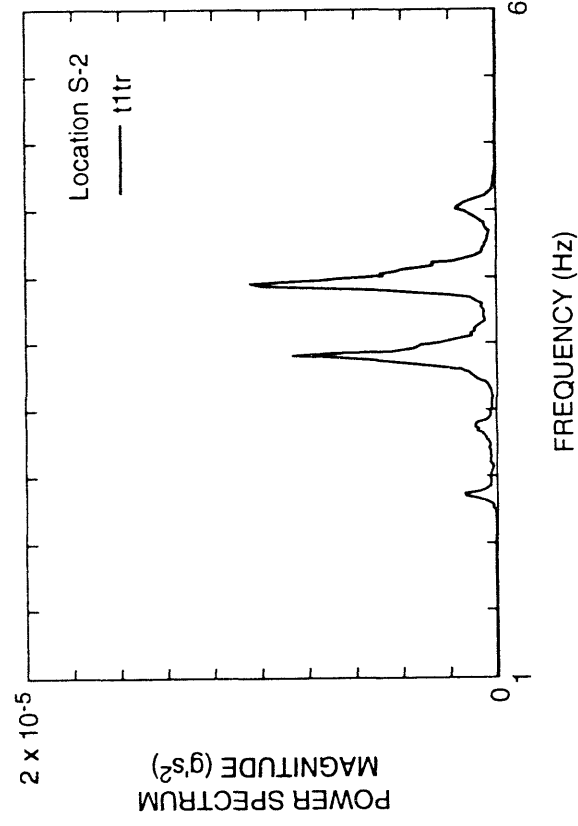
Fig. 37. The power spectrum for S-2 measured during test t1tr.
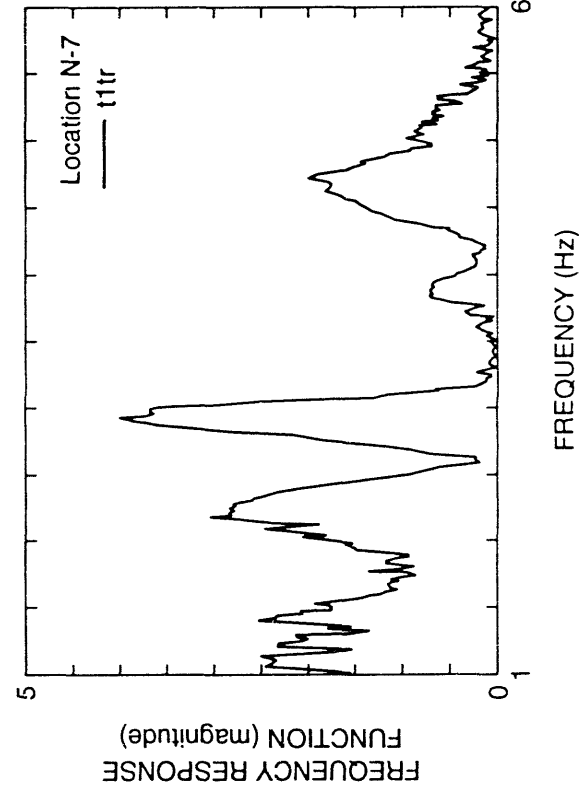
Fig. 38. The frequency response function calculated with N-7 considered as the response and S-2 as the input for test t1tr.

60

peaks. This method has been used in numerous previous investigations, McLamore, et al. (1971) for example. Drawbacks of this method that have been previously identified by Abdel Gaffar and Housner (1978) are the need for very high frequency resolution (the necessary resolution has been quantified by Bendat and Piersol, (1980)) around the resonance to adequately define the half-power points and the difficulties in identifying closely spaced modes.

To circumvent the drawbacks of the methods discussed above, an ambient vibration system identification method developed at SNL was applied to the measured response data obtained on the I-40 bridge. James, Carne, and Lauffer (1993), have shown that for an input, which is not measured but assumed to be white noise, the cross-correlation function between two response measurements (the inverse Fourier transform of the CPS) is the sum of decaying sinusoids and these decaying sinusoids have the same damped resonant frequencies and damping ratios as the modes of the system. Therefore, the cross-correlation functions will have the same form as the system's impulse response function, and, hence, time domain curve-fitting algorithms such as the polyreference method (Vold and Rocklin, 1982) or complex exponential method (Ewins, 1989) can be applied to these functions to obtain the resonant frequencies and modal damping exhibited by the structure. These curve-fitting methods have the ability to identify closely spaced modes and, in general, provide a more accurate method for estimating damping than the HPBW method. Mode shapes are determined from magnitudes and phases in the CPS at the identified resonant frequencies. An overview of the ambient vibration system identification method developed at SNL and the complex exponential curve-fitting method is presented in Appendix A.

The mode shapes for the first six modes identified from test t1tr are shown in Figs 39 through 44. Mode shapes from other ambient vibration tests are tabulated in Appendix B. Table IV summarizes the resonant frequencies and modal damping values calculated from the different tests where the global Y direction response was measured. Both parameters were calculated in a global manner using a complex exponential curve-fitting method, that is, each measured CPS was used to estimate the parameter and the mean value from the 26 measurements was then calculated. These mean values appear in Table IV .
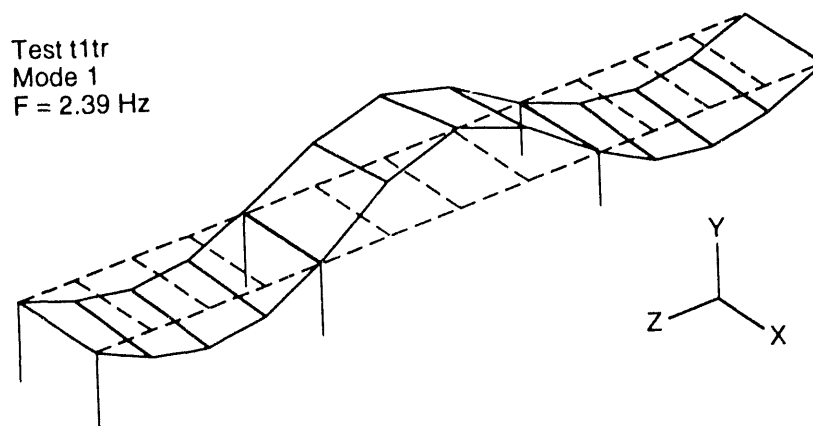
Test t1tr
Mode 1
F = 2.39 Hz

Fig. 39. First flexural mode identified from ambient vibration data, test t1tr.

61

Test t1tr
Mode 2
F = 2.92 Hz
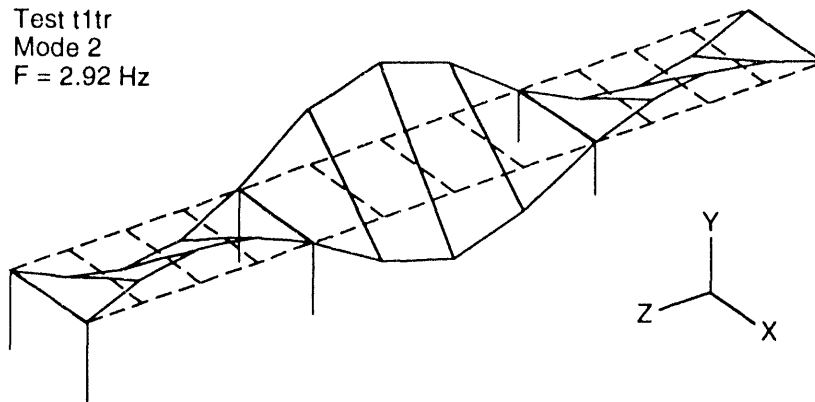
Fig. 40. First torsional mode identified from ambient vibration data, test t1tr.

Test t1tr
Mode 3
F = 3.42 Hz
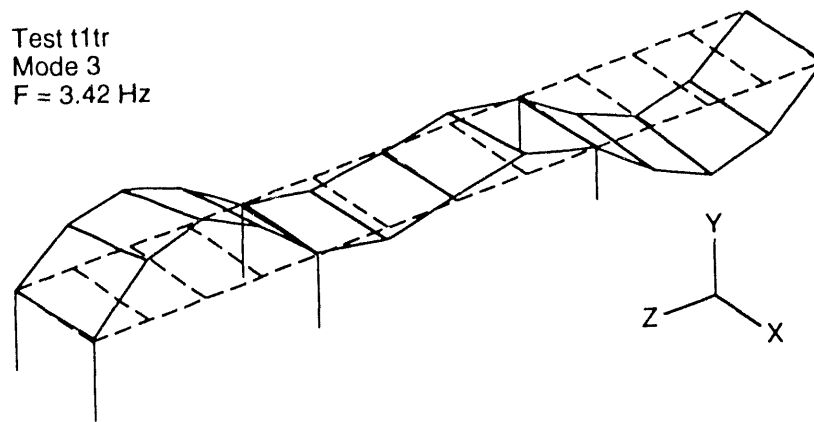
Fig. 41. Second flexural mode identified from ambient vibration data, test t1tr.

Test t1tr
Mode 4
F = 3.96 Hz
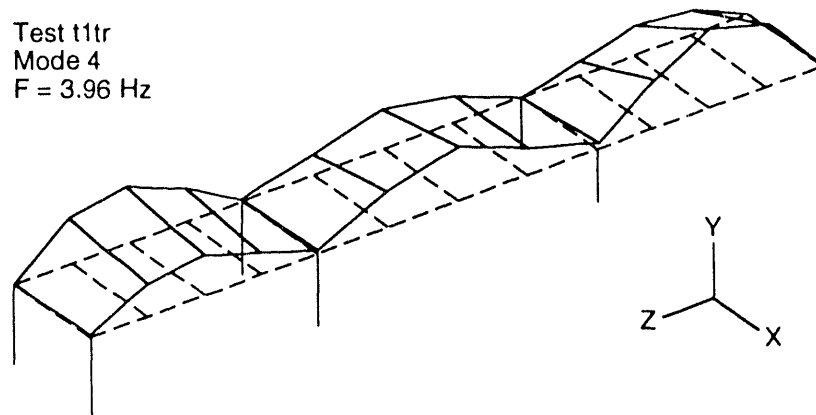
Fig. 42. Third flexural mode identified from ambient vibration data, test t1tr.

Test t1tr
Mode 5
F = 4.10 Hz
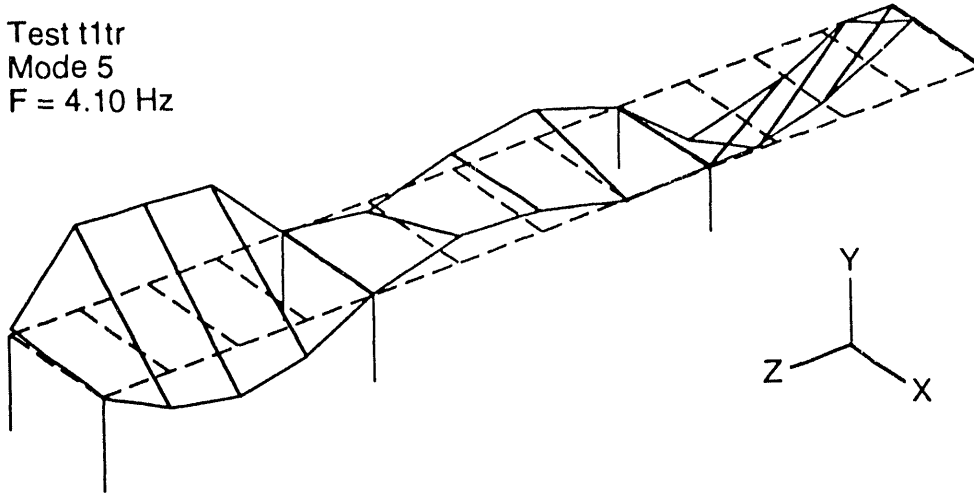
Fig. 43. Second torsional mode identified from ambient vibration data, test t1tr.

Test t1tr
Mode 6
F = 4.56 Hz
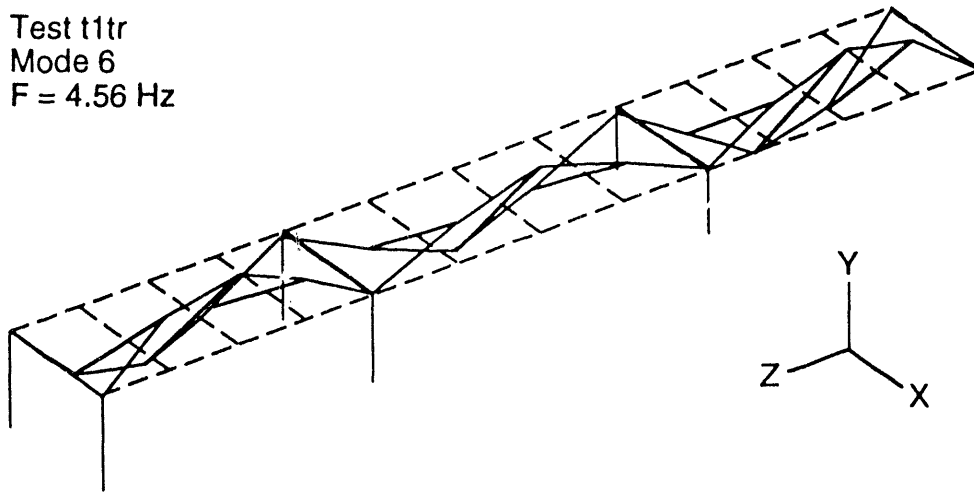
Fig. 44. Third torsional mode identified from ambient vibration data, test t1tr.

Table IV						
Resonant Frequencies and Modal Damping Values Identified from Ambient Vibration Response in the Global Y-Direction						
	Mode 1	Mode 2	Mode 3	Mode 4	Mode 5	Mode 6
Test	Freq. (Hz)/ Damp. (%)	Freq. (Hz)/ Damp. (%)	Freq. (Hz)/ Damp. (%)	Freq. (Hz)/ Damp. (%)	Freq. (Hz)/ Damp. (%)	Freq. (Hz)/ Damp. (%)
t1tr	2.39/ 1.28	2.92/ 1.18	3.42/ 1.00	3.96/ 0.94	4.10/ 1.58	4.56/ 1.56
t2tr	2.43/ 2.39	2.98/ 2.52	3.51/ 1.06	3.97/ 1.20	4.17/ 1.79	4.64/ 1.29
t10tr	2.42/ 1.15	2.93/ 1.18	3.46/ 0.85	3.99/ 0.70	4.12/ 0.59	4.61/ 0.97
t11tr	2.42/ 2.15	2.99/ 1.78	3.51/ 1.37	4.03/ 1.74	4.18/ 1.52	4.70/ 1.18
t15tr	2.52/ 1.28	3.04/ 0.38	3.53/ 0.89	4.10/ 1.08	4.17/ 0.92	4.71/ 0.60

A modal assurance criterion (MAC), sometimes referred to as a modal correlation coefficient (Ewins, 1989) was calculated to quantify the correlation between mode shapes measured during different tests and to check the orthogonality of mode shapes measured during a particular test. The MAC makes use of the orthogonality properties of the mode shapes to compare either two modes from the same test or two modes from different tests. If the modes are identical, a scalar value of one is calculated by the MAC. If the modes are orthogonal and dissimilar, a value of zero is calculated. The MAC that compares mode i and j has the form

$$MAC(i,j) = \frac{\left| \sum_{k=1}^{n} (\phi_j)_k (\phi_i)_k^* \right|^2}{\left(\sum_{k=1}^{n} (\phi_j)_k (\phi_j)_k^* \right) \left(\sum_{k=1}^{n} (\phi_i)_k (\phi_i)_k^* \right)}$$

(9)

where $(\phi)_k$ is an element of the mode shape vector. The value of the MAC does not actually quantify the correlation between modes. Ewins points out that, in practice, correlated modes will yield a value greater than 0.9 and uncorrelated modes will yield a value less than 0.05. The MAC is not affected by a scalar multiple.

The matrix listed below in Table V show the MACs that compares modes identified from data measured during test t1tr with itself, essentially an orthogonality check. This matrix shows that the six modes identified from this data are, in fact, orthogonal to each other. The matrix of MACs listed in Table VI compares the first six modes obtained from data measured during test t1tr and the first six modes measured during test t2tr. From this matrix it is evident that the same modes are being identified in each test. A complete set of matrices comparing the first six modes identified during various ambient vibration tests listed in Table III are given in Appendix B.

Table V

Modal Assurance Criteria: Test t1tr Compared with Test t1tr

Mode	1	2	3	4	5	6
1	1.000	0.006	0.001	0.005	0.001	0.001
2	0.006	1.000	0.003	0.000	0.002	0.004
3	0.001	0.003	1.000	0.004	0.015	0.003
4	0.005	0.000	0.004	1.000	0.218	0.027
5	0.001	0.002	0.015	0.218	1.000	0.024
6	0.001	0.004	0.003	0.027	0.024	1.000

Table VI

Modal Assurance Criteria: Test t1tr Compared with Test t2tr

Mode/Test	1/t2tr	2/t2tr	3/t2tr	4/t2tr	5/t2tr	6/t2tr
1/t1tr	0.999	0.011	0.001	0.001	0.000	0.000
2/t1tr	0.006	0.990	0.001	0.000	0.002	0.004
3/t1tr	0.001	0.012	0.994	0.025	0.018	0.001
4/t1tr	0.004	0.001	0.007	0.789	0.516	0.019
5/t1tr	0.001	0.006	0.026	0.645	0.845	0.017
6/t1tr	0.001	0.004	0.003	0.023	0.093	0.997

The following conclusions can be obtained from the ambient vibration results summarized in Tables III through VI, the mode shapes shown in Figs. 39-44, and the data summarized in Appendix B.

1. Ambient vibration from traffic provides an adequate source of input for identifying the dynamic properties of the bridge. An ambient vibration system identification method developed by SNL was applied to the inverse Fourier transform of the CPS measurements. The results obtained with this method were repeatable (resonant frequency values measured with traffic on the bridge did not vary more than 3%) and were independent of the selected reference measurement. This method allowed closely spaced modes such as modes 4 and 5 to be identified, and this method identified the associated modal damping values.

2. During test t15tr, when traffic was not on the bridge, generally higher frequencies were measured for each mode as compared to the results from tests when traffic was on the bridge. These higher frequencies are attributed to the reduced mass of the system that resulted from removing the traffic from the bridge.

3. Doubling the frequency resolution had little effect on the identified resonant frequencies. The increased frequency resolution did improve the ability to identify the closely space modes. Damping values were particularly sensitive to the increased frequency resolution and these values appeared to decrease with the increased frequency resolution.

65

4. Closely spaced modes, such as modes 4 and 5, showed strong coupling through the MAC values.

5. The modes are lightly damped with modal damping values ranging from 0.4 to 2.59 %, and can be accurately approximated as real modes. Phase angles were typically close to either 0 or 180 degrees.

6. Background sources of ambient vibration from traffic on the adjacent bridges were of sufficient magnitude that the dynamic properties of the structure could be determined by measuring the response to this excitation source as was done in test t15tr.

F. Forced Vibration (undamaged)

From August 31, through September 2nd, 1993 a series of forced vibration tests were conducted on the undamaged bridge. Eastbound traffic had been transferred to a new bridge just south of the one being tested. The westbound traffic continued on the original westbound bridge. Sandia National Laboratory provided a hydraulic shaker that generated the measured force input. Excitation from traffic on the adjacent bridges could be felt when the shaker was not running. The load cell located between the Sandia hydraulic actuator and reaction mass showed that the vibration from traffic on the adjacent bridges, transferred through the ground to the piers and abutment of the bridge being tested, caused the bridge deck to put a peak force of 150 lb. into the reaction mass.

Demolition of the concrete deck at the west end of the bridge was started before the forced vibration tests and continued while they were underway proceeding to the third span in from the west end as shown in Fig. 9. Portions of the foundation around the north side of the east abutment were removed to build an access ramp for construction work. The amount of material removal can be seen in Fig. 45. Both the demolition and the construction of the access ramp can be viewed as changing the boundary conditions of the test structure. Forced vibration measurements taken before and after the access ramp was constructed showed no changes in the resonant frequencies of the structure. Because forced vibration measurements were not made before the demolition of the west end began, the extent of this change can only be quantified by comparing the results of the forced vibration tests to the results from the previous ambient vibration tests. Temperature ranged from morning lows of 56 degrees F to afternoon highs of 80 degrees F. The east end of the south girder was observed to no longer be in contact with the concrete on the top of the abutment. Wind, although not measured, was not considered significant during these tests.

The Sandia shaker consists of a 21,700 lb. reaction mass supported by three air springs resting on top of 55 gallon drums filled with sand. A 2200 lb. hydraulic actuator bolted under the center of the mass and anchored to the top of the bridge deck provided the input force to the bridge. A schematic of the shaker is shown in Fig. 46, and Fig. 47 shows the shaker in place on the bridge. A portable 460 volt, three phase diesel generator provided power to the hydraulic pump necessary to operate the actuator. A water truck supplied by the NMSH&TD provided cooling water for the power supply. The shaker could produce either a random or stepped sine input. A random signal generator was used to produced a uniform random signal that was

Fig. 45. Material removed around the east abutment.
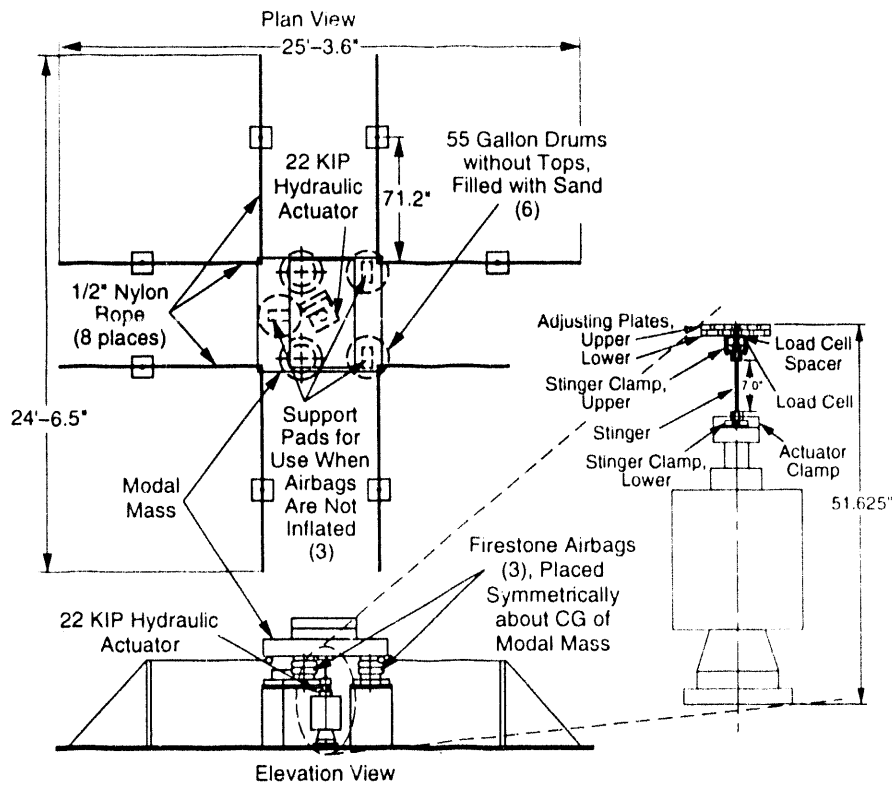
Fig. 46. Schematic depiction of the Sandia Shaker.

67

Fig. 47. The Sandia shaker in place on the I-40 bridge.

band-passed between 2 and 12 Hz before inputting the signal to an amplifier. A sinusoidal signal generator provided the stepped sign input. The amplifier gain was controlled manually to provide 500 lb. peak sinusoidal force input or an approximately 2000 lb. peak random force input. An accelerometer mounted on the reaction mass was used to measure the force input to the bridge. This indirect force measurement gives the total force transferred to the bridge through the 55 gallon drums as well as the actuator. The shaker was located over the south plate girder directly above point S-3 in Fig. 31. The accelerometer used to measure force was oriented such that a positive force corresponded to the positive global Y direction shown in Fig. 31.

   1. MEE-13 forced vibration tests. Forced vibration tests were conducted using a random input so that MEE-13 personnel could perform experimental modal analyses of the bridge. In this context experimental modal analysis refers to the procedure whereby a measured excitation (random, sine, or impact force) is applied to a structure and the structure's response (acceleration, velocity, or displacement); is measured at discrete locations that are representative of the structure's motion. Both the excitation and the response time histories are transformed into the frequency domain so that modal parameters (resonant frequencies, mode shapes, modal damping) can be determined by curve fitting a Laplace domain representation of the equations of motion to the measured frequency domain data (Ewins, 1989).

a. Experimental procedure and equipment. The data acquisition system, mounting blocks, cabling, accelerometers, and generator used for the forced vibration tests were identical to those used for the ambient vibration tests. An additional input module was used to monitor the accelerometer located on the reaction mass. Because there was no traffic on the bridge, the double-backed tape used to mechanically isolate the accelerometers from high frequency inputs caused by traffic impact was not used during these tests.

Sampling parameters were specified so that responses with frequency content in the range of 0 - 12.5 Hz could be measured. All computed frequency domain quantities (power spectra, cross-power spectra, FRFs, and coherence functions) were based on 30 averages with no overlap. A Hanning window was applied to all time samples used in these calculations. Pre-test checks showed that several accelerometers were not functioning properly. Accelerometers at locations S-1, S-6, and S-11 were replaced with Endevco Model 7751-500 integrated circuit, piezoelectric accelerometers supplied by SNL. These accelerometers had a nominal sensitivity of 500 mV/g, a specified frequency range of 0.4 to 1500 Hz, and a amplitude range of ± 10 g's. Because of their larger dimensions, these accelerometers had to be attached to the aluminum mounting blocks with the double - backed tape previously used for mechanical isolation during the ambient vibration tests. It is of interest to note that the three accelerometers that were replaced and their associated wiring responded properly when each was tested with a small hand held shaker adjacent to the mounting block. When returned to the mounting block, they continued to malfunction. Also, when the malfunctioning ones were replaced by similar PCB 336C accelerometers, the replacement accelerometers would not work at these locations either. It is believed that increased surface and air moisture caused by recent rain storms coupled with leakage and random electrical noise caused these problems. Unlike the PCB units, the Endevco replacements have their cases grounded to the mounting surface

b. Results. A typical 16-s response time history measured at location S-7 is shown in Fig. 48 for comparison with the time history measured during the ambient vibration tests, Fig. 35. These figures show that the level of excitation during the forced test was less than the levels produced by the large trucks passing the bridge, but was higher than the level of excitation produced by cars.

Figure 49 shows the power spectrum of the force input from the Sandia shaker. From this plot it is evident that the input excites frequencies in the range of 2 to 10 Hz. The power spectrum of the response measured at location S-3 is shown in Fig. 50. This function can be compared to a similar spectrum calculated from ambient vibration data and shown in Fig. 37. The similarity of these two plots and the flat input power spectrum indicate that the peaks in both tests correspond to resonances of the structure rather than frequencies where the energy content of the input is strong.

Coherence functions can be used to determine if sources of excitation other than the Sandia shaker are significantly contributing to the measured response. The
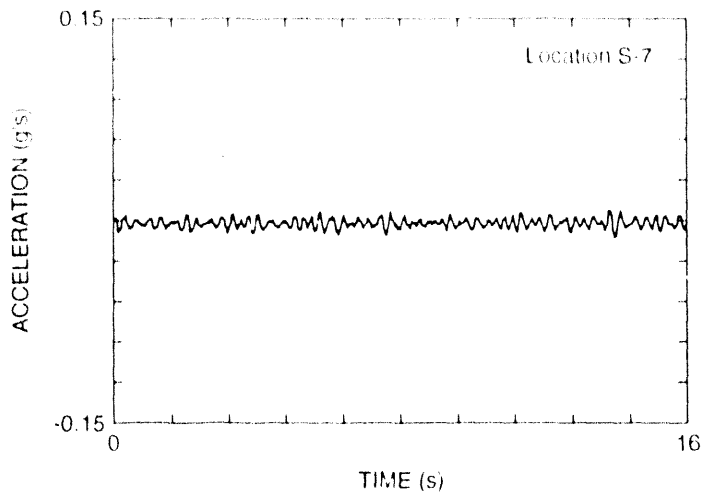
Fig. 48. Time history measured at location S-7 during the undamaged forced vibration test.
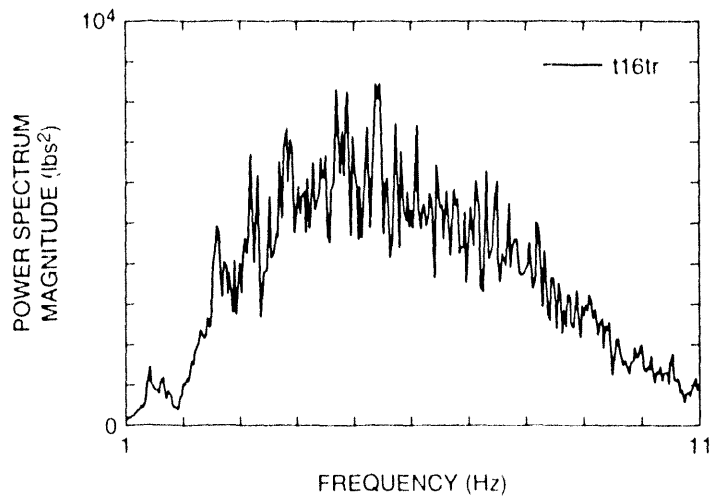
Fig. 49. Power spectrum of the input force from the Sandia shaker measured during the undamaged forced vibration test.
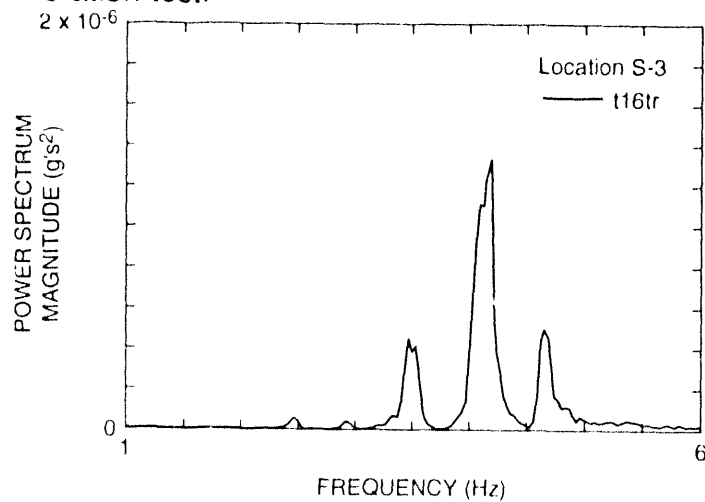
Fig. 50. Power spectrum of the response measured at location S-3 during the undamaged forced vibration test.

coherence function, $\gamma_{xy}^2(\omega)$, is defined as

$$\gamma_{xy}^2(\omega) = \frac{\left|G_{xy}(\omega)\right|^2}{G_{xx}(\omega)G_{yy}(\omega)}.$$

(10)

For an ideal linear system the coherence function will yield a value of one. If the response is completely unrelated to the input, this function will yield a value of zero. Values between zero and one result when there is extraneous noise in the measurements, the structure is responding in a nonlinear manner, or sources of input other than the one being monitored are causing the response. For lightly damped structures, low coherence can also occur around resonances when the system response is calculated from a series of time windows as was done in these tests. The response in a particular window is strongly dependent on energy input during the previous window, particularly at resonance, and this response will be uncorrelated with input measured during the current window.

A plot of the coherence function for location S-3, Fig. 51 shows poor coherence up to 2 Hz that results from attenuation of the input and response signals caused by the AC coupling filter. From 2 to 11 Hz the coherence is close to unity except at the resonant frequencies of the structure. These results imply that the structure is responding in a linear manner and the response is caused primarily by the measured input. Coherence functions for measurements made at N-7 and N-11, Figs 52 and 53, show decreasing coherence as the measurement location is located further from the excitation source. This reduction in coherence is caused by the inputs that result from extraneous sources of noise (traffic on the adjacent spans) causing a greater portion of the measured response at locations further from the excitation source. The effects of the extraneous inputs are minimized by the averaging process used to calculate the FRFs.

Figure 54 shows a FRF that was measured at location N-7 during the forced vibration test. A rational-fraction polynomial global curve-fitting algorithm in a commercial modal analysis software package (Structural Measurements Systems, 1987) was used to fit the analytical models to the measured FRF data and extract resonant frequencies, mode shapes and modal damping values. Figures 55 through 60 shows the first six modes of the undamaged bridge identified from these data. A comparison of these figures with Figs 39 through 44 show that the dynamic properties identified from the forced vibration tests are similar to those identified by the ambient vibration tests.

Table VII compares the resonant frequencies and modal damping values determined from the ambient vibration tests with those determined during the forced vibration tests. From this table it is evident that the dynamic properties measured during the forced vibration test fall within the range of those measured during the various ambient vibration tests. The dynamic properties measured during the forced vibration tests are nearly identical to those measured during ambient vibration test t15tr that was conducted immediately before the forced vibration test.

71
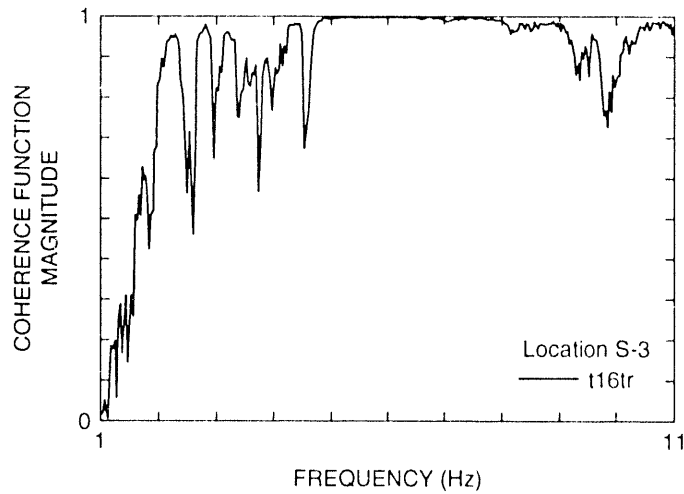
Fig. 51. Coherence function for location S-3 measured during undamaged forced vibration test t16tr
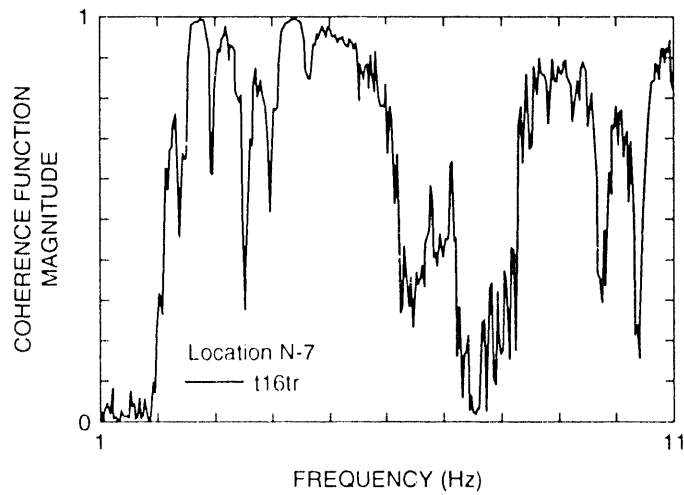
Fig. 52. Coherence function for location N-7 measured during undamaged forced vibration test, t16tr.
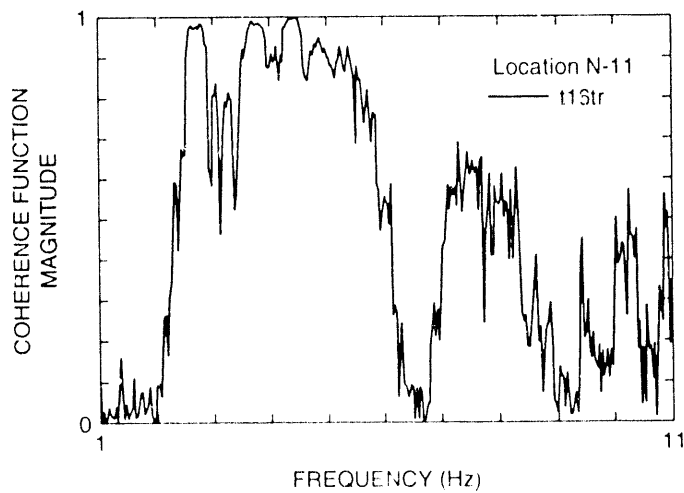
Fig. 53. Coherence function for location N-11 measured during undamaged forced vibration test t16tr.
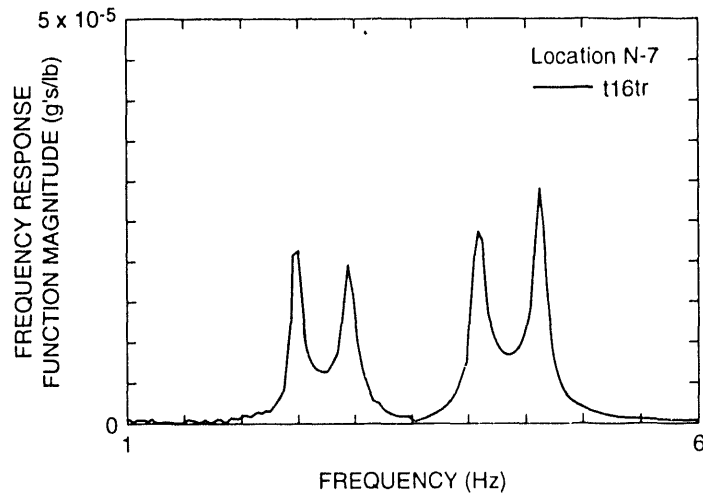
Fig. 54. Frequency response function measured at location N-7 during the undamaged forced vibration test.

Test t16tr
Mode 1
F = 2.48 Hz
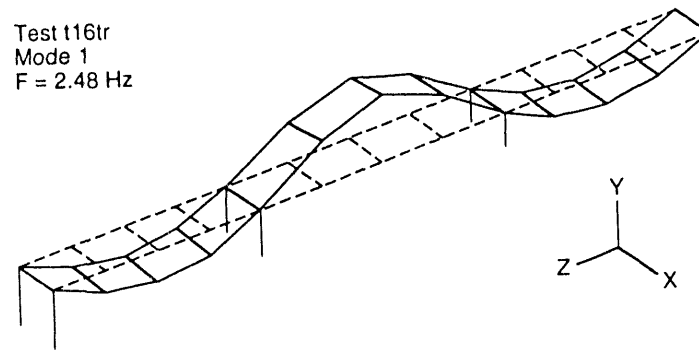
Fig. 55. First flexural mode identified from undamaged forced vibration data, test t16tr.

Test t16tr
Mode 2
F = 2.96 Hz
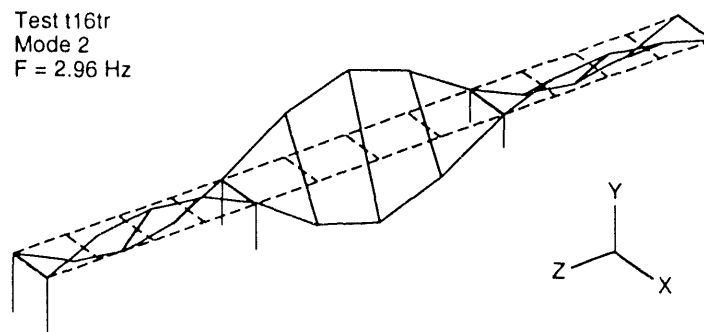
Fig. 56. First torsional mode identified from undamaged forced vibration data, test t16tr.

73
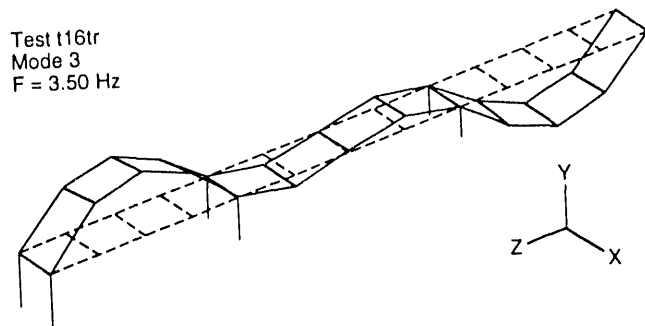
Fig. 57. Second flexural mode identified from undamaged forced vibration data, test t16tr.
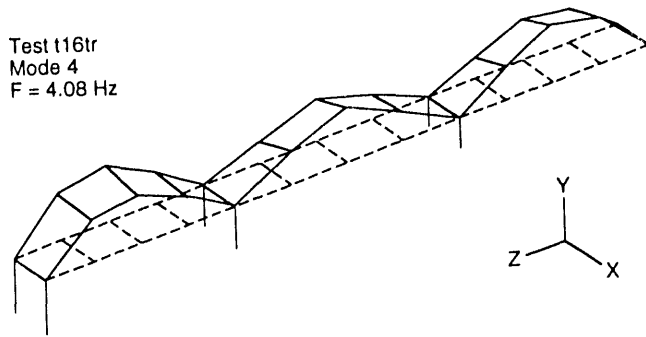
Fig. 58. Third flexural mode identified from undamaged forced vibration data, test t16tr.
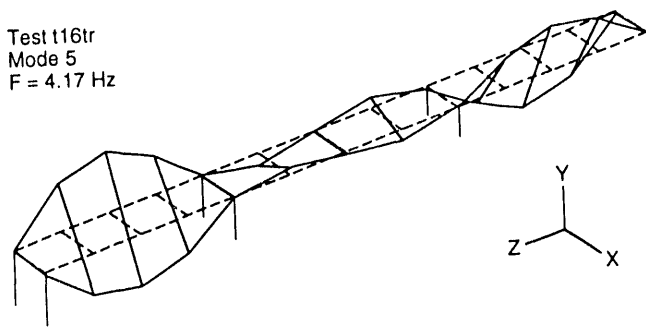
Fig. 59. Second torsional mode identified from undamaged forced vibration data, test t16tr.
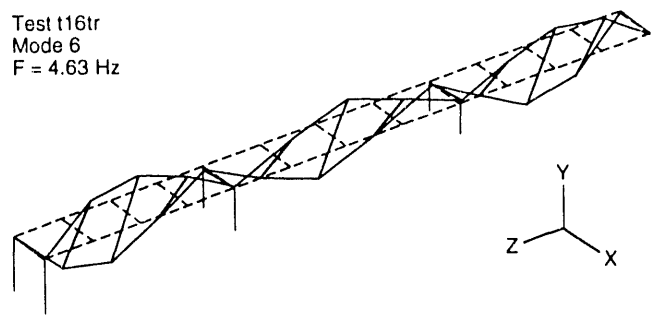
Fig. 60. Third torsional mode identified from undamaged forced vibration data, test t16tr.

Table VII						
Resonant Frequencies and Modal Damping Values Identified from Ambient Vibration Response Compared with Similar Quantities Identified from Forced Vibration Tests						
	Mode 1	Mode 2	Mode 3	Mode 4	Mode 5	Mode 6
Test	Freq. (Hz)/ Damp. (%)	Freq. (Hz)/ Damp. (%)	Freq. (Hz)/ Damp. (%)	Freq. (Hz)/ Damp. (%)	Freq. (Hz)/ Damp. (%)	Freq. (Hz)/ Damp. (%)
t1tr (ambient)	2.39/ 1.28	2.92/ 1.18	3.42/ 1.00	3.96/ 0.94	4.10/ 1.58	4.56/ 1.56
t2tr (ambient)	2.43/ 2.39	2.98/ 2.52	3.51/ 1.06	3.97/ 1.20	4.17/ 1.79	4.64/ 1.29
t10tr (ambient)	2.42/ 1.15	2.93/ 1.18	3.46/ 0.85	3.99/ 0.70	4.12/ 0.59	4.61/ 0.97
t11tr (ambient)	2.42/ 2.15	2.99/ 1.78	3.51/ 1.37	4.03/ 1.74	4.18/ 1.52	4.70/ 1.18
t15tr (ambient)	2.52/ 1.28	3.04/ 0.38	3.53/ 0.89	4.10/ 1.08	4.17/ 0.92	4.71/ 0.60
t16tr (forced)	2.48/ 1.06	2.96/ 1.29	3.50/ 1.52	4.08/ 1.10	4.17/ 0.86	4.63/ 0.92

The MAC can be applied to compare the mode shapes from the forced vibration tests with the modes determined during the ambient vibration testing. Table VIII shows such a comparison with the ambient vibration mode shape data obtained during test t1tr. Table VIII shows that similar mode shapes are being identified in each case. MAC comparisons with other ambient vibration mode shapes are summarized in Appendix C. The matrices in Appendix C show that the mode shapes determined during the ambient vibration tests are similar to those determined during the forced vibration test. Modes 4 and 5, which are closely spaced and which were difficult to identify during several ambient vibration tests did not always show good correlation with the modes determined during the forced vibration tests.

Table VIII						
Modal Assurance Criteria: Mode Shapes Identified from Ambient Vibration Test t1tr Compared with Mode Shapes Identified from Forced Vibration Tests on the Undamaged Structure, Test t16tr						
Mode/test	1/t16tr	2/t16tr	3/t16tr	4/t16tr	5/t16tr	6/t16tr
1/t1tr	0.989	0.008	0.000	0.004	0.002	0.001
2/t1tr	0.004	0.985	0.000	0.001	0.001	0.004
3/t1tr	0.002	0.003	0.984	0.000	0.009	0.001
4/t1tr	0.005	0.002	0.001	0.901	0.102	0.009
5/t1tr	0.000	0.001	0.005	0.066	0.917	0.005
6/t1tr	0.001	0.003	0.002	0.004	0.004	0.984

c. Data acquired for Texas A&M. Additional data were acquired for investigators at Texas A&M who have developed very sensitive damage identification procedures based on changes in the mode shapes of a structure. Based on instructions received from these investigators, 11 Endevco 7751-500 accelerometers were placed in the global Y direction at a nominal spacing of 16 ft along the midspan of the north plated girder. All accelerometers were located at midheight of the girder. The actual spacing of these accelerometers is shown in Fig. 61 . To accommodate the dimensions of these accelerometers, aluminum mounting blocks 1.5 inches long were fabricated by dental cementing an aluminum plate to the base of the 1 in square blocks. These blocks were then mounted in a similar fashion as the blocks used for the ambient and forced vibration tests. When the dental cement cured, some of the blocks were no longer vertical. X-3 was tilted 3.3 degrees to the east, X-5 was tilted 1.2 degrees to the west, X-8 was tilted 1.2 degrees to the east, and X-10 was tilted 1.8 degrees to east. The same data acquisition system, similar wiring, and identical sampling parameters as those used for the forced vibration test were again used when acquiring data for Texas A&M.

Mode shapes were determined from cross-power spectra of the various accelerometer readings relative to accelerometer X-3 shown in Fig. 61. The amplitude of a mode corresponding tɔ location X-3 was obtained from the power spectrum of the signal measured at this location. The mode shape data obtained from this set of accelerometers for the first three modes of the bridge in the undamaged state are tabulated in Appendix D.

2. P-10 forced vibration tests. There were two main motives for doing this experiment, firstly to test the remote measurement capability of these sensors, and secondly, to compare the results of single-point remote measurements with the results of the conventional modal testing measurements that were made by MEE-13.

The forced vibration tests carried out by P-10 used the microwave interferometer displacement detection sensors described in Sections III. A and III. D., and a variation of the homodyne detection scheme also discussed in Section III. A. A computer controlled sine wave generator provided a fixed frequency harmonic input to drive the SNL hydraulic shaker. The amplitude of the vertical response of the plate girder's bottom flange was measured remotely, at only two places, Pts. N-6 and S-6 in Fig. 31, by the microwave interferometers. For a given excitation frequency, the response at that frequency was extracted by the homodyne detection system. The computer then stepped to another frequency to repeat the measurement. This measurement method has very little noise associated with it because large excitation amplitudes can be applied at each frequency and the homodyne system provides narrow band detection at that frequency. The response of the bridge was measured over a frequency range of 2 to 5 Hz, in steps of 0.05 Hz. The accumulated data set was then fit with an analytical function (representing the sum of the real part of Fourier spectra of SDOF system's response to a harmonic excitation plus a term to account for crosstalk between the drive signal and the measured response) to extract the resonant frequencies and modal damping associated with each resonance peak.
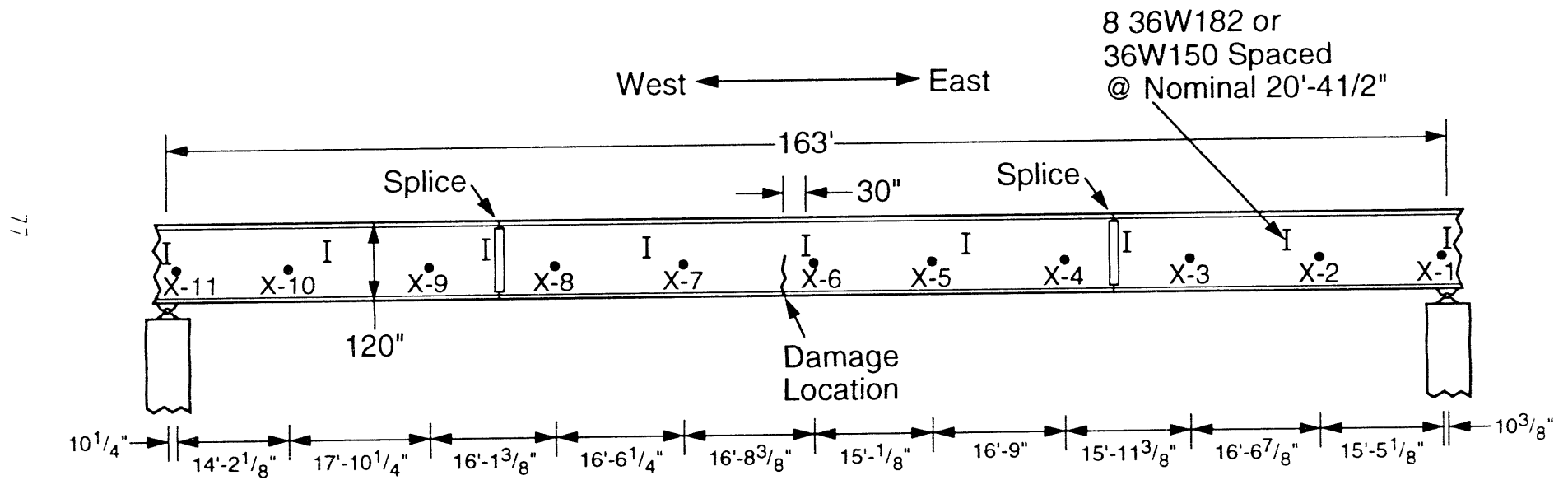
Fig. 61. Locations of accelerometers used to measure responses for Texas A&M.

a. Experimental procedure and equipment. Data for these measurements were acquired at only two points on the bridge structure as discussed in the previous section. These points were selected for convenience, as they are directly above the access embankment that permitted the microwave dishes to be set up easily.

Each microwave interferometer consisted of a 24" diameter aluminum parabolic dish, with a 10.25 GHz Gunn diode transceiver unit mounted near the focus. Figure 62 shows the microwave interferometer supported by a 55 gallon drum under the plate girder whose displacement was being monitored. The optical axis of the system is aligned with the aid of a bubble level so that the axis points at the bottom of the girder flange, and is perpendicular to it. The Gunn diode source is positioned so the focus of the microwaves is on the flange. Microwaves reflected from the flange are focused by the dish back into the transceiver where they interfere with the emitted waves and form a standing wave pattern. The amplitude of the standing wave, which is detected by a Schottky diode in the transceiver, depends on the cavity length. The cavity length is the distance from the transceiver to the bridge. When the bridge moves vertically, the signal amplitude changes as the cavity length changes. This measurement method is entirely analogous to optical interferometry. To stay on a monotonic part of the interference pattern, adjustments were made to the phase of the pattern by changing the frequency of the source a small amount. This change was accomplished by putting a tuning voltage on the varactor diode capacitor which is also part of the transceiver. With this adjustment a good measurement of the cavity length change over a dynamic range of about 6 mm was obtained. This system was able to measure displacement response over a frequency range from DC to several kHz.

Fig. 62. Microwave interferometer supported by a 55 gallon drum.

The signal from the interferometer was amplified and then digitized using an Analogic LSDAS-16 16-bit plug-in ADC card. The computer also has a programmable, high accuracy sine wave generator board which creates the input signal, under software control. This board is manufactured by Quatro Corp. who has a manufacturing license for the technology developed by P-10. The digitized signal, which is the time domain amplitude signal of the plate girder, can then be Fourier transformed to obtain a frequency spectrum (which was done in earlier tests, see Section III. D.) or used in the homodyne detection mode (which was also done earlier, see Section III. A.).

A complete scan from 2 Hz to 5 Hz in 0.05 Hz steps took approximately 1.5 hours and was fully automatic. At the end of the scan the plot of the vertical amplitude response against frequency was obtained for the two specified points on the bridge. The equipment for this experiment and the software was produced at LANL, with the exception of some hardware components which were manufactured by Quatro Corp.

b. Results. The plots of the scans for the North and South girders are shown in Figs. 63 and 64, respectively, and the identified resonant frequencies and modal damping values are summarized in Table IX. Although mode shapes can not be extracted from these measurements, these data can be fit with the analytical model discussed above to extract the resonant frequencies and modal damping. Also, the fit can be used to reconstruct some phase information and determine the relative phase of motion caused by each resonance. This phase information was determined by examining the interference between close resonances. This method allows the relative motions of the North and South girders at the measured points to be compared, which provides some mode shape information.

The analytical function that was fit to the measured data (by minimizing a chi-squared error term) was

$$F(\omega) = \text{Re}\left[\sum_{n=1}^{6} \frac{A_n e^{i\omega t}}{\omega_n^2 - \omega^2 + i\omega^2 4\zeta^2 \omega_n^2} + A_0 e^{i\omega t}\right], \tag{11}$$

where $F(\omega)$ = the real portion of the measured displacement Fourier spectrum,

ω_n = resonant frequency,

ζ = modal damping, and

A_n = the amplitude of the spectrum associated with ω_n.

A_0 is a background amplitude at ω, such as might occur with crosstalk between the harmonic input signal and the measured response signal.

The phase information only returns an "in phase" (+) or "opposite phase" (-) with the preceding resonance. It was assumed (and subsequently verified by the mode shapes calculated from measured response data by MEE-13) that the first resonance has (+) phase for both the North and South girders. All relative phase information agreed with that obtained by MEE-13.

Fig. 63. Fourier spectrum of the north girder displacement response obtained with the microwave interferometer during sine-sweep tests on the undamaged bridge.

Fig. 64. Fourier spectrum of the south girder response obtained with the microwave interferometer during sine-sweep tests on the undamaged bridge.

Table IX					
Resonance Frequencies and Modal Damping Identified from the Fits of Analytical Models to the Undamaged Data Measured with the Microwave Interferometer					
Mode 1	Mode 2	Mode 3	Mode 4	Mode 5	Mode 6
Freq. (Hz)/ Damp. (%)	Freq. (Hz)/ Damp. (%)	Freq. (Hz)/ Damp. (%)	Freq. (Hz)/ Damp. (%)	Freq. (Hz)/ Damp. (%)	Freq. (Hz)/ Damp. (%)
2.48/ 0.91	2.98/ 1.61	3.53/ 3.19	4.12/ 0.79		4.67/ 0.65

The curve-fitting routine was unable to distinguish modes 4 and 5, primarily as a result of the frequency resolution, but partially as a result of a lack of sophistication in the curve-fitting algorithm.

3. Comparison of different vibration measurement methods. For the modes that could be identified with the microwave interferometer (modes 1-3, 6), the resonant frequencies measured with the interferometer agree well with corresponding values identified by MEE-13's more conventional modal analysis methods as listed in Table VII (all modes showed less than 1 percent difference). Damping values, which are typically a difficult parameter to identify, did not compare well with values obtained by MEE-13. This lack of agreement is attributed to the curve fitting algorithm used with the microwave interferometer data and frequency resolution of these data, and does not reflect an inherent inability of the interferometer to measure the widths of the resonance peaks. The limited mode shape information (phase values (+)/(-)) also agree with the mode shape information obtained by MEE-13 and shown in Figs 55 through 60.

From these results it is apparent that the modal information being obtained with the interferometer is as accurate as that being obtained with the conventional accelerometers. These interferometers cost approximately $200 (U.S., 1993), which is about the same cost as the accelerometers that were used by MEE-13. Complete mode shape data can be obtained if more interferometers were placed along the length of the beam at similar locations as the accelerometers (see Fig. 31). An obvious improvement to the data acquisition from the interferometers would be to feed a calibrated analog displacement - time history from the interferometer directly into MEE-13's data acquisition system where this signal could be digitized and analyzed with the more refined commercial modal analysis and digital signal processing software available on this system. The non-contact nature of the interferometers offers many advantages over conventional accelerometers, particularly for testing large civil engineering structures.

G. Forced Vibration (Damaged)
From September 3 through 11, 1993 four different levels of damage were introduced into the middle span of north plate girder. Forced vibration tests similar to those done on the undamaged structure were repeated after each level of damage had been introduced. The information obtained form these tests was subsequently used to develop, refine, and experimentally verify damage detection schemes. Weather conditions during these tests were similar to those reported for the forced

vibration tests. Background sources of vibration were also similar. No new demolition of the bridge was done during this time period and work on the access ramp near the east abutment was complete before these tests started.

1. Damage Description. The damage that was introduced was intended to simulate fatigue cracking that has been observed in plate girder bridges. This type of cracking results from out of plane bending of the web and usually begins at welded attachments to the web such as the seats supporting the floor beams. Four levels of damage were introduced to the middle span of the north plate girder close to the seat supporting the floor beam at midspan. Damage was introduced by making various torch cuts in the web and flange of the girder. The first level of damage consisted of a two-foot-long cut through the web approximately 3/8-in-wide centered a midheight of the web. Next, this cut was continued to the bottom of the web . During this cut the web, on either side of the cut, bent out of plane approximately 1 in. The flange was then cut half way in from either side directly below cut in the web. Finally, the flange was cut completely through leaving the top 4 ft of the web and the top flange to carry the load at this location. The various levels of damage are shown in Figs. 65 through 68.
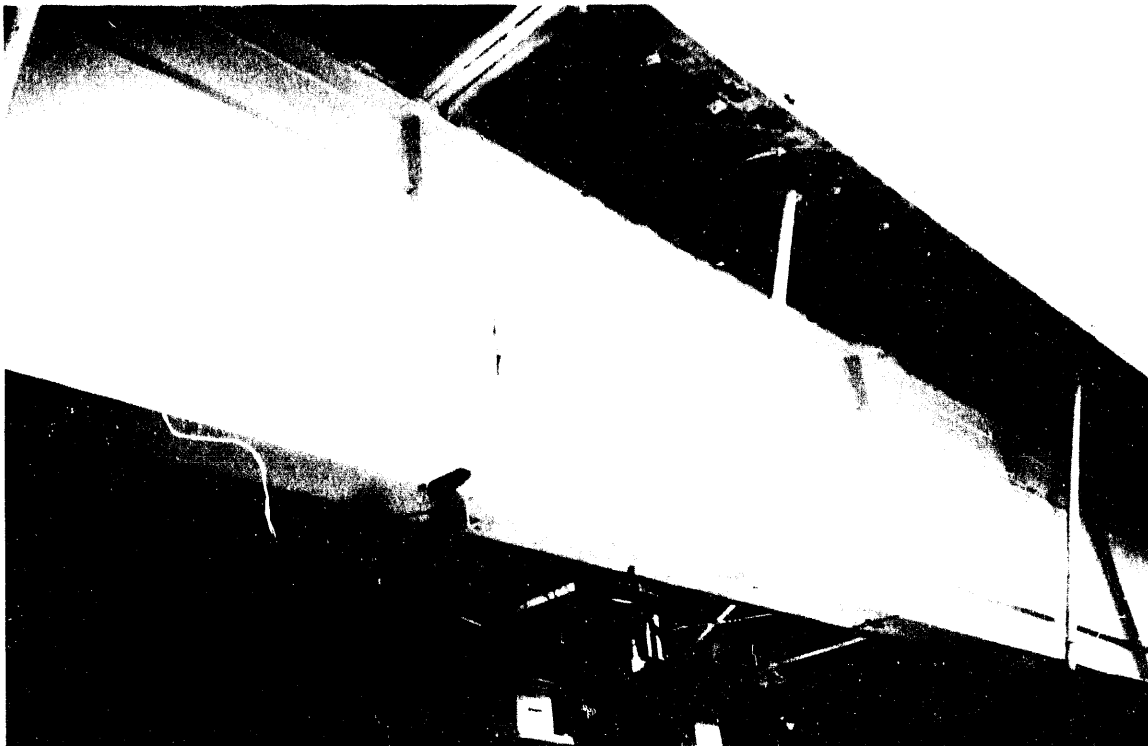
Fig. 65. First Stage of Damage: Two-foot cut at the center of the web.
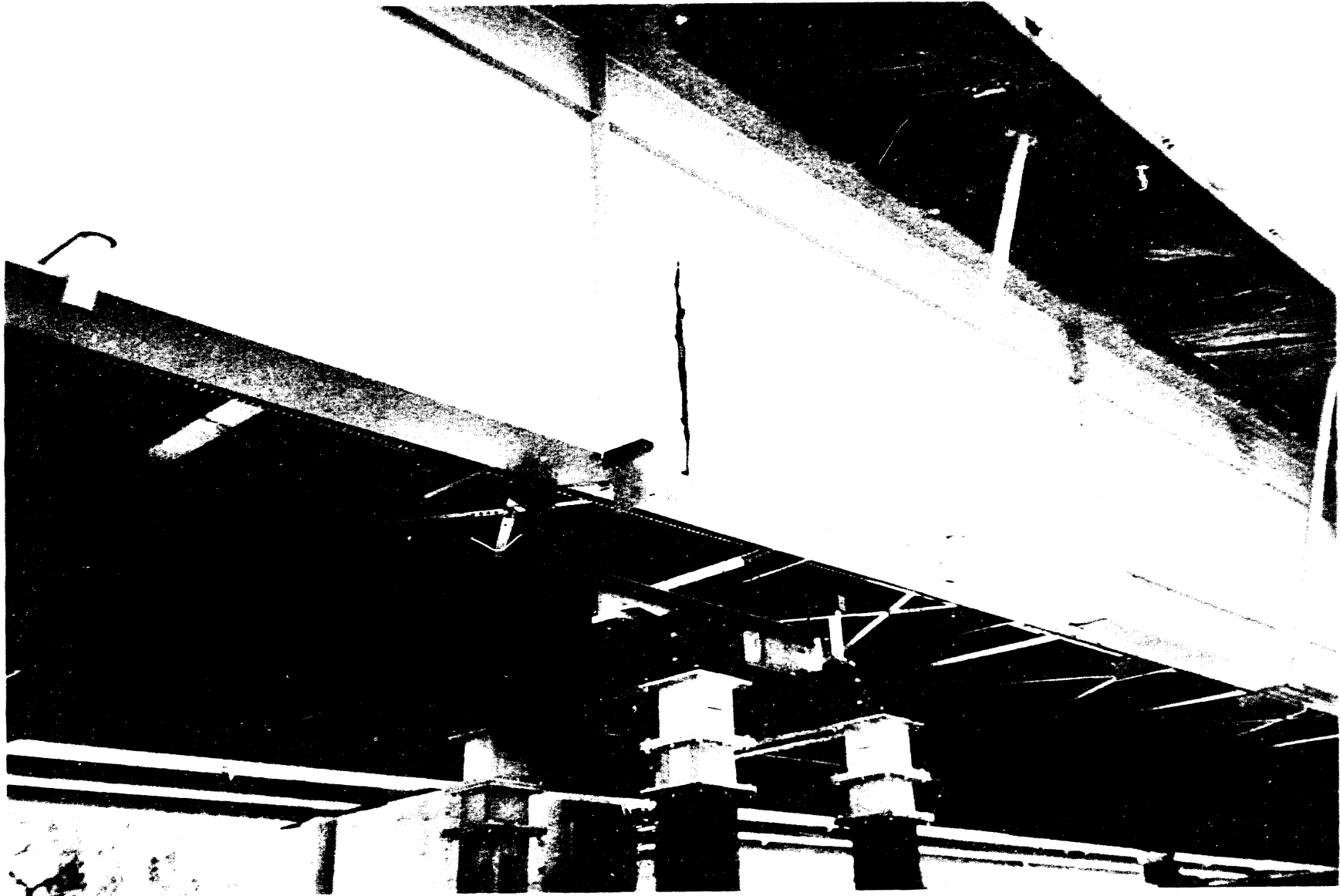
Fig. 66. Second Stage of damage: Six-foot cut from the center of the web to the bottom flange.

Fig. 67. Third Stage of Damage: Six foot cut in the web and cuts through half the bottom flange on either side of the web.

2. MEE-13 forced vibration tests (damaged). Experimental modal analyses were repeated after each level of damage had been introduced. The experimental procedures and data acquisition equipment used were identical to those used for the undamaged forced vibration tests summarized in section III.F.1.a. Accelerometer N - 10 had to replaced with an Endevco 7751-500 before the test that was performed after the cuts in the outer edge of the flange were made. The dynamic range for the accelerometer and force readings had to be adjusted during the testing sequence. Table X summarizes the forced vibration tests that were performed.

Centimeter

1   2   3   4   5   6   7   8   9   10   11   12   13   14   15   mm

1   2   3   4   5

Inches

1.0

2.8   2.5
3.2   2.2
3.6
4.0   2.0

1.1

1.8

1.25   1.4   1.6
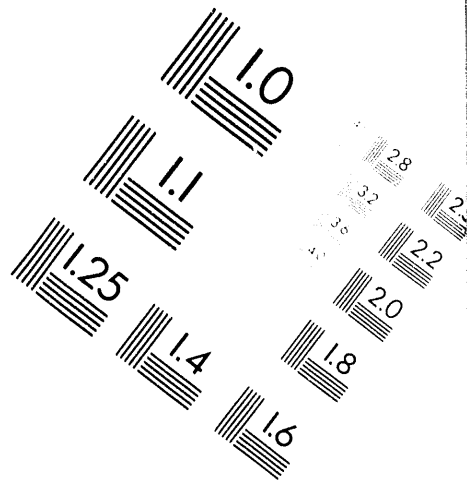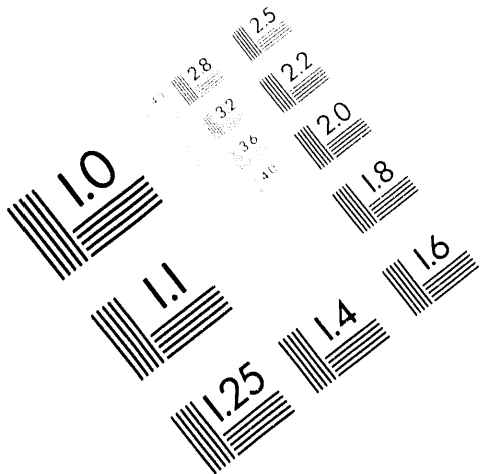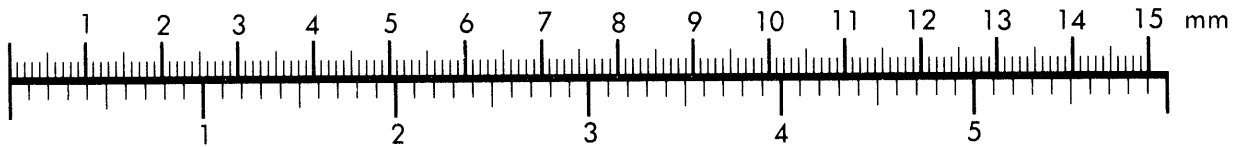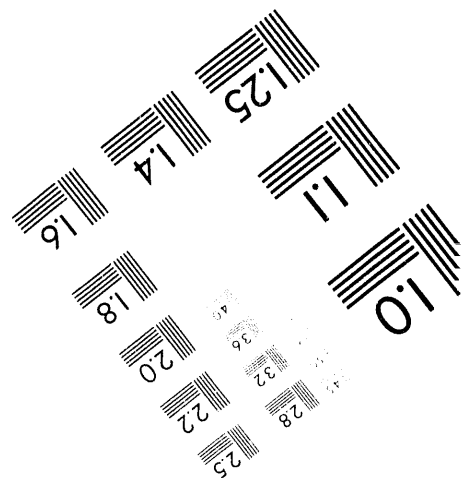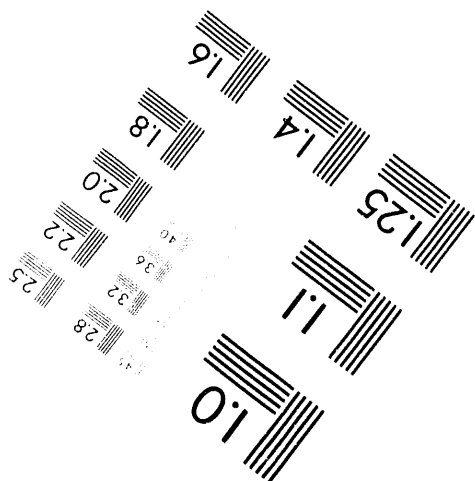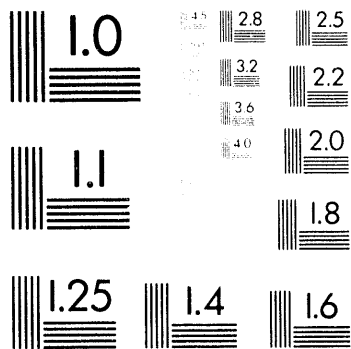
MANUFACTURED TO AIIM STANDARDS

BY APPLIED IMAGE, INC.
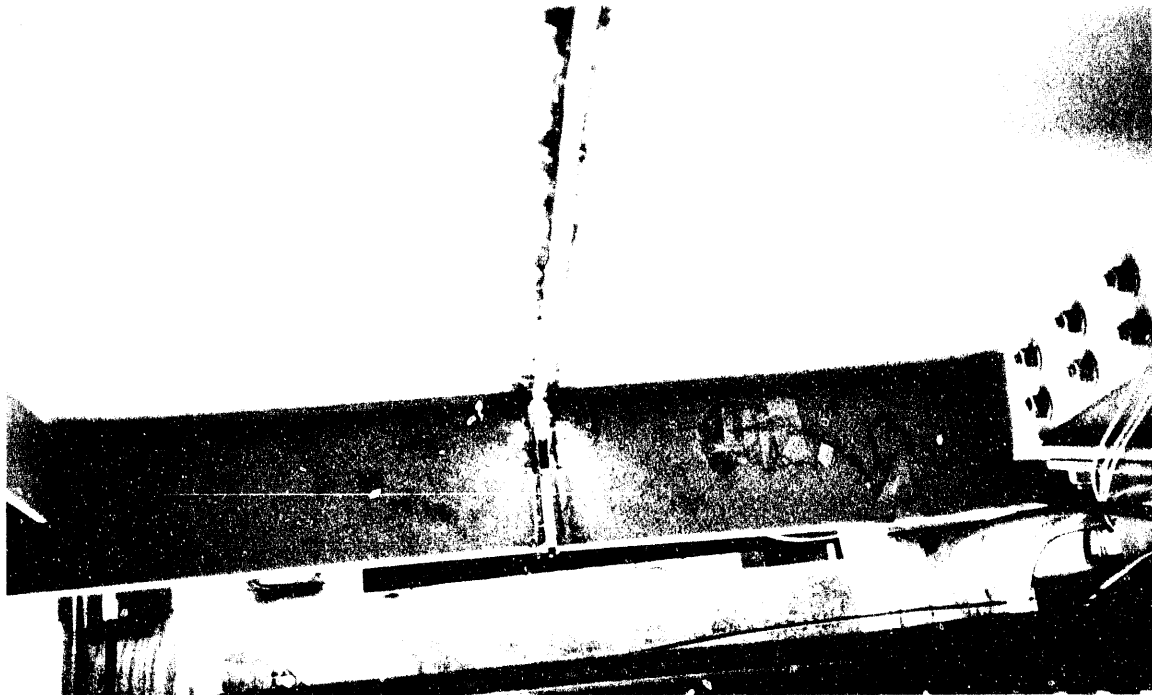
Fig. 68. Fourth Stage of Damage: Six -foot cut in the web and cut through the entire bottom flange.

Table X

<table>
<tr><td colspan="6">Summary of Forced Vibration Tests</td></tr>
<tr><td>Test Designation</td><td>Frequency Range (Hz)</td><td>No. of Averages</td><td>Date/Time</td><td>Dynamic Range Accelerometers / Force Transducer</td><td>Damage Description</td></tr>
<tr><td>t16tr</td><td>0-12.5</td><td>30</td><td>Sept. 2, 11:08 - 11:33 AM</td><td>1 Vp, 3.16 Vp</td><td>undamaged</td></tr>
<tr><td>t17tr</td><td>0-12.5</td><td>30</td><td>Sept. 2, 2:25 - 2:40 PM</td><td>1 Vp, 3.16 Vp</td><td>2 ft. cut at the center of the web</td></tr>
<tr><td>t18tr</td><td>0-12.5</td><td>30</td><td>Sept. 3, 12:00 - 12:46 PM</td><td>2 Vp, 6.31 Vp</td><td>6 ft cut in the web to the bottom flange</td></tr>
<tr><td>t19tr</td><td>0-12.5</td><td>30</td><td>Sept. 7, 9:32 - 9:55 AM</td><td>2 Vp, 6.31 Vp</td><td>bottom 6 ft of the web and half of the flange cut</td></tr>
<tr><td>t22tr</td><td>0-12.5</td><td>30</td><td>Sept. 8, 9:52 - 10:17 AM</td><td>3.98 Vp, 6.31 Vp</td><td>bottom 6 ft of the web and entire flange cut</td></tr>
</table>

a. Results. Figure 69 shows the power spectrum for the input during each test performed on the damaged structure. This figure shows that inputs with similar frequency content but different amplitude were applied during each test of the damaged structure and these inputs have similar frequency content to the one applied during the test of the bridge in its undamaged condition.

Figures 70 shows the coherence functions measured at location S-3 during each test of the damaged structure compared to the coherence functions measured at this location during the undamaged forced vibration test. The area between the undamaged and damaged coherence functions has been shaded to highlight the changes in coherence with increased damage. Figures 71 shows similar results for location N-7. Increasing loss in coherence is observed at both locations with the increased levels of damage that have been introduced. Assuming that the other sources of input from traffic on the adjacent bridges were similar during each test, this result would imply that the structure is behaving in an increasingly nonlinear manner with each increased damage level.

FRF magnitudes for locations S-3 and N-7 are plotted for each level of damaged and compared to the similar FRFs measured on the undamaged structure in Figures 72 and 73, respectively. The figures show that little change in the resonant frequencies and widths of the resonance (damping) occur until the final stage of damage is introduced.

Table XI summarizes the resonant frequency and modal damping data obtained during each modal test of the damaged bridge. Also show in Table XI are similar results from the ambient vibration tests and the undamaged forced vibration test. No change in the dynamic properties can be observed until the final level of damage is introduced. At the final level, test t22tr, the resonant frequencies for the first two modes have dropped to values 7.6 and 4.4 percent less, respectively, than those measured during the undamaged tests. It is of interest to note that changes of similar magnitude are observed between the two ambient vibration tests performed on the undamaged structure at different times. For modes where the damage was introduced near a stress node for that mode (modes 3 and 5) no significant changes in resonant frequencies can be observed.
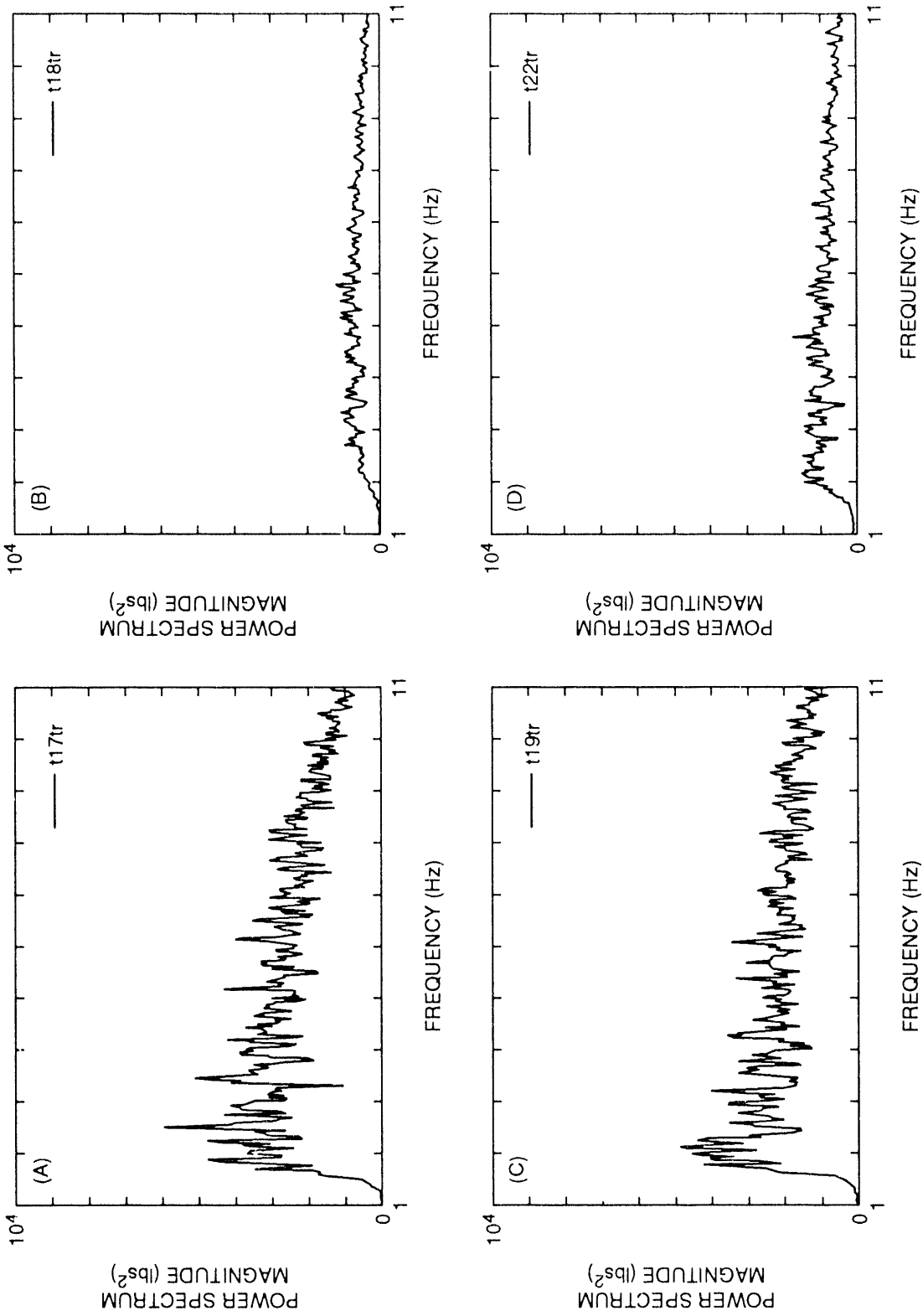
Fig. 69. Power spectra of the force input from Sandia's shaker measured during each forced vibration test on the damaged structure (test t16tr).
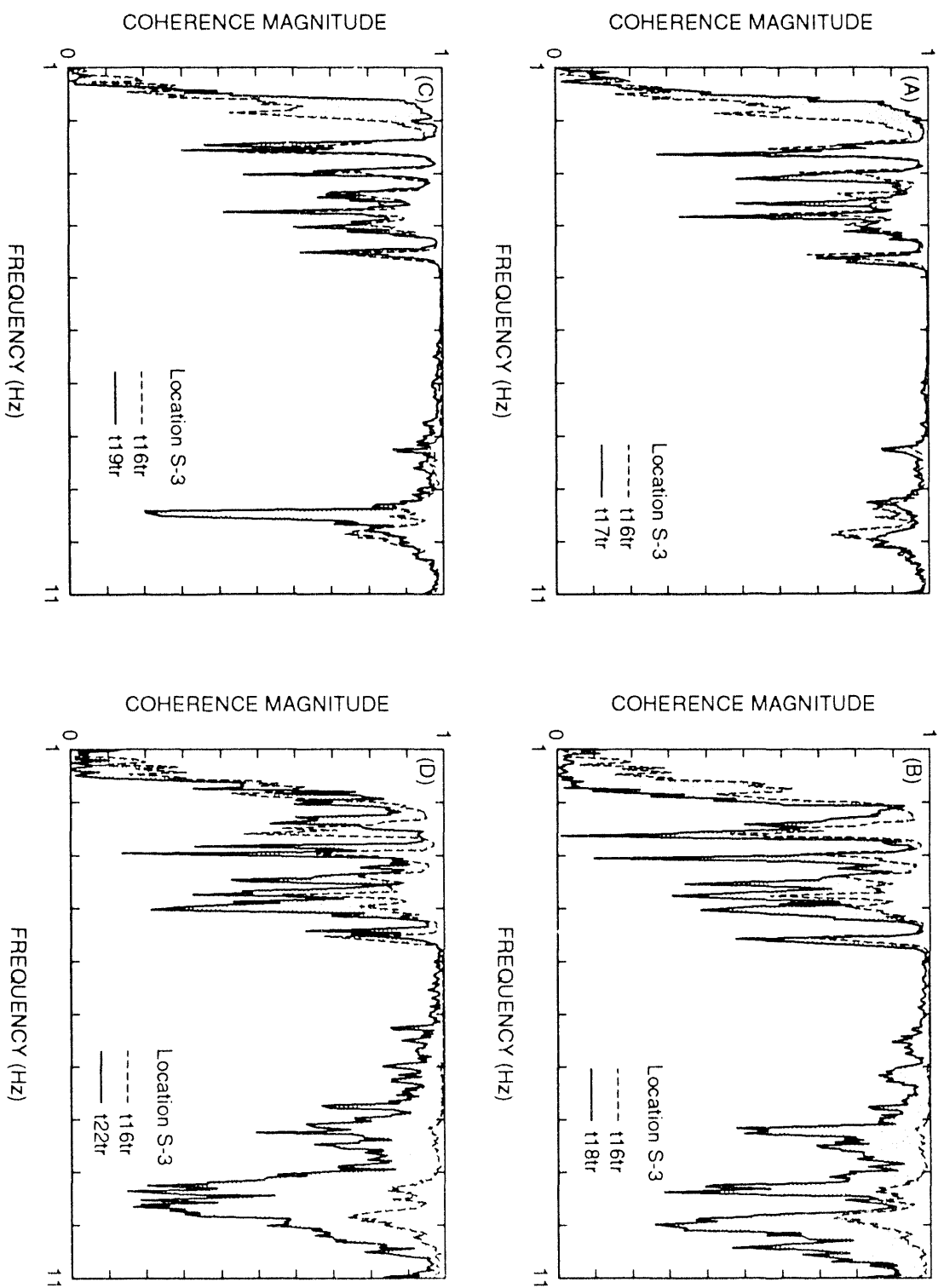
Fig. 70. Coherence measured at location S-3 after each stage of damage compared to a similar function measured during the undamaged forced vibration test (test t16tr).
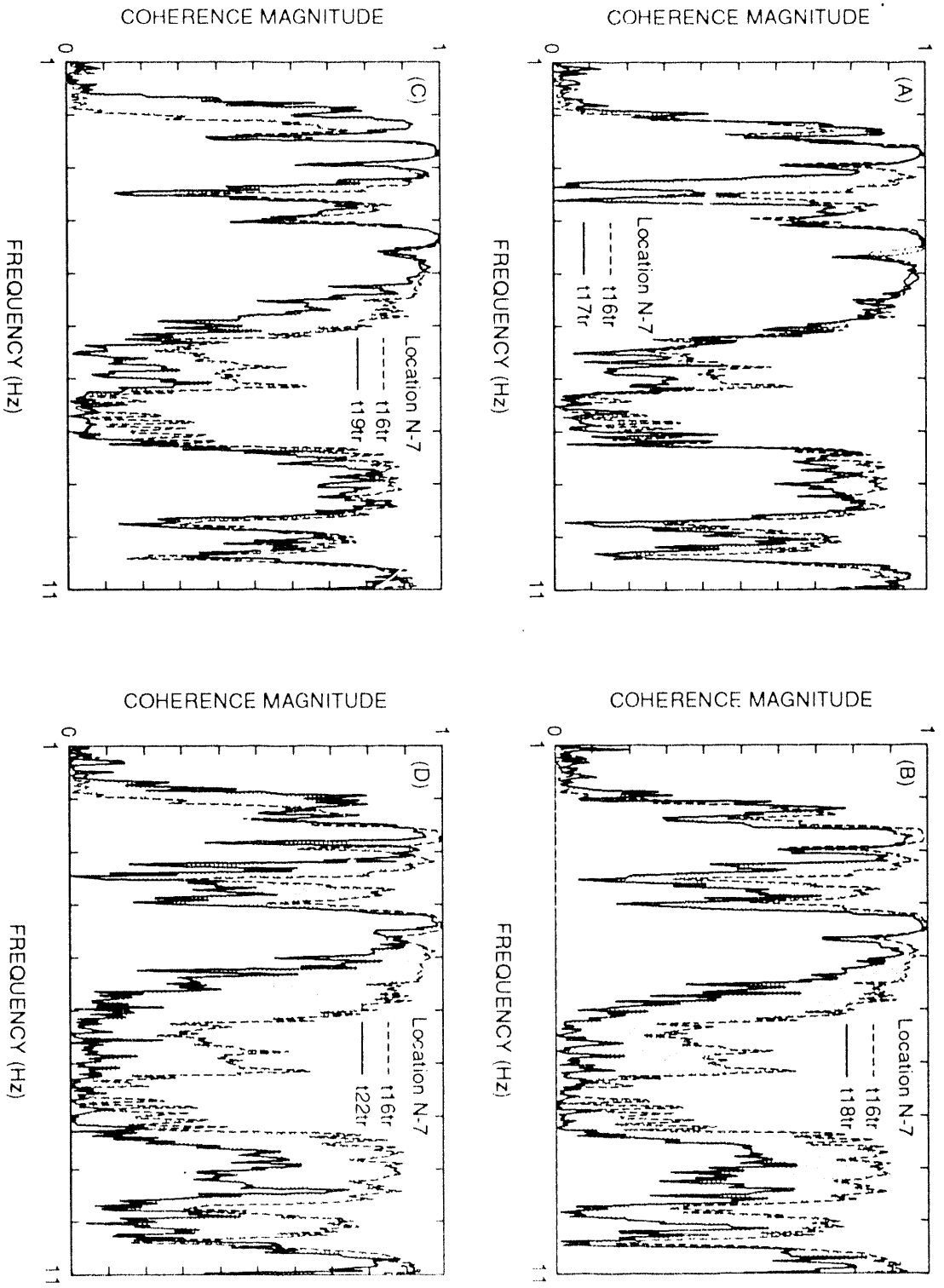
Fig. 71. Coherence measured at location N-7 after each stage of damage compared to a similar function measured during the undamaged forced vibration test (test t16tr).
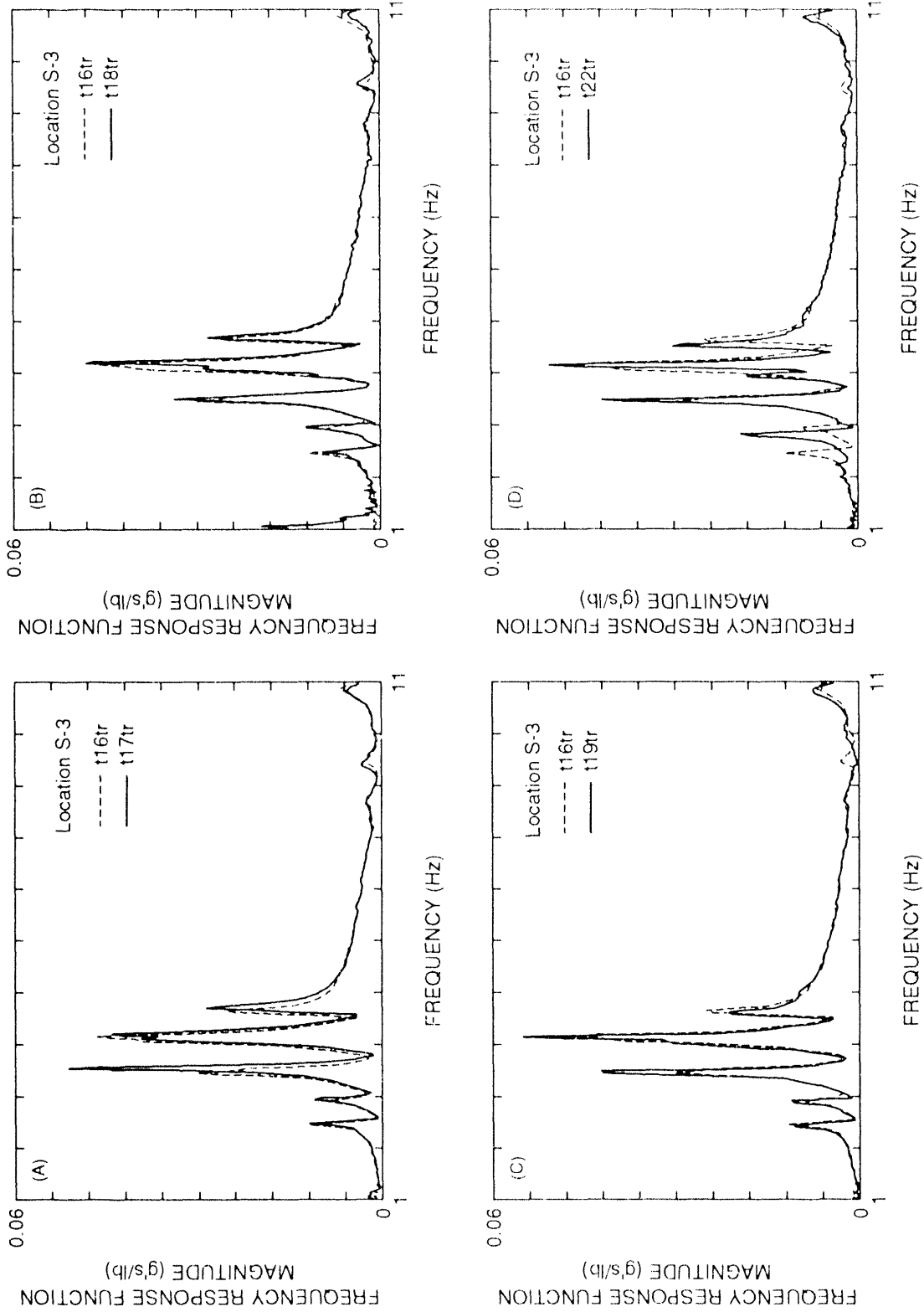
Fig. 72. FRF magnitude measured at location S-3 during each of the damaged forced vibration tests compared with the FRF measured at location S-3 during the undamaged forced vibration test (test t16tr).

FREQUENCY RESPONSE FUNCTION
MAGNITUDE (g's/lb)

FREQUENCY RESPONSE FUNCTION
MAGNITUDE (g's/lb)

(A)

(C)

FREQUENCY (Hz)

FREQUENCY (Hz)

Location N-7
---- t16tr
—— t17tr

Location N-7
---- t16tr
—— t19tr

FREQUENCY RESPONSE FUNCTION
MAGNITUDE (g's/lb)

FREQUENCY RESPONSE FUNCTION
MAGNITUDE (g's/lb)

(B)

(D)

FREQUENCY (Hz)

FREQUENCY (Hz)

Location N-7
---- t16tr
—— t18tr

Location N-7
---- t16tr
—— t22tr
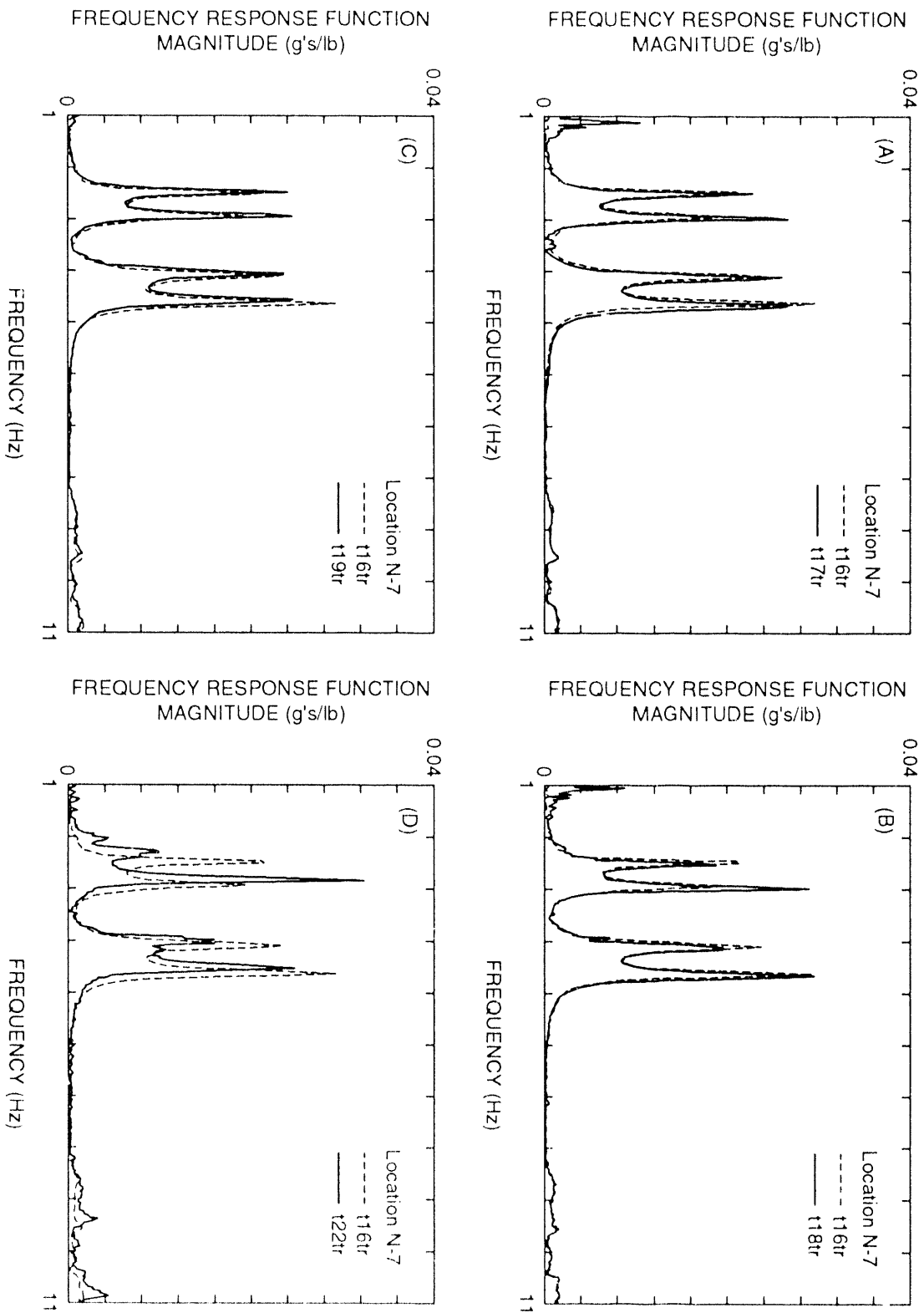
Fig. 73. FRF magnitude measured at location N-7 during each of the damaged forced vibration tests compared with the FRF measured at location N-7 during the undamaged forced vibration test (test t16tr).

Table XI						
Resonant Frequencies and Modal Damping Values Identified from Ambient Vibration Response Compared with Similar Quantities Identified from Undamaged and Damaged Forced Vibration Tests						
	Mode 1	Mode 2	Mode 3	Mode 4	Mode 5	Mode 6
Test	Freq. (Hz)/ Damp. (%)	Freq. (Hz)/ Damp. (%)	Freq. (Hz)/ Damp. (%)	Freq. (Hz)/ Damp. (%)	Freq. (Hz)/ Damp. (%)	Freq. (Hz)/ Damp. (%)
t1tr (ambient)	2.39/ 1.28	2.92/ 1.18	3.42/ 1.00	3.96/ 0.94	4.10/ 1.58	4.56/ 1.56
t15tr (ambient)	2.52/ 1.28	3.04/ 0.38	3.53/ 0.89	4.10/ 1.08	4.17/ 0.92	4.71/ 0.60
t16tr (forced, undamaged)	2.48/ 1.06	2.96/ 1.29	3.50/ 1.52	4.08/ 1.10	4.17/ 0.86	4.63/ 0.92
t17tr (forced, after 1st cut)	2.52/ 1.20	3.00/ 0.80	3.57/ 0.87	4.12/ 1.00	4.21/ 1.04	4.69/ 0.90
t18tr (forced, after 2nd cut)	2.52/ 1.33	2.99/ 0.82	3.52/ 0.95	4.09/ 0.85	4.19/ 0.65	4.66/ 0.84
t19tr (forced, after 3rd cut)	2.46/ 0.82	2.95/ 0.89	3.48/ 0.92	4.04/ 0.81	4.14/ 0.62	4.58/ 1.06
t22tr (forced, after final cut)	2.30/ 1.60	2.84/ 0.66	3.49/ 0.80	3.99/ 0.80	4.15/ 0.71	4.52/ 1.06

Table XII shows the MAC values that are calculated when mode shapes from test t17tr, t18tr, t19tr, and t22tr are compared to the modes calculated from the undamaged forced vibration test, t16tr. The MAC values show no change in the mode shapes for the first three stages of damage. When the final level of damage is introduced, significant drops in the MAC values for modes 1 and 2 are noticed. These two modes are shown in Figs. 74 and 75 and can be compared to similar modes identified for the undamaged bridge in Figs. 55 and 56. When the modes have a node near the damage location (modes 3 and 5), no significant reduction in the MAC values are observed, even for the final stage of damage, and a plot of this mode shape from test t22tr, Fig. 76, shows no change from the corresponding undamaged mode, Fig. 57. Plots of mode shapes from other forced vibration tests on the damaged structure have been included in Appendix E. It is should be noted that examination of these mode shapes reveals no change from the undamaged mode shapes shown in Figs. 55 through 60, as would be indicated from the MAC values shown in Table XII.

92

Test t22tr
Mode 1
F = 2.30 Hz
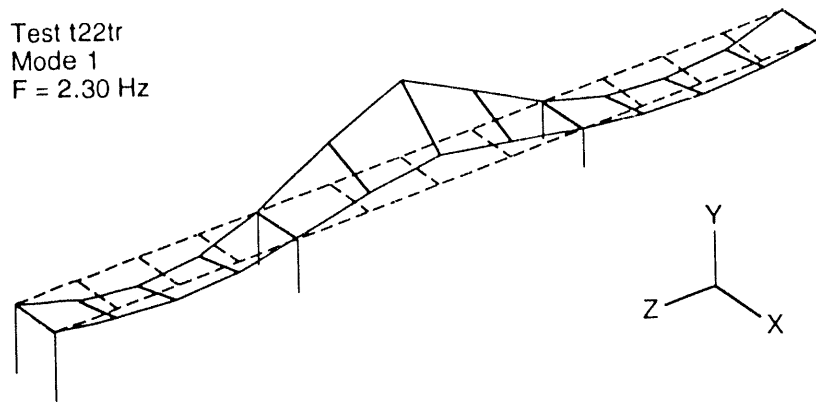
Fig. 74. The first flexural mode measured after the final damage stage, test t22tr.

Test t22tr
Mode 2
F = 2.84 Hz
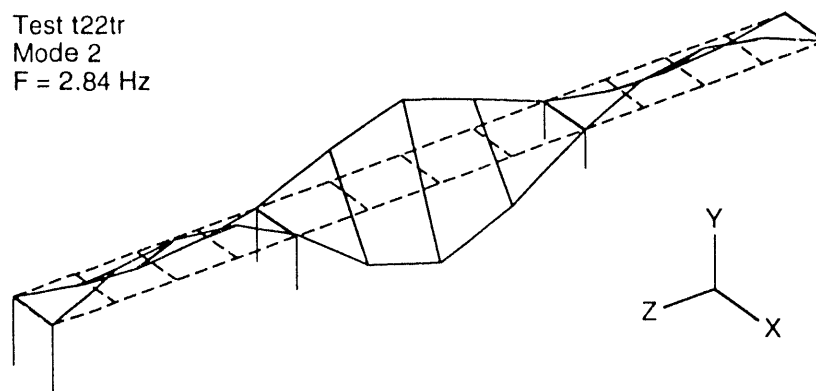
Fig. 75. The first torsional mode measured after the final damage stage, test t22tr.

Test t22tr
Mode 3
F = 3.49 Hz
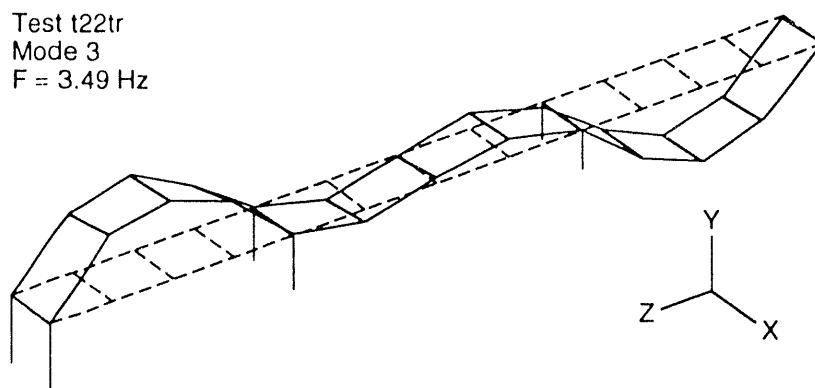
Fig. 76. The second flexural mode measured after the final damage stage, test t22tr.

Table XII

Modal Assurance Criteria:
Undamaged and Damaged Forced Vibration Tests

Modal Assurance Criteria	t16tr X t17tr					
Mode	1	2	3	4	5	6
1	0.996	0.006	0.000	0.003	0.001	0.003
2	0.000	0.997	0.000	0.005	0.004	0.003
3	0.000	0.000	0.997	0.003	0.008	0.001
4	0.004	0.003	0.006	0.984	0.026	0.011
5	0.001	0.008	0.003	0.048	0.991	0.001
6	0.001	0.006	0.000	0.005	0.005	0.996

Modal Assurance Criteria	t16tr X t18tr					
Mode	1	2	3	4	5	6
1	0.995	0.004	0.000	0.004	0.001	0.002
2	0.000	0.996	0.000	0.003	0.002	0.002
3	0.000	0.000	0.999	0.006	0.004	0.000
4	0.003	0.006	0.005	0.992	0.032	0.011
5	0.001	0.006	0.008	0.061	0.997	0.004
6	0.002	0.004	0.000	0.005	0.005	0.997

Modal Assurance Criteria	t16tr X t19tr					
Mode	1	2	3	4	5	6
1	0.997	0.002	0.000	0.005	0.001	0.001
2	0.000	0.996	0.001	0.003	0.002	0.002
3	0.000	0.000	0.999	0.006	0.006	0.000
4	0.003	0.005	0.004	0.981	0.032	0.011
5	0.001	0.006	0.004	0.064	0.995	0.003
6	0.002	0.002	0.000	0.004	0.009	0.995

Modal Assurance Criteria	t16tr X t22tr					
Mode	1	2	3	4	5	6
1	0.821	0.168	0.002	0.001	0.000	0.001
2	0.083	0.884	0.001	0.004	0.001	0.002
3	0.000	0.000	0.997	0.005	0.007	0.001
4	0.011	0.022	0.006	0.917	0.010	0.048
5	0.001	0.006	0.003	0.046	0.988	0.002
6	0.005	0.005	0.000	0.004	0.009	0.965

b. Data acquired for Texas A&M. Data similar to that acquired during the undamaged forced vibration tests were again acquired after each level of damage had been introduced into the plate girder. Experimental procedures and equipment were identical to those used to acquire data for Texas A&M during the undamaged forced vibration test. The resonant frequencies and complex mode shape data corresponding to the different levels of damage are summarized in Appendix D.

3. P-10 forced vibration tests (damaged). Scientists from P-10 performed swept-sine modal tests after each stage of damage. The following sections summarize the experimental procedures and equipment used during these tests and the results that were obtained.

a. Experimental procedure and equipment. Measurements made after each stage of damage was inflicted on the North girder followed the same procedure as the measurements made on the undamaged bridge. Additional measurements were made after the first cut and after the final cut, using the counter-rotating weight shaker supplied by NMSU. This shaker is well suited to generating stepped sine inputs, but the amplitude of the driving force is frequency dependent. This shaker did not have an external input, so the drive frequency was adjusted manually, with the shaker operator in walkie-talkie contact with the person at the data acquisition computer. To reduce the frequency dependence, scans were made over the range of 3.8 Hz to 4.4 Hz to better examine the closely spaced modes (Modes 4 and 5). The frequency step used was 0.025 Hz. The frequency was read out from an optical encoder wheel attached to one of the flywheels. Data were recorded separately from each of these frequency steps and later analyzed by the same homodyne software used when responses induced by the SNL shaker were measured.

b. Results. Figures 77-80 show Fourier spectra of the north girder's displacement response corresponding to each stage of damage. Figure 81 compares the spectrum from the undamaged state with the spectrum corresponding to the final damage state. Table XIII summarizes the results from applying the fitting procedure (described in Section III. F. 2. b) to data corresponding to each stage of damage. Modes 4 and 5 are sometimes separated by the fitting routine and sometimes they are not. Where there is only one fitted value, it is in the middle of the table. It is clear from the data gathered here and from the MEE-13 data, that these modes are separated by approximately 0.1 Hz, which corresponds to only two data points with the 0.05 Hz resolution, so it is not surprising that the fitting routine has difficulty separating these modes. Also noticeable is the inconsistency of the modal damping values for modes 3, 4 and 5. These changes seem uncorrelated with the damage being inflicted on the North girder and may be caused by the fitting routine.

There is a systematic increase in the resonant frequencies of all the modes after the second cut, the average increase being about 0.05 Hz. These increases are also seen in the MEE-13 data (See Table XI) and are believed to result from changes in the static loads on the bridge. This particular data scan was made unusually late in the afternoon when contractors vehicles may have been removed from the surface of the bridge.

In general, while the microwave interferometer stepped sine measurements have excellent noise reduction properties, they are susceptible to systematic errors, such as a truck parked on the bridge for several minutes. The data points recorded in those few minutes will accurately reflect the loading change, but will be inconsistent with the data obtained before the trucks came onto the bridge and after the trucks were removed.
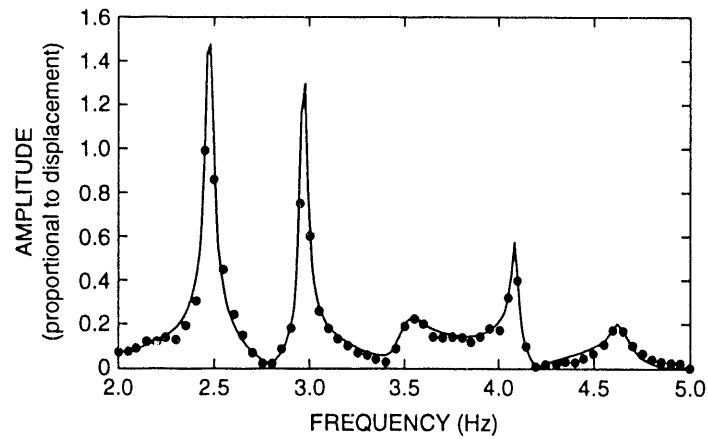
Fig. 77. Fourier spectrum of the south girder displacement response obtained with the microwave interferometer during sine-sweep tests on the bridge after the first cut.
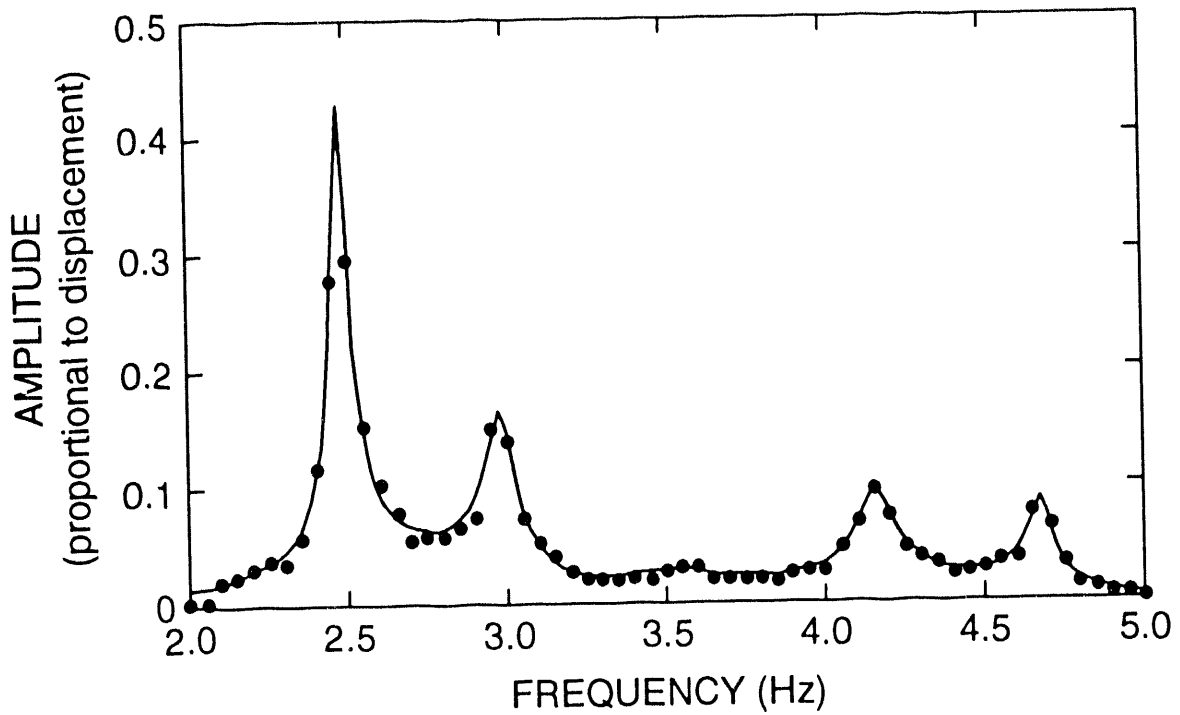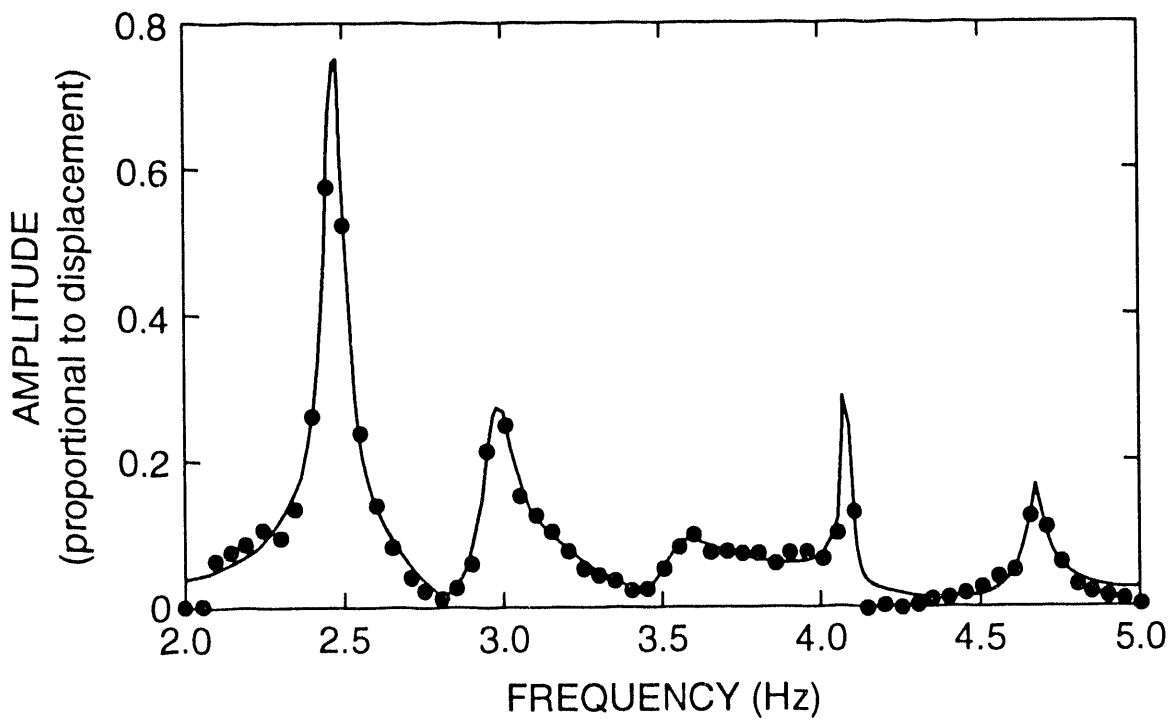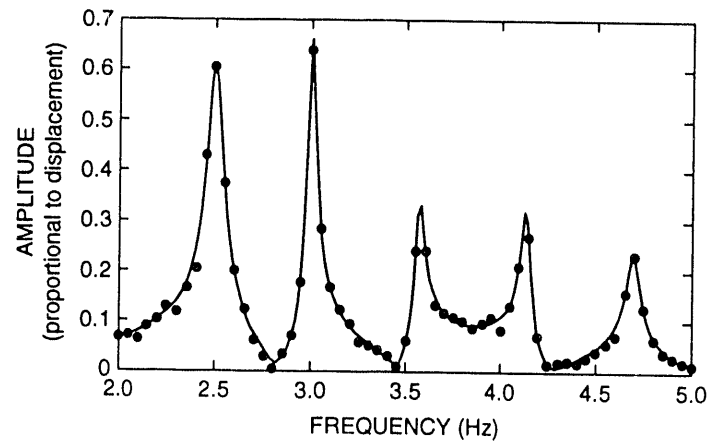

Fig. 78. Fourier spectrum of the south girder displacement response obtained with the microwave interferometer during sine-sweep tests on the bridge after the second cut.
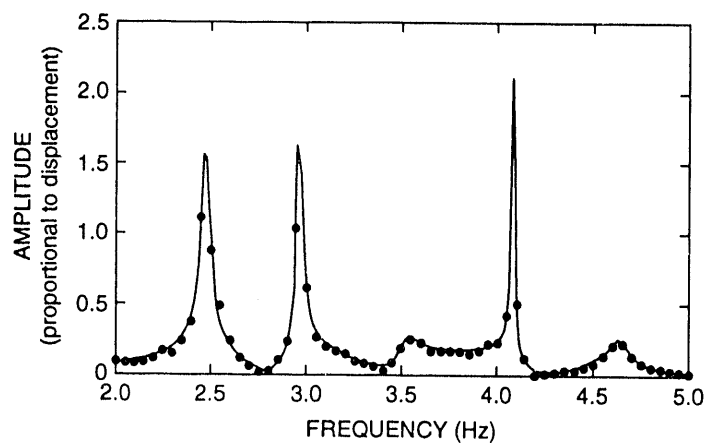
Fig. 79. Fourier spectrum of the south girder displacement response obtained with the microwave interferometer during sine-sweep tests on the bridge after the third cut.
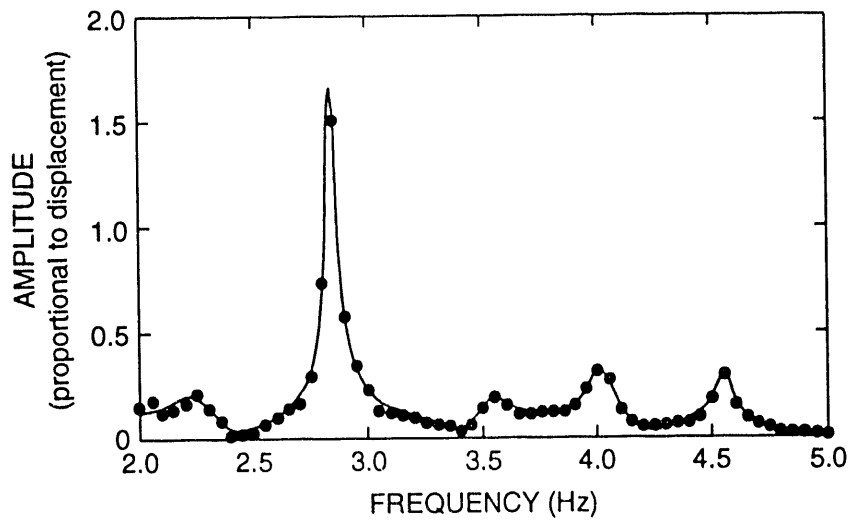
Fig. 80. Fourier spectrum of the south girder displacement response obtained with the microwave interferometer during sine-sweep tests on the bridge after the final cut.
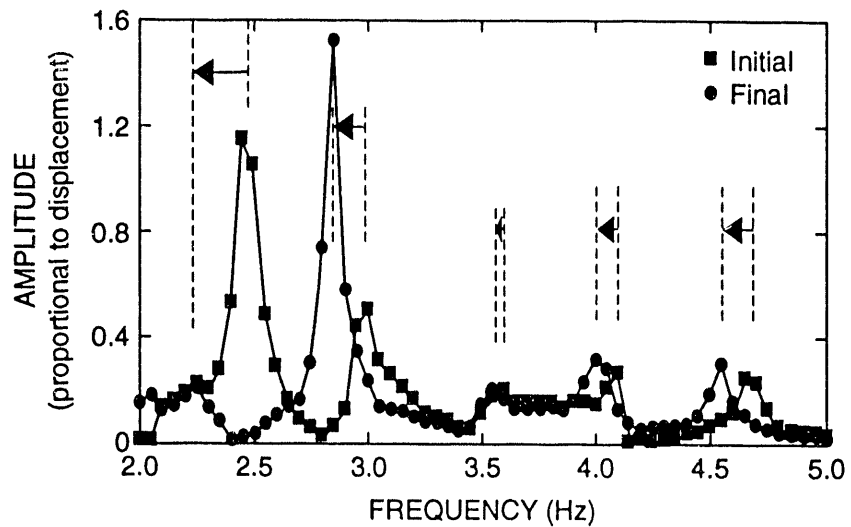
Fig. 81. A comparison of the Fourier spectra from the south girder of the undamaged bridge with a similar plot corresponding to data obtained after the final stage of damage.

Table XIII

A Comparison of Resonance Frequencies and Modal Damping, Identified from the Fits of Analytical Models to the Undamaged and Damaged Data Measured with the Microwave Interferometer

Test	Mode 1	Mode 2	Mode 3	Mode 4	Mode 5	Mode 6
	Freq. (Hz)/ Damp. (%)	Freq. (Hz)/ Damp. (%)	Freq. (Hz)/ Damp. (%)	Freq. (Hz)/ Damp. (%)	Freq. (Hz)/ Damp. (%)	Freq. (Hz)/ Damp. (%)
Undamaged	2.48/ 0.91	2.98/ 1.61	3.53/ 3.19	4.12/ 0.79		4.67/ 0.65
After first cut	2.47/ 0.81	2.97/ 0.59	3.50/ 1.86	4.08/ 0.49		4.62/ 1.03
After second cut	2.50/ 1.59	3.00/ 0.67	3.57/ 0.56	3.98/ 1.01	4.14/ 0.72	4.70/ 0.79
After third cut	2.47/ 0.71	2.97/ 0.42	3.50/ 1.93	4.03/ 2.92	4.11/ 1.03	4.62/ 1.02
After final cut	2.25/ 3.56	2.84/ 0.70	3.45/ 2.39	3.96/ 1.96	4.12/ 2.61	4.55/ 0.93

Figures 82 and 83 show the results of the measurements made in the 3.8-4.4 Hz range using the NMSU shaker. The "before" plots show clearly the peak near 4.07 Hz and an indication of another peak in the region 4.15 - 4.2 Hz. The relative size of these two peaks in the North and South data sets agrees with the SNL shaker data. These refined measurements were a cumbersome method of separating closely spaced modes, but results indicated that they can be an effective tool for separating closely spaced modes.

H. Comparison of Results From Damaged and Undamaged Data

A review of the data obtained by P-10 and MEE-13 during the undamaged and damaged forced vibration tests shows that damage must be significant before the global dynamic properties of the structure are affected. Both measurement systems only identified damage after the final cut had been made in the plate girder. From a practical point of view this would be considered too late to prevent a catastrophic failure. After the initial stage of damage, resonant frequencies were observed to increase slightly, even though damage typically increases the flexibility of the structure and, hence, would be expected to cause reductions in the structure's resonant frequencies. This change is assumed to be related to either changes in the dead loads being carried by the bridge such as parked cars and trucks on the deck, changes resulting from demolition of the other end of the bridge, or changes to the boundary conditions from ongoing construction. At this time the specific cause of the increased frequency cannot be identified. Because the result appears in both the P-10 and MEE-13 data, which were measured at different times, with different types of transducers and with different types of excitation, these results do not represent anomalies in the data acquisition.
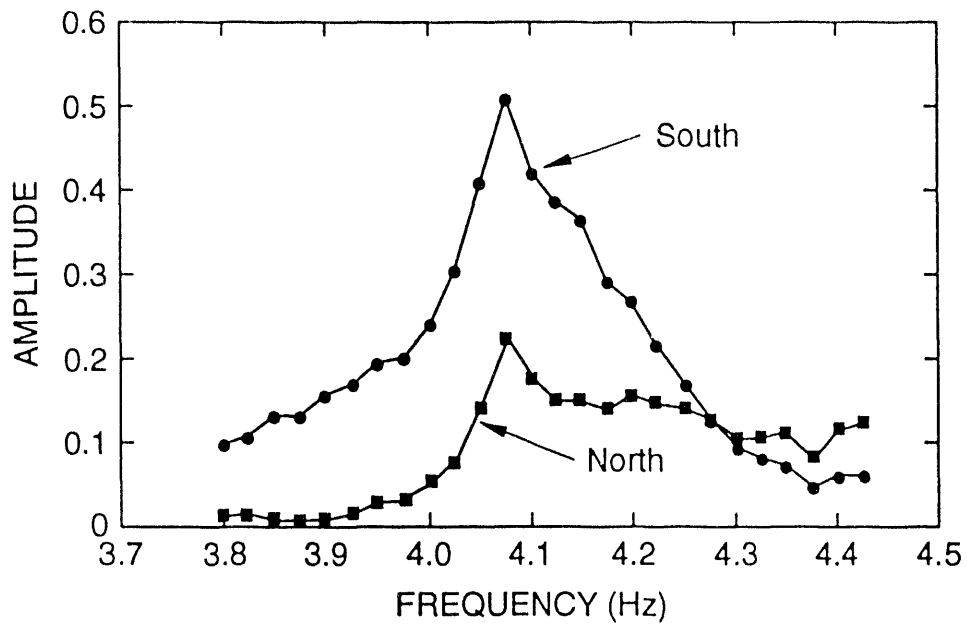
Fig. 82. Refined Fourier spectra before damage.
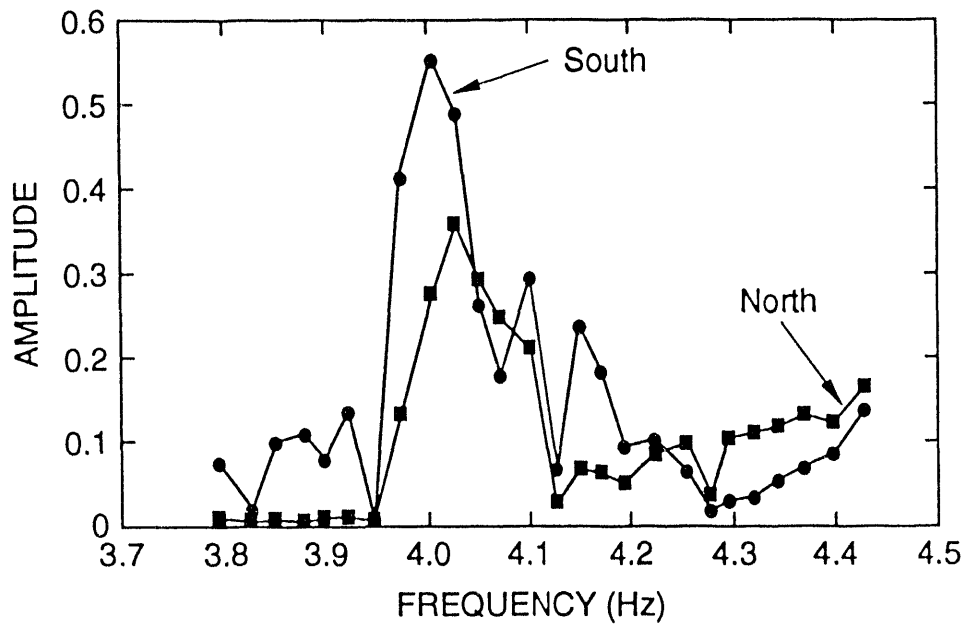
Fig. 83. Refined Fourier spectra after final stage of damage.

Both sets of measurements showed similar reductions in the resonant frequencies associated with the final stage of damage. Changes in the mode shapes were also observed, but if the mode had a node point at the location of damage, as was the case for mode 3, no changes in the dynamic properties (mode shapes or resonant frequencies) could be observed. At this point more refined analysis procedures such as those being developed at Texas A&M or the Stretch technique being developed at SNL need to be applied to these data to better quantify and locate the damage in the structure. The tests performed do quantify the limitations of examining changes in the global mode shapes and resonant frequencies only for the purpose of damage identification.

IV. SUMMARY & CONCLUSIONS

Extensive modal testing of the I-40 bridge over the Rio Grande in Albuquerque, New Mexico has been reported herein. These tests were intended to characterize the dynamic properties of the bridge and show how these dynamic properties change as damage is introduced. The tests also allowed data to be acquired that could subsequently be used with state-of-the-art damage identification methods to better characterize and locate the damage. Initial tests performed on the bridge were ambient vibration tests that used traffic as an excitation source. The NExT method, developed at Sandia National Laboratory, which can be used to identify dynamic properties (resonant frequencies and modal damping) of a structure from ambient vibration response measurements, was applied to these data. Mode shapes were determined from relative amplitude and phase information contained in the cross-power spectra between a reference response channel and other response measurements. The ambient vibration measurements were repeated several times with different locations designated as the reference, with different frequency resolution in the measurements, and with different sources of ambient vibration. The first source of ambient vibration was traffic on the bridge being tested. After traffic had been removed from the bridge being tested, traffic from the adjacent bridge, as it was filtered through the ground to the piers and abutment of the bridge that was instrumented, was used as the ambient source. In all cases the ambient source was not characterized, but assumed to be white noise.

Results of the ambient tests were repeatable and the dynamic properties associated with the first six modes of the structure were identified. A review of the literature on ambient vibration testing of bridges showed that previous tests and their associated data reduction methods have difficulty identifying closely spaced modes and modal damping. The NExT method handled both of these problems quite well as two modes approximately 0.1 Hz apart (frequency resolution was 0.016 Hz) were identified and these modes were subsequently shown to agree with results from forced vibration tests summarized below. Damping values identified by the NExT method also agreed with those determined by forced vibration tests. The sensitivity of the measurement and data reduction methods was demonstrated during test t15tr when excitation from traffic on the adjacent bridge, as it was filtered through the soil to the piers and abutment of the instrumented bridge, was used to successfully identify the dynamic properties of the instrumented bridge.

Following the ambient vibration tests, forced vibration tests were performed on the undamaged bridge using a shakers provided by SNL and NMSU. Both random and harmonic inputs were used. The random input was used with conventional, forced-vibration experimental modal analysis techniques to again characterize the dynamic properties of the bridge. The harmonic inputs were used with an experimental homodyne data acquisition system and microwave interferometer non-contact absolute-displacement sensors to also characterize the bridge's dynamic properties. Both measurement methods gave comparable results for the resonant frequencies and mode shapes of the first six modes of vibration. Damping values identified by analysis of data from the microwave sensors were inconsistent with damping values identified by the conventional modal analysis methods and the NExT method. This inconsistency is attributed to the analysis methods and is not an inherent shortcoming of the microwave interferometer. Dynamic properties identified by the conventional modal analysis methods were in agreement with results obtained during the ambient vibration tests when the difference in mass caused by the traffic was taken into account. All data from the forced vibration tests were forwarded to investigators at SNL for use with their damage detection algorithms.

Next, cuts were made in the plate girder to simulate the formation of fatigue cracks that occur under actual field conditions. The cuts were made in four stages and forced vibration tests were repeated after each stage. Both the conventional modal analyses and the measurements made with the microwave interferometers showed no change in the global dynamic properties of the bridge until the final stage of damage was introduced. After the final stage of damage had been introduced, changes in the resonant frequencies and their associated mode shapes could be identified. However, the dynamic properties of modes that have a node point at the location of damage did not change even after the final stage of damage. These results emphasize the need for more work in the development of damage identification algorithms.

In addition to the data collected for the experimental modal analysis, additional accelerometers were mounted on the span of the girder that was damaged. Measurements of the response before damage and after each stage of damage were made while a random input was applied with the Sandia shaker. These data were subsequently forwarded to faculty members at Texas A&M University where sophisticated damage detection algorithms will be used to assess the damage in the bridge.

Significant contributions of this work include: (1) the demonstration of the NExT method for identification of bridge dynamic properties from ambient response to traffic excitation and the benchmarking of this procedure against conventional forced vibration test results; (2) the demonstration of the microwave interferometer non-contact absolute displacement dynamic measurement system and the benchmarking of results obtained from it with a conventional modal analysis data acquisition system; and (3) a quantification of the amount of damage that must be present before conventional modal analysis methods identify a change in the structure's global dynamic properties. The combination of the NExT method with the microwave

interferometer sensors provides a quick, accurate, inexpensive (hardware for the prototype sensors cost approximately $200 (U.S., 1993)), nonintrusive method to obtain the dynamic properties of a wide variety of large civil engineering structures.

ACKNOWLEDGMENTS

APPENDIX A: Modal Testing Theory

This appendix presents a brief summary of some of the concepts related to modal testing used throughout the report. The concepts outlined in this appendix are not found in typical vibration texts. First, the partial fraction representation of the frequency response function (FRF) will be developed. This development is taken from Formenti (1977). Next, the global frequency domain parameter estimation method used to determine the dynamic properties of the bridge during forced vibration tests is outlined. This discussion is taken from Richardson and Formenti (1985). A summary of the development given by James, Lauffer and Carne (1993), which shows that cross-correlation function (the inverse Fourier transform of the cross-power spectrum) relating two response measurements has the same form as an impulse response function, is given. This relationship allows time domain curve-fitting method to be used to extract modal parameters from ambient vibration data. Finally, a summary of the complex exponential curve fitting method described by Ewins (1988) which was used to obtain resonant frequencies and modal damping values from cross-correlation functions measured during the ambient vibration tests of the bridge, is presented.

A.1 Partial Fraction Representation of the Frequency Response Function

The equation of motion for a single degree of freedom (SDOF) system is

$$m\ddot{x} + c\dot{x} + kx = f(t),$$
(A-1)

where m = mass of the system,
  c = viscous damping of the system,
  k = stiffness of the system,
  f(t) = the applied force as a function of time (t),
  $\ddot{x}$ = acceleration,
  $\dot{x}$ = velocity, and
  x = displacement.

Equation A-1 can be transformed into the Laplace Domain (sometimes referred to as the S domain) by taking the Laplace transform of both sides yielding

$$(ms^2 + cs + k)X(s) = F(s) + (ms + c)x(0) + m\dot{x}(0),$$
(A-2)

where x(0) and $\dot{x}$(0) are the displacement and velocity at time t=0. Assuming zero initial conditions, Eq. A-2 reduces to

$$(ms^2 + cs + k)X(s) = F(s),$$
(A-3)

Typically, the response of a system caused by a known input, F(s), is of interest and Eq. A-3 can be written as

$$F(s)H(s) = X(s)$$
(A-4)

where $H(s)$ is referred to as the system's transfer function. For the SDOF system described by Eq. A-1, the transfer function has the form

$$H(s) = \frac{1/m}{s^2 + \frac{c}{m}s + \frac{k}{m}}.$$

(A-5)

The denominator of Eq. A-5 is referred to as the system's characteristic equation and the roots of this equation, $s_{1,2}$, are

$$s_{1,2} = -\frac{c}{2m} \pm \sqrt{\left(\frac{c}{2m}\right)^2 - \frac{k}{m}}.$$

(A-6)

Using the following definitions for resonant frequency, ω_n, and critical damping, c_c,

$$\omega_n = \sqrt{\frac{k}{m}},$$

$$c_c = 2m\omega_n,$$

Eq. A-6 can be written in terms of ω_n and a damping ratio, $\zeta = \frac{c}{c_c}$, as

$$s_{1,2} = \left(-\zeta \pm \sqrt{\zeta^2 - 1}\right)\omega_n.$$

(A-7)

Restricting this study to an underdamped system (as is the case for most real structures), the roots of the characteristic equation can be written as

$$s_{1,2} = \sigma \pm i\omega_d,$$

(A-8)

where σ = damping factor,

ω_d = damped natural frequency, and

$i = \sqrt{-1}$.

The system's transfer function can now be written as

$$H(s) = \frac{1/m}{(s-p)(s-p^*)},$$

(A-9)

where $p = \sigma + i\omega_d$, and

$p^* = \sigma - i\omega_d$.

p is referred to as the pole of the transfer function.

Now H(s) can be written in terms of partial fractions as

$$H(s) = \frac{c_1}{\left(s-p\right)} + \frac{c_2}{\left(s-p^*\right)}. \qquad \text{(A-10)}$$

c_1 and c_2 are referred to as the residues of the transfer function and they are obtained from Eqs A-9 and A-10 by multiplying both equations by (s - p) and evaluating the equations at s=p yielding

$$c_1 = \frac{1/m}{2i\omega_d} = A, \text{ and}$$

$$c_2 = \frac{1/m}{-2i\omega_d} = A^*.$$

In actual vibration testing the transfer function is evaluated along the $i\omega$ axis and this function is referred to as the frequency response function (FRF). The FRF can be written as

$$H(\omega) = H(s)|_{s=i\omega} = \frac{A}{\left(i\omega - p\right)} + \frac{A^*}{\left(i\omega - p^*\right)}. \qquad \text{(A-11)}$$

Substituting the values for p and p^* yields

$$H(\omega) = \frac{A}{i\left(\omega - \omega_d\right) - \sigma} + \frac{A^*}{i\left(\omega + \omega_d\right) - \sigma}. \qquad \text{(A-12)}$$

Equation A-12 shows that the value of the FRF at a particular frequency is a function of the residues, the damping factor, and the damped natural frequency of the system.

Assuming zero initial conditions and that the F(s)=1 for an impulse applied to the system, the impulse response function, h(t), can be obtained from the inverse transform of the transfer function defined by Eq. A-10

$$L^{-1}[H(s)] = h(t) = Ae^{pt} + A^*e^{p^*t} = e^{\sigma t}\left[Ae^{i\omega_d t} + A^*e^{-i\omega_d t}\right]. \qquad \text{(A-13)}$$

From Eq. A-13 it is evident that the residue controls the initial amplitude of h(t), the real part of the pole is the decay rate, and the imaginary part of the pole is the frequency of oscillation.

The partial fraction form of the transfer function and FRF can now be extended to multi-degree-of-freedom systems. For an n degree of freedom system, the equation of motion is

$$[m]\{\ddot{x}\} + [c]\{\dot{x}\} + [k]\{x\} = \{f(t)\}, \tag{A-14}$$

where [m] = n×n mass matrix,
    [c] = nxn damping matrix
    [k] = nxn stiffness matrix,
    $\{\ddot{x}\}$ = nx1 acceleration vector,
    $\{\dot{x}\}$ = nx1 velocity vector,
    $\{x\}$ = nx1 displacement vector, and
    $\{f(t)\}$ = nx1 applied force vector.

Assuming zero initial conditions, the Laplace transform of Eq. A-14 yields

$$\left[[m]s^2 + [c]s + [k]\right]\{X(s)\} = \{F(s)\}. \tag{A-15}$$

A relation for the system response, {X(s)}, to the system excitations, {F(s)}, is

$$[H(s)] \{F(s)\} = \{X(s)\}, \tag{A-16}$$

where $H(s) = \left[[m]s^2 + [c]s + [k]\right]^{-1}$.

[H(s)] is referred to as the transfer function matrix. Because the transfer functions are a function of a complex variable, they describe a surface above the complex plane. Experimentally this surface can only be evaluated where it intersects the iω axis and the functions described by this intersection are the frequency response functions.

Analogous to the SDOF case, Eq. A-16 reduces to

$$[H(\omega)] \{F(\omega)\} = \{X(\omega)\}, \tag{A-17}$$

when evaluated along the iω axis. [H(ω)] is the frequency response function matrix whose elements are denoted $h_{ij}(\omega)$. The elements of this matrix can each be thought of as the frequency response function that relates the response at degree of freedom i to an input at degree of freedom j. Applying the theory of superposition, $h_{ij}(\omega)$ can be shown to be the sum of SDOF FRFs expressed in partial fraction form as

$$h_{ij}(\omega) = \sum_{n=1}^{N} \left[\frac{A_{ijn}}{(i\omega - p_n)} + \frac{A_{ijn}^*}{(i\omega - p_n^*)} \right], \tag{A-18}$$

where N = the number of DOFs,

A_{ij_n} = the residue, and

p_n = the pole for the nth mode.

The residue is also referred to as the amplitude coefficient of the nth mode and is defined as a scaling constant for the nth mode multiplied by the components of the mode shape vector corresponding to the response and excitation locations. The residue has the form

$$A_{ij_n} = c_n \phi_{i_n} \phi_{j_n}$$

where c_n = the scaling constant,

ϕ_{i_n} = the mode shape coefficient for the nth mode at location i, and

ϕ_{j_n} = the mode shape coefficient for the nth mode at location j.

The scaling constant is defined as

$$c_n = \frac{1/m_n}{i2\omega_{d_n}},$$

where m_n = the modal mass for the nth mode.

An important property of the FRF matrix that is evident from Eq. A-18 is that all the information necessary to define the dynamic properties of the system (resonant frequencies, modal damping, and mode shapes) is contained in one row or one column of the FRF matrix. The implication of this property for modal testing is that an excitation source need only be applied at one location, as was done with the Sandia shaker (See Section III.F.1.a), to adequately identify the dynamic properties of the structure.

The inverse transform of A-18 yields the impulse response function $h_{ij}(t)$ and this function has the form

$$h_{ij}(t) = \sum_{n=1}^{N} \left[A_{ij_n} e^{p_n t} + A^*_{ij_n} e^{p^*_n t} \right]. \tag{A-19}$$

A.2 Global Frequency Domain Parameter Estimation From Forced Vibration Data

The method of analysis used to estimate dynamic properties from the FRFs measured during the forced vibration tests is now summarized. Frequency response functions can also be written as the ratio of two polynomials. This representation is referred to as the rational fraction form of the FRF. The polynomials in the numerator and denominator that make up the rational fraction are typically independent and, in general, of different order. Again the denominator represents the characteristic equation of the system. As an example, Eq. A-11 can be written as

$$H(\omega) = \frac{a_1(i\omega) + a_0}{b_2(i\omega)^2 + b_1(i\omega) + b_0},$$ (A-20)

where $a_0 = A + A^*$,

$a_1 = A^*p + Ap^*$,

$b_0 = pp^*$,

$b_1 = -(p + p^*)$, and

$b_2 = 1$.

The rational fraction form of the FRF shown in Eq. A-20 can be extended to MDOF systems. The MDOF FRF has the general form

$$H(\omega) = \frac{\displaystyle\sum_{k=0}^{m} a_k(i\omega)^k}{\displaystyle\sum_{k=0}^{n} b_k(i\omega)^k},$$ (A-21)

where the coefficients a_k and b_k are functions of the systems poles and residues.

Experimental modal analysis, as defined in this report, refers to the procedure whereby an analytical form of the FRF given in Eq. A-21 is fit to a set of measured FRFs to estimate the values of the coefficients a_k and b_k such that the error between the analytical FRF and the measured FRF is minimized. The values of the coefficients a_k and b_k are then used to estimate the poles and residues of the system, which, in turn, are used to determine the resonant frequencies, modal damping, and mode shapes of the system.

To determine the coefficients a_k and b_k, the error, e_i, between the measured and analytical FRF at a frequency ω_i is defined as

$$e_i = \sum_{k=0}^{m} a_k(i\omega_i)^k - h_i\left[\left(\sum_{k=0}^{n-1} b_k(i\omega_i)^k\right) + (i\omega_i)^n\right],$$ (A-22)

where h_i = the measured FRF value at ω_i.

A squared error criterion, J, is defined as

$$J = \sum_{i=1}^{L} e_i^* e_i = \{E^*\}^T\{E\},$$ (A-23)

where $\{E\} = \begin{Bmatrix} e_1 \\ e_2 \\ \vdots \\ e_L \end{Bmatrix}$,

T denotes transpose, and

L = the number of frequency values that form the specified frequency range to be analyzed.

The error vector can be written in matrix form as

$$\{E\} = [P]\{A\} - [T]\{B\} - \{W\},\tag{A-24}$$

where $[P] = \begin{bmatrix} 1 & i\omega_1 & (i\omega_1)^2 & \cdots(i\omega_1)^m \\ 1 & i\omega_2 & (i\omega_2)^2 & \cdots(i\omega_2)^m \\ \vdots & \vdots & \vdots & \vdots \\ 1 & i\omega_L & (i\omega_L)^2 & \cdots(i\omega_L)^m \end{bmatrix}$,

$$[T] = \begin{bmatrix} h_1 & h_1(i\omega_1) & h_1(i\omega_1)^2 & \cdots h_1(i\omega_1)^{n-1} \\ h_2 & h_2(i\omega_2) & h_2(i\omega_2)^2 & \cdots h_2(i\omega_2)^{n-1} \\ \vdots & \vdots & \vdots & \vdots \\ h_L & h_L(i\omega_L) & h_L(i\omega_L)^2 & \cdots h_L(i\omega_L)^{n-1} \end{bmatrix},$$

$$\{A\} = \begin{Bmatrix} a_0 \\ \vdots \\ a_m \end{Bmatrix}, \quad \{B\} = \begin{Bmatrix} b_0 \\ \vdots \\ b_{n-1} \end{Bmatrix}, \quad \text{and} \quad \{W\} = \begin{Bmatrix} h_1(i\omega_1)^n \\ \vdots \\ h_L(i\omega_L)^n \end{Bmatrix}.$$

Note that it has been assumed that the highest order denominator coefficient, b_n, is equal to 1, which can be accomplished by normalizing the other coefficients by this value. The squared error criteria can be expressed in matrix form as

$$J(A,B) = \{A\}^T[P^*]^T[P]\{A\} + \{B\}^T[T^*]^T[T]\{B\} + \{W^*\}^T\{W\}$$
$$- 2\operatorname{Re}(\{A\}^T[P^*]^T[T]\{B\}) - 2\operatorname{Re}(\{A\}^T[P^*]^T\{W\}) - 2\operatorname{Re}(\{B\}^T[T^*]^T\{W\}).\tag{A-25}$$

where Re denotes the real portion of the quantity in parentheses.

The values of $\{A\}$ and $\{B\}$ that will yield a minimum value for J can be determined by setting the partial derivatives of Eq. A-25 with respect to $\{A\}$ and $\{B\}$ equal to zero yielding

$$\frac{\partial J(A,B)}{\partial A} = 2[P^*]^T[P]\{A\} - 2\,\mathrm{Re}([P^*]^T[T]\{B\}) - 2\,\mathrm{Re}([P^*]^T\{W\}) = \{0\}, \text{ and} \qquad \text{(A-26)}$$

$$\frac{\partial J(A,B)}{\partial B} = 2[T^*]^T[T]\{B\} - 2\,\mathrm{Re}([T^*]^T[P]\{A\}) - 2\,\mathrm{Re}([T^{*}]^T\{W\}) = \{0\}. \qquad \text{(A-27)}$$

These equations are coupled in the vectors {A} and {B}, hence, they must be solved simultaneously which leads to a set of n+m+1 equations that can be written as

$$\begin{bmatrix} [Y] & [X] \\ [X^T] & [Z] \end{bmatrix} \begin{Bmatrix} \{A\} \\ \{B\} \end{Bmatrix} = \begin{Bmatrix} \{G\} \\ \{F\} \end{Bmatrix}, \qquad \text{(A-28)}$$

where $[X] = -\mathrm{Re}([P^*]^T[T])$,

$$[Y] = ([P^*]^T[P]),$$

$$[Z] = ([T^*]^T[T]),$$

$$\{G\} = \mathrm{Re}([P^*]^T\{W\}), \text{and}$$

$$\{F\} = \mathrm{Re}([T^*]^T\{W\}).$$

Typically in a modal test there are numerous FRFs that can be used to solve for the vectors {A} and {B}. Equation A-28 can be extended to the case where p measurements are available and the least squares solution then takes on the form

$$\sum_{k=1}^{p}[u_k]^2 \begin{Bmatrix} \{A\} \\ \{B\} \end{Bmatrix} = \sum_{k=1}^{p}[u_k]\{v_k\} \qquad \text{(A-29)}$$

where $[u_k] = \begin{bmatrix} [Y] & [X] \\ [X^T] & [Z] \end{bmatrix}$ corresponds to the *kth* measurement, and

$[v_k] = \begin{Bmatrix} \{G\} \\ \{F\} \end{Bmatrix}$ also corresponds to the *kth* measurement.

This discussion summarizes the method used to estimate the dynamic properties of a system from measured FRF data. The actual implementation of an algorithm to perform the computations outlined above is more complex. In general, Eq. A-28 is ill-conditioned and this equation is reformulated in terms of orthogonal polynomials. Also, the frequency values must be scaled to avoid out-of-range numerical problems. Because the curve-fit is usually performed over a limited frequency range surrounding a resonant peak, a method to compensate for residual effects from out-of-band resonances is required. A detailed discussion of these topics is not presented and the reader is referred to Richardson and Formenti (1985) for a summary of how each of these topics is addressed in an actual curve-fitting algorithm.

A. 3 The NExT Technique

When ambient vibration data such as that cause by the traffic on the bridge is measured, the response is typically unknown, and the parameter estimation method discussed in A. 2 cannot be used. The development presented in this section shows that the cross-correlation function between two measured response signals from a discrete, MDOF system excited by multiple white noise random inputs has the same form as the impulse response function. Once this relationship has been established, time-domain parameter estimation methods, such as the complex exponential method discussed in A-4, can be used to estimate the dynamic properties of the structure. This method was applied to all ambient vibration data obtained on the I-40 bridge.

When proportional damping is assumed and Eq. A-14 is transformed into modal coordinates, a set of uncoupled scalar equations of the following form results

$$\ddot{q}^r + 2\zeta^r \omega_n^r \dot{q}^r + \left(\omega_n^r\right)^2 q^r = \frac{1}{m^r}\left\{\phi^r\right\}^T \left\{f(t)\right\}, \tag{A-30}$$

where the superscript r denotes values associated with the rth mode, $q, \dot{q}$, and $\ddot{q}$ are the displacement, velocity and acceleration in modal coordinates, and m is the modal mass.

These equations may be solved by the convolution integral, assuming a general forcing function and zero initial condition, and back-transformed into the original coordinates yielding

$$\{x\} = \sum_{r=1}^{n}\left\{\phi^r\right\}^T \int_{-\infty}^{t}\left\{\phi^r\right\}^T \{f(\tau)\} g^r(t-\tau)d\tau, \tag{A-31}$$

where $g^r(t) = \dfrac{1}{m^r \omega_d^r} e^{-\zeta^r \omega_n^r t} \sin(\omega_d^r t)$ is the impulse response function associated with mode r, and n is the number of modes.

The response at location i caused by an input at location k, x_{ik} and $f_k(t)$, respectively, can be expressed as

$$x_{ik} = \sum_{r=1}^{n}\phi_i^r \phi_k^r \int_{-\infty}^{t} f_k(\tau)\, g^r(t-\tau)d\tau, \tag{A-32}$$

where ϕ_i^r is the ith component of the mode shape vector.

If $f(\tau)$ is a Dirac delta function at $\tau=0$, then the response at location i resulting from the impulse at location k is

$$x_{ik} = \sum_{r=1}^{n} \frac{\phi_i^r \phi_k^r}{m^r \omega_d^r} e^{-\zeta^r \omega_n^r t} \sin(\omega_d^r t).$$

(A-33)

The cross-correlation function $R_{ijk}(t)$ relating two measure responses at locations i and j caused by a white noise random input at k is given by Bendat and Piersol (1980) as

$$R_{ijk}(T) = E\{x_{ik}(t+T)x_{jk}(t)\}.$$

(A-34)

Substituting Eq. A-32 into A-34 and noting that $f_k(t)$ is the only random variable yields

$$R_{ijk}(T) = \sum_{r=1}^{n} \sum_{s=1}^{n} \phi_i^r \phi_k^r \phi_j^s \phi_k^s \int_{-\infty}^{t} \int_{-\infty}^{t+T} g^r(t+T-\sigma) \ g^s(t-\tau) \ E\{f_k(\sigma)f_k(\tau)\} \ d\sigma d\tau.$$

(A-35)

Based on the assumption that $f(t)$ is a white noise function and using the definition of the autocorrelation function given in Bendat and Piersol (1980), the following relationship can be established for the autocorrelation function of f

$$E\{f_k(\sigma)f_k(\tau)\} = \alpha_k \delta(\tau - \sigma)$$

(A-36)

where α_k is a constant and $\delta(t)$ is the Dirac delta function.

Substituting A-36 into A-35 and changing the variable of integration to $\lambda = t - \tau$ yields

$$R_{ijk}(T) = \sum_{r=1}^{n} \sum_{s=1}^{n} \alpha_k \phi_i^r \phi_k^r \phi_j^s \phi_k^s \int_{0}^{\infty} g^r(\lambda + T) \ g^s(\lambda) \ d\lambda.$$

(A-37)

From the previous definition of g^r and the trigonometric identity for the sine of a sum, $g^r(\lambda + T)$ can be expressed with terms involving T separated from those involving λ resulting in

$$g^r(\lambda + T) = \left[e^{-\zeta^r \omega_n^r T} \cos(\omega_d^r T) \right] \frac{e^{-\zeta^r \omega_n^r \lambda} \sin(\omega_d^r \lambda)}{m^r \omega_d^r} + \left[e^{-\zeta^r \omega_n^r T} \sin(\omega_d^r T) \right] \frac{e^{-\zeta^r \omega_n^r \lambda} \cos(\omega_d^r \lambda)}{m^r \omega_d^r}$$

(A-38)

When Eq. A-38 is substituted into A-37 along with the corresponding term for $g^s(\lambda)$, the terms involving T can be factored out of the integral and the summation on s yielding the following form for the cross-correlation function

$$R_{ijk}(T) = \sum_{r=1}^{n} G_{ijk}^r \left[e^{-\zeta^r \omega_n^r T} \cos(\omega_d^r T) \right] + H_{ijk}^r \left[e^{-\zeta^r \omega_n^r T} \sin(\omega_d^r T) \right], \qquad (A\text{-}39)$$

where

$$\begin{Bmatrix} G_{ijk}^r \\ H_{ijk}^r \end{Bmatrix} = \sum_{s=1}^{n} \frac{\alpha_k \phi_i^r \phi_k^r \phi_j^s \phi_k^s}{m^r \omega_d^r m^s \omega_d^s} \int_0^\infty e^{(-\zeta^r \omega_n^r - \zeta^s \omega_n^s)\lambda} \sin(\omega_d^r \lambda) \begin{Bmatrix} \sin(\omega_d^r \lambda) \\ \cos(\omega_d^r \lambda) \end{Bmatrix} d\lambda. \qquad (A\text{-}40)$$

From Eqs A-39 and A-40 it is evident that the cross-correlation function between two response measurements that result from an unknown white noise excitation have the form of decaying sinusoids, and these decaying sinusoids have the same characteristics as the system's impulse response function. Therefore time-domain modal identification techniques such as the complex exponential method can be applied to these cross-correlation functions (again, the inverse Fourier transform of the cross-power spectrum) to estimate the systems resonant frequencies and modal damping values.

A. 4 Complex Exponential Curve Fitting Method

Previously, it was shown that the measured cross-correlation function relating two response measurements have the same form as the system's impulse response functions. The complex exponential curve-fitting method, which analyzes impulse response functions to determine dynamic properties of the system, will now be summarized. This method was used to analyze the measured ambient vibration data obtained in this study. This method is a multi-degree-of-freedom curve fitting algorithm, that is, the response in a particular frequency window is assumed to result from the superposition of several modes of response, and this method attempts to identify modal parameters for all modes contributing to this response. The method is particularly well suited for response caused by closely coupled modes and for lightly damped systems.

To begin, Eq. A-19 is written with the following substitutions

$$A_{ijN+1\ldots2N} = A_{ij1\ldots N}^*, \text{ and}$$

$$p_{N+1\ldots2N} = p_{1\ldots N}^*,$$

resulting in

$$h_{ij}(t) = \sum_{n=1}^{2N} A_{ijn} e^{p_n t}. \qquad (A\text{-}41)$$

The inverse Fourier transform of $H(\omega)$, which is defined for discrete, equally spaced frequencies will yield a discrete time domain function defined at equally spaced time intervals, $t_k = k\delta t$. Therefore

$$h_{ij}(t_k) = \sum_{n=1}^{2N} A_{ij_n} e^{P_n(k\delta t)}, \qquad k = 0....m, \qquad (A\text{-}42)$$

where m = the number of discrete time points. The subscripts ij are dropped for convenience and the following substitution is made to linearize the equation

$$z_n = e^{P_n(\delta t)}, \qquad (A\text{-}43)$$

so that Eq. A-42 can now be written as

$$h(t_k) = \sum_{n=1}^{2N} A_n(z_n)^k, \qquad k = 0....m, \qquad (A\text{-}44)$$

The method of collocation is now employed to define a polynomial whose 2N roots are the complex exponentials, z_n,

$$\prod_{n=1}^{2N}(z - z_n) = \sum_{k=0}^{2N} c_k(z_n)^k = 0. \qquad (A\text{-}45)$$

Next, both sides of Eq. A-44 are multiplied by the autoregression coefficients, c_k, and the equations are summed over the number of time points, which have been limited to 2N resulting in

$$\sum_{k=0}^{2N} c_k h(t_k) = \sum_{n=1}^{2N} \left(A_n \sum_{k=0}^{2N} c_k (z_n)^k \right). \qquad (A\text{-}46)$$

Substituting Eq. A-45 into A-46 yields

$$\sum_{k=0}^{2N} c_k h(t_k) = 0 \qquad (A\text{-}47)$$

Setting c_{2N} equal to one (which essentially scales to vector {c} by c_{2N}), and defining an initial time index, i, yields

$$\sum_{k=0}^{2N-1} c_k h(t_{i+k}) = -h(t_{i+2N}). \qquad (A\text{-}48)$$

Allowing i to very from 0 to 2N-1 yields 2N equations with 2N unknowns c_0 through c_{2N-1}. These equations can be expressed in matrix form as

$$\begin{bmatrix} h(t_0) & h(t_1) & \cdots & h(t_{2N-1}) \\ h(t_1) & h(t_2) & \cdots & h(t_{2N}) \\ \vdots & \vdots & \ddots & \vdots \\ h(t_{2N-1}) & h(t_{2N}) & \cdots & h(t_{4N-2}) \end{bmatrix} \begin{bmatrix} c_0 \\ c_1 \\ \vdots \\ c_{2N-1} \end{bmatrix} = \begin{bmatrix} h(t_{2N}) \\ h(t_{2N+1}) \\ \vdots \\ h(t_{4N-1}) \end{bmatrix}. \tag{A-49}$$

This equation can be solved for the values of c_k, and these values can be substituted into Eq. A-46 to solve for the 2N values of z_n. The poles of the system, which contain the resonant frequency and modal damping information can then be obtained from Eq. A-43.

APPENDIX B
Ambient Vibration Test Data

Modal Assurance Criteria   t2tr X t2tr

Mode	1	2	3	4	5	6
1	1.000	0.009	0.001	0.001	0.000	0.000
2	0.009	1.000	0.006	0.002	0.006	0.005
3	0.001	0.006	1.000	0.039	0.027	0.002
4	0.001	0.002	0.039	1.000	0.846	0.015
5	0.000	0.006	0.027	0.846	1.000	0.076
6	0.000	0.005	0.002	0.015	0.076	1.000

Modal Assurance Criteria   t4tr X t4tr

Mode	1	2	3	4	5	6
1	1.000	0.008	0.001	0.017	0.001	0.005
2	0.008	1.000	0.000	0.001	0.003	0.010
3	0.001	0.000	1.000	0.001	0.001	0.009
4	0.017	0.001	0.001	1.000	0.239	0.013
5	0.001	0.003	0.001	0.239	1.000	0.088
6	0.005	0.010	0.009	0.013	0.088	1.000

Modal Assurance Criteria   t5tr X t5tr

Mode	1	2	3	4	5	6
1	1.000	0.005	0.003	0.013	0.017	0.002
2	0.005	1.000	0.011	0.002	0.004	0.019
3	0.003	0.011	1.000	0.002	0.011	0.000
4	0.013	0.002	0.002	1.000	0.942	0.002
5	0.017	0.004	0.011	0.942	1.000	0.001
6	0.002	0.019	0.000	0.002	0.001	1.000

Modal Assurance Criteria   t10tr X t10tr

Mode	1	2	3	4	5	6
1	1.000	0.009	0.000	0.009	0.003	0.001
2	0.009	1.000	0.002	0.001	0.008	0.005
3	0.000	0.002	1.000	0.000	0.002	0.003
4	0.009	0.001	0.000	1.000	0.754	0.014
5	0.003	0.008	0.002	0.754	1.000	0.080
6	0.001	0.005	0.003	0.014	0.080	1.000

Modal Assurance Criteria   t11tr X t11tr

Mode	1	2	3	4	5	6
1	1.000	0.012	0.001	0.006	0.002	0.001
2	0.012	1.000	0.006	0.001	0.011	0.005
3	0.001	0.006	1.000	0.012	0.002	0.000
4	0.006	0.001	0.012	1.000	0.762	0.022
5	0.002	0.011	0.002	0.762	1.000	0.079
6	0.001	0.005	0.000	0.022	0.079	1.000

t15tr x t15tr

mode	1	2	3	4	5	6
1	1.000	0.002	0.001	0.007	0.006	0.004
2	0.002	1.000	0.005	0.002	0.001	0.003
3	0.001	0.005	1.000	0.000	0.000	0.003
4	0.007	0.002	0.000	1.000	0.962	0.002
5	0.006	0.001	0.000	0.962	1.000	0.004
6	0.004	0.003	0.003	0.002	0.004	1.000

Modal Assurance Criteria   t4tr X t1tr

Mode	1	2	3	4	5	6
1	0.997	0.008	0.001	0.013	0.001	0.004
2	0.007	0.954	0.004	0.001	0.002	0.009
3	0.001	0.001	0.993	0.000	0.007	0.004
4	0.007	0.001	0.002	0.887	0.436	0.044
5	0.002	0.000	0.006	0.050	0.804	0.064
6	0.002	0.007	0.005	0.013	0.024	0.911

Modal Assurance Criteria   t5tr X t1tr

Mode	1	2	3	4	5	6
1	0.997	0.006	0.003	0.013	0.017	0.001
2	0.004	0.906	0.006	0.001	0.000	0.014
3	0.001	0.015	0.989	0.001	0.002	0.002
4	0.005	0.003	0.000	0.928	0.974	0.016
5	0.001	0.006	0.011	0.079	0.187	0.043
6	0.001	0.008	0.001	0.013	0.004	0.978

Modal Assurance Criteria   t10tr X t1tr

Mode	1	2	3	4	5	6
1	0.998	0.007	0.001	0.007	0.002	0.000
2	0.007	0.997	0.003	0.001	0.010	0.005
3	0.000	0.005	0.997	0.001	0.005	0.004
4	0.007	0.000	0.002	0.896	0.511	0.029
5	0.001	0.003	0.012	0.031	0.103	0.030
6	0.001	0.003	0.002	0.016	0.082	0.996

Modal Assurance Criteria   t11tr X t1tr

Mode	1	2	3	4	5	6
1	0.996	0.007	0.001	0.008	0.002	0.000
2	0.012	0.998	0.004	0.000	0.011	0.007
3	0.001	0.007	0.991	0.005	0.001	0.002
4	0.004	0.000	0.002	0.827	0.590	0.022
5	0.001	0.004	0.010	0.006	0.120	0.017
6	0.001	0.003	0.000	0.020	0.076	0.997

Modal Assurance Criteria   t15tr X t1tr

mode	1	2	3	4	5	6
1	0.992	0.006	0.002	0.003	0.002	0.003
2	0.003	0.967	0.008	0.004	0.003	0.003
3	0.001	0.010	0.964	0.010	0.004	0.006

4	0.010	0.001	0.028	0.934	0.855	0.005
5	0.000	0.002	0.002	0.336	0.417	0.010
6	0.001	0.003	0.001	0.020	0.021	0.983

Modal Assurance Criteria   t10tr X t2tr

Mode	1	2	3	4	5	6
1	0.997	0.007	0.001	0.006	0.002	0.000
2	0.010	0.985	0.011	0.002	0.017	0.005
3	0.000	0.003	0.990	0.000	0.005	0.005
4	0.003	0.000	0.017	0.487	0.155	0.029
5	0.001	0.002	0.021	0.220	0.048	0.102
6	0.001	0.003	0.001	0.012	0.075	0.995

Modal Assurance Criteria   t11tr X t2tr

Mode	1	2	3	4	5	6
1	0.996	0.006	0.001	0.007	0.002	0.000
2	0.014	0.991	0.013	0.001	0.019	0.008
3	0.000	0.003	0.987	0.003	0.000	0.002
4	0.001	0.000	0.013	0.392	0.244	0.015
5	0.000	0.003	0.023	0.152	0.113	0.079
6	0.001	0.002	0.001	0.019	0.067	0.998

Modal Assurance Criteria   t15tr X t2tr

Mode	1	2	3	4	5	6
1	0.993	0.002	0.000	0.004	0.001	0.001
2	0.004	0.944	0.014	0.000	0.000	0.005
3	0.002	0.016	0.951	0.036	0.003	0.001
4	0.002	0.007	0.011	0.821	0.620	0.014
5	0.002	0.007	0.005	0.798	0.618	0.015
6	0.003	0.003	0.005	0.003	0.062	0.988

Modal Assurance Criteria   t11tr X t10tr

Mode	1	2	3	4	5	6
1	0.998	0.008	0.001	0.010	0.003	0.001
2	0.013	0.998	0.003	0.001	0.008	0.006
3	0.000	0.005	0.996	0.004	0.001	0.001
4	0.005	0.001	0.002	0.982	0.791	0.015
5	0.002	0.010	0.003	0.748	0.981	0.085
6	0.001	0.003	0.002	0.017	0.071	0.992

Modal Assurance Criteria   t5tr X t15tr

Mode	1	2	3	4	5	6
1	0.993	0.003	0.003	0.020	0.025	0.002
2	0.005	0.937	0.015	0.000	0.002	0.013
3	0.002	0.026	0.942	0.025	0.009	0.001
4	0.003	0.008	0.032	0.801	0.930	0.013
5	0.003	0.009	0.021	0.673	0.839	0.017
6	0.004	0.008	0.002	0.006	0.001	0.970

		Mode 1 F=2.39 Hz ζ=1.28%	Mode 2 F=2.92Hz ζ=1.18%	Mode 3 F=3.42Hz ζ=1.00%	Mode 4 F=3.96 Hz ζ=0.94%	Mode 5 F=4.10Hz ζ=1.58%	Mode 6 F=4.56 Hz ζ=1.56%
Test t1tr Undamaged Ambient Vibration Results							
Resonant Frequencies and Modal Damping From NExT Method, Mode Shapes From CPS							
Location							
S1	M =	27.6	25.4	248.0	351.0	111.0	63.7
	P =	15.8	-8.9	39.0	18.7	-0.2	17.3
S2	M =	1320.0	839.0	8250.0	9890.0	2510.0	1580.0
	P =	-1.9	-0.8	-0.8	-0.5	-0.4	0.5
S3	M =	1950.0	1260.0	11000.0	12600.0	3310.0	2040.0
	P =	-2.2	-1.1	-1.2	-0.6	-0.3	0.2
S4	M =	1520.0	1020.0	7330.0	7680.0	2180.0	1270.0
	P =	0.3	0.2	-0.2	-0.4	0.4	0.7
S5	M =	16.8	4.2	460.0	784.0	166.0	145.0
	P =	28.2	9.4	2.0	-3.1	-0.3	-2.1
S6	M =	2720.0	1910.0	2760.0	4130.0	142.0	1060.0
	P =	179.0	178.0	178.0	1.2	-171.0	-9.0
S7	M =	4070.0	2800.0	564.0	8660.0	692.0	1900.0
	P =	-179.0	179.0	173.0	1.0	-4.7	-7.5
S8	M =	2770.0	1920.0	2040.0	5700.0	896.0	1180.0
	P =	-179.0	177.0	0.0	-0.2	-3.3	-7.5
S9	M =	60.9	65.7	173.0	508.0	18.4	145.0
	P =	-173.0	172.0	170.0	-8.9	-126.0	-5.3
S10	M =	1610.0	1070.0	7540.0	3230.0	1290.0	1150.0
	P =	0.4	-6.8	178.0	3.3	-179.0	-4.2
S11	M =	2070.0	1400.0	11700.0	6220.0	1850.0	1960.0
	P =	2.1	-7.7	178.0	4.4	-179.0	-4.6
S12	M =	1400.0	955.0	8800.0	5120.0	1340.0	1580.0
	P =	3.8	-7.2	179.0	4.6	-178.0	-4.1
S13	M =	58.6	52.0	440.0	295.0	54.6	107.0
	P =	5.0	-4.2	178.0	5.6	172.0	-4.0
N1	M =	50.5	32.7	373.0	227.0	126.0	123.0
	P =	10.7	170.0	14.6	26.1	-177.0	-177.0
N2	M =	1130.0	1090.0	7210.0	3920.0	2460.0	2290.0
	P =	2.7	168.0	11.4	27.5	174.0	172.0
N3	M =	1630.0	1560.0	9370.0	4690.0	3260.0	2780.0
	P =	2.9	168.0	10.9	29.8	174.0	173.0
N4	M =	1220.0	1160.0	5840.0	2390.0	2090.0	1510.0
	P =	2.4	168.0	9.6	33.8	174.0	173.0
N5	M =	30.0	10.8	429.0	340.0	123.0	185.0
	P =	8.7	-156.0	20.7	12.3	167.0	169.0
N6	M =	2160.0	2210.0	1800.0	4420.0	1020.0	1400.0
	P =	-177.0	-10.4	-175.0	3.3	6.7	163.0
N7	M =	3240.0	3310.0	285.0	6680.0	552.0	2410.0
	P =	-175.0	-8.5	-31.9	8.1	18.8	167.0
N8	M =	2200.0	2320.0	2010.0	3240.0	404.0	1400.0
	P =	-177.0	-7.6	8.1	9.3	166.0	166.0
N9	M =	65.1	88.9	99.3	422.0	88.1	167.0
	P =	174.0	-14.4	-143.0	17.3	-12.5	161.0
N10	M =	1280.0	1290.0	6000.0	5330.0	2520.0	1410.0
	P =	6.1	180.0	-173.0	2.2	-4.2	164.0
N11	M =	1640.0	1660.0	8980.0	8960.0	2800.0	2370.0
	P =	7.2	-180.0	-173.0	3.2	-2.6	165.0
N12	M =	1160.0	1160.0	6920.0	7300.0	2930.0	1940.0
	P =	7.7	-180.0	-174.0	3.0	-2.4	166.0
N13	M =	71.7	77.2	419.0	537.0	175.0	150.0
	P =	10.1	-178.0	-179.0	2.3	1.5	172.0
ref	M =	1380.0	917.7	8634.0	10400.0	2670.0	1704.0
M = magnitude in g^2 *10^{-9}, P = phase in degrees, reference acceleration near S2							

120

		Mode 1 F=2.43 Hz ζ= 2.39%	Mode 2 F=2.98 Hz ζ= 2.52%	Mode 3 F=3.51 Hz ζ= 1.06%	Mode 4 F=3.97 Hz ζ= 1.20%	Mode 5 F=4.17 Hz ζ= 1.79%	Mode 6 F=4.64 Hz ζ= 1.29%
Location							
S1	M =	72.2	82.7	842.0	726.0	251.0	210.0
	P =	1.1	-8.7	42.5	14.5	7.6	-2.3
S2	M =	3350.0	2700.0	31200.0	17800.0	5780.0	5410.0
	P =	-2.1	-0.5	-0.7	-0.5	-0.2	-0.3
S3	M =	4950.0	4010.0	42100.0	23300.0	7580.0	7090.0
	P =	-1.6	-1.3	-0.6	-0.3	0.2	-0.1
S4	M =	3860.0	3210.0	28000.0	14700.0	4840.0	4410.0
	P =	0.6	-0.5	0.3	0.1	1.0	0.2
S5	M =	17.0	21.1	1620.0	1350.0	449.0	513.0
	P =	22.9	-26.3	5.7	-2.5	-1.6	0.3
S6	M =	7010.0	5980.0	10900.0	3900.0	1360.0	3530.0
	P =	179.0	175.0	-177.0	-7.1	-12.3	-2.5
S7	M =	10500.0	8810.0	2710.0	11100.0	3690.0	6310.0
	P =	-179.0	175.0	-157.0	-3.1	-7.5	-1.6
S8	M =	7160.0	5980.0	8090.0	8450.0	2900.0	3870.0
	P =	180.0	173.0	-5.7	-2.7	-6.5	-2.2
S9	M =	255.0	45.9	745.0	104.0	132.0	503.0
	P =	168.0	-160.0	157.0	-12.9	-5.7	2.5
S10	M =	3980.0	4340.0	28200.0	3890.0	553.0	3950.0
	P =	7.8	-9.5	175.0	171.0	-149.0	4.0
S11	M =	5300.0	4500.0	45900.0	539.0	626.0	6690.0
	P =	2.4	-14.9	-180.0	-47.1	-84.7	-0.7
S12	M =	3570.0	2970.0	34400.0	1270.0	651.0	5330.0
	P =	2.9	-15.5	-179.0	-16.5	-64.6	-0.4
S13	M =	125.0	201.0	1480.0	93.4	29.9	317.0
	P =	10.2	-10.5	-178.0	-159.0	65.7	0.6
N1	M =	161.0	67.7	1060.0	167.0	193.0	405.0
	P =	-0.2	140.0	20.5	86.2	-173.0	-180.0
N2	M =	3100.0	3070.0	25700.0	3670.0	3690.0	7880.0
	P =	3.0	154.0	12.7	113.0	176.0	177.0
N3	M =	4410.0	4480.0	33600.0	4920.0	4880.0	9660.0
	P =	3.1	155.0	12.3	121.0	176.0	177.0
N4	M =	3260.0	3310.0	21000.0	3370.0	3050.0	5270.0
	P =	2.4	155.0	11.8	131.0	176.0	177.0
N5	M =	37.8	28.7	1210.0	251.0	162.0	650.0
	P =	7.7	137.0	24.6	47.8	171.0	174.0
N6	M =	5770.0	6500.0	7610.0	7890.0	1810.0	4810.0
	P =	-176.0	-17.8	-169.0	-1.6	11.2	170.0
N7	M =	8590.0	9810.0	599.0	9300.0	1130.0	8490.0
	P =	-175.0	-14.3	-118.0	4.0	18.3	173.0
N8	M =	5810.0	6920.0	6600.0	2920.0	477.0	4990.0
	P =	-177.0	-12.1	14.1	11.5	178.0	175.0
N9	M =	601.0	950.0	1680.0	1350.0	479.0	684.0
	P =	145.0	-2.3	51.5	170.0	75.7	150.0
N10	M =	3230.0	3980.0	22500.0	11400.0	4190.0	5320.0
	P =	7.8	-179.0	-165.0	-4.5	3.2	168.0
N11	M =	4280.0	5420.0	34500.0	18800.0	6320.0	8820.0
	P =	7.1	-175.0	-163.0	-2.9	1.2	170.0
N12	M =	3000.0	3800.0	26100.0	15000.0	4800.0	7130.0
	P =	6.8	-174.0	-163.0	-3.2	0.7	170.0
N13	M =	165.0	243.0	1450.0	1130.0	263.0	508.0
	P =	0.0	-173.0	-163.0	-3.2	-5.3	173.0
ref	M =	3490.0	2892.0	32720.0	18880.0	6163.0	5858.0

M = magnitude in $g^2 * 10^{-9}$, P = phase in degrees, reference acceleration near S2

		Mode 1 F=2.41 Hz	Mode 2 F=2.94 Hz	Mode 3 F=3.45 Hz	Mode 4 F=3.98 Hz	Mode 5 F=4.17 Hz	Mode 6 F=4.62 Hz
			Test t4tr Cross Spectral Density Values Undamaged Ambient Vibration (Peak Amplitude Estimation)				
Location							
S1	M =	3.8	3.8	39.3	73.6	52.1	18.8
	P =	50.1	-28.3	22.8	6.2	12.7	15.7
S2	M =	100.0	97.0	2850.0	3620.0	1130.0	514.0
	P =	-3.8	-0.5	1.0	-0.4	-0.1	-1.0
S3	M =	142.0	146.0	3810.0	4580.0	1460.0	656.0
	P =	-4.3	1.4	-0.9	-0.2	0.0	0.1
S4	M =	114.0	115.0	2570.0	2710.0	932.0	411.0
	P =	-2.8	2.4	-0.7	1.7	1.0	-1.0
S5	M =	1.6	3.3	161.0	329.0	79.2	48.6
	P =	-107.0	-109.0	8.8	-2.8	3.7	5.5
S6	M =	198.0	227.0	1060.0	2170.0	180.0	298.0
	P =	178.0	-175.0	178.0	-10.7	-9.5	2.4
S7	M =	294.0	348.0	231.0	3930.0	608.0	547.0
	P =	177.0	-174.0	174.0	-6.3	1.1	-2.2
S8	M =	203.0	244.0	738.0	2350.0	576.0	347.0
	P =	177.0	-174.0	1.4	-3.4	3.4	-3.0
S9	M =	3.3	8.9	116.0	311.0	15.2	46.6
	P =	-124.0	-168.0	171.0	-9.2	-62.6	2.4
S10	M =	124.0	120.0	2780.0	2520.0	307.0	341.0
	P =	-6.0	3.9	-180.0	-16.5	-172.0	-1.7
S11	M =	152.0	176.0	4270.0	4370.0	350.0	586.0
	P =	2.6	8.2	180.0	-13.2	-166.0	47.1
S12	M =	107.0	119.0	3160.0	3410.0	229.0	460.0
	P =	2.2	12.2	-179.0	-12.0	-162.0	1.2
S13	M =	3.1	5.4	72.4	167.0	19.8	24.0
	P =	-40.2	15.2	171.0	-0.2	-140.0	4.5
N1	M =	2.9	5.7	109.0	149.0	19.1	38.6
	P =	25.6	-121.0	7.3	-10.1	-158.0	-170.0
N2	M =	93.6	125.0	2720.0	2900.0	585.0	631.0
	P =	7.4	-175.0	2.9	-8.8	-167.0	177.0
N3	M =	134.0	182.0	3580.0	3600.0	792.0	790.0
	P =	3.7	-175.0	3.0	-9.5	-169.0	177.0
N4	M =	95.7	142.0	2280.0	1980.0	526.0	447.0
	P =	0.3	-178.0	2.5	-11.5	-172.0	177.0
N5	M =	6.3	4.4	145.0	247.0	30.6	46.2
	P =	8.9	117.0	-3.0	-12.1	-145.0	171.0
N6	M =	147.0	97.7	545.0	1390.0	125.0	109.0
	P =	177.0	13.1	-170.0	7.9	-28.2	177.0
N7	M =	243.0	415.0	155.0	3380.0	341.0	608.0
	P =	-179.0	2.9	-120.0	1.1	-12.8	176.0
N8	M =	163.0	280.0	676.0	1870.0	35.4	386.0
	P =	-179.0	1.7	-6.5	-1.9	-153.0	173.0
N9	M =	4.1	10.2	53.9	250.0	68.1	48.6
	P =	156.0	1.2	-154.0	1.5	1.9	165.0
N10	M =	93.4	155.0	2270.0	2300.0	99.3	368.0
	P =	7.9	178.0	-179.0	6.0	-3.4	-178.0
N11	M =	119.0	198.0	3410.0	3840.0	1530.0	366.0
	P =	6.1	-179.0	-178.0	5.8	-3.5	-179.0
N12	M =	82.9	137.0	2560.0	3150.0	1170.0	512.0
	P =	5.8	179.0	-178.0	5.7	-4.0	179.0
N13	M =	4.1	10.3	134.0	208.0	66.4	42.1
	P =	30.1	-153.0	178.0	15.3	2.3	170.0
ref	M =	103.3	101.9	3002.0	3810.0	1188.0	557.1

M = magnitude in $g^2 \cdot 10^{-9}$, P = phase in degrees, reference acceleration near S2

Location		Mode 1 F=2.36 Hz	Mode 2 F=2.92 Hz	Mode 3 F=3.45 Hz	Mode 4 F=3.98 Hz	Mode 5 F=4.06 Hz	Mode 6 F=4.61 Hz
S1	M =	1.6	3.4	164.0	90.3	25.9	75.8
	P =	2.2	15.2	31.2	24.0	13.6	-8.3
S2	M =	249.0	187.0	9800.0	3300.0	1200.0	1490.0
	P =	-1.8	-1.9	-0.8	-0.5	-0.3	-0.2
S3	M =	376.0	275.0	13200.0	4190.0	1550.0	1880.0
	P =	-1.4	0.7	-0.6	-0.3	0.1	0.7
S4	M =	297.0	230.0	8910.0	2530.0	960.0	1170.0
	P =	1.1	3.5	-0.2	1.3	-0.4	2.1
S5	M =	5.9	1.4	501.0	272.0	97.7	150.0
	P =	8.3	-47.1	2.4	-4.7	-3.1	-1.7
S6	M =	535.0	467.0	3870.0	1670.0	532.0	855.0
	P =	-179.0	-170.0	178.0	-10.5	1.5	-5.2
S7	M =	802.0	706.0	1230.0	3210.0	1030.0	1470.0
	P =	-178.0	-167.0	175.0	-5.6	3.7	-3.2
S8	M =	539.0	492.0	2380.0	1990.0	669.0	866.0
	P =	-178.0	167.0	2.0	-1.8	3.9	-2.5
S9	M =	12.1	11.8	367.0	236.0	73.1	109.0
	P =	175.0	-160.0	170.0	-5.0	-5.4	-14.2
S10	M =	319.0	274.0	9940.0	1800.0	575.0	912.0
	P =	3.0	19.3	178.0	-16.8	2.1	-7.5
S11	M =	397.0	363.0	15300.0	3170.0	995.0	1560.0
	P =	3.6	19.8	179.0	-13.5	2.2	-4.9
S12	M =	266.0	245.0	11300.0	2500.0	780.0	1220.0
	P =	6.0	23.0	180.0	-11.9	4.0	-3.8
S13	M =	8.5	6.5	428.0	106.0	57.0	53.1
	P =	1.9	23.5	-178.0	-0.8	-21.1	-15.2
N1	M =	3.0	11.9	326.0	106.0	10.9	97.2
	P =	11.9	-143.0	16.8	-2.7	-10.4	-171.0
N2	M =	244.0	315.0	8340.0	2340.0	496.0	2010.0
	P =	1.8	-149.0	9.7	-6.3	10.5	-178.0
N3	M =	346.0	451.0	10900.0	2830.0	615.0	2480.0
	P =	1.1	-151.0	9.3	-5.9	13.8	-178.0
N4	M =	257.0	326.0	6800.0	1520.0	324.0	1390.0
	P =	1.6	-155.0	8.4	-6.8	24.5	-178.0
N5	M =	5.0	5.0	387.0	173.0	42.4	157.0
	P =	-22.4	-170.0	8.4	-11.2	1.8	175.0
N6	M =	364.0	214.0	1650.0	1170.0	380.0	471.0
	P =	-177.0	15.9	-171.0	5.7	-2.1	-174.0
N7	M =	665.0	810.0	373.0	2800.0	932.0	1930.0
	P =	-175.0	13.8	-27.1	1.3	-7.1	176.0
N8	M =	449.0	542.0	2680.0	1490.0	448.0	1190.0
	P =	-177.0	10.2	3.5	-0.5	-3.8	175.0
N9	M =	19.2	24.0	243.0	190.0	80.2	136.0
	P =	162.0	8.9	174.0	-0.9	-6.7	170.0
N10	M =	252.0	271.0	9190.0	2010.0	868.0	1130.0
	P =	4.5	178.0	-178.0	2.3	-4.8	170.0
N11	M =	324.0	351.0	13600.0	3320.0	1370.0	1950.0
	P =	3.4	177.0	-177.0	2.8	-4.0	172.0
N12	M =	235.0	239.0	10200.0	2690.0	1090.0	1590.0
	P =	3.2	174.0	-177.0	2.6	-5.3	172.0
N13	M =	7.1	12.9	517.0	165.0	78.2	90.1
	P =	-23.0	174.0	-175.0	4.2	-5.6	165.0
ref	M =	268.9	201.4	10320.0	3465.0	1279.0	1567.0

Test t5tr Cross Spectral Density Values
Undamaged Ambient Vibration (Peak Amplitude Estimation)

M = magnitude in $g^2 * 10^{-9}$, P = phase in degrees, reference acceleration near S2

		Mode 1 F=2.38 Hz	Mode 2 F=2.92 Hz	Mode 3 F=3.45 Hz	Mode 4 F=4.00 Hz	Mode 5 F=4.12 Hz	Mode 6 F=4.59 Hz
Test t6tr Cross Spectral Density Values Undamaged Ambient Vibration (Peak Amplitude Estimation)

Location		Mode 1 F=2.38 Hz	Mode 2 F=2.92 Hz	Mode 3 F=3.45 Hz	Mode 4 F=4.00 Hz	Mode 5 F=4.12 Hz	Mode 6 F=4.59 Hz
S1	M =	11.4	89.8	334.8	271.7	98.8	178.6
	P =	-88.4	-175.9	143.1	145.4	154.7	166.8
S2	M =	39.7	635.6	526.6	1120.0	1042.0	1471.0
	P =	-22.3	178.7	144.8	152.2	168.4	174.9
S3	M =	77.4	875.6	596.6	1295.0	1163.0	1540.0
	P =	-19.1	179.4	143.4	153.1	168.2	175.6
S4	M =	143.1	789.9	461.2	1027.0	775.0	1020.0
	P =	-17.8	-176.2	144.0	155.0	166.0	177.5
S5	M =	162.1	210.0	148.1	227.9	89.9	60.1
	P =	-19.0	-153.0	151.0	156.0	30.8	-176.3
S6	M =	257.1	788.8	12.7	44.0	322.2	541.1
	P =	-24.4	-16.9	-120.3	27.1	2.2	177.3
S7	M =	330.1	1340.0	162.0	125.3	25.1	1007.0
	P =	-18.3	-9.6	6.5	-179.8	-17.8	177.1
S8	M =	257.4	883.4	119.1	158.6	228.4	546.3
	P =	-21.0	-9.6	-1.1	-164.0	-167.0	177.7
S9	M =	76.8	125.0	116.5	182.3	84.6	56.6
	P =	-29.2	178.0	-75.8	-38.6	-119.0	-18.0
S10	M =	54.5	683.6	487.6	481.2	479.6	968.0
	P =	-3.8	172.2	-49.4	-41.2	-22.2	175.3
S11	M =	103.9	851.9	754.5	617.0	656.9	1403.0
	P =	172.5	171.2	-41.7	-23.7	-13.8	174.8
S12	M =	147.9	551.8	355.0	570.1	401.9	1294.0
	P =	170.4	163.5	-71.7	-12.1	-8.9	174.7
S13	M =	172.0	157.4	45.7	96.4	228.9	163.2
	P =	174.0	74.6	-56.8	72.5	151.9	167.7
N1	M =	28.5	90.6	27.7	133.3	88.4	183.5
	P =	158.5	5.8	-125.5	-42.5	-21.6	-13.1
N2	M =	39.5	632.2	1039.0	1391.0	1027.0	1390.0
	P =	155.3	1.6	-12.5	-16.3	-9.9	-4.6
N3	M =	44.1	840.6	1440.0	1630.0	1157.0	1459.0
	P =	146.0	2.1	-11.3	-17.0	-9.6	-3.0
N4	M =	128.8	795.2	927.0	1207.0	770.4	943.3
	P =	162.3	4.1	-15.0	-19.0	-12.8	-2.1
N5	M =	157.2	197.6	143.9	181.3	104.2	40.2
	P =	160.9	29.6	-22.6	-24.8	-151.6	13.1
N6	M =	313.2	804.6	255.1	145.7	284.9	541.2
	P =	165.0	165.7	-174.5	1.3	-177.6	-2.1
N7	M =	369.1	1269.0	163.8	401.0	23.9	939.7
	P =	166.4	171.4	-167.5	5.7	34.9	-1.3
N8	M =	231.1	855.0	40.9	158.1	237.4	528.3
	P =	157.3	170.8	-82.4	26.0	9.5	-1.6
N9	M =	71.2	130.6	114.2	188.7	86.6	36.1
	P =	148.3	1.2	139.6	136.9	65.4	162.6
N10	M =	69.1	740.8	1129.0	424.4	481.7	940.3
	P =	14.1	-7.5	162.8	133.7	158.5	-4.7
N11	M =	107.7	889.1	972.1	494.8	658.9	1451.0
	P =	-8.9	-8.7	156.8	140.8	166.4	-5.0
N12	M =	190.3	556.2	1172.0	193.1	317.2	1220.0
	P =	-7.2	-18.6	165.8	115.4	168.5	-6.1
N13	M =	153.0	152.8	201.2	195.1	219.1	184.3
	P =	-8.6	-104.2	6.4	-147.7	-30.1	-11.4
ref	M =	891.2	872.4	11980.0	6224.0	2382.0	2165.0
M = magnitude in $g^2 \cdot 10^{-9}$, P = phase in degrees, reference acceleration near S2

Location		Mode 1 F=2.38 Hz	Mode 2 F=2.89 Hz	Mode 3 F=3.41 Hz	Mode 4 F=3.95 Hz	Mode 5 F=4.08 Hz	Mode 6 F=4.56 Hz
		Test t8tr Cross Spectral Density Values					
		Undamaged Ambient Vibration (Peak Amplitude Estimation)					
S1	M =	115.0	168.3	700.5	723.6	701.3	115.6
	P =	-33.0	19.3	-45.2	12.5	4.5	-11.1
S2	M =	124.4	124.3	859.6	706.1	548.8	69.5
	P =	-29.7	31.6	-42.1	5.4	8.1	1.7
S3	M =	80.4	108.8	599.7	241.5	243.8	54.1
	P =	-49.4	36.7	-85.3	9.3	11.5	-60.8
S4	M =	86.2	165.7	947.6	361.6	411.5	97.0
	P =	-133.9	155.0	-137.9	173.9	172.2	-150.4
S5	M =	114.2	169.7	889.2	66.9	249.0	67.2
	P =	-143.0	152.5	-131.4	159.1	169.3	-97.1
S6	M =	96.0	178.1	720.1	249.5	57.8	70.6
	P =	-131.2	145.2	-103.8	12.4	114.2	-42.7
S7	M =	68.6	104.1	702.4	131.8	79.2	10.3
	P =	-93.3	91.4	-85.5	12.2	35.8	-13.1
S8	M =	160.3	226.7	734.9	318.4	160.8	92.5
	P =	-25.9	29.6	-101.9	168.8	164.3	131.4
S9	M =	170.9	271.0	912.6	130.7	361.6	89.2
	P =	-24.7	20.1	-131.8	150.9	165.6	102.2
S10	M =	78.9	124.7	654.1	166.7	156.4	100.6
	P =	-70.2	58.1	-96.4	156.3	141.9	98.6
S11	M =	74.5	118.3	737.2	97.3	123.6	107.2
	P =	-72.8	66.2	-103.4	103.6	126.4	94.1
S12	M =	96.6	158.7	879.1	406.4	327.0	176.5
	P =	-127.2	132.0	-48.0	171.7	5.2	134.0
S13	M =	105.7	161.0	1014.0	496.0	407.1	173.0
	P =	-133.1	135.0	-40.8	173.0	2.8	140.4
N1	M =	116.4	178.1	740.4	397.9	610.4	207.3
	P =	-25.9	146.1	-35.1	34.4	163.7	154.6
N2	M =	88.7	95.4	554.0	203.5	217.8	99.0
	P =	-38.5	110.0	-70.2	40.5	155.5	139.7
N3	M =	60.5	147.9	724.2	29.3	343.4	87.9
	P =	-80.8	26.1	-117.9	103.3	-1.5	38.4
N4	M =	68.1	161.7	800.3	48.4	385.0	100.2
	P =	-111.9	20.5	-123.0	142.0	2.1	63.0
N5	M =	98.6	291.0	813.9	120.9	459.2	108.1
	P =	-136.4	7.6	-123.3	23.8	2.8	96.0
N6	M =	131.6	409.8	675.4	394.5	321.8	177.8
	P =	-143.8	2.9	-103.0	19.1	17.6	138.2
N7	M =	155.1	254.0	682.8	231.5	54.8	66.0
	P =	-23.3	152.6	-76.6	164.7	77.6	8.1
N8	M =	133.7	180.0	713.2	175.4	188.2	54.7
	P =	-26.1	148.8	-91.6	163.0	12.1	-15.8
N9	M =	171.1	274.9	900.1	135.3	587.8	15.9
	P =	-23.1	161.1	-118.1	30.5	0.6	-107.6
N10	M =	153.1	231.1	1100.0	489.5	905.7	111.7
	P =	-24.7	161.5	-130.6	8.6	-3.7	177.4
N11	M =	80.0	82.8	769.9	85.7	323.0	50.0
	P =	-62.2	107.4	-99.1	20.9	1.4	-130.3
N12	M =	89.3	186.3	764.9	426.7	433.9	166.6
	P =	-111.6	20.8	-55.6	-168.7	170.8	-37.9
N13	M =	80.1	234.9	809.0	426.2	550.2	212.0
	P =	-114.6	32.4	-51.2	-176.2	168.7	-33.0
ref	M =	891.2	1407.0	8226.0	7294.0	5919.0	67.2
M = magnitude in $g^2 \cdot 10^{-9}$, P = phase in degrees, reference acceleration near S2							

| | Test t10tr Undamaged Ambient Vibration Results | | | | | |
| | Resonant Frequencies and Modal Damping From NExT Method, Mode Shapes From CPS | | | | | |
Location	Mode 1 F=2.42 Hz ζ=1.15%	Mode 2 F=2.93 Hz ζ=1.18%	Mode 3 F=3.46 Hz ζ=0.85%	Mode 4 F=3.99Hz ζ=0.70%	Mode 5 F=4.12 Hz ζ=0.59%	Mode 6 F=4.61 Hz ζ=0.97%
S1 M =	26.6	49.6	49.2	108.0	12.8	67.4
P =	174.0	175.0	-150.0	25.1	17.9	3.8
S2 M =	1970.0	1430.0	2920.0	3730.0	554.0	1530.0
P =	176.0	-178.0	177.0	-4.5	-20.5	4.9
S3 M =	2900.0	2180.0	3920.0	4710.0	687.0	1980.0
P =	177.0	-179.0	178.0	-4.7	-21.9	4.8
S4 M =	2260.0	1750.0	2620.0	2780.0	390.0	1210.0
P =	179.0	-178.0	178.0	-4.6	-25.9	5.5
S5 M =	58.1	6.7	151.0	328.0	55.7	145.0
P =	-155.0	-70.6	177.0	-7.6	-21.6	4.5
S6 M =	4100.0	3710.0	1090.0	2330.0	528.0	989.0
P =	-1.7	-1.4	-1.2	-0.6	-0.6	-0.7
S7 M =	6120.0	5470.0	315.0	4200.0	835.0	1760.0
P =	-0.2	-1.1	4.4	-1.2	-4.7	0.6
S8 M =	4210.0	3850.0	659.0	2480.0	435.0	1110.0
P =	-1.1	-2.5	177.0	-2.8	-11.8	0.5
S9 M =	131.0	123.0	107.0	307.0	74.8	147.0
P =	6.7	-1.4	-7.5	-3.8	-6.4	-1.7
S10 M =	2450.0	2180.0	2700.0	2680.0	763.0	1140.0
P =	178.0	175.0	-2.9	2.1	7.0	-1.8
S11 M =	3180.0	2860.0	4190.0	4690.0	1280.0	1940.0
P =	179.0	174.0	-2.1	2.4	6.4	1.3
S12 M =	2130.0	1960.0	3120.0	3700.0	991.0	1530.0
P =	-180.0	175.0	-1.1	3.1	7.2	-0.6
S13 M =	75.6	89.3	140.0	200.0	60.4	84.5
P =	170.0	169.0	-4.5	3.5	17.2	-5.3
N1 M =	26.0	71.2	96.1	157.0	36.4	97.2
P =	-127.0	-15.1	-173.0	15.7	19.9	-180.0
N2 M =	1890.0	2290.0	2600.0	3200.0	638.0	2090.0
P =	-175.0	-12.6	-174.0	12.0	22.9	-179.0
N3 M =	2710.0	3330.0	3380.0	3930.0	786.0	2630.0
P =	-176.0	-12.2	-174.0	12.7	24.4	-178.0
N4 M =	2010.0	2470.0	2100.0	2160.0	459.0	1470.0
P =	-177.0	-12.8	-175.0	12.8	23.9	-177.0
N5 M =	21.6	34.0	121.0	250.0	41.6	180.0
P =	169.0	-23.2	-176.0	4.8	12.0	175.0
N6 M =	3450.0	4380.0	690.0	1980.0	186.0	1290.0
P =	3.5	170.0	1.4	-2.1	-2.9	168.0
N7 M =	5170.0	6490.0	129.0	3520.0	444.0	2180.0
P =	5.1	172.0	-151.0	1.6	8.5	174.0
N8 M =	3510.0	4420.0	787.0	2060.0	318.0	1230.0
P =	3.2	173.0	-173.0	2.8	11.6	176.0
N9 M =	111.0	175.0	63.6	216.0	14.7	164.0
P =	7.4	174.0	0.3	1.2	-10.8	168.0
N10 M =	2140.0	2290.0	2410.0	1760.0	142.0	1400.0
P =	-178.0	-2.5	3.8	-0.6	-149.0	164.0
N11 M =	2780.0	2940.0	3570.0	3040.0	185.0	2320.0
P =	-178.0	0.0	4.9	0.5	-147.0	166.0
N12 M =	1950.0	2030.0	2710.0	2500.0	143.0	1880.0
P =	-179.0	0.2	4.2	0.4	-148.0	167.0
N13 M =	87.6	118.0	153.0	157.0	21.3	133.0
P =	172.0	6.0	1.0	-0.3	-125.0	171.0
ref M =	4053.0	3619.0	1085.0	2290.0	519.0	961.7

M = magnitude in $g^2 * 10^{-9}$, P = phase in degrees, reference acceleration near S6

126

Location	Mode 1 F=2.42 Hz ζ=2.15%	Mode 2 F=2.99 Hz ζ=1.78%	Mode 3 F=3.51 Hz ζ=1.37%	Mode 4 F=4.03 Hz ζ=1.74%	Mode 5 F=4.18 Hz ζ=1.52%	Mode 6 F=4.70 Hz ζ=1.18%
Test t11tr Undamaged Ambient Vibration Results						
Resonant Frequencies and Modal Damping From NExT Method, Mode Shapes From CPS						
S1 M =	117.0	213.0	149.0	278.0	68.2	211.0
P =	163.0	179.0	-135.0	16.8	14.6	-4.4
S2 M =	7300.0	7300.0	9470.0	8870.0	1720.0	5030.0
P =	177.0	-178.0	178.0	-6.3	-20.5	0.6
S3 M =	10800.0	11000.0	12700.0	11100.0	2160.0	6510.0
P =	177.0	-178.0	179.0	-6.4	-21.8	1.0
S4 M =	8400.0	8830.0	8570.0	6390.0	1260.0	3970.0
P =	179.0	-177.0	179.0	-6.9	-24.8	1.4
S5 M =	63.9	50.3	464.0	833.0	177.0	486.0
P =	-126.0	-99.3	178.0	-7.6	-15.1	-0.7
S6 M =	15400.0	18100.0	3740.0	6570.0	1470.0	3250.0
P =	-1.5	-1.5	-1.1	-0.6	-0.9	-0.8
S7 M =	23000.0	26500.0	1300.0	11300.0	2350.0	5730.0
P =	0.0	-1.3	-1.5	-1.5	-5.8	0.0
S8 M =	15800.0	18600.0	2110.0	6350.0	1260.0	3540.0
P =	-0.7	-3.1	-179.0	-2.8	-12.9	0.3
S9 M =	449.0	621.0	356.0	891.0	196.0	462.0
P =	-0.7	-1.4	-11.1	-2.5	-2.5	-0.6
S10 M =	9000.0	10400.0	9430.0	8320.0	2080.0	3730.0
P =	178.0	172.0	-1.4	0.1	7.5	-0.2
S11 M =	11600.0	13700.0	14700.0	14200.0	3430.0	6320.0
P =	179.0	171.0	-0.5	0.4	7.0	0.0
S12 M =	7780.0	9200.0	10900.0	11100.0	2640.0	4940.0
P =	-180.0	173.0	0.4	1.3	7.2	0.7
S13 M =	222.0	341.0	401.0	605.0	167.0	246.0
P =	-178.0	179.0	5.5	0.3	10.0	-0.7
N1 M =	197.0	381.0	235.0	623.0	96.6	395.0
P =	-166.0	-24.2	-168.0	5.4	51.7	178.0
N2 M =	6890.0	10400.0	7800.0	10200.0	1790.0	7260.0
P =	-175.0	-16.7	-173.0	4.7	34.3	175.0
N3 M =	9990.0	15300.0	10200.0	12400.0	2270.0	9060.0
P =	-174.0	-15.6	-173.0	5.3	34.4	174.0
N4 M =	7490.0	11400.0	6410.0	6740.0	1350.0	5100.0
P =	-175.0	-15.7	-174.0	4.0	35.1	174.0
N5 M =	61.5	120.0	349.0	787.0	132.0	611.0
P =	177.0	-36.4	-175.0	0.6	21.3	172.0
N6 M =	13700.0	21000.0	2570.0	5690.0	702.0	4160.0
P =	4.7	169.0	7.0	0.6	-6.2	172.0
N7 M =	20400.0	31400.0	329.0	10500.0	1360.0	7430.0
P =	6.7	172.0	22.3	1.2	10.1	172.0
N8 M =	13900.0	21700.0	2070.0	6320.0	889.0	4420.0
P =	5.0	173.0	-173.0	-0.2	19.3	171.0
N9 M =	471.0	890.0	291.0	671.0	50.9	594.0
P =	-1.9	172.0	-3.5	1.2	-16.3	168.0
N10 M =	7910.0	11400.0	8410.0	5250.0	463.0	4750.0
P =	-172.0	2.0	4.5	9.9	-99.0	171.0
N11 M =	10200.0	14500.0	12500.0	9060.0	683.0	7910.0
P =	-171.0	3.7	5.6	10.6	-96.6	172.0
N12 M =	7190.0	9980.0	9510.0	7480.0	545.0	6420.0
P =	-171.0	4.2	5.2	10.1	-95.6	172.0
N13 M =	314.0	606.0	509.0	459.0	83.7	398.0
P =	-158.0	6.3	4.7	13.1	-139.0	171.0
ref M =	15200.0	17680.0	3716.0	6455.0	7199.0	3169.0

M = magnitude in $g^2 *10^{-9}$, P = phase in degrees, reference acceleration near S6

		Mode 1 F=2.52 Hz ζ=1.28%	Mode 2 F=3.04 Hz ζ=0.38%	Mode 3 F=3.53 Hz ζ=0.89%	Mode 4 F=4.10 Hz ζ=1.08%	Mode 5 F=4.17 Hz ζ=0.92%	Mode 6 F=4.71 Hz ζ=0.60%
S1	M =	2.9	72.9	17.2	57.2	94.6	2.5
	P =	-39.6	20.1	-14.1	-60.7	-40.0	-28.6
S2	M =	48.7	2790.0	201.0	1570.0	1580.0	51.9
	P =	0.0	0.0	0.0	0.0	0.0	0.0
S3	M =	70.2	4120.0	265.0	2010.0	2040.0	67.1
	P =	-3.8	0.8	0.5	-0.3	-1.2	2.9
S4	M =	55.6	3160.0	174.0	1210.0	1240.0	38.3
	P =	2.1	3.4	-0.8	-0.6	-2.2	0.7
S5	M =	3.2	24.5	22.2	156.0	153.0	4.0
	P =	-6.0	-11.8	16.4	3.4	4.0	-3.8
S6	M =	92.6	5530.0	17.0	833.0	821.0	43.8
	P =	180.0	-174.0	175.0	12.4	22.3	6.8
S7	M =	137.0	7960.0	49.9	1650.0	1610.0	74.0
	P =	-179.0	-171.0	9.5	9.6	16.1	6.5
S8	M =	92.2	5370.0	90.8	1070.0	1050.0	46.0
	P =	-179.0	-171.0	1.9	4.4	8.3	5.8
S9	M =	3.1	209.0	4.9	112.0	115.0	5.4
	P =	-135.0	175.0	-33.5	9.5	21.0	6.8
S10	M =	54.8	2670.0	163.0	652.0	748.0	42.3
	P =	3.0	21.9	-178.0	30.6	54.9	4.8
S11	M =	71.0	3400.0	247.0	1210.0	1310.0	72.3
	P =	4.0	26.3	-176.0	29.8	51.2	6.4
S12	M =	47.0	2350.0	180.0	1010.0	1070.0	59.0
	P =	4.7	28.1	-176.0	29.6	50.2	8.5
S13	M =	3.2	135.0	5.2	61.7	61.2	4.4
	P =	-9.2	34.3	-144.0	27.8	42.4	-8.9
N1	M =	2.4	93.5	16.0	18.3	37.6	3.7
	P =	-40.1	-178.0	-6.7	77.4	53.1	-175.0
N2	M =	46.4	2590.0	184.0	483.0	795.0	87.7
	P =	1.1	-161.0	0.9	66.6	89.8	-174.0
N3	M =	66.1	3740.0	235.0	572.0	1000.0	108.0
	P =	-2.0	-162.0	0.9	73.4	94.7	-175.0
N4	M =	48.4	2780.0	157.0	328.0	601.0	58.0
	P =	-0.3	-163.0	4.6	86.4	101.0	-178.0
N5	M =	2.4	10.8	21.0	53.4	63.7	6.4
	P =	19.6	-177.0	2.3	59.9	75.2	178.0
N6	M =	82.0	5480.0	40.8	760.0	725.0	48.7
	P =	-180.0	15.2	-176.0	11.5	10.9	-171.0
N7	M =	124.0	8350.0	4.6	1080.0	1020.0	88.9
	P =	-179.0	15.3	-8.6	17.8	25.7	-172.0
N8	M =	81.8	5810.0	49.8	442.0	459.0	56.4
	P =	-179.0	13.3	0.5	23.8	42.7	-173.0
N9	M =	3.5	249.0	14.7	74.0	81.9	6.7
	P =	162.0	17.2	8.4	-4.0	-12.6	-178.0
N10	M =	51.9	3350.0	121.0	1330.0	1290.0	57.1
	P =	-2.4	-171.0	-178.0	3.5	-2.2	-176.0
N11	M =	67.9	4440.0	196.0	2140.0	2100.0	92.6
	P =	-0.6	-171.0	-177.0	4.6	-0.6	-176.0
N12	M =	46.5	3080.0	143.0	1710.0	1670.0	72.7
	P =	-2.5	-171.0	-177.0	4.6	0.1	-173.0
N13	M =	5.8	190.0	3.2	128.0	114.0	6.2
	P =	-1.8	-169.0	-45.9	2.4	-2.4	-157.0

Test t15tr Undamaged Ambient Vibration Results
Resonant Frequencies and Modal Damping From NExT Method, Mode Shapes From CPS

M = magnitude in $g^2 * 10^{-9}$, P = phase in degrees, reference acceleration is S2

APPENDIX C

Comparison of Ambient and Undamaged Forced Vibration Test Results

Modal Assurance Criteria   t2tr X t16tr

Mode	1	2	3	4	5	6
1	0.991	0.006	0.000	0.004	0.002	0.001
2	0.003	0.969	0.001	0.003	0.002	0.004
3	0.002	0.012	0.968	0.003	0.022	0.002
4	0.004	0.002	0.005	0.594	0.350	0.012
5	0.000	0.007	0.014	0.431	0.640	0.004
6	0.001	0.004	0.001	0.003	0.047	0.988

Modal Assurance Criteria   t4tr X t16tr

Mode	1	2	3	4	5	6
1	0.985	0.002	0.000	0.007	0.0C0	0.005
2	0.004	0.961	0.000	0.002	0.008	0.007
3	0.001	0.001	0.992	0.003	0.001	0.007
4	0.008	0.005	0.002	0.978	0.323	0.001
5	0.001	0.003	0.001	0.032	0.687	0.015
6	0.002	0.006	0.003	0.003	0.010	0.883

Modal Assurance Criteria   t5tr X t16tr

Mode	1	2	3	4	5	6
1	0.989	0.001	0.002	0.008	0.012	0.002
2	0.002	0.930	0.002	0.003	0.002	0.013
3	0.001	0.017	0.987	0.000	0.005	0.002
4	0.005	0.004	0.011	0.982	0.929	0.003
5	0.000	0.004	0.002	0.029	0.053	0.010
6	0.002	0.006	0.001	0.003	0.002	0.965

Modal Assurance Criteria   t10tr X t16tr

Mode	1	2	3	4	5	6
1	0.993	0.009	0.000	0.005	0.002	0.001
2	0.002	0.982	0.001	0.000	0.007	0.006
3	0.001	0.005	0.990	0.001	0.002	0.004
4	0.007	0.002	0.004	0.909	0.491	0.008
5	0.000	0.001	0.003	0.004	0.219	0.012
6	0.002	0.002	0.001	0.001	0.081	0.977

Modal Assurance Criteria   t11tr X t16tr

Mode	1	2	3	4	5	6
1	0.993	0.008	0.000	0.005	0.002	0.001
2	0.003	0.979	0.000	0.000	0.007	0.007
3	0.001	0.007	0.986	0.008	0.000	0.001
4	0.004	0.002	0.013	0.908	0.519	0.012
5	0.000	0.002	0.002	0.022	0.179	0.002
6	0.001	0.002	0.000	0.006	0.068	0.986

Modal Assurance Criteria t15tr X t16tr

mode	1	2	3	4	5	6
1	0.992	0.000	0.001	0.003	0.004	0.004
2	0.000	0.977	0.007	0.010	0.011	0.002
3	0.001	0.009	0.961	0.030	0.021	0.003
4	0.010	0.002	0.009	0.798	0.651	0.014
5	0.000	0.001	0.001	0.148	0.228	0.001
6	0.002	0.002	0.000	0.001	0.001	0.991

APPENDIX D
Data Transmitted to Texas A&M

TABLE D-1						
Undamaged Mode Shape Data for Texas A&M From Cross-Power Spectra						
	Mode 1 :	2.500 Hz	Mode 2 :	2.969 Hz	mode 3 :	3.562 Hz
Pt.	mag. $g^2 \times 10^{-9}$	phase (degrees)	mag. $g^2 \times 10^{-9}$	phase (degrees)	mag. $g^2 \times 10^{-9}$	phase (degrees)
X1	2.202E+01	-2.532E+00	3.219E+01	-5.971E-01	1.010E+01	1.760E+02
X2	2.827E+02	6.782E-01	3.789E+02	2.114E-01	1.074E+02	1.862E+00
X3	5.698E+02	0.000E+00	7.582E+02	0.000E+00	1.790E+02	0.000E+00
X4	8.051E+02	5.495E-01	1.084E+03	4.129E-01	1.697E+02	1.111E+00
X5	9.764E+02	2.727E-01	1.306E+03	3.224E-01	1.007E+02	2.866E+00
X6	1.004E+03	3.346E-02	1.351E+03	4.066E-01	1.702E+01	9.825E+00
X7	9.478E+02	6.762E-02	1.256E+03	8.007E-01	7.686E+01	-1.791E+02
X8	7.933E+02	-7.207E-02	1.059E+03	7.976E-01	1.478E+02	1.791E+02
X9	5.827E+02	2.871E-01	7.872E+02	1.106E+00	1.682E+02	1.790E+02
X10	2.647E+02	-2.878E-01	3.643E+02	8.772E-01	9.043E+01	-1.789E+02
X11	2.550E+01	-7.886E-01	4.064E+01	-4.411E+00	1.555E+01	-2.091E+01

TABLE D-2						
Damaged Mode Shape Data for Texas A&M From Cross-Power Spectra						
Two-Foot-Cut at Center of the Web						
	Mode 1 :	2.531 Hz	Mode 2 :	3.000 Hz	mode 3 :	3.594 Hz
Pt.	mag. $g^2 \times 10^{-9}$	phase (degrees)	mag. $g^2 \times 10^{-9}$	phase (degrees)	mag. $g^2 \times 10^{-9}$	phase (degrees)
X1	1.672E+01	-6.427E+00	2.703E+01	2.436E+00	1.684E+01	1.648E+02
X2	2.180E+02	8.009E-01	3.145E+02	4.196E-01	1.360E+02	7.140E-01
X3	4.389E+02	0.000E+00	6.257E+02	0.000E+00	2.285E+02	0.000E+00
X4	6.196E+02	7.284E-01	8.937E+02	6.380E-01	2.087E+02	7.099E-01
X5	7.508E+02	4.059E-01	1.074E+03	4.360E-01	1.106E+02	4.188E+00
X6	7.797E+02	2.343E-01	1.117E+03	4.838E-01	1.692E+01	1.167E+02
X7	7.322E+02	1.180E-01	1.034E+03	9.206E-01	1.362E+02	1.709E+02
X8	6.124E+02	3.210E-02	8.697E+02	8.814E-01	2.236E+02	1.735E+02
X9	4.487E+02	3.473E-01	6.446E+02	1.315E+00	2.408E+02	1.750E+02
X10	2.039E+02	-3.884E-01	2.989E+02	1.185E+00	1.306E+02	1.758E+02
X11	1.927E+01	-5.214E+00	3.205E+01	9.973E-01	1.931E+01	-1.828E+01

TABLE D-3 Damaged Mode Shape Data for Texas A&M From Cross-Power Spectra Six-Foot-Cut to Bottom of the Web					
	Mode 1 : 2.531 Hz		Mode 2 : 3.000 Hz		mode 3 : 3.531 Hz	
Pt.	mag. $g^2 \times 10^{-9}$	phase (degrees)	mag. $g^2 \times 10^{-9}$	phase (degrees)	mag. $g^2 \times 10^{-9}$	phase (degrees)
X1	2.251E+00	1.277E+00	1.096E+01	7.615E+00	4.838E+00	1.715E+02
X2	2.757E+01	5.624E-01	1.247E+02	4.957E-01	3.667E+01	1.639E+00
X3	5.504E+01	0.000E+00	2.511E+02	0.000E+00	6.263E+01	0.000E+00
X4	7.915E+01	5.758E-01	3.584E+02	2.468E-01	5.941E+01	1.028E+00
X5	9.636E+01	2.272E-01	4.314E+02	7.153E-02	3.533E+01	1.918E+00
X6	9.941E+01	1.606E-01	4.470E+02	6.585E-02	5.963E+00	1.430E+01
X7	9.346E+01	1.084E-01	4.142E+02	3.891E-01	2.770E+01	1.764E+02
X8	7.826E+01	-1.151E-01	3.462E+02	4.062E-01	5.162E+01	1.776E+02
X9	5.739E+01	2.789E-01	2.568E+02	9.323E-01	5.798E+01	1.780E+02
X10	2.621E+01	-1.641E-01	1.186E+02	1.199E+00	3.134E+01	1.788E+02
X11	2.555E+00	4.546E+00	1.350E+01	1.000E+01	5.119E+00	-8.770E+00

TABLE D-4 Damaged Mode Shape Data for Texas A&M From Cross-Power Spectra Six-Foot-Cut to the Bottom of the Web and Cut Through Half the Bottom Flange					
	Mode 1 : 2.469 Hz		Mode 2 : 2.938 Hz		mode 3 : 3.500 Hz	
Pt.	mag. $g^2 \times 10^{-9}$	phase (degrees)	mag. $g^2 \times 10^{-9}$	phase (degrees)	mag. $g^2 \times 10^{-9}$	phase (degrees)
X1	1.604E+01	-7.263E-01	3.612E+01	7.879E-01	7.300E+00	1.751E+02
X2	1.951E+02	3 378E-01	4.225E+02	4.739E-02	6.524E+01	1.112E+00
X3	3.907E+02	0.000E+00	8.506E+02	0.000E+00	1.099E+02	0.000E+00
X4	5.560E+02	5.551E-01	1.221E+03	2.726E-01	1.035E+02	6.430E-01
X5	6.787E+02	1.996E-01	1.480E+03	1.559E-01	5.986E+01	1.800E+00
X6	7.001E+02	-2.605E-02	1.535E+03	1.540E-01	8.325E+00	8.103E+00
X7	6.569E+02	-4.889E-02	1.427E+03	4.738E-01	5.129E+01	-1.799E+02
X8	5.493E+02	-6.362E-02	1.196E+03	5.469E-01	9.388E+01	1.793E+02
X9	4.031E+02	5.275E-01	8.842E+02	9.250E-01	1.045E+02	1.794E+02
X10	1.824E+02	-2.169E-01	4.062E+02	4.199E-01	5.656E+01	-1.797E+02
X11	1.851E+01	-3.758E+00	4.229E+01	-1.675E+00	8.894E+00	-1.922E+01

TABLE D-5 Damaged Mode Shape Data for Texas A&M From Cross-Power Spectra Six-Foot-Cut to the Bottom of the Web and Cut Through the Entire Bottom Flange					
Mode 1 :	2.312 Hz	Mode 2 :	2.844 Hz	mode 3 :	3.500 Hz
mag. g^2x10^{-9}	phase (degrees)	mag. g^2x10^{-9}	phase (degrees)	mag. g^2x10^{-9}	phase (degrees)
Pt.					
X1	1.230E+00	1.070E+01	9.110E+00	-1.472E+00	3.862E+00	-1.791E+02
X2	1.577E+01	4.181E-01	1.079E+02	4.261E-01	3.866E+01	1.152E+00
X3	3.252E+01	0.000E+00	2.228E+02	0.000E+00	6.535E+01	0.000E+00
X4	4.938E+01	3.772E-01	3.417E+02	2.078E-01	6.257E+01	2.756E-01
X5	6.509E+01	-7.649E-02	4.445E+02	5.227E-02	3.870E+01	-5.862E-02
X6	7.350E+01	-4.978E-01	5.035E+02	2.559E-02	8.478E+00	-2.865E+00
X7	6.477E+01	-4.358E-01	4.363E+02	2.366E-01	2.647E+01	-1.788E+02
X8	5.053E+01	-3.573E-01	3.405E+02	1.365E-01	5.048E+01	1.798E+02
X9	3.508E+01	1.584E-01	2.388E+02	4.811E-01	5.770E+01	1.793E+02
X10	1.504E+01	6.280E-01	1.059E+02	-2.621E-01	3.171E+01	1.790E+02
X11	1.354E+00	8.664E+00	1.172E+01	1.527E+00	4.446E+00	1.856E+00

	Test t16tr Undamaged Forced Vibration Global Polynomial Curve-Fit Results					
Location	Mode 1 F=2.48 Hz, ζ=1.06 %	Mode 2 F=2.96 Hz, ζ=1.29 %	Mode 3 F=3.50 Hz, ζ=1.52 %	Mode 4 F=4.08 Hz, ζ=1.10 %	Mode 5 F=4.17 Hz, ζ=0.86 %	Mode 6 F=4.63 Hz, ζ=0.92 %
S1	M=257u P=184	173u 353	472u 12.9	702u 358	513u 176	414u 5.63
S2	M=6.90m P=174	5.55m 360	0.014 1.72	0.013 6.25	0.011 172	9.88m 2.90
S3	M=0.010 P=174	8.38m 1.39	0.019 1.99	0.017 6.99	0.015 173	0.013 2.99
S4	M=8.01m P=178	6.98m 4.00	0.013 3.08	9.94m 8.91	0.010 175	7.67m 4.04
S5	M=16.6u P=70.3	137u 165	716u 3.55	1.17m 2.70	609u 172	1.03m 1.59
S6	M=0.014 P=358	0.014 180	4.48m 172	7.72m 355	3.44m 10.8	7.49m 357
S7	M=0.023 P=3.33	0.024 183	1.04m 139	0.015 0.626	1.89m 58.4	0.014 0.09
S8	M=0.015 P=2.84	0.016 182	3.87m 5.74	9.44m 2.45	2.71m 158	8.43m 360
S9	M=456u P=353	535u 176	511u 164	1.06m 352	491u 13.8	1.08m 0.168
S10	M=8.62m P=183	8.87m 0.053	0.014 178	7.73m 350	0.012 4.50	8.61m 2.15
S11	M=0.010 P=177	0.011 356	0.020 174	0.013 349	0.017 2.41	0.014 360
S12	M=7.54m P=184	8.43m 359	0.016 177	0.011 352	0.013 5.210	0.012 1.76
S13	M=423u P=181	472u 9.33	895u 178	697u 355	918u 6.95	827u 5.18
N1	M=302u P=202	293u 150	478u 10.0	610u 351	735u 2.03	552u 193
N2	M=7.46m P=183	7.62m 185	0.014 0.555	0.010 348	0.015 2.33	0.015 184
N3	M=0.010 P=183	0.011 186	0.018 0.954	0.012 347	0.019 2.57	0.018 184
N4	M=8.12m P=184	8.42m 184	0.011 360	6.58m 343	0.012 1.32	9.92m 184
N5	M=201u P=205	111u 136	652u 0.569	900u 349	869u 1.38	1.26m 181
N6	M=0.014 P=2.66	0.016 2.61	4.28m 179	7.71m 2.75	4.25m 177	9.68m 181
N7	M=0.021 P=4.04	0.024 2.32	464u 202	0.013 360	879u 143	0.017 182
N8	M=0.014 P=3.34	0.017 2.28	3.39m 0.195	6.85m 355	3.38m 5.00	0.010 182
N9	M=367u P=325	783u 347	427u 160	942u 1.73	605u 176	1.50m 179
N10	M=7.52m P=185	9.97m 182	0.012 180	0.010 10.4	0.013 182	0.011 186
N11	M=0.010 P=179	0.014 178	0.019 177	0.017 6.54	0.020 179	0.019 183
N12	M=6.99m P=178	9.54m 178	0.015 176	0.014 5.73	0.016 178	0.015 183
N13	M=434u P=188	561u 183	981u 170	1.04m 5.53	1.18m 179	1.23m 185
m = x 10^{-3}, u = x 10^{-6}, M = magnitude, P = phase in degrees						

135

	Mode 1 F=2.52 Hz, ζ=1.20 %	Mode 2 F=3.00 Hz, ζ=0.80 %	Mode 3 F=3.57 Hz, ζ=0.87 %	Mode 4 F=4.12 Hz, ζ=1.00 %	Mode 5 F=4.21 Hz, ζ=1.04 %	Mode 6 F=4.69 Hz, ζ=0.90 %
Location						
S1	M=3.95m P=178	3.70m 159	8.17m 176	9.66m 357	8.19m 181	7.19m 2.48
S2	M=0.218 P=170	0.171 168	0.443 179	0.393 3.79	0.392 178	0.346 3.47
S3	M=0.320 P=171	0.258 169	0.597 179	0.497 4.18	0.532 178	0.449 3.62
S4	M=0.257 P=175	0.218 172	0.404 180	0.293 5.68	0.363 178	0.278 4.15
S5	M=6.08m P=113	3.76m 103	0.024 175	0.034 3.03	0.024 177	0.035 3.97
S6	M=0.454 P=358	0.433 355	0.151 349	0.248 356	0.090 359	0.219 358
S7	M=0.732 P=4.27	0.715 359	0.049 316	0.473 0.468	0.020 142	0.423 1.54
S8	M=0.491 P=4.74	0.490 359	0.119 189	0.275 1.98	0.120 175	0.255 1.98
S9	M=0.015 P=6.04	0.016 4.92	0.016 345	0.035 353	0.012 7.55	0.034 0.641
S10	M=0.268 P=181	0.273 177	0.435 358	0.294 354	0.367 0.742	0.275 1.68
S11	M=0.314 P=175	0.322 172	0.603 356	0.465 353	0.494 358	0.421 359
S12	M=0.230 P=179	0.246 176	0.497 359	0.403 356	0.411 1.27	0.374 1.44
S13	M=0.015 P=161	0.014 175	0.019 6.35	0.019 5.36	0.025 8.86	0.020 11.1
N1	M=0.010 P=194	6.18m 346	0.015 183	0.018 0.438	0.020 359	0.017 190
N2	M=0.263 P=186	0.222 357	0.448 181	0.371 355	0.471 0.170	0.453 183
N3	M=0.372 P=186	0.322 358	0.581 182	0.451 355	0.617 0.320	0.565 183
N4	M=0.279 P=185	0.242 356	0.368 181	0.248 353	0.390 359	0.315 183
N5	M=4.90m P=226	1.73m 203	0.024 175	0.031 356	0.028 0.386	0.039 181
N6	M=0.494 P=4.80	0.468 177	0.125 4.32	0.238 5.12	0.126 173	0.273 181
N7	M=0.741 P=5.93	0.714 178	0.011 101	0.418 2.80	0.024 119	0.486 181
N8	M=0.486 P=3.07	0.490 177	0.123 177	0.239 359	0.115 3.76	0.291 181
N9	M=0.019 P=346	0.030 199	0.013 336	0.032 10.7	0.013 169	0.044 175
N10	M=0.278 P=181	0.292 358	0.396 359	0.283 9.98	0.420 178	0.332 181
N11	M=0.353 P=179	0.390 357	0.599 358	0.478 9.65	0.637 177	0.557 181
N12	M=0.247 P=176	0.268 358	0.463 358	0.394 7.85	0.491 176	0.452 181
N13	M=0.013 P=176	0.014 7.86	0.026 355	0.023 6.92	0.036 176	0.032 184

Test t17tr
Undamaged Forced Vibration
Global Polynomial Curve-Fit Results

$m = \times 10^{-3}$, $u = \times 10^{-6}$, M = magnitude, P = phase in degrees

Test t18tr Undamaged Forced Vibration Global Polynomial Curve-Fit Results						
Location	Mode 1 F=2.52 Hz, ζ=1.33 %	Mode 2 F=2.99 Hz, ζ=0.82 %	Mode 3 F=3.52 Hz, ζ=0.95 %	Mode 4 F=4.09 Hz, ζ=0.85 %	Mode 5 F=4.19 Hz, ζ=0.65 %	Mode 6 F=4.66 Hz, ζ=0.84 %
S1	M=5.56m P=178	3.15m 162	6.18m 356	9.92m 5.32	7.41m 173	6.28m 3.56
S2	M=0.226 P=173	0.194 174	0.393 1.48	0.339 7.73	0.353 176	0.332 3.38
S3	M=0.316 P=165	0.285 174	0.530 2.33	0.421 9.00	0.475 175	0.420 1.53
S4	M=0.246 P=171	0.236 178	0.355 2.79	0.247 10.8	0.324 176	0.257 2.00
S5	M=0.037 P=237	8.37m 159	0.017 339	0.032 356	0.024 180	0.034 357
S6	M=0.425 P=353	0.435 357	0.134 172	0.209 360	0.096 13.4	0.230 355
S7	M=0.684 P=359	0.711 0.703	0.043 135	0.407 4.70	0.047 83.6	0.429 358
S8	M=0.475 P=359	0.495 360	0.105 13.6	0.248 6.06	0.098 164	0.263 358
S9	M=0.16 P=359	0.016 359	0.015 165	0.028 358	0.014 21.8	0.035 360
S10	M=0.255 P=174	0.263 178	0.392 181	0.224 357	0.344 5.44	0.265 358
S11	M=0.306 P=170	0.307 174	0.558 178	0.361 355	0.472 3.69	0.408 356
S12	M=0.225 P=171	0.234 178	0.464 181	0.322 359	0.395 6.72	0.368 358
S13	M=9.16m P=167	0.015 188	0.025 185	0.021 358	0.026 6.49	0.27 357
N1	M=0.013 P=197	7.03m 339	0.013 4.34	0.018 0.301	0.022 8.60	0.016 191
N2	M=0.223 P=182	0.211 360	0.384 2.46	0.307 357	0.459 4.90	0.444 180
N3	M=0.331 P=183	0.313 0.619	0.502 3.56	0.369 357	0.604 5.33	0.562 181
N4	M=0.260 P=184	0.229 359	0.311 2.28	0.197 355	0.381 4.77	0.311 182
N5	M=7.27m P=201	4.84m 221	0.019 348	0.027 353	0.026 1.53	0.036 179
N6	M=0.441 P=1.68	0.464 181	0.123 184	0.196 9.22	0.128 177	0.270 179
N7	M=0.680 P=3.20	0.711 181	0.015 187	0.344 6.38	0.032 130	0.493 179
N8	M=0.454 P=358	0.479 180	0.088 4.20	0.188 4.15	0.112 12.3	0.295 178
N9	M=0.014 P=338	0.022 176	9.05m 175	0.026 9.87	0.016 177	0.042 176
N10	M=0.250 P=176	0.279 0.511	0.343 180	0.243 15.1	0.410 180	0.320 180
N11	M=0.329 P=173	0.377 0.484	0.534 180	0.419 13.2	0.636 180	0.549 179
N12	M=0.221 P=170	0.258 0.259	0.415 179	0.343 12.5	0.486 179	0.441 179
N13	M=0.014 P=179	0.016 3.30	0.027 181	0.024 14.0	0.034 181	0.033 179
m = x 10⁻³, u = x 10⁻⁶, M = magnitude, P = phase in degrees						

m = x 10^{-3}, u = x 10^{-6}, M = magnitude, P = phase in degrees

	Mode 1 F=2.46 Hz, ζ=0.82 %	Mode 2 F=2.95 Hz, ζ=0.89 %	Mode 3 F=3.48 Hz, ζ=0.92 %	Mode 4 F=4.04 Hz, ζ=0.81%	Mode 5 F=4.14 Hz, ζ=0.62 %	Mode 6 F=4.58 Hz, ζ=1.06 %
Test t19tr **Undamaged Forced Vibration** **Global Polynomial Curve-Fit Results**						
Location						
S1	M=4.48m P=171	2.90m 149	8.38m 3.78	0.011 357	0.010 171	6.52m 15.3
S2	M=0.200 P=174	0.182 178	0.433 2.94	0.352 6.36	0.374 174	0.315 7.43
S3	M=0.295 P=175	0.277 179	0.583 3.00	0.441 7.15	0.502 174	0.409 7.26
S4	M=0.231 P=179	0.230 182	0 392 4.36	0.259 8.92	0.342 176	0.250 8.44
S5	M=3.07m P=162	429u 53.2	0.021 6.78	0.034 2.97	0.023 172	0.035 4.35 ,
S6	M=0.389 P=360	0.441 359	0.152 175	0.228 357	0.092 11.6	0.236 357
S7	M=0.636 P=4.92	0.730 2.62	0.051 158	0.444 2.53	0.045 96.2	0.452 0.738
S8	M=0.427 P=3.71	0.498 1.67	0.105 10.5	0.267 3.66	0.111 166	0.284 0.729
S9	M=0.012 P=4.72	0.016 5.46	0.016 166	0.032 355	0.011 17.0	0.036 0.271
S10	M=0.250 P=181	0.277 178	0.423 180	0.255 355	0.351 3.76	0.247 0.944
S11	M=0.293 P=176	0.322 174	0.597 177	0.409 354	0.478 2.03	0.388 359
S12	M=0.218 P=180	0.252 177	0.501 180	0.366 357	0.403 5.12	0.360 1.18
S13	M=0.014 P=180	0.017 177	0.032 179	0.025 355	0.028 5.08	0.027 1.70
N1	M=9.50m P=194	8.38m 355	0.019 7.78	0.020 357	0.024 4.88	0.015 204
N2	M=0.208 P=185	0.234 0.612	0.428 2.78	0.354 354	0.454 4.06	0.417 186
N3	M=0.297 P=185	0.340 1.08	0.559 2.90	0.435 354	0.597 4.10	0.518 186
N4	M=0.226 P=184	0.252 359	0.349 2.03	0.240 351	0.373 3.04	0.279 186
N5	M=2.68m P=209	1.24m 321	0.19 2.39	0.029 354	0.025 2.85	0.035 184
N6	M=0.405 P=4.30	0.480 181	0.129 181	0.205 6.78	0.132 177	0.284 180
N7	M=0.625 P=5.40	0.737 182	7.65m 197	0.375 3.87	0.033 143	0.510 181
N8	M=0.418 P=3.01	0.504 180	0.114 1.31	0.215 359	0.107 7.60	0.300 181
N9	M=0.013 P=2.24	0.021 174	0.012 166	0.025 6.23	0.015 172	0.043 178
N10	M=0.226 P=175	0.260 359	0.366 176	0.234 9.30	0.388 176	0.298 179
N11	M=0.313 P=179	0.378 2.30	0.588 180	0.423 11.7	0.640 179	0.544 182
N12	M=0.217 P=177	0.261 2.89	0.458 179	0.351 10.7	0.493 178	0.439 182
N13	M=0.011 P=174	0.021 12.7	0.036 176	0.026 10.4	0.036 178	0.038 181
m = x 10^{-3}, u = x 10^{-6}, M = magnitude, P = phase in degrees						

	Test t22tr Undamaged Forced Vibration Global Polynomial Curve-Fit Results					
Location	Mode 1 F=2.30 Hz, ζ=1.60 %	Mode 2 F=2.84 Hz, ζ=0.66 %	Mode 3 F=3.49 Hz, ζ=0.80 %	Mode 4 F=3.99 Hz, ζ=0.80 %	Mode 5 F=4.15 Hz, ζ=0.71 %	Mode 6 F=4.52 Hz, ζ=1.06 %
S1	M=8.40m P=135	6.64m 141	0.016 9.20	9.55m 337	0.016 176	0.012 8.34
S2	M=0.101 P=161	0.247 176	0.405 1.92	0.278 1.73	0.414 180	0.365 3.25
S3	M=0.143 P=162	0.365 175	0.543 2.20	0.339 1.39	0.553 180	0.469 3.56
S4	M=0.110 P=169	0.292 179	0.364 3.68	0.193 1.98	0.377 181	0.284 4.40
S5	M=0.013 P=152	2.19m 185	0.021 13.8	0.022 360	0.025 176	0.037 359
S6	M=0.204 P=347	0.495 355	0.135 176	0.220 4.91	0.090 360	0.282 355
S7	M=0.368 P=354	0.797 359	0.036 177	0.411 5.90	0.019 160	0.513 359
S8	M=0.251 P=356	0.550 358	0.102 6.93	0.236 6.02	0.118 179	0.311 359
S9	M=7.19m P=67.0	0.015 360	0.015 158	0.028 357	0.011 5.34	0.038 357
S10	M=0.131 P=168	0.322 178	0.399 181	0.249 6.03	0.370 1.09	0.312 359
S11	M=0.177 P=169	0.384 174	0.560 179	0.394 3.46	0.498 359	0.485 357
S12	M=0.118 P=170	0.297 179	0.469 182	0.352 6.69	0.419 1.60	0.444 359
S13	M=0.013 P=113	0.017 182	0.029 174	0.022 9.86	0.028 1.84	0.032 4.16
N1	M=0.012 P=207	478u 351	0.021 17.3	0.022 9.75	0.027 1.83	9.95m 199
N2	M=0.204 P=181	0.104 0.076	0.418 4.76	0.435 4.94	0.480 1.83	0.383 180
N3	M=0.292 P=179	0.154 360	0.543 5.02	0.546 5.28	0.630 1.98	0.487 180
N4	M=0.232 P=178	0.122 359	0.341 4.32	0.309 3.86	0.395 1.35	0.272 180
N5	M=0.014 P=156	741u 85.5	0.022 17.3	0.027 10.8	0.027 2.58	0.029 180
N6	M=0.500 P=2.24	0.298 179	0.130 181	0.140 8.63	0.145 182	0.171 179
N7	M=0.964 P=3.61	0.559 180	0.013 167	0.386 6.93	0.026 192	0.446 179
N8	M=0.535 P=1.25	0.323 179	0.105 6.16	0.170 4.28	0.111 1.39	0.199 177
N9	M=0.023 P=343	0.016 167	9.99m 148	0.023 0.811	0.015 183	0.034 173
N10	M=0.252 P=177	0.116 353	0.338 178	0.265 3.58	0.398 179	0.275 179
N11	M=0.342 P=182	0.169 357	0.563 182	0.482 8.37	0.679 182	0.510 181
N12	M=0.226 P=181	0.108 355	0.435 182	0.388 7.92	0.519 182	0.401 181
N13	M=0.011 P=187	6.02m 0.846	0.033 172	0.031 9.52	0.041 183	0.034 179
m = x 10^{-3}, u = x 10^{-6}, M = magnitude, P = phase in degrees						

REFERENCES

Abdel-Ghaffar, A. M. and R. H. Scanlan (1985) "Ambient Vibration Studies of Golden Gate Bridge: I. Suspended Structure," *ASCE Journal of Engineering Mechanics*, **111**, 463-482.

Abdel-Ghaffar, A. M. and R. H. Scanlan (1985) "Ambient Vibration Studies of Golden Gate Bridge: II. Pier-Tower Structure," *ASCE Journal of Engineering Mechanics*, **111**, 483-499.

Abdel-Ghaffar, A. M. and G. W. Housner (1978) "Ambient Vibration Tests of Suspension Bridge," *ASCE Journal of the Engineering Mechanics Division*, **104**, 983-999.

Agbabian, M. S. (1980) "Simulation of Dynamic Environments for Design Verification," *Nuclear Engineering and Design*, **59**, 127-141.

American Society of Civil Engineers Committee on Bridge Safety, (1980) *A Guide For Field Testing of Bridges*, New York.

Applied Technology Council, (1979) *Proceedings of a Workshop on Earthquake Resistance of Highway Bridges*, Palo Alto, CA.

Bakht B. and S. G. Pinjarkar (1989) "Dynamic Testing of Highway Bridges- A Review," *Transportation Research Record* **1223**, 93-100.

Bendat, J. S., and A. G. Piersol (1980) *Engineering Applications of Correlation and Spectral Analysis*, John Wiley, New York.

Benuska, K. L., G. Y. Matsummoto, E. H. Killam, and J. G. Diehl, (1981) "Structural Characterization of Concrete Chimneys", *Proceedings of the Second Specialty Conference on Dynamic Response of Structures*, American Society of Civil Engineers.

Billing, J. R. (1984) "Dynamic Loading and Testing of Bridges in Ontario," *Canadian Journal of Civil Engineering*, **11**, 833-843.

Biswas, M., A. K. Pandey and M. M. Samman (1989) "Diagnostic Experimental Spectral/Modal Analysis of a Highway Bridge," *The International Journal of Analytical and Experimental Modal Analysis*, **5**, 33-42.

Breen, J. M. E. Kreger, C. D. White and G. C. Clark (1987) "Field Evaluation and Model Test of a Composite Wing-Girder Bridge," *Canadian Journal of Civil Engineering*, **14**, 753-762.

Brownjohn, J. M., A. A. Dumanoglu, R. T. Severn and A. Blakeborough (1989) "Ambient Vibration Survey of the Bosporus Suspension Bridge," *Earthquake Engineering and Structural Dynamics*, **18**, 263-283.

Brownjohn, J. M., Dumanoglu and R. T. Severn (1992) "Ambient Vibration Survey of the Fatih Sultan Mehmet (Second Bosporus) Suspension Bridge," *Earthquake Engineering and Structural Dynamics*, **21**, 907-924.

Brownjohn, J. M., Dumanoglu, R. T. Steven and C. A. Taylor (1987) "Ambient Vibration Measurements of the Humber Suspension Bridge and Comparison with Calculated Results," *Proc. Institute for Civil Eng. Pt. 2*, **83**, 561-600.

Buckland, P. G., R. Hooley, B. D. Morgenstern, J. H. Rainer and A. M. van Selst (1979) "Suspension Bridge Vibrations: Computed and Measured," *ASCE Journal of the Structural Division*, **105**, 859-874.

Burdette, E. G. and D. W. Goodpasture (1972) "Comparison of Measured and Computed Ultimate Strengths of Four Highway Bridges," *Highway Research Record*, No. 382, 38-49.

Cantieni, R. (1984) "Dynamic Load Testing of Highway Bridges," *Transportation Research Record* **950,** 141-148.

Cantieni, R. And S. Pietrzko (1993), "Modal Testing of a Wooden Footbridge Using Random Excitation", *Proceedings of the 11th International Modal Analysis Conference,* Kissimmee, Florida, 1230-1236.

Carne, T. G., J. P. Lauffer, A. J. Gomez, and H. Benjannet (1988), "Modal Testing an Immense Flexible Structure Using Natural and Artificial Excitation", *Journal of Modal Analysis,* 117-122, October 1988.

Chen, C. K., R. M. Czarnecki, and R. E. Scholl (1977) "Vibration Tests of a 4-story Concrete Structure". *Proc. Second ASCE Engineering Mechanics Specialty Conf.,* Raleigh, NC, 2753-2758.

Crawford, R., and H. S. Ward (1964), "Determination of the Natural Periods of Buildings", *Bulletin of the Seismological Society of America,* **54**, 1743-1756.

Crouse, C. B., B. Hushmand and G. R. Martin (1987) "Dynamic Soil-Structure Interaction of a Single-Span Bridge," *Earthquake Engineering and Structural Dynamics*, **15**, 711-729.

Dorton, R. A., M. Holowka, and J. P. King (1977) "The Conestogo River Bridge - Design and Testing," *Canadian Journal of Civil Engineering*, 4, No. 1.

Douglas, B. M. and W. H. Reid (1982) "Dynamic Tests and System Identification of Bridges," *ASCE Journal of Structural Engineering*, **108**, 2295-2312.

Douglas, B. M. (1976) "Quick Release Pullback Testing and Analytical Seismic Analysis of Six Span Composite Girder Bridge," FHWA-RD-76-173.

Douglas, B. M., C. D. Brown and M. L. Gordon (1981) "Experimental Dynamics of Highway Bridges," *Conference on Dynamic Response of Structures: Experimentation, Observation, Prediction and Control*, 98-712.

Ellis, B. R. and A. P. Jeary (1979) "An Initial Study of the Dynamic Behavior of the New Christchurch Bay Tower," *Proc. Second Int. Conf. on Behavior of Off-Shore Structures*, Vol 2., Imperial College, London, 87-96.

Ewins, D. J. (1985), *Modal Testing: Theory and Practice*, John Wiley, New York.

Filiatrault, A., R. Tinawi, A. Felber, C. E. Ventura, and S. F. Stiemer (1993), "Modal Analysis and Testing of the Cable-Stayed Shipshaw Bridge in Jonquiere, Quebec", *Proceedings of the 11th International Modal Analysis Conference*, Kissimmee, Florida, 14-20.

Formenti, D. (1977) "Analytical and Experimental Modal Analysis," notes from short course *Experimental Modal Analysis*, University of Cincinnati.

Galambos, T. V., and R. C. Mayes (1979) "Lessons from dynamic tests of an Eleven Story Building," *Engineering Structures*, 1, 264-273.

Ganga Rao, H. V. S. (1977), "Survey of Field and Laboratory Tests on Bridge Systems", *Bridge Tests*, Transportation Research Record 645, National Academy of Sciences, Washington D.C.

Gates, J. H. (1976) "California's Seismic Design Criteria For Bridges," *ASCE Journal of Structural Engineering*, 102, 2301-2313.

Gates, J. H. and M. J. Smith (1982) "Verification of Dynamic Modeling Methods by Prototype Experiments," FHWA/CA/SD-82/07.

Gersch, W. and T. Brotherton (1982) "Estimation of Stationary Structural System Parameters from Non-Stationary Random Vibration Data: A Locally Stationary Model Method," *Journal of Sound and Vibration*, 81, 215-227.

Gersch, W. and F. Martinelli (1979) "Estimation of Structural System Parameters from Stationary and Non-Stationary Ambient Vibrations: An Exploratory-Comfirmatory Analysis," *Journal of Sound and Vibration*, 65, 303-318.

Gorlov, A. M. (1984) "Disaster of the I-95 Mianus River Bridge - Where Could Lateral Vibration Come From?," *ASME Journal of Applied Mechanics*, 51, 694-696.

Grace, N. F. and J. B. Kennedy (1988) "Dynamic Response of Two-Span Continuous Composite Bridges," *Canadian Journal of Civil Engineering*, 15, 579-588.

Granga Rao, H. V. S. (1977) "Survey of Field and Laboratory Tests on bridge Systems," *Transportation Research Record* 645, 10-15.

Green, R. and D. Strevel (1977) "Composite Box-Girder Bridges During Construction," *Transportation Research Record* **645**, 1-6.

Green, M. F. and D. Cebon (1993), "Modal Testing of Two Highway Bridges", *Proceedings of the 11th International Modal Analysis Conference,* Kissimmee, Florida, 838-844.

Hall, W. J., and N. M. Newmark (1979) "Seismic Design of Bridges -- Research Needs," *Proceedings of a Workshop on Earthquake Resistance of Highway Bridges,* Palo Alto, California.

Hashimoto, P. S., L. K. Steele, J. J. Johnson, and R. W. Mensing (1993), *Review of Structure Damping Values for Elastic Seismic Analysis of Nuclear Power Plants,* NUREG/CR-6011, U.S. Nuclear Regulatory Commission, Washington, D.C.

Higashihara, H., T. Moriya and J. Tajima (1987) "Ambient Vibration Test of an Anchorage of South Bisan-Seto Suspension Bridge," *Earthquake Engineering and Structural Dynamics,* **15**, 679-695.

Hudson, D. E. (1977) " Dynamic Tests of Full-Scale Structures," *Journal of the Engineering Mechanics Division,* **103**, 1141-1157.

Hudson, D. E. (1970) "Dynamic Tests of Full-Scale Structures", *Earthquake Engineering,* R. L. Wiegel, Ed., Prentice-Hall, Inc., Englewood Cliffs, N.J.

Hudson, D. E., W. O. Keightley and N. N. Nielsen (1964) "A New method for the Measurement of the Natural Periods of Buildings," *Bulletin of the Seismological Society of America,* **54**, 233-241.

Ismail, F., A. Ibrahim, and H. R. Martin (1990), "Identification of Fatigue Cracks from Vibration Testing", *Journal of Sound and Vibration,* Vol. **140**, 305-317.

Iwasaki, T., Penzien, J., and Clough, R., (1972) "Literature Survey - Seismic Effects on Highway Bridges," EERC report 72-11, University of California, Berkeley.

Jain, B. K. (1991) "Diagnostics Through Experimental Vibration Signature Analysis of Prestressed Concrete Bridges," *International Symposium on Fracture in Steel and Concrete Structures,* 1123-1136.

James, G. H., T. G. Carne, and J. P. Lauffer (1993) "The Natural Excitation Technique (NExT) for Modal Parameter Extraction From Operating Wind Turbines," Sandia National Laboratory report SAND92-1666.

Jennings, P. C., R. B. Matthiesen and J. B. Hoerner (1972) " Forced Vibration of a Tall Steel Frame Building," *Earthquake Engineering and Structural Dynamics,* **1**, 107-132.

Jorgenson, L. J and W. Larson (1972) "Field Testing of a Reinforced Concrete Highway Bridge to Collapse," *Transportation Research Record,* 66-71.

Kato, M. and S. Shimada (1984) "Vibration of PC Bridge During Failure Process," *ASCE Journal of Structural Engineering*, **112**, 1692-1703,

Kennedy, J. B. and N. F. Grace (1990) "Prestressed Continuous Composite Bridges Under Dynamic Load," *ASCE Journal of Structural Engineering*, **116**, 1660-1678.

Kim, J.-T., and N. Stubbs (1993), *Assessment of the Relative Impact of Model Uncertainty on the Accuracy of Global Nondestructive Damage Detection in Structures*, report prepared for New Mexico State University.

Kohoutek, R. (1993), "Tests on Bridge over Talbragar River at Dubbo", *Proceedings of the 11th International Modal Analysis Conference*, Kissimmee, FL., 1168-1174.

Kumarasena, T. , R. H. Scanlon, and G. R. Morris (1989) "Deer Isle Bridge: field and Computed Vibrations," *ASCE Journal of Structural Engineering*, **115**, 2313-2328.

Kuribayashi, E. and T. Iwasaki (1973), "Dynamic Properties of Highway Bridges", *Proc. 5th World Conf. on Earthquake Engineering*, Rome, 938-941.

Kussmaul, K., E. Luz, K. Kerkhof, R. Haas and C. Gurr-Beyer (1992) "System Control by Ambient Vibration Analysis," VDI Berichte NR. 940, 153-162.

Lee, P. K., D. Ho and H. W. Chung (1987) "Static and Dynamic Tests of Concrete Bridge," *ASCE Journal of Structural Engineering,* **113**, 61-73.

Leonard, D. R. (1974), *Dynamic Tests on Highway Bridges - Test Procedures and Equipment,* TRRL Laboratory Report 654, Transport and Road Research Laboratory, Berkshire, England.

Leonard, D. R. and Eyre, R. (1975), *Damping and Frequency Measurements of Eight Box Girder Bridges,* TRRL Laboratory Report 682, Transport and Road Research laboratory, Berkshire, England.

Levine, M. B. and R. F. Scott (1989) "Dynamic Response Verification of Simplified Bridge-Foundation Model," *ASCE Journal of Geotechnical Engineering*, **115**, 246-260.

Luz, E. and J. Wallaschek (1992) "Experimental Modal Analysis Using Ambient Vibration," *Int. J. of Analytical and Experimental Modal Analysis*, **7**, n1, 29-39.

Mazurek, D. F. and J. T. DeWolf (1990) "Experimental Study of Bridge Monitoring Technique," *ASCE Journal of Structural Engineering*, **116**, 2532-2549.

McClure, R. M. and H. H. West (1984) "Full-Scale Testing of a Prestressed Concrete Segmental Bridge," *Canadian Journal of Civil Engineering*, **11**, 505-515.

McLamore, V. R., G. C. Hart and I. R. Stubbs (1971) "Ambient Vibration of Two Suspension Bridges," *Proceedings of the ASCE Journal of the Structural Division*, **97**, 2567-2582.

Miller, R. A., A. E. Aktan, and B. M. Sharooz (1992) "Nondestructive and Destructive Testing of a Three Span Skewed R. C. Slab Bridge," in *Proc. of Conference on Nondestructive Testing of Concrete Elements and Structures*, ASCE, San Antonio 150-161

Muria-Vila, D, R. Gomez and C. King (1991) "Dynamic Structural Properties of Cable-Stayed Tampico Bridge," *ASCE Journal of Structural Engineering*, **117**, 3396-3416.

O'Connor, C. and R. Pritchard (1985) "Impact Studies on Small Composite Girder Bridge," *ASCE Journal of Structural Engineering*, **111**, 641-653.

Oehler, L. T. (1957) "Vibration Susceptibilities of Various Highway Bridge Types," *Proceedings of the ASCE, Journal of the Structural Division*, **83**, 1-41.

Pardoen, G. C., A. J. Carr and P. J. Moss (1981) "Bridge Modal Identification Problems," Proceedings of the Second Specialty Conference on Dynamic Response of Structures: Experimentation, Observation, Prediction and Control, ASCE, 29-45.

Paultre, P., O. Chaallal and J. Proulx (1992) "Bridge Dynamics and Dynamic Amplification Factors - A Review of the Analytical and Experimental Findings," *Canadian Journal of Engineering*, **19**, 260-278.

Radkowski, A. F., B. Bakht, and J. Billing (1984) "Design and Testing of a 400 Ft Span Plate Girder Bridge," *Proc. U.S./Japan Joint Seminar on Composite and Mixed Construction, Seattle*, WA, 60-70.

Raghavendrachar, M. and A. E. Aktan (1992) "Flexibility by Multireference Impact Testing for Bridge Diagnostics," *ASCE Journal of Structural Engineering*, **118**, 2186-2203.

Richardson, M. H. (1980), *Detection of Damage in Structures from Changes in their Dynamic (Modal) Properties- A survey*, NUREG/CR-1431, U.S. Nuclear Regulatory Commission, Washington, D.C.

Richardson, M. H. and D. L. Formenti (1985) "Parameter Estimation From Frequency Response Function Measurements Using Rational Fraction Polynomials," Technical Note 85-3, Structural Measurements Systems, San Jose, CA.

Richardson, J. A. and B. M. Douglas (1987) "Identifying Frequencies and Three-Dimensional Mode Shapes From a Full Scale Bridge Test," *Proceedings of the 5th International Modal Analysis Conference*, **1**, 160-165.

Saiidi, M. and B. M. Douglas (1984) "Effect of Design Seismic Loads on a Highway Bridge," *ASCE Journal of Structural Engineering*, **110**, 2723-2737.

Salane, H. J., J. W. Baldwin and R. C. Duffield (1981) "Dynamics Approach for Monitoring Bridge Deterioration," *Transportation Research Record* **832**, 21-28.

Samman, M. M., M. Biswas and A. K. Pandey (1991) "Employing Pattern Recognition for Detecting Cracks in a Bridge Model," *The International Journal of Analytical and Experimental Modal Analysis*, **6**, 35-44.

Sanders, D. R., N. Stubbs and Y. I. Kim (1989) "Global Nondestructive Damage Detection in Composite Structures," *Proceedings of the 7th International Modal Analysis Conference*, **2**, 1501-1507.

Scanlon, A. and L. Mikhailovsky (1987) "Full-Scale Load Test of Three-Span Concrete Bridge," *Canadian Journal of Engineering*, **14**, 19-23.

Scordelis, A. C., T. Wasti and F. Seible (1982) "Structural Response of Skew RC Box Girder Bridge," *ASCE Journal of the Structural Division*, **108**, 89-104.

Severn, R. T. (1988) "A Review of Dynamic Testing Methods for Civil Engineering Structures," *1988 Conference on Earthquake and Civil Engineering Dynamics*, 1-23

Severn, R. T., J. M. W. Brownjohn, A. A. Dumanoglu, and C. A. Taylor (1988), "A Review of Dynamic Testing Methods for Civil Engineering Structures", *Civil Engineering Dynamics*, University of Bristol, 1-23.

Shepherd, R., Brown, H. E. E., and Wood, J. H. (1979) "Dynamic Investigations of the Mohaka River Bridge," *Proc. of the Institution of Civil Engineers*, Part 1, **66**, 457-469.

Shepherd, R. and A. W. Charleson (1971) "Experimental Determination of the Dynamic Properties of a Bridge Substructure," *Bulletin of the Seismological Society of America*, **61**, 1529-1548.

Shepherd, R. and G. K. Sidwell (1973) "Investigations of the Dynamic Properties of Five Concrete Bridges," Fourth Australian conference on the Mechanics of Structures and Materials, University of Queensland, Brisbane, 261-268.

Shirole, A. M. and R. C. Holt (1991), "Planning for a Comprehensive Bridge Safety Assurance Program", *Transportation Research Record 1290*, 39-50.

Spyrakos, C., H. L. Chen, J. Stephens, and V. Govidaraj (1990), "Evaluating Structural Deterioration Using Dynamic Response Characterization", *Proceedings Intelligent Structures*, Elsevier Applied Science, 137-154.

Srinivasan, M. G., C. A. Kot, B. J. Hsieh and H. H. Chung (1981) "Dynamic Testing of As-built Power Plant Buildings: An Evaluation Review," *Nuclear Engineering and Design*, **66**, 97-115.

Srinivasan, M. G., C. A. Kot, and B. J. Hsieh (1984) *Dynamic Testing of As-Built Civil Engineering Structures - A Review and Evaluation*, NUREG/CR-3649, U.S. Nuclear Regulatory Commission, Washington, D.C.

Tanaka, H. and A. G. Davenport (1983) "Wind-Induced Response Golden Gate Bridge," *ASCE Journal of Engineering Mechanics*, **109**, 296-312.

Tang, J. P., and K.-M. Leu (1991), "Vibration Tests and Damage Detection of P/C Bridges", *Journal of the Chinese Institute of Engineers*, Vol. 14, 531-536.

Taskov, L. A. (1988) "Dynamic testing of Bridge Structures Applying Force and Ambient Vibration methods," *1988 Conference on Earthquake and Civil Engineering Dynamics*, 81-92.

Thoman, S. J., C. M. Redfield and R. E. Hollenbeck (1984) "Load Test of Single-Cell Box Girder Bridge Cantilever Deck," *ASCE Journal of Structural Engineering*, **110**, 1773-1785.

Turner, J. D. and A. J. Pretlove (1988) "A Study of the Spectrum of Traffic-Induced Bridge Vibration," *Journal of Sound and Vibration*, **122**, 31-42.

Van Nunen, J. W. G., and A. J. Persoon (1982), "Investigation of the Vibrational Behavior of a Cable-Stayed Bridge Under Wind Loads", *Eng. Struct.*, **4**, 99-105.

Varney R. F. and C. F. Galambos (1966) "Field Dynamic Loading Studies of Highway Bridges in the U. S., 1948-1965," *Transportation Research Record*, 285-304.

Vold, H. and G. F. Rocklin (1982) "The Numerical Implementation of a Multi-Input Modal Estimation Method for Mini-Computers," *Proc. 1st International Modal Analysis Conference*, Kissimmee, FA.

Wang, T., D. Huang and M. Shahawy (1992) "Dynamic Response of Multigirder Bridges," *ASCE Journal of Structural Engineering*, 118, 2222-2238.

Ward, H. S. (1984) "Traffic Generated Vibrations and Bridge Integrity," *ASCE Journal of Structural Engineering*, **110**, 2487-2498.

Weaver, H. J. (1980) "Dynamic Testing of Nuclear Power Plant Structures - An Evaluation," UCRL-52732, Lawrence Livermore Laboratory.

Werner, S. D., J. L. Beck and B. Levine (1987) "Seismic Response Evaluation of Meloland Road Overpass Using 1979 Imperial Valley Earthquake Records," *Earthquake Engineering and Structural Dynamics*, **15**, 249-274.

White, J. M. and G. C. Pardoen (1987) "Modal Identification of the Golden Gate Bridge Tower Using Ambient Vibration Data," *Proceedings of the 5th International Modal Analysis Conference*, **1**, 16-20.

White, K. R., J. Minor, and K. N. Derucher (1992), *Bridge Maintenance, Inspection and Evaluation*, Marcel Dekker, New York.

Wilson, J. C. (1986) "Analysis of the Observed Seismic Response of a Highway Bridge," *Earthquake Engineering and Structural Dynamics*, **14**, 339-354.

Wilson, J. C. and B. S. Tan (1990) "Bridge Abutments - Assessing Their Influence on Earthquake Response of Meloland Road Overpass," *ASCE Journal of Engineering Mechanics,* **116**, 1838-1856.

Wilson, J. C. and T. Liu (1991) "Ambient Vibration Measurements on a Cable-Stayed Bridge," *Earthquake Engineering and Structural Dynamics,* **20**, 723-747.

Dr. John D. Stevenson
Stevenson & Associates
9217 Midwest Avenue
Cleveland, Ohio 44125

Dr. Mete Sozen
3112 Newmark Civil Engineering Lab
208 North Romine Street
Urbana, IL 61801

Dr. Robert P. Kennedy
18971 Villa Terrace
Yorba Linda, CA 92686

Mr. Phil Hashimoto
EQE Engineering, Inc.
Lakeshore Towers
18101 Von Karman Ave., Suite 400
Irvine, CA 92715

Mr. Mike Salmon
EQE Engineering, Inc.
Lakeshore Towers
18101 Von Karman Ave., Suite 400
Irvine, CA 92715

Dr. Mike Bohn
Sandia National Laboratory
Division 6447
P.O. Box 5800
Albuquerque, NM 87185

Mr. Claude Griffin
Geiner, Inc.
4742 N. Oracle Road, Suite 310
Tucson, AZ 85705

Mr. Eric Klamerous
Sandia National Laboratory
Division 6447
P.O. Box 5800
Albuquerque, NM 87185

Professor Jack P. Moehle
University of California
Department of Civil Engineering
775 Davis Hall
Berkeley, CA 94720

Ms. Cecily Sobey
Gift & Exchange Dept.
Earthquake Engineering Research
Center Library
University of California/RFS 453
1306 South 46th Street
Richmond, CA 94804-4698

Professor Peter Gergely
Cornell Univesity
Hollister Hall
Ithica, NY 14853

Prof. Ming L. Wang
University of New Mexico
Department of Civil Engineering
209 Tapy Hall
Albuquerque, New Mexico 87131

Dr. James E. Beavers
Martin Marietta Energy Systems, Inc.
P.O. Box Y
Oak Ridge, Tennessee 37831

Dr. John W. Reed
Jack Benjamin & Associates
Mountain Bay Plaza
444 Castro St. Suite 501
Mountain View, CA 94041

Dr. Gerard C. Pardoen
101 ICEF-Civil Eng.
Univ. of California-Irvine
Irvine, CA. 92717

Dr. J. Altes
Institute of Safety Research and Reactor
Technology
Research Center Juelich
5170 Juelich
Postbox 1913
Germany

Ms. F. Gantenbein
C.E.A.- CE/Saclay - DMT/SEMT/EMS
91191 - GIF - SUR - YVETTE Cedex
Fra ice

Mr. Jeffrey Kimball
Department of Energy
DP-12, E-136A
19901 Germantown Rd.
Germantown, MD 20585

Dr. Robert Murray
Lawrence Livermore National
Laboratory
P. O. Box 808, L-197
Livermore, CA 94550

Dr. J. J. Johnson
EQE, Inc.,
44 Montgomery St., Suite 3200
San Francisco, CA 94104

Dr. Alejandro Asfura
EQE, Inc.,
44 Montgomery St., Suite 3200
San Francisco, CA 94104

Mr. Steve Eder
EQE, Inc.,
44 Montgomery St., Suite 3200
San Francisco, CA 94104

Dr. Ron Polivka
EQE, Inc.,
44 Montgomery St., Suite 3200
San Francisco, CA 94104

Mr. Dan Nuta
EBASCO Services, Inc.,
Two World Trade Center
New York, NY 10048

Prof. Ken White   (10 copies)
Dept. of Civil, Agricultural, and
Geological Eng.
Box 30001/Dept. 3CE
Las Cruces, NM 88003-0001

William L. Barringer
Alliance for Transportation Research
1001 University Blvd., SE Suite 103
Albuquerque, NM 87106

Larry Blair
Alliance for Transportation Research
1001 University Blvd., SE Suite 103
Albuquerque, NM 87106

David Albright
Alliance for Transportation Research
1001 University Blvd., SE Suite 103
Albuquerque, NM 87106

Dr. Christian A. Kot
Argonne National Laboratory
9700 South Cass Ave. RE/331
Argonne, IL 60439-4817

Dipl. ING Klaus Kerkhoff
Staatliche Materialprufungsanstalt
Universitat Stuttgart
D-70569 Stuttgart (Vaihingen)
Germany

Randy Mayes
MS 0557
Sandia National Laboratory
Albuquerque, NM 87185

George James
MS 0557
Sandia National Laboratory
Albuquerque, NM 87185

Robert Redden
P.O. Box 1628
Santa Fe, NM 87504-1628

Dr. Mrinmay Biswas
Dept. of Civil Engineering
Duke University
Durham, NC 27706

Anshel Schiff
Stanford University
Dept. of Civil Eng.
Standford, CA 94305

Stuart Werner
Dames and Moore
221 Main St., Suite 600
San Francisco, CA 94607

Shorchi Nakai
Fukoku Seimei Bldg.
2-2-2 Uchisaiwai - Cho
Chiyoda - ku
Tokyo, 100 Japan

Prof. A. K. Gupta
Civil Eng. Dept.
Box 7908
Raleigh, NC 27695-7908

Prof. Franklin Cheng
Dept. of Civil Eng.
University of Missouri, Rolla
Rolla, MO 65401

Tom Duffey
P.O. Box 1239
Tijeras, NM 87059

M. Saiidi
Dept. of Civil Eng./258
College of Engineering
Reno, NV 89557-0152

Dr. Lee Peterson
Center for Aerospace Structures
Univ. Colorado, Boulder
Campus Box 429
Boulder, CO 80309-0429

Prof. Norris Stubbs
Mechanics and Materials Center
Dept. of Civil Engineering
Texas A&M University
College Station, TX 77843-3136

Los Alamos National Laboratory
Tim Darling, MTL-10, MS K764
Al Migliori, MTL-10, MS K764
Tom Bell, MTL-10, MS K764
Richard Burick, ESA-DO, MS P945
John Ruminer, ESA-DO, MS P945
Mike Berger, ET, MS D453
Paul Smith, ESA-11, MS C931
Kerry Cone, ESA-13, MS J576
Bill Baker, ESA-13, MS J576
Chuck Anderson, ESA-13, MS J576
Wayne McCabe, ESA-13, MS J576

DATE
FILMED
7 / 8 / 94

END